DISTRIBUTED-PARAMETER STATE-VARIABLE TECHNIQUES

APPLIED TO COMMUNICATION OVER DISPERSIVE CHANNELS

by

RICHARD ROBERT KURTH

B.S., Massachusetts Institute of Technology
(1965)

M.S., Massachusetts Institute of Technology
(1965)

E.E., Massachusetts Institute of Technology
(1968)

SUBMITTED IN PARTIAL FULFILLMENT OF THE

REQUIREMENTS FOR THE DEGREE OF

DOCTOR OF SCIENCE

at the

MASSACHUSETTS INSTITUTE OF TECHNOLOGY

June, 1969

Signature of Author _____

Department of Electrical Engineering, May 16, 1969

Certified by ___   _____

Thesis Supervisor

Accepted by ___   _____

Chairman, Departmental Committee on Graduate Students

DISTRIBUTED-PARAMETER STATE-VARIABLE TECHNIQUES

APPLIED TO COMMUNICATION OVER DISPERSIVE CHANNELS

by

RICHARD ROBERT KURTH

Submitted to the Department of Electrical Engineering on May 16, 1969
in partial fulfillment of the requirements for the degree of Doctor
of Science.

ABSTRACT

This thesis considers the problem of detecting known narrowband
signals transmitted over random dispersive channels and received in addi-
tive white Gaussian noise. Methods for calculating error probabilities
and performance comparisons between optimum and suboptimum receivers are
presented for doppler-spread, delay-spread, and doubly-spread channels.

The doppler-spread channel is assumed to have a finite state-
variable representation. Asymptotic expressions for the error probabili-
ties of suboptimum receivers are derived in terms of the semi-invariant
moment-generating functions of the receiver decision statistic. The per-
formance of two suboptimum receivers, a filter-squarer-integrator and a
sampled correlator followed by square-law detection, come within one or
two dB of the optimum receiver performance in a number of examples.

The delay-spread channel is related to the doppler-spread model
by time-frequency duality. Two suboptimum receiver structures are sug-
gested for the delay-spread channel: a two-filter radiometer, and a bank
of delayed replica correlators followed by square-law detection. A di-
rect method for finding the performance of the optimum and these subopti-
mum receivers is given which is convenient for transmitted signals and
scattering distributions with finite durations. The suboptimum receiver
performance is shown to be close to optimum in several examples.

A distributed-parameter state-variable model is given for the
doubly-spread channel. It is a linear distributed system whose dynamics
are described by partial differential equations and whose input is a dis-
tributed, temporally white noise. The model is specialized to the case
of stationary, uncorrelated scattering, and the class of scattering func-
tions which can be described by the model are given. The realizable
minimum mean-square error estimator for the distributed state vector in
the channel model is used to construct a realizable optimum detector. A
by-product of the estimator structure is a partial differential equation

for the estimation error covariance matrix, which is necessary for the calculation of the error probabilities.

A modal technique for solving the estimator and error covariance equations of the distributed doubly-spread channel model is given. It reduces the distributed model to a finite state system. This approximate model is compared with a tapped delay line model for the channel. The performance of the optimum receiver is computed for an example. The technique for finding the optimum receiver error probabilities is useful for arbitrary signals and energy-to-noise ratios, and for a large class of doubly-spread channel scattering functions.

Finally, several suboptimum receivers for the doubly-spread channel are considered. It is shown that their performance can be found by the methods used to obtain the optimum receiver performance.

THESIS SUPERVISOR: Harry L. Van Trees
TITLE: Associate Professor of Electrical Engineering

ACKNOWLEDGEMENT

TABLE OF CONTENTS

To my parents and Mary

CHAPTER I

INTRODUCTION

An appropriate model for many detection and communication

problems is one that describes the received waveform as the sum of a

signal term which is a Gaussian random process and a noise term which

is also Gaussian. For example, in sonar and radar detection a known

signal is transmitted and may be reflected by a target. If the target

is not a point reflector of constant intensity, the received waveform

can be characterized as a random process with properties that are related

to the transmitted signal and the target scattering mechanism. Signals

received after transmission over certain communication channels often

exhibit a similar random behavior. Such channels include underwater

acoustic paths, orbiting dipole belts, chaff clouds, and the tropo-

sphere. The Gaussian signal in Gaussian noise model is also appli-

cable in many situations which do not involve the initial transmission

of a known waveform: passive acoustic detection of submarines, the

discrimination between various types of seismic disturbances, or the

detection of extraterrestial radio sources.

The optimum reception of Gaussian signals in Gaussian noise

has received considerable attention [1-8]. Van Trees [8] contains

a thorough discussion of optimum receivers, their realization, and

performance evaluation for a wide class of Gaussian signal in Gaussian

noise detection problems. A familiarity with these results is assumed

here.

The detection problem which is considered in the sequel is formulated as a binary hypothesis test. With $r(t)$ denoting the received waveform, the two hypotheses are

$$H_1: r(t) = s_1(t) + w(t),$$

$$H_0: r(t) = s_0(t) + w(t), \qquad T_o \leq t \leq T_f \qquad (1.1)$$

The observation interval is $[T_o, T_f]$ and the signals $s_k(t)$ are sample functions of zero-mean, narrowband Gaussian random processes. That is, the $s_k(t)$ can be written in terms of their complex amplitudes as

$$s_k(t) = \sqrt{2} \, \text{Re}[\tilde{s}_k(t) \, e^{j\omega_k t}], \quad k = 0,1 \qquad (1.2)$$

with covariance functions

$$E[\tilde{s}_k(t)\tilde{s}_k^*(u)] = \tilde{K}_{s_k}(t,u)$$

$$ \qquad (1.3)$$

$$E[\tilde{s}_k(t)\tilde{s}_k(u)] = 0$$

$$E[s(t)s(u)] = K_{s_k}(t,u) = \text{Re}[\tilde{K}_{s_k}(t,u)e^{j\omega_k(t-u)}] \qquad (1.4)$$

The superscript $*$ indicates complex conjugation and $E[\cdot]$ expectation. Details of the representation of complex random processes are contained in Van Trees [8,15].

The additive noise $w(t)$ in (1.1) is assumed to be a sample function from a zero-mean, white Gaussian random process. In terms of complex amplitudes

$$w(t) = \sqrt{2} \, \text{Re}[\tilde{w}_k(t) \, e^{j\omega_k t}], \quad k = 0,1 \qquad (1.5)$$

$$E[\tilde{w}_k(t)\tilde{w}_k^*(u)] = N_o\delta(t-u)$$

$$\text{(1.6)}$$

$$E[\tilde{w}_k(t)\tilde{w}_k(u)] = 0$$

The subscript k in $\tilde{w}_k(t)$ indicates that the lowpass processes $\tilde{w}_k(t)$ are different if the ω_k are not identical. When the ω_k are the same or when the meaning is clear, the subscript will be dropped. The received waveform r(t) may be expressed as

$$r(t) = \sqrt{2}\ \text{Re}[\tilde{r}_k(t)e^{j\omega_k t}], \quad k = 0,1 \tag{1.7}$$

$$\tilde{K}_{\tilde{r}_k}(t,u) = E[\tilde{r}_k(t)\tilde{r}_k^*(u)] = \tilde{K}_{\tilde{s}_k}(t,u) + N_o\delta(t-u) \tag{1.8}$$

The detection problem of (2.1) may now be restated in terms of complex processes

$$H_1: \tilde{r}_1(t) = \tilde{s}_1(t) + \tilde{w}_1(t)$$

$$T_o \leq t \leq T_f \tag{1.9}$$

$$H_0: \tilde{r}_0(t) = \tilde{s}_0(t) + \tilde{w}_0(t)$$

A special case of the binary detection problem of (1.9) occurs when H_0 is taken to be the absence of the signal. Then the carrier frequencies are identical and the problem is one of deciding between

$$H_1: \tilde{r}(t) = \tilde{s}(t) + \tilde{w}(t)$$

$$T_o \leq t \leq T_f \tag{1.10}$$

$$H_0: \tilde{r}(t) = \tilde{w}(t)$$

The hypothesis test of (1.10) will be called the simple binary detection problem.

A communication problem that also receives attention in the sequel involves the reception of one of M equally likely, narrowband Gaussian random processes, $s_k(t)$, in white Gaussian noise. It will be assumed that the zero-mean $s_k(t)$ are sufficiently separated in carrier frequency to ensure that they are essentially orthogonal. Furthermore, the covariance functions of the $s_k(t)$ differ only in carrier frequency.

$$K_{s_k}(t,u) = \text{Re } [\tilde{K}_{s}(t,u) \, e^{j\omega_k(t-u)}] \, , \quad k = 1,\ldots,M \qquad (1.11)$$

The receiver decides at which one of the M carrier frequencies a signal is present. In complex notation there are M hypotheses

$$H_k: \tilde{r}_k(t) = \tilde{s}_k(t) + \tilde{w}_k(t) \, , \quad k = 1,\ldots,M \qquad (1.12)$$

This will be called the M-ary symmetric, orthogonal communication problem. Note that when $M = 2$, the formulation of (1.12) is the same as the problem of (1.9) when the model of (1.9) has identical covariance functions, $\tilde{K}_{s_k}(t,u)$, and widely separated carrier frequencies.

The optimum receivers for the detection and communication problems presented above are well known [1-8]. For a large class of criteria both receivers compare the likelihood ratio to a threshold. Both receivers utilize the statistics

$$\ell_k = \int_{T_o}^{T_f} \int_{T_o}^{T_f} \tilde{r}_k^*(t)\tilde{h}_{ku}(t,u)\tilde{r}_k(u)dtdu \qquad (1.13)$$

The complex impulse responses $\tilde{h}_{ku}(t,u)$ are solutions to the integral equations

$$N_o \tilde{h}_{ku}(t,u) + \int_{T_o}^{T_f} \tilde{K}_{s_k}(t,x) \tilde{h}_{ku}(x,u) dx = \tilde{K}_{s_k}(t,u), \quad T_o \leq t,u \leq T_f$$

(1.14)

Figure 1.1 show the optimum receiver for the binary detection problem of (1.9) as an unrealizable estimator-correlator; the block ILPF denotes an ideal lowpass filter. Figure 1.2 shows the optimum receiver for the M-ary communication problem of (1.12).

Several other realizations of the operations which generate the statistics ℓ_k are possible. If $\tilde{h}_{ku}(t,u)$ in (1.13) is factored [8]

$$\tilde{h}_{ku}(t,u) = \int_{T_o}^{T_f} \tilde{g}_k^*(x,t) \tilde{g}_k(x,u) dx, \quad T_o \leq t,u \leq T_f$$

(1.15)

then (1.13) becomes

$$\ell_k = \int_{T_o}^{T_f} \left| \int_{T_o}^{T_f} \tilde{g}_k(x,u) \tilde{r}_k(u) du \right|^2 dx$$

(1.16)

The resulting structure, shown in Figure 1.3, will be called a filter-squarer-integrator branch. Whenever $\hat{\tilde{s}}_{kr}(t)$, the minimum-mean-square-error realizable estimate of the signal $\tilde{s}_k(t)$, is available, the ℓ_k can be generated as shown in Figure 1.4 [8-10]. The realizable filter $\tilde{h}_{kr}(t,u)$ produces the estimate $\hat{\tilde{s}}_{kr}(t)$ from $\tilde{r}_k(t)$.

In order to find the configurations of Figures 1.1 - 1.3, one of the integral equations (1.14) or (1.15) must be solved. In
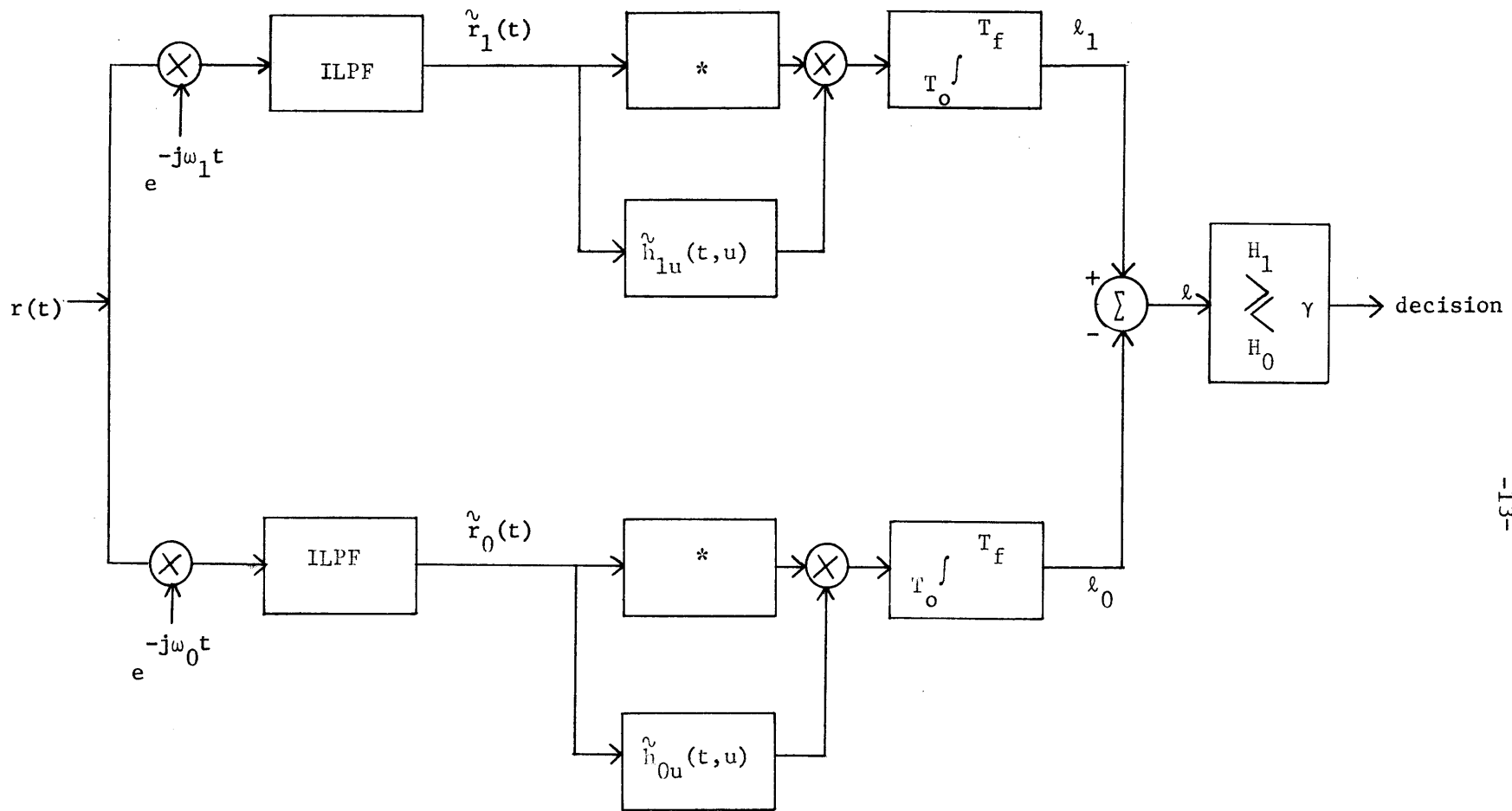
Figure 1.1. Complex representation of the estimator-correlator version of the optimum receiver for detecting Gaussian signals in white Gaussian noise.
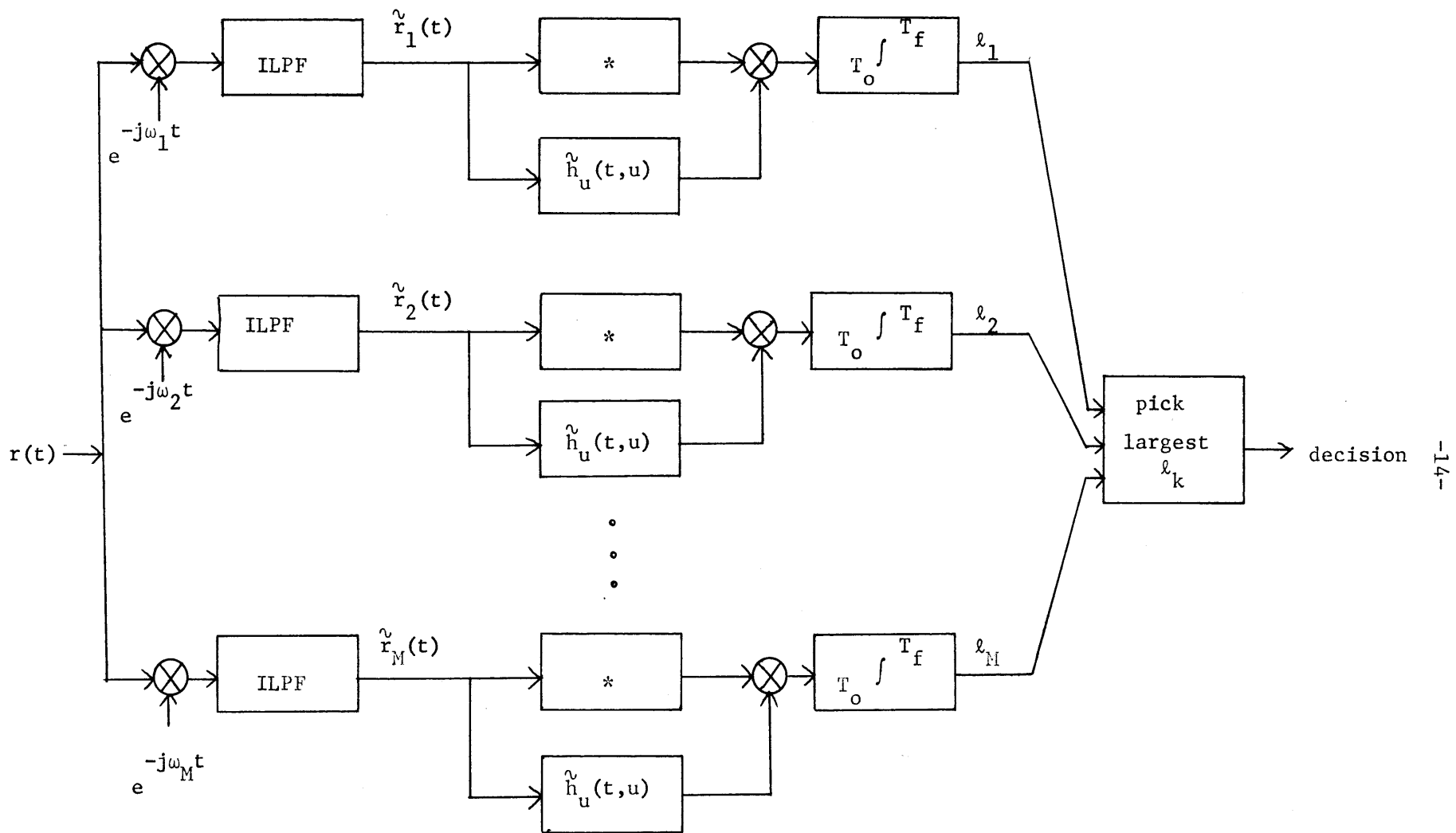
Figure 1.2. Complex version of the optimum receiver for M-ary communication with orthogonal Gaussian signals.
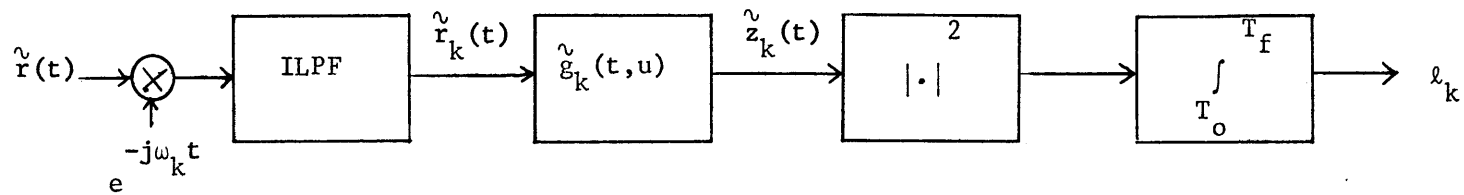
Figure 1.3. Complex version of the kth branch of the optimum receiver, filter-squarer-integrator realization.
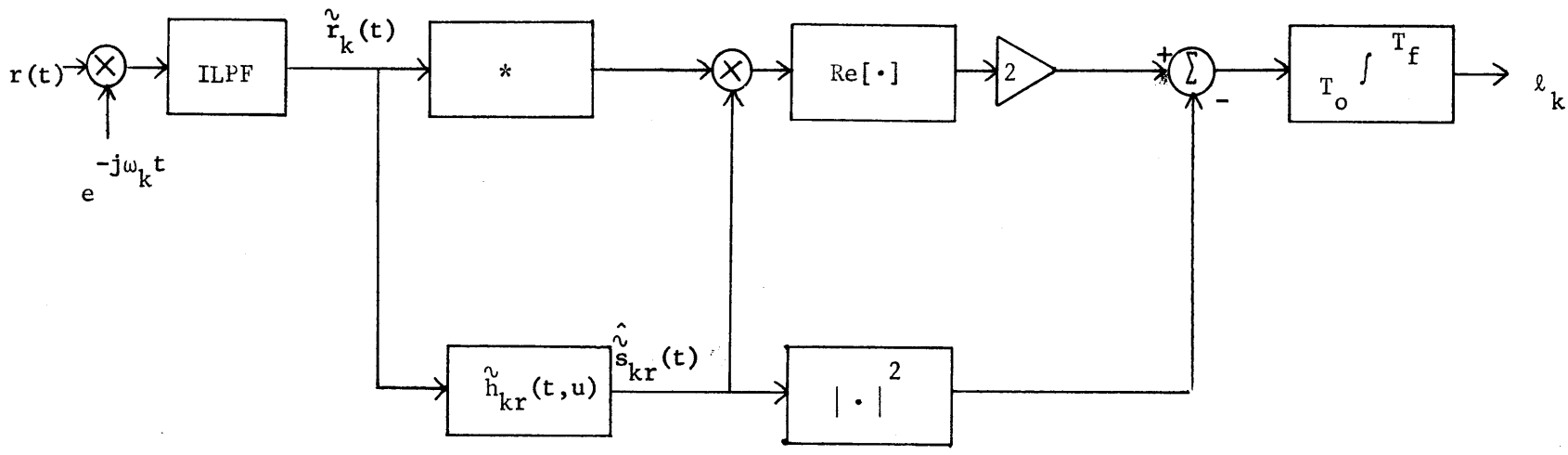
Figure 1.4. Complex representation of a realizable structure for generating the optimum ℓ_k.

general this is difficult. Several special cases which have solutions

arise when the covariance functions $\tilde{K}_{\tilde{s}_k}(t,u)$ satisfy a "low-energy-

coherence" condition [2,7,8], or are separable [8], or when the $\tilde{s}_k(t)$

are stationary and the observation interval is long [8]. The structure

of Figure 1.4 can be realized for a considerably wider class of prob-

lems: whenever the processes $\tilde{s}_k(t)$ have finite state representations

[8,15,20].

Several measures of the performance of the optimum receiver

for the binary detection problem of (1.1) have seen use [2,11,12].

A popular one is the output "signal-to-noise" ratio of the detector,

but it is strictly valid only under low-energy-coherence conditions

[2,7]. Collins [13,14] has derived asymptotic expressions for the

detection error probabilities, $Pr(\varepsilon|H_1)$ and $Pr(\varepsilon|H_0)$, for the optimum

receiver in the general case. His method involves the use of tilted

probability distributions, and the error probabilities are given in

terms of the moment-generating function of the likelihood ratio. This

function can be found for the special cases of low-energy-coherence,

separable kernels, or stationary processes-long observation. When

the $\tilde{s}_k(t)$ have state-variable representations, the moment-generating

functions can also be conveniently computed.

For the M-ary symmetric, orthogonal communication problem

of (1.12), the probability of error of the optimum receiver is not

known. Kennedy [6] has derived bounds on $Pr(\varepsilon)$ which also involve

moment-generating functions of the decision statistics ℓ_k. When $M = 2$

the asymptotic expressions for the error probabilities in the detection

problem can be applied to evaluate $Pr(\varepsilon)$ for the communication case.

A special case of the Gaussian signal in Gaussian noise model which is treated in detail in this thesis arises when a known waveform is transmitted over a "dispersive" or "spread" channel [2,6,8,16, 17]. The transmitted signal is

$$f_k(t) = \sqrt{2} \ \text{Re}[\tilde{f}_k(t)e^{j\omega_k t}], \quad 0 \le t \le T \qquad (1.17)$$

An appropriate physical model for the channel is a collection of moving point scatterers which reflect the transmitted signal. The portion of the received signal due to $f_k(t)$ is then modeled as a random process. It is convenient to classify this type of dispersive channel by its effect on the transmitted signal as doppler-spread, delay-spread, or doubly-spread.

The doppler-spread channel arises when the moving scatterers are distributed over a region of space which is small, in units of propagation time, compared to the duration of $f_k(t)$. As a result the amplitudes of the quadrature components of the reflected $f_k(t)$ vary randomly with time. The complex amplitude of the scattered return can be modeled as [8]

$$\tilde{s}_k(t) = \tilde{f}_k(t)\tilde{y}(t) \qquad (1.18)$$

where $\tilde{y}(t)$ is a complex Gaussian random process. The multiplicative disturbance in (1.18) causes $s_k(t)$ to exhibit time-selective fading; in the frequency domain this appears as a broadening of the spectrum of $f_k(t)$. The doppler spread channel is also referred to as a fluc-

tuating point target model.

When the scatterers are moving at a rate which is small compared with 1/T, but have a spatial distribution in units of propagation time which is significant compared to T, the result is the delay-spread channel. Here each scattering element returns $f_k(t)$ with a random phase and amplitude which do not vary with time. Mathematically, the total return is given by

$$\tilde{s}_k(t) = \int_{-\infty}^{\infty} \tilde{f}_k(t - \lambda)\tilde{y}(\lambda)d\lambda \qquad (1.18)$$

where $\tilde{y}(\lambda)$ is a complex Gaussian random process. Equation (1.18) indicates that the duration of $s_k(t)$ exceeds that of $f_k(t)$; $s_k(t)$ also exhibits frequency-selective fading. The delay-spread channel is also called a deep or extended target model.

A combination of the effects which produce the doppler- and delay-spread models results in the doubly-spread channel model. Here each spatial element of the moving scatterer distribution acts as a point fluctuating target. The integrated return is

$$\tilde{s}_k(t) = \int_{-\infty}^{\infty} \tilde{f}_k(t - \lambda)\tilde{y}(\lambda,t)d\lambda \qquad (1.19)$$

where $\tilde{y}(\lambda,t)$ is a two parameter, complex Gaussian random process. The received signal exhibits both time- and frequency-selective fading in this case; both the duration and bandwidth of $f_k(t)$ are increased. The doubly-spread channel is also termed the deep fluctuating target model.

Construction of optimum receivers and evaluation of their

performance for detection or communication with the spread channel

model above is feasible in certain situations. Price [1,2,7] has

considered this problem in detail when a low-energy-coherence condition

prevails. Stated briefly, this condition requires the eigenvalues of

the kernel $\tilde{K}_{\tilde{s}_k}(t,u)$ all to be much smaller than the additive white

noise spectral density, N_o. Physically, this means that no time

interval over which $\tilde{s}_k(t)$ is significantly correlated can contain an

appreciable portion of the total average received signal energy. In

this case, optimum receiver structures and performance expressions are

available. However, the most comprehensive treatment of the Gaussian

signal in Gaussian noise problem is possible only with the state-

variable techniques outlined above. For the case of the transmission

of known signals over dispersive channels only the doppler-spread

model can be solved in general, since it is possible to specify a

state-variable model for the multiplicative fading process $\tilde{y}(t)$ and

hence for $\tilde{s}_k(t)$.

A considerable protion of this thesis is devoted to the

derivation and discussion of techniques for specifying the optimum

receivers for delay-spread and doubly-spread channels, and for eval-

uating their performance. These methods involve distributed-para-

meter state-variable representations for random processes. Evaluation

of the moment-generating functions of the optimum receiver decision

statistic allows the calculation of the appropriate error probabilities.

Of the optimum receiver structures in Figures 1.1 - 1.4, the

filter-squarer-integrator of Figure 1.3 is the easiest to implement

from a practical point of view. However, the solution of (1.15) is not

known except in a few special cases. The filter-squarer-integrator receiver may still be used with a different filter, although it will then be no longer optimum. Its performance may not suffer much, provided that the filter is chosen properly. In order to compare the optimum receiver with any supoptimum receiver, a technique for the evaluation of the suboptimum receiver error probabilities must be available.

This thesis presents a method of evaluating the detection error probabilities for any suboptimum binary receiver. The technique is similar to that described above for the evaluation of optimum receiver error probabilities. The results are asymptotic expressions which involve the moment-generating functions of the receiver decision statistic. For the M-ary orthogonal communication problem, bounds on suboptimum receiver error probabilities are evaluated.

The application of the expressions for the suboptimum error probabilities depends on the ability to compute the moment-generating functions of the suboptimum receiver decision statistic. This is done for two classes of suboptimum receivers: the filter-squarer-integrator structure and the finite quadratic form. The latter term describes a receiver with a decision statistic that can be written

$$\ell_k = \sum_{i=1}^{N} \sum_{j=1}^{N} \tilde{r}_i^* \tilde{W}_{ij} \tilde{r}_j \tag{1.20}$$

where the $\tilde{r}_i$ are complex Gaussian random variables [8]. The resulting expressions for the receiver error probabilities are evaluated for the spread channel detection problem and compared with the optimum receiver

performance. These comparisons provide insight into the design of suboptimum receivers and signals for the dispersive channel model.

A brief outline of the thesis follows:

Chapter II derives asymptotic expressions for the error probabilities of any suboptimum receiver used for binary detection. Bounds are given on the probability of error for the M-ary symmetric, orthogonal communication problem. Moment generating functions for optimum, filter-squarer-integrator, and finite quadratic form receivers are specified for the Gaussian signal in white Gaussian noise model.

Chapter III considers the doppler-spread channel model. A particular filter-squarer-integrator suboptimum receiver is specified and its performance is evaluated. A second suboptimum receiver is suggested and error probabilities for it are calculated. A comparison of the performance of optimum and suboptimum detectors is given.

Chapter IV treats the delay-spread channel model. The notions of time and frequency duality [6,18] are used to relate the delay-spread model to the doppler-spread problem. An alternative technique is established for finding the performance of the optimum receiver. Two suboptimum receiver structures are specified and their error probabilities are evaluated using the results of Chapter II.

Chapter V presents a distributed-parameter state-variable model for the doubly-spread channel model. A realization for the optimum detector is given and a method for evaluating the error probabilities is derived. An example is discussed in detail.

Chapter VI considers two suboptimum receiver structures for the doubly-spread channel detection problem. They are related to the suboptimum receivers treated earlier in the doppler-spread and delay-spread models. A method of evaluating their performance is given. The suboptimum receivers are compared with the optimum receiver for the same example presented in Chapter V.

Chapter VII is a summary of the results of the thesis. Some comments on signal design for dispersive channels are included. Suggestions for further research are given.

CHAPTER II

ASYMPTOTIC ERROR PROBABILITY EXPRESSIONS

FOR THE DETECTION OF GAUSSIAN SIGNALS

IN GAUSSIAN NOISE

The problem of finding the detection error probabilities for a receiver which makes a decision by comparing a random variable with a threshold can be approached in several ways. The most direct is to find the probability density function of the decision statistic and integrate over the tails of the density to get the error probabilities. For the detection of Gaussian signals in Gaussian noise, the optimum receiver of Chapter I performs a non-linear operation on the process $\tilde{r}(t)$. In this case the probability density of the decision statistic is not known. Even in problems where the density function is known, it may be difficult to perform analytically or numerically the integration required to obtain the error probabilities.

For the Gaussian signal, binary detection problem of Chapter I, it is possible to write the optimum receiver decision statistic as an infinite, weighted sum of squared, independent Gaussian random variables with known variances [8]

$$\ell = \sum_{i=1}^{\infty} \alpha_i |\tilde{R}_i|^2 \tag{2.1}$$

This suggests two possibilities for finding the error probabilities. The first is the application of the central limit theorem to the sum

of (2.1) to establish that ℓ is a Gaussian random variable. This fails because (2.1) violates a necessary condition for the use of the central limit theorem [8]. The second approach is based upon the fact that an expression for the characteristic function of ℓ is available [8,13]. Inversion of the characteristic function gives the desired density function, but in this case the inversion must be done numerically. This is impractical due to the form of the characteristic function and the necessity of accurately obtaining the tails of the density function [13].

Collins [13,14] has developed an alternate method of computing the optimum receiver error probabilities provided that the semi-invariant moment-generating function of the logarithm of the likelihood ratio is available. This technique involves the notion of tilted probability densities and the resulting error probability expressions are in series form. The semi-invariant moment-generating function is closely related to the characteristic function of ℓ in (2.1); thus for the Gaussian signal in Gaussian noise problem the optimum receiver error probabilities can be evaluated.

Essential to Collins' derivation is the fact that the receiver is optimum: it compares the likelihood ratio with a threshold. The discussion above on the calculation of error probabilities is relevant also when a receiver which is not optimum is being used. This is the case in many practical situations. Hence a generalization of Collins' results would be useful, if the moment-generation function of the output of this receiver is available.

This chapter derives expressions for the binary detection

error probabilities of receivers which are not necessarily optimum. The
results are evaluated in terms of the semi-invariant moment-generating
functions of the receiver decision statistic. Bounds on these error
probabilities are also given, as well as bounds on the error probability
of a certain class of receivers for the M-ary orthogonal communication
problem of Chapter I. The techniques of Collins [13,14] and Kennedy
[6] are used in the derivations. Moment-generating functions for
several receiver structures, including the optimum, are presented for
the Gaussian signal in Gaussian noise model.

A. Bounds on and Asymptotic Expressions for Binary Detection Error Probabilities

This section derives bounds on, and asymptotic expressions
for, the detection error probabilities for any receiver which decides
on one of two hypotheses by comparing a statistic ℓ with a threshold γ.
The development of the results is similar to that used by Collins
[13,14] for the optimum receiver error probabilities.

The conditional error probabilities for this problem are
given by

$$Pr(\varepsilon|H_0) = Pr(\ell > \gamma) = \int_{\gamma}^{\infty} p_{\ell|H_0}(L)dL \qquad (2.2)$$

$$Pr(\varepsilon|H_1) = Pr(\ell < \gamma) = \int_{-\infty}^{\gamma} p_{\ell|H_1}(L)dL \qquad (2.3)$$

The semi-invariant moment-generating functions of ℓ on the two hypo-
theses are

$$\mu_i(s) = \ell n M_{\ell|H_i}(s) = \ell n \, E[e^{s\ell}|H_i], \quad i = 0,1 \tag{2.4}$$

The functions $\mu_i(s)$ generally exist only for some range of values of s.

Given H_0 a tilted random variable ℓ_{0s} is defined to have a probability density function

$$p_{\ell_{0s}}(L) = e^{sL-\mu_0(s)} \, p_{\ell|H_0}(L) \tag{2.5}$$

From (2.2) the probability of error give H_0 is

$$Pr(\epsilon|H_0) = \int_\gamma^\infty p_{\ell_{0s}}(L) e^{\mu_0(s)-sL} \, dL \tag{2.6}$$

Note that

$$\frac{d^n \mu_0(s)}{ds^n} = \text{nth semi-invariant of } \ell_{0s} \overset{\Delta}{=} \mu_0^{(n)}(s) \tag{2.7}$$

Thus the random variable

$$y = \frac{\ell_{0s} - \dot{\mu}_0(s)}{\sqrt{\ddot{\mu}_0(s)}} \tag{2.8}$$

is zero-mean and has a unit variance. Rewriting (2.6) in terms of the density function $p_y(Y)$ gives

$$\Pr(\epsilon|H_0) = e^{\mu_0(s) - s\dot{\mu}_0(s)} \int_\delta^\infty e^{-s\sqrt{\dot{\mu}_0(s)}\,Y} p_y(Y)dY \qquad (2.9)$$

where

$$p_y(Y) = \sqrt{\ddot{\mu}_0(s)}\; p_{\ell_{0s}}(Y\sqrt{\ddot{\mu}_0(s)} + \dot{\mu}_0(s)) \qquad (2.10)$$

$$\delta = \frac{\gamma - \dot{\mu}_0(s)}{\sqrt{\ddot{\mu}_0(s)}} \qquad (2.11)$$

An upper bound on $\Pr(\epsilon|H_0)$ is obtained from (2.9) by noting that

$$\exp(-s\,\sqrt{\ddot{\mu}_0(s)}\; Y) \leq 1 \qquad (2.12)$$

if

$$s \geq 0, \; Y \geq 0 \qquad (2.13a)$$

Then if

$$\gamma \geq \dot{\mu}_0(s) \qquad (2.13b)$$

(2.9) becomes

$$\Pr(\epsilon|H_0) \leq e^{\mu_0(s) - s\dot{\mu}_0(s)} \int_\delta^\infty p_y(Y)dY$$

$$\leq e^{\mu_0(s) - s\dot{\mu}_0(s)}, \; s \geq 0, \; \gamma \geq \dot{\mu}_0(s)$$

$$(2.14)$$

Note that the bound of (2.14) is valid for any s that satisfies the conditions of (2.13).

If the random variable y in (2.8) is Gaussian, the evaluation of the integral in (2.9) is straightforward. In general y is not Gaussian, but it is often the sum of a large number of random variables. Thus for cases in which $p_y(Y)$ bears some similarity to a Gaussian density it appears reasonable to expand $p_y(Y)$ in an Edgeworth series [13,21]

$$p_y(Y) = \phi(Y) - \frac{\gamma_3}{3!} \phi^{(3)}(Y) + \left[\frac{1}{4!} \gamma_4 \phi^{(4)}(Y) \right.$$

$$+ \frac{10}{6!} \gamma_3^2 \phi^{(6)}(Y) \left. \right] - \left[\frac{1}{5!} \gamma_5 \phi^{(5)}(Y) + \frac{35}{7!} \gamma_3\gamma_4 \phi^{(7)}(Y) \right.$$

$$+ \frac{280}{9!} \gamma_3^3 \phi^{(9)}(Y) \left. \right] + \ldots \qquad (2.15)$$

where

$$\gamma_k = \frac{\mu_0^{(k)}(s)}{\left[\mu_0(s) \right]^{\frac{k}{2}}} \qquad , \ k \geq 2 \qquad (2.16)$$

$$\phi(Y) = \frac{1}{\sqrt{2\pi}} \exp\left(-\frac{Y^2}{2} \right) \qquad (2.17)$$

(The superscript (k) denotes the kth derivative.) Introducing (2.15) into (2.9) gives

$$\Pr(\epsilon \mid H_0) = e^{\mu_0(s) - s\dot{\mu}_0(s)} \left\{ I_0 - \frac{\gamma_3}{3!} I_3 + \left[\frac{\gamma_4}{4!} I_4 \right. \right.$$

$$\left. \left. + \frac{10}{6!} \gamma_3^2 I_6 \right] - \cdots \right\} \tag{2.18}$$

where

$$I_k = \int_\delta^\infty e^{-aY} \phi^{(k)}(Y) dY \tag{2.19}$$

$$a = s \sqrt{\ddot{\mu}_0(s)} \tag{2.20}$$

Integration of (2.19) by parts yields the relations

$$I_o = \exp\left(\frac{a^2}{2}\right) \mathrm{erfc}_*(\delta + a)$$

$$I_k = a I_{k-1} - \exp(-a\delta)\, \phi^{(k-1)}(\delta), \quad k \geq 2 \tag{2.21}$$

with

$$\mathrm{erfc}_*(x) = \int_x^\infty \frac{1}{\sqrt{2\pi}} \exp\left(\frac{u^2}{2}\right) du \tag{2.22}$$

Equation (2.18) gives an asymptotic expansion for $\Pr(\epsilon \mid H_0)$ in terms of $\mu_0(s)$ and its derivatives. Truncating the series provides an approximate expression for the error probability. Any non-negative value of s for which $\mu_0(s)$ and its derivatives exists is valid in (2.18 - 2.20); a desirable value is one for which the series converges

rapidly.

To obtain a similar series for $\Pr(\epsilon | H_1)$ a second tilted random variable ℓ_{1s} is defined

$$P_{\ell_{1s}}(L) = e^{sL-\mu_1(s)} P_{\ell | H_1}(L) \qquad (2.23)$$

where $\mu_1(s)$ is given by (2.4). From (2.3)

$$\Pr(\epsilon | H_1) = \int_{-\infty}^{\gamma} e^{\mu_1(s) - sL} P_{\ell_{1s}}(L)dL \qquad (2.24)$$

With the normalized random variable

$$x = \frac{\ell_{1s} - \dot{\mu}_1(s)}{\sqrt{\ddot{\mu}_1(s)}} \qquad (2.25)$$

(2.24) becomes

$$\Pr(\epsilon | H_0) = e^{\mu_1(s) - s\dot{\mu}_1(s)} \int_{-\infty}^{\Delta} e^{-s\sqrt{\ddot{\mu}_1(s)} X} p_X(X)dX \qquad (2.26)$$

where

$$p_X(X) = \sqrt{\ddot{\mu}_1(s)} \, P_{\ell_{1s}}(X \sqrt{\ddot{\mu}_1(s)} + \dot{\mu}_1(s)) \qquad (2.27)$$

$$\Delta = \frac{\gamma - \dot{\mu}_1(s)}{\sqrt{\ddot{\mu}_1(s)}} \qquad (2.28)$$

An upper bound on $\Pr(\epsilon | H_1)$ is obtained by noting that

$$\exp(-s\sqrt{\ddot{\mu}_1(s)}X) \leq 1 \qquad (2.29)$$

when

$$s \leq 0, \quad X \leq 0 \qquad (2.30a)$$

Thus if

$$\gamma \leq \dot{\mu}_1(s) \qquad\qquad (2.30b)$$

(2.26) becomes

$$\Pr(\epsilon \mid H_1) \leq e^{\mu_1(s) - s\dot{\mu}_1(s)} \int_{-\infty}^{\Delta} p_x(X)dX$$

$$\leq e^{\mu_1(s) - s\dot{\mu}_1(s)}, \quad s \leq 0, \quad \gamma \leq \dot{\mu}_1(s) \qquad (2.31)$$

Note that the bound of (2.31) is valid for any s satisfying the conditions of (2.30).

An asymptotic expansion for $\Pr(\epsilon \mid H_1)$ is obtained by the same procedure used for $\Pr(\epsilon \mid H_0)$. The density $p_x(X)$ is expanded in the series of (2.15) and introduced into (2.26). The result is

$$\Pr(\epsilon \mid H_1) = e^{\mu_1(s) - s\dot{\mu}_1(s)} \left\{ I_0' - \frac{\gamma_3'}{3!} I_3' + \left[\frac{\gamma_4'}{4!} I_4' + \frac{10}{6!} \gamma_3'^2 I_6' \right] - \ldots \right\}$$

$$(2.32)$$

where

$$I_k' = \int_{-\infty}^{\Delta} e^{-\beta x} \phi^{(k)}(x)dx \qquad\qquad (2.33)$$

$$\gamma_k' = \frac{\mu_1^{(k)}(s)}{\left[\ddot{\mu}_1(s) \right]^{\frac{k}{2}}} \qquad\qquad (2.34)$$

$$\beta = s \sqrt{\ddot{\mu}_1(s)}$$

The integral I_k' can be expressed recursively as

$$I_0' = \exp \left(\frac{\beta^2}{2} \right) \text{erfc}_* (-\Delta - \beta)$$

$$I_k' = \beta I_{k-1}' + \exp(-\beta\Delta) \, \phi^{(k-1)}(\Delta), \qquad k \geq 1 \qquad (2.35)$$

Approximations to $\Pr(\epsilon | H_1)$ are obtained by truncating the series (2.32). Equation (2.32) is valid for any non-positive s for which $\mu_1(s)$ and its derivatives exist.

The error probability bounds (2.14) and (2.31) deserve further attention. The constraints of (2.13) and (2.30) limit the range of the threshold γ. Since $\ddot{\mu}_0(s)$ and $\ddot{\mu}_1(s)$ are variances, they are positive, and thus the $\dot{\mu}_i(s)$ are monotonically increasing functions. Then the conditions (2.13) and (2.30) imply that

$$\gamma \geq \dot{\mu}_0(0) = E[\ell | H_0]$$

$$(2.36)$$

$$\gamma \leq \dot{\mu}_1(0) = E[\ell | H_1]$$

This indicates that the threshold γ must lie between the means of ℓ on H_0 and H_1 if the bounds of (2.14) and (2.31) are to be used.

The bounds on the error probabilities may be optimized by the proper choice of s. The derivative of the exponents in each of the bounds (2.14) and (2.31) is $-s\ddot{\mu}_i(s)$. Since s is constrained to be positive on H_1 and negative on H_0, and since the $\ddot{\mu}_i(s)$ are positive, this implies that $|s|$ should be made as large as possible in each case. The conditions (2.13b) and (2.30b) limit how large $|s|$ can be. Hence

the optimized bounds are

$$Pr(\varepsilon \mid H_0) \leq e^{\mu_0(s_0)-s_0\dot{\mu}_0(s_0)} \tag{2.37}$$

$$Pr(\varepsilon \mid H_1) \leq e^{\mu_1(s_1)-s_1\dot{\mu}_1(s_1)} \tag{2.38}$$

where s_0 and s_1 are determined by

$$\dot{\mu}_0(s_0) = \dot{\mu}_1(s_1) = \gamma$$

$$\tag{2.39}$$

$$s_0 \geq 0, \quad s_1 \leq 0$$

Since the values s_0 and s_1 in (2.39) optimize the bounds, they are good candidates for use in the series expansions for the error probabilities.

The bounds on, and asymptotic expressions for $Pr(\varepsilon \mid H_0)$ and $Pr(\varepsilon \mid H_1)$ given above hold for any binary receiver that compares a random variable to a threshold. For these results to be useful, the semi-invariant moment-generating function $\mu_i(s)$ must be available. Also convergence of the series expressions is not likely to be rapid if the tilted probability densities differ greatly from a Gaussian density. Unfortunately, little is known about the convergence of the error probability expressions in general; see Collins [13] for a discussion of this issue.

When the decision statistic ℓ is the logarithm of the likelihood ratio, $Pr(\varepsilon \mid H_1)$ and $Pr(\varepsilon \mid H_0)$ are related. The connection is established by noting that

$$\ell_{op} = \ell n \, \Lambda(r(t)) = \ell n \frac{p(\underline{R}|H_1)}{p(\underline{R}|H_0)} \tag{2.40}$$

where $\underline{R}$ is a sufficient statistic [20] and $\Lambda(r(t))$ is the likelihood ratio. Then

$$\mu_1(s) = \ell n \, E[e^{s\ell_{op}}|H_1]$$

$$= \ell n \int_{-\infty}^{\infty} e^{sL} \, p_{\ell_{op}|H_1}(L)dL$$

$$= \ell n \int_{-\infty}^{\infty} e^{sL + L} \, p_{\ell_{op}|H_0}(L)dL$$

$$= \mu_0(s + 1) , \quad 0 \leq s \leq 1 \tag{2.41}$$

The condition on s comes from the relation of (2.41) and the simultaneous satisfaction of (2.11) and (2.28). Thus both of the optimum receiver error probabilities, or their bounds, can be written in terms of one of the $\mu_i(s)$, where the value of s is determined by the threshold; usually $\mu_0(s)$ is used [13].

B. **Error Probability Bounds for M-ary Orthogonal Communication**

This section evaluates upper and lower bounds on the probability of error of a receiver deciding which one of M bandpass Gaussian random processes is present. The receiver structure is similar to that shown in Figure 1.2: the complex representation of each branch is identical; only the carrier frequencies differ. It will be assumed that the ω_k are sufficiently separated to ensure that the

branch outputs are independent random variables. Furthermore, it is
assumed that the outputs of all the branches which have inputs con-
sisting of white noise alone are identically distributed. The re-
ceiver makes a decision by choosing the largest of the branch outputs,
ℓ_k. Equally likely hypotheses are also assumed. Note that the re-
ceiver is not necessarily optimum. This section uses the results of
Section A to evaluate bounds originally established by Kennedy [6].

The probability of error is given by

$$Pr(\varepsilon) = Pr(\varepsilon | H_i)$$

$$= 1 - Pr(\ell_i > \text{all } \ell_k, \ k \neq i | \ H_i)$$

(2.42)

From Kennedy [6], $Pr(\varepsilon)$ may be bounded by

$$Pr(\varepsilon) \leq Pr(\ell_s \leq h) + M \ Pr(h < \ell_s \leq \ell_n)$$

(2.43)

$$Pr(\varepsilon) \geq \frac{M}{4} \ Pr(\ell_s \leq h) \ Pr(\ell_n \geq h)$$

(2.44)

where the latter bound holds provided that

$$M \ Pr \ (\ell_n \geq h) \leq 1$$

(2.45)

The random variables ℓ_s and ℓ_n are branch outputs when $s(t) + w(t)$ and $w(t)$,
respectively, are inputs. The variable h may take on different values
in the two bounds.

The lower bound (2.44) is composed of factors for which
expressions are available from Section A. From (2.32)

$$\Pr(\ell_s \leq h) = e^{\mu_{1c}(s) - s\dot{\mu}_{1c}(s)} \; [I_0' - \frac{\gamma'_3}{3!} \; I_3' + \dots] \tag{2.46}$$

where

$$I_k' = \int_{-\infty}^{\Delta} \exp\left(-s \sqrt{\ddot{\mu}_{1c}(s)} \; x\right) \phi^{(k)}(x) dx \tag{2.47}$$

$$\Delta = \frac{h - \dot{\mu}_{1c}(s)}{\sqrt{\ddot{\mu}_{1c}(s)}} \tag{2.48}$$

$$\gamma_k' = \frac{\mu^{(k)}_{1c}(s)}{\left[\ddot{\mu}_{1c}(s)\right]^{\frac{k}{2}}} \tag{2.49}$$

The semi-invariant moment-generating function for ℓ_s, the branch output when a signal is present, is

$$\mu_{1c}(s) = \ln E[\, e^{s\ell_s}] \tag{2.50}$$

Similarly, from (2.18)

$$\Pr(\ell_n \geq h) = e^{\mu_{0c}(s) - s\dot{\mu}_{0c}(s)} [I_0 - \frac{\gamma_3}{3!} I_3 + \dots] \tag{2.51}$$

$$I_k = \int_{0}^{\infty} \exp\left(-s \sqrt{\ddot{\mu}_{0c}(s)} \, u\right) \phi^{(k)}(u) du \tag{2.52}$$

$$\gamma_k = \frac{\mu_{0c}^{(k)}(s)}{\left[\ddot{\mu}_{0c}(s)\right]^{\frac{k}{2}}} \tag{2.53}$$

$$= \frac{h - \dot{\mu}_{0c}(s)}{\sqrt{\ddot{\mu}_{0c}(s)}} \tag{2.53a}$$

$$\mu_{0c}(s) = \ln E[e^{s\ell_n}] \tag{2.54}$$

Equations (2.46) and (2.51) permit evaluation of the lower bound (2.44) and the condition (2.45). The value of h can be varied to maximize the lower bound.

The upper bound of (2.43) is first replaced by a looser bound. From Appendix III of Kennedy [6]

$$\Pr(h < \ell_s \le \ell_n) = \int_h^\infty \int_{L_s}^\infty p_{\ell_s}(L_s) p_{\ell_n}(L_n) dL_n dL_s$$

$$\le \int_h^\infty \int_{L_s}^\infty e^{t(L_n - L_s)} p_{\ell_s}(L_s) p_{\ell_n}(L_n) dL_n dL_s$$

$$\le e^{\mu_{0c}(t)} \int_h^\infty p_{\ell_s}(L_s) e^{-tL_s} dL_s$$

$$= e^{\mu_{0c}(t)+\mu_{1c}(-t)} \int_h^\infty p_{\ell_s}(L_s) e^{-tL_s - \mu_{1c}(-t)} dL_s \tag{2.55}$$

where $t > 0$. Equation (2.55) can be evaluated by noting that the integrand is a density function with semi-invariant moment-generating function

$$\mu(r) = \int_{-\infty}^{\infty} e^{rL_s} P_{\ell_s}(L_s) e^{-tL_s - \mu_{1c}(-t)} dL_s$$

$$= \mu_{1c}(r-t) - \mu_{1c}(-t) \tag{2.56}$$

Then by (2.18)

$$Pr(h < \ell_s \leq \ell_n) \leq e^{\mu_{0c}(t) + \mu_{1c}(r-t) - r\dot{\mu}_{1c}(r-t)} [I_0 - \frac{3}{3!} I_3 + \ldots] \tag{2.57}$$

where the I_k and γ_k of (2.52) and (2.53) can be used with the $\mu(r)$ of (2.56). Equations (2.46) and (2.57) provide the expressions necessary for the evaluation of the upper bound; the value of h can be varied to minimize the bound.

Somewhat looser bounds on $Pr(\epsilon)$ when the suboptimum receiver is of the type considered in Section D are derived in Appendix I. The derivation is related to one carried out for the optimum receiver by Kennedy [6]. The results are

$$Pr(\epsilon) \leq k_u 2^{-\tau C E^0 (\frac{R}{C})} \tag{2.58}$$

$$Pr(\epsilon) \geq k_\ell 2^{-\tau C E^0 (\frac{R}{C})} \tag{2.59}$$

where

$$\tau = T_f - T_o \tag{2.60}$$

$$R = \frac{\log_2 M}{\tau} \tag{2.61}$$

$$C = \frac{\alpha}{\tau \ln 2} \tag{2.62}$$

$$\alpha = \frac{E_r}{N_o} \tag{2.63}$$

and k_u, k_ℓ are constants. E_r is the expected value of the received energy in $s_k(t)$ over the **observation** interval, and C is the infinite bandwidth, additive white Gaussian noise channel capacity in bits/second. The function $E^o(\frac{R}{C})$ is termed the system reliability function, and it is discussed by Kennedy [6]. Appendix I shows that

$$E^o(\frac{R}{C}) = \begin{cases} E_\ell(\frac{R}{C}) & R \leq R_{crit} \\ \\ E_h(\frac{R}{C}) & R > R_{crit} \end{cases} \tag{2.64}$$

where R_{crit} is determined by the equations

$$\frac{R_{crit}\,\alpha}{C} = -s\dot{\mu}_{1c}(s) - \mu_{0c}(-s)$$

$$\dot{\mu}_{1c}(s) = \dot{\mu}_{0c}(-s) , \quad s \leq 0 \tag{2.65}$$

The function $E_\ell(\frac{R}{C})$ is

$$E_\ell \left(\frac{R}{C} \right) \;\; = \;\; -\frac{R}{C} \; - \; \frac{1}{\alpha} \left[\mu_{1c}(s) + \mu_{0c}(-s) \right]$$

(2.66)

$$\dot{\mu}_{1c}(s) = \dot{\mu}_{0c}(-s) \qquad s \leq 0$$

and $E_h \left(\frac{R}{C} \right)$ is

$$E_h \left(\frac{R}{C} \right) = \frac{1}{\alpha} \left[s\dot{\mu}_{1c}(s) - \mu_{1c}(s) \right]$$

$$\dot{\mu}_{1c}(s) = \dot{\mu}_{0c}(t), \qquad t \geq 0, \; s \leq 0$$

(2.67)

$$\frac{R\alpha}{C} \;\;\; = \; t\,\dot{\mu}_{0c}(t) \, - \, \mu_{0c}(t)$$

The $\mu_{ic}(s)$ are the semi-invariant moment-generating functions of (2.50) and (2.54).

An expression for $Pr(\varepsilon)$ can be derived when $M = 2$. Then

$$Pr(\varepsilon) = Pr(\ell_s - \ell_n < 0)$$

(2.68)

The semi-invariant moment-generating function of $\ell_s - \ell_n$ is

$$\mu_{bc}(s) = \ln E[\, e^{s(\ell_s - \ell_n)} \,]$$

$$= \ln E[e^{s\ell_s}] + \ln E[e^{-s\ell_n}]$$

$$= \mu_{1c}(s) + \mu_{0c}(-s)$$

(2.69)

The asymptotic expansion for $Pr(\varepsilon)$ follows directly from (2.32)

$$Pr(\varepsilon) = e^{\mu_{bc}(s) - s\dot{\mu}_{bc}(s)} [I_0' - \frac{\gamma_3'}{3!} I_3 + \ldots] \tag{2.70}$$

$$I_k' = \int_{-\infty}^{\Delta} \exp(-s \sqrt{\ddot{\mu}_{bc}(s)} x) \phi^{(k)}(x) dx \tag{2.71}$$

$$\gamma_k' = \frac{\mu_{bc}^{(k)}(s)}{\left[\ddot{\mu}_{bc}(s)\right]^{\frac{k}{2}}} \tag{2.72}$$

$$\Delta = \frac{-\dot{\mu}_{bc}(s)}{\sqrt{\ddot{\mu}_{bc}(s)}} \tag{2.73}$$

A bound on $Pr(\varepsilon)$ is available from (2.38)

$$Pr(\varepsilon) \leq e^{\mu_{bc}(s)} \tag{2.74}$$

$$\dot{\mu}_{bc}(s) = 0 , \quad s \leq 0 \tag{2.75}$$

When $M = 2$ and the optimum receiver is used, tight bounds on $Pr(\varepsilon)$ are available from Pierce [27]. From (2.69) and (2.41)

$$\mu_{*bc}(s) = \mu_{*0c}(s + 1) + \mu_{*0c}(-s) \tag{2.76}$$

where the * indicates that the optimum receiver is used. Then $Pr(\varepsilon)$ may be bounded by [13]

$$\frac{\exp(\mu_{*bc}(-.5))}{2[1+\sqrt{.125\pi\ddot{\mu}_{*bc}(-.5)}]} \leq \Pr(\varepsilon) \leq \frac{\exp(\mu_{*bc}(-.5))}{2[1+\sqrt{.125\ddot{\mu}_{*bc}(-.5)}]} \qquad (2.77)$$

Note that this is consistent with (2.74). Equation (2.77) indicates that for optimum reception in the binary symmetric orthogonal communication problem, the quantity $\mu_{*bc}(-.5)$ is an accurate performance indicator.

This section has evaluated bounds on the $\Pr(\varepsilon)$ for the M-ary communication problem of (1.12). Any receiver may be used that has identical branch structures and statistically independent branch outputs. The expressions given are not useful, however, unless the moment-generating functions are available. The remainder of Chapter II considers the moment-generating functions associated with the optimum receiver and with two classes of suboptimum receivers for the Gaussian signal in white Gaussian noise model outlined in Chapter I.

C. Moment-Generating Functions for Optimum Receivers

This section reviews the semi-invariant moment-generating functions for the optimum receivers in the detection problems (1.9) and (1.10), and the communication problem (1.12). These results are due to Collins [13] and Baggeroer [24]. The evaluation of the re-sulting expressions is considered for situations in which the random processes in the models have finite state-variable representations.

For the binary detection problem of (1.10) the moment-generating function for the optimum receiver decision statistic on H_0 is

$$\mu_{*0}(s) = (1-s) \sum_{n=1}^{\infty} \ell n(1 + \frac{\lambda_{1n}}{N_0}) + s \sum_{n=1}^{\infty} \ell n (1 + \frac{\lambda_{0n}}{N_0}) - \sum_{n=1}^{\infty} \ell n(1 + \frac{\lambda_{cn}}{N_0}),$$

$$0 \leq s \leq 1 \qquad (2.78)$$

where the $\{\lambda_{1n}\}$, $\{\lambda_{0n}\}$, and $\{\lambda_{cn}\}$ are the eigenvalues of the process $\tilde{s}_1(t)$, $\tilde{s}_0(t)$, and the composite process $\tilde{s}_c(t)$:

$$\tilde{s}_c(t) = \sqrt{s} \; \tilde{s}_1(t) + \sqrt{1 - s} \; \tilde{s}_0(t) \qquad (2.79)$$

Equation (2.41) gives the moment-generating function on H_1

$$\mu_{*1}(s) = \mu_{*0}(s + 1) \qquad (2.80)$$

For the special case of (1.10), simple binary detection, (2.78) reduces to

$$\mu_{*0}(s) = (1-s) \sum_{n=1}^{\infty} \ell n(1 + \frac{\lambda_n}{N_0}) - \sum_{n=1}^{\infty} \ell n(1 + \frac{(1-s)\lambda_n}{N_0})$$

$$0 \leq s \leq 1 \qquad (2.81)$$

Here the $\{\lambda_n\}$ are eigenvalues of the process $\tilde{s}(t)$ in (1.10).

For the M-ary communication problem of (1.12) the moment-generating function of (2.54) is identical with that of (2.81)

$$\mu_{*0c}(s) = (1-s) \sum_{n=1}^{\infty} \ell n(1+ \frac{\lambda_n}{N_0}) - \sum_{n=1}^{\infty} \ell n(1+ \frac{(1-s)\lambda_n}{N_0})$$

$$(2.82)$$

$$\mu_{*1c}(s) = \mu_{*0c}(1 + s)$$

Here the $\{\lambda_n\}$ are the eigenvalues of the complex process $\tilde{s}_k(t)$ which has the same complex covariance function for all k. For the binary symmetric communication problem (M = 2), $\mu_{*bc}(s)$ is given by (2.76) and (2.82)

$$\mu_{*bc}(s) = \sum_{n=1}^{\infty} \ell n(1 + \frac{\lambda_n}{N_0}) - \sum_{n=1}^{\infty} \ell n(1 - \frac{s\lambda_n}{N_0})$$

$$- \sum_{n=1}^{\infty} \ell n(1 + \frac{(1 + s)\lambda_n}{N_0}) \qquad (2.83)$$

Closed form expressions for the moment-generating functions given above exist under certain circumstances. All of these formulas involve the Fredholm determinant associated with the random process $\tilde{s}(t)$ [22]

$$D_F(\alpha) = \prod_{i=1}^{\infty} (1 + \alpha\lambda_i) \qquad (2.84)$$

The $\{\lambda_i\}$ are the eigenvalues of $\tilde{K}_s(t,u)$. This function can be related to a filtering error [8,24]

$$\ell n D_F(\alpha) = \alpha \int_{T_0}^{T_f} \xi_p(t,\tilde{s}(t),\alpha)\ dt \qquad (2.85)$$

where $\xi_p(t)$ is the minimum-mean-square realizable filtering error obtained in estimating the random process $\tilde{s}(t)$ which is imbedded in complex white Gaussian noise of spectral density α.

When $\tilde{s}(t)$ has a finite state-variable representation, (2.85)

can be evaluated, since $\xi_p(t,\tilde{s}(t),\alpha)$ is available as the solution of a non-linear differential equation obtained in solving the estimation problem [20]. A more convenient method for evaluating the Fredholm determinant is known [10, 24]. Suppose $\tilde{s}(t)$ has the complex state-variable representation [15]

$$\dot{\tilde{\underline{x}}}(t) = \tilde{\underline{F}}(t)\tilde{\underline{x}}(t) + \tilde{\underline{G}}(t)\tilde{\underline{u}}(t)$$

$$\tilde{s}(t) = \tilde{\underline{C}}(t)\tilde{\underline{x}}(t) \tag{2.86}$$

$$E[\tilde{\underline{u}}(t)\tilde{\underline{u}}^{\dagger}(\sigma)] = \underline{Q}\delta(t-\sigma)$$

$$E[\tilde{\underline{x}}(T_o)\tilde{\underline{x}}^{\dagger}(T_o)] = \underline{P}_o \tag{2.87}$$

$$E[\tilde{\underline{u}}(t)\tilde{\underline{u}}^{T}(\sigma)] = E[\tilde{\underline{x}}(t)\tilde{\underline{x}}^{T}(\sigma)] = \underline{0} \tag{2.88}$$

where the superscripts ^{T} and † denote transpose and conjugate transpose, respectively. Then the Fredholm determinant for $\tilde{s}(t)$ is given by

$$\ell n D_F(\alpha) = \ell n \det \underline{\phi}_2(T_f) + \int_{T_o}^{T_f} tr[\tilde{\underline{F}}^{\dagger}(t)]dt \tag{2.89}$$

where $\phi_2(T_f)$ is the solution at $t = T_f$ of the matrix differential equation

$$\frac{d}{dt}\begin{bmatrix} \underline{\phi}_1(t) \\ \underline{\phi}_2(t) \end{bmatrix} = \begin{bmatrix} \tilde{\underline{F}}(t) & \tilde{\underline{G}}(t)\underline{Q}\tilde{\underline{G}}^{\dagger}(t) \\ \alpha\tilde{\underline{C}}^{\dagger}(t)\tilde{\underline{C}}(t) & -\tilde{\underline{F}}^{\dagger}(t) \end{bmatrix}\begin{bmatrix} \underline{\phi}_1(t) \\ \underline{\phi}_2(t) \end{bmatrix} \tag{2.90}$$

$$
\begin{bmatrix} \underline{\psi}_1 (T_o) \\ \\ \underline{\psi}_2 (T_o) \end{bmatrix} = \begin{bmatrix} \underline{P}_o \\ \\ I \end{bmatrix}
\tag{2.91}
$$

The functions det $(\cdot)$ and tr$(\cdot)$ are the determinant and trace, respectively, of their matrix arguments.

Thus either (2.85) or (2.89) provides a way to evaluate the Fredholm determinant for a wide class of signal processes. This in turn allows computation of the optimum receiver error probabilities or bounds on those probabilities.

D. Moment-Generating Functions for Filter-Squarer-Integration Receivers

This section obtains the moment-generating functions for a class of receivers which are generally suboptimum. The structure of each branch in the receivers for the binary detection problem and M-ary communication problem of Chapter I is a linear filter followed by a square-law device and an integrator. This filter-squarer-integrator (FSI) receiver is shown in Figure 2.1. The filter may be time-varying. The choice of $\tilde{g}(t,u)$ which makes the FSI receiver an optimum receiver is unknown except in a few special cases.

The moment-generating function for the FSI receiver output statistic ℓ can be obtained by first writing the random process $\tilde{z}(t)$ in Figure 2.1 in a Karhunen-Loeve expansion [20,22]

$$
\tilde{z}(t) = \sum_{n=1}^{\infty} \tilde{z}_n \overset{\sim}{\psi}_n(t), \qquad T_o \le t \le T_f
\tag{2.92}
$$

$r(t) \rightarrow \bigotimes \rightarrow \boxed{\text{ILPF}} \xrightarrow{\tilde{r}(t)} \boxed{\tilde{g}(t,u)} \xrightarrow{\tilde{z}(t)} \boxed{|\cdot|^2} \rightarrow \boxed{\int_{T_o}^{T_f}} \rightarrow$

$e^{-j\omega t}$

LINEAR
FILTER
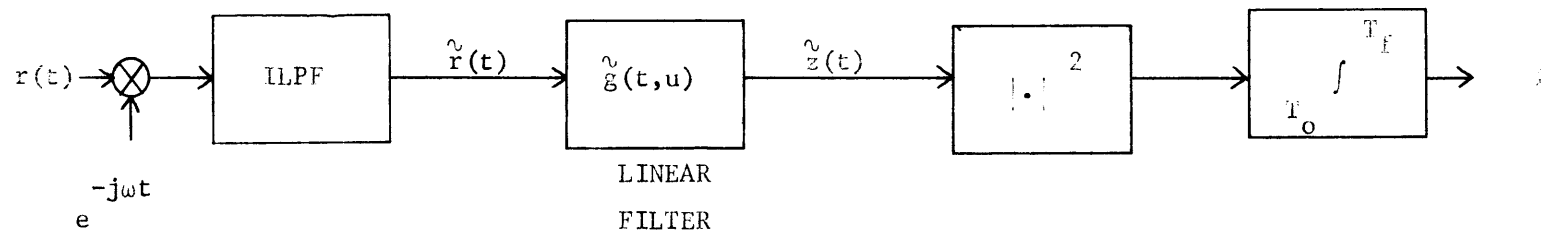
Figure 2.1.   Complex version of the filter-squarer-integrator receiver branch.

where

$$\int_{T_o}^{T_f} \tilde{\psi}_n(t)\tilde{\psi}_m^*(t)dt = \delta_{nm} \qquad (2.93)$$

$$E[\tilde{z}_n \tilde{z}_m^*] = \lambda_n \delta_{nm} \qquad (2.94)$$

Then

$$\ell = \int_{T_o}^{T_f} |\tilde{z}(t)|^2 dt$$

$$= \int_{T_o}^{T_f} (\sum_{n,m} \tilde{z}_n \tilde{z}_m^* \tilde{\psi}_n(t)\tilde{\psi}_m^*(t))dt$$

$$= \sum_{n=1}^{\infty} |\tilde{z}_n|^2 \qquad (2.95)$$

Hence ℓ is the sum of the squares of statistically independent, complex Gaussian random variables [8], with variances given by (2.94). The moment-generating function of ℓ under H_i is

$$\ln E[e^{s\ell} | H_i] = \ln E[\exp(s \sum |\tilde{z}_n|^2) H_i]$$

$$= \sum_{n=1}^{\infty} \ln E[e^{s|\tilde{z}_n|^2} | H_i]$$

$$= -\sum_{n=1}^{\infty} \ln(1 - s\lambda_{in}) \qquad (2.96)$$

by (9.87) of [22]. The first $\{\lambda_{in}\}$ are the eigenvalues of $\overset{\backsim}{z}(t)$ given that H_i is true. Equation (2.96) is valid for

$$s < \left[\max_n \{\lambda_{in}\}\right]^{-1} \qquad (2.97)$$

For the simple binary detection problem of (1.10), the $\mu_i(s)$ of (2.4) follow directly from (2.96)

$$\mu_0(s) = -\sum_{n=1}^{\infty} \ln(1 - s\lambda_{0n}) \qquad (2.98)$$

$$\mu_1(s) = -\sum_{n=1}^{\infty} \ln(1 - s\lambda_{1n}) \qquad (2.99)$$

The $\{\lambda_{0n}\}$ and the $\{\lambda_{1n}\}$ are the eigenvalues of $\overset{\backsim}{z}(t)$ in Figure 2.1 when $\overset{\backsim}{r}(t) = \overset{\backsim}{w}(t)$ and $\overset{\backsim}{r}(t) = \overset{\backsim}{s}(t) + \overset{\backsim}{w}(t)$, respectively, are inputs. For the general binary problem of (1.9) with branch outputs ℓ_1 and ℓ_0 which are independent, the $\mu_i(s)$ are

$$\mu_0(s) = -\sum_{n=1}^{\infty} \ln(1 - s\lambda_{01n}) - \sum_{n=1}^{\infty} \ln(1 + s\lambda_{00n}) \qquad (2.100)$$

$$\mu_1(s) = -\sum_{n=1}^{\infty} \ln(1 - s\lambda_{11n}) - \sum_{n=1}^{\infty} \ln(+s\lambda_{10n}) \qquad (2.101)$$

The $\{\lambda_{ijn}\}$ are the eigenvalues of $\overset{\backsim}{z}_j(t)$ on H_i.

For the M-ary communication problem of (1.12), $\mu_{0c}(s)$ and $\mu_{1c}(s)$ in (2.54) and (2.50) are identical to $\mu_0(s)$ and $\mu_1(s)$, respectively, given by (2.98) and (2.99). When $M = 2$, $\mu_{bc}(s)$ in (2.69) is

$$\mu_{bc}(s) = - \sum_{n=1}^{\infty} \ln(1-s\lambda_{1n}) - \sum_{n=1}^{\infty} \ln(1 + s\lambda_{0n}) \qquad (2.102)$$

The moment-generating functions (2.98 -2.102) can all be expressed in terms of Fredholm determinants, (2.84). The previous section indicated that computation of $D_F(\alpha)$ is feasible whenever the $\{\lambda_i\}$ of $D_F(\alpha)$ are eigenvalues of a state representable process. In the case of the FSI receiver, then, the error probability expressions can be conveniently computed when $\tilde{z}(t)$ in Figure 2.1 has a finite state representation. For this to happen, both $\tilde{r}(t)$ and the filter $\tilde{g}(t,u)$ should have state-variable representations.

Figure 2.2 shows a model in which the filter in the FSI receiver has a finite number of states and the signal $\tilde{s}(t)$ is represented as the output of a finite state system driven by white noise. Figure 2.2a is the model when the receiver input is signal plus noise. The signal state equations are

$$\overset{\sim}{\underline{x}}_s(t) = \overset{\sim}{\underline{F}}_s(t)\overset{\sim}{\underline{x}}_s(t) + \overset{\sim}{\underline{G}}_s(t)\overset{\sim}{\underline{u}}_s(t)$$

$$\tilde{s}(t) = \overset{\sim}{\underline{C}}_s(t)\overset{\sim}{\underline{x}}_s(t) \qquad (2.103)$$

$$E[\overset{\sim}{\underline{u}}_s(t)\overset{\sim}{\underline{u}}_s^{\dagger}(\sigma)] = \underline{Q}_s\delta(t - \sigma) \qquad (2.104)$$

$$E[\overset{\sim}{\underline{x}}_s(T_o)\overset{\sim}{\underline{x}}_s^{\dagger}(T_o)] = \underline{P}_{os}$$

and those for the receiver
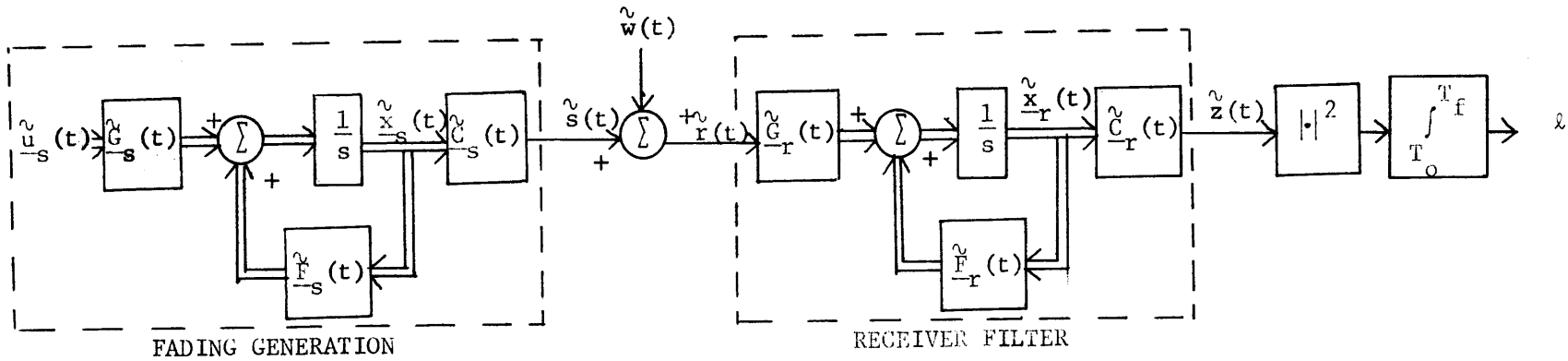
a) Signal plus noise input.
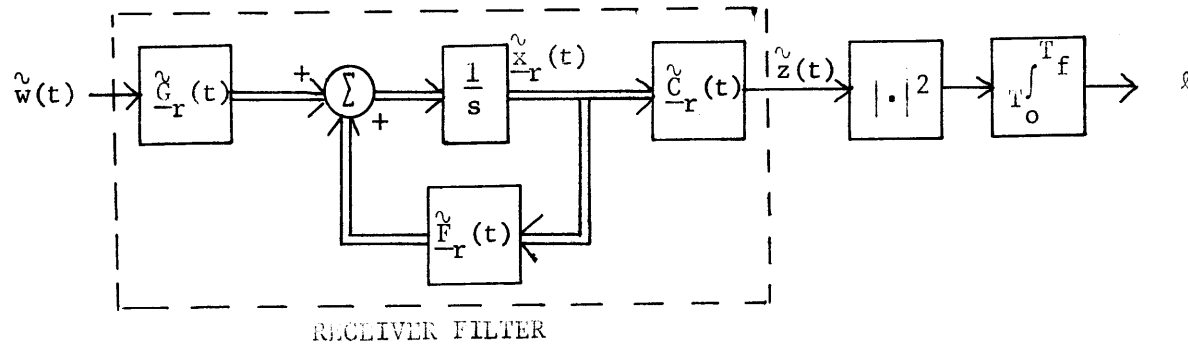
b) Noise input.

Figure 2.2. Complex state-variable model for the detection of a Gaussian signal in white Gaussian noise with a filter-squarer-integrator receiver.

$$\dot{\tilde{\underline{x}}}_r(t) = \tilde{\underline{F}}_r(t)\tilde{\underline{x}}_r(t) + \tilde{\underline{G}}_r(t)\tilde{r}(t)$$

$$\tilde{z}(t) = \tilde{\underline{C}}_r(t)\tilde{\underline{x}}_r(t) \tag{2.105}$$

$$E[\tilde{\underline{x}}_r(T_o)\tilde{\underline{x}}_r^{\dagger}(T_o)] = \underline{P}_{or} \tag{2.106}$$

The receiver initial condition $\underline{P}_{or}$ is arbitrary. A composite state-variable model for the system of **Figure** 2.2a can be defined by letting

$$\tilde{\underline{x}}(t) = \begin{bmatrix} \tilde{\underline{x}}_s(t) \\ \\ \tilde{\underline{x}}_r(t) \end{bmatrix} \tag{2.107a}$$

$$\tilde{\underline{F}}(t) = \begin{bmatrix} \tilde{\underline{F}}_s(t) & \underline{0} \\ \\ \tilde{\underline{G}}_r(t)\tilde{\underline{C}}_s(t) & \tilde{\underline{F}}_r(t) \end{bmatrix} \tag{2.107b}$$

$$\tilde{\underline{G}}(t) = \begin{bmatrix} \tilde{\underline{G}}_s(t) & \underline{0} \\ \\ \underline{0} & \underline{G}_r(t) \end{bmatrix} \tag{2.107c}$$

$$\underline{Q} = \begin{bmatrix} \underline{Q}_s & \underline{0} \\ \\ \underline{0} & N_0 \end{bmatrix} \tag{2.107d}$$

$$\tilde{\underline{C}}(t) = \begin{bmatrix} \underline{0} & , & \tilde{\underline{C}}_r(t) \end{bmatrix} \tag{2.107e}$$

$$\tilde{u}(t) = \begin{bmatrix} \tilde{\underline{u}}_s(t) \\ \\ \tilde{\underline{w}}(t) \end{bmatrix} \qquad\qquad (2.107f)$$

$$\underline{P}_o = \begin{bmatrix} \underline{P}_{os} & \underline{0} \\ \\ \underline{0} & \underline{P}_{or} \end{bmatrix}$$

Equations (2.84 - 2.91) can be used directly to give the Fredholm determinant for the model above. This in turn provides a means of obtaining $\mu_1(s)$ in (2.99).

When the input to the FSI is just $\tilde{w}(t)$, the model of Figure 2.2b is appropriate. The system of differential equations is defined by letting

$$\tilde{\underline{x}}(t) = \tilde{\underline{x}}_r(t)$$

$$\tilde{\underline{F}}(t) = \tilde{\underline{F}}_r(t)$$

$$\tilde{\underline{G}}(t) = \tilde{\underline{G}}_r(t)$$

$$\tilde{\underline{C}}(t) = \tilde{\underline{C}}_r(t) \qquad\qquad (2.108)$$

$$\underline{Q} = N_0$$

$$\tilde{\underline{u}}(t) = \tilde{\underline{w}}(t)$$

$$\underline{P}_o = \underline{P}_{or}$$

Again the results of the previous section provide the Fredholm determinant for $\tilde{z}(t)$ when noise alone is the input to the FSI receiver; then (2.98) follows immediately. The rest of the moment-generating

functions of this section can then be expressed in terms of (2.98) and (2.99).

Although it is necessary that both the signal $\tilde{s}(t)$ and the receiver filter have state-variable representations for easy computation of the Fredholm determinant, a wide class of signals and filters fall into this category. Once the semi-invariant moment-generating functions are available for the FSI receivers, the error probabilities can be calculated. The resulting suboptimum performances can be compared with the optimum.

E. Moment-Generating Functions for Quadratic Forms

In the following chapters another receiver which is generally suboptimum will be considered. It is one composed of branches with outputs that can be written as finite quadratic forms

$$\ell = \sum_{i=1}^{N} \sum_{j=1}^{N} \tilde{r}_i^* \tilde{W}_{ij} \tilde{r}_j \tag{2.109}$$

The $\{r_i\}$ are complex Gaussian random variables (see [8] for details). If a vector $\overset{\sim}{\underline{R}}$ and Hermetian matrix $\overset{\sim}{\underline{W}}$ are defined

$$\overset{\sim}{\underline{R}} = \begin{bmatrix} \tilde{r}_1 \\ \cdot \\ \cdot \\ \cdot \\ \tilde{r}_N \end{bmatrix} \tag{2.110}$$

$$\overset{\sim}{\underline{W}} = \begin{bmatrix} \tilde{W}_{ij} \end{bmatrix} \tag{2.111}$$

then

$$\ell = \underline{\tilde{R}}^\dagger \underline{\tilde{W}} \underline{\tilde{R}} \tag{2.112}$$

An example of a receiver with this decision statistic is one in which $\tilde{r}(t)$ is passed into a bank of linear filters. The sampled filter outputs, $\tilde{r}_i$, are quadratically combined, as in (2.109). This type of receiver will be considered in the following chapters. The optimum receiver for a diversity communication system operating over a Rayleigh fading channel is another case in which the operation of (2.109) appears.

The moment-generating functions of ℓ can be found by first defining the conditional covariance matrices

$$\underline{\Lambda}_s = E[\underline{\tilde{R}}\,\underline{\tilde{R}}^\dagger \mid \text{signal} + \text{noise}] \tag{2.113}$$

$$\underline{\Lambda}_n = E[\underline{\tilde{R}}\,\underline{\tilde{R}}^\dagger \mid \text{noise}] \tag{2.114}$$

where the conditions refer to the branch input. The joint probability density function for $\underline{\tilde{R}}$ given noise only is

$$P_{\underline{\tilde{R}}}(\underline{\rho}) = \frac{1}{\pi^N |\underline{\Lambda}_n|} \exp\{-\underline{\rho}^\dagger \underline{\Lambda}_n^{-1} \underline{\rho}\} \tag{2.115}$$

where the notation $|\cdot|$ means determinant. Then

$$\mu_0(s) = \ell n \, E[e^{s\ell} \, \text{noise}]$$

$$= \ell n \int_{-\infty}^{\infty} e^{s\dot{\rho}\tilde{W}\rho} \; p_{\underline{R}}^{\sim}(\underline{\rho})d\underline{\rho}$$

$$= \ell n \left[\frac{|\underline{\Sigma}_n|}{|\underline{\Lambda}_n|} \int_{-\infty}^{\infty} \frac{1}{\pi^N |\Sigma_n|} \exp\left(- \underline{\rho}^\dagger \underline{\Sigma}_n^{-1} \underline{\rho}\right) d\underline{\rho} \right]$$

$$= -\ell n \; \det \left(\underline{\Sigma}_n^{-1} \underline{\Lambda}_n \right) \tag{2.116}$$

with

$$\underline{\Sigma}_n^{-1} = \underline{\Lambda}_n^{-1} - s \tilde{\underline{W}} \tag{2.117}$$

Thus

$$\mu_0(s) = -\ell n \; \det(\underline{I} - s \tilde{\underline{W}} \underline{\Lambda}_n) \tag{2.118}$$

and correspondingly

$$\mu_1(s) = -\ell n \; \det (\underline{I} - s \tilde{\underline{W}} \underline{\Lambda}_s) \tag{2.119}$$

The expressions of (2.118) and (2.119) can be used in place of (2.98) and (2.99) for simple binary detection. Equations (2.100 - 2.102) for the other cases follow directly. Thus the error probabilities for another class of generally suboptimum receivers can be evaluated, provied that the matrices $\tilde{\underline{W}}$, $\underline{\Lambda}_s$, and $\underline{\Lambda}_n$ in (2.118) and (2.119) are known.

F. Summary

This chapter has considered methods of computing error prob-
abilities for receivers which use a threshold comparison to make a
binary decision. A technique for evaluating the error probabilities is
derived which depends on the knowledge of the semi-invariant moment-
generating function of the decision statistic. The derivation uses
tilted probability densities and is similar to one devised previously
for optimum receivers. The asymptotic expressions for the error
probabilities are also used to evaluate error probability bounds for
an M-ary communication problem.

The case of the detection of Gaussian signals in Gaussian noise
is considered next. Moment-generating functions for the optimum
receiver are reviewed, as well as an efficient technique for computing
them when finite state-variable models are available for the received
signal processes. Moment-generating functions for two classes of generally
suboptimum receivers are derived: filter-squarer-integrator receivers
and quadratic form receivers. The moment-generating functions of the
first class can be conveniently computed if the receiver filter has
finite state representation. The error probabilities of the optimum and
suboptimum receivers can then be compared.

The following chapter considers a particular example of the
Gaussian signal in Gaussian noise model: the reception of known signals
transmitted over a doppler-spread channel. Since a state-variable
representation is available for the signals in this model, it is
possible to directly apply the results of this chapter. The

performance of two classes of suboptimum receivers for the doppler-spread channel will be compared with the optimum receiver performance. Insight into the design of signals and suboptimum receivers will be provided by numerical examples. The delay-spread and doubly-spread channel models are considered in subsequent chapters.

CHAPTER III

DETECTION OF KNOWN SIGNALS TRANSMITTED

OVER DOPPLER-SPREAD CHANNELS

This chapter considers the problem of detecting known signals which are transmitted over doppler-spread dispersive channels. This problem is a special case of the Gaussian signal in Gaussian noise detection problem of Chapter I. The results of Chapter II can be applied here if a state-variable model for the doppler-spread channel is available. Such a model is specified, and the performance of the optimum receiver and several suboptimum receivers is analyzed.

The first section gives a model for the doppler-spread channel. Implementation and the performance of the optimum receiver is reviewed. Filter-squarer-integrator (FSI) suboptimum receivers are discussed. A particular FSI configuration is chosen, and the results of Chapter II are used to evaluate its performance. A second suboptimum structure, called a correlator-squarer-sum (CSS) receiver, is suggested. Its performance is analyzed and is compared to that of the optimum and FSI receivers for a variety of signal and channel parameters.

A. The Doppler-Spread Channel Model

The doppler-spread channel model considered here can be derived [6,8] by assuming that a narrowband transmitted signal

$$f(t) = \sqrt{2} \, \text{Re}[\tilde{f}(t) \, e^{j\omega t}], \qquad 0 \le t \le T \tag{3.1}$$

is reflected by a collection of moving point scatterers. The dimensions of the spatial distribution of the scatterers are small, in units of propagation time, compared to the transmitted signal duration T. It can be shown [6] that the random movement of the scatters produces a fluctuation in the amplitudes of the quadrature components of $\tilde{f}(t)$. In terms of complex amplitudes, a suitable model for the scattered return in white noise is then

$$\tilde{r}(t) = \tilde{f}(t)\tilde{y}(t) + \tilde{w}(t)$$

$$= \tilde{s}(t) + \tilde{w}(t) \qquad 0 \leq t \leq T \qquad (3.2)$$

The multiplicative disturbance $\tilde{y}(t)$ is a complex Gaussian random process. Any pure delay or doppler shift in the channel is assumed to be known and therefore is not included in the formulation of (3.2). The observation interval in (3.2) takes into account that the only interval during which a scattered return may be present is [0,T]. This model is also known as a fluctuating point target model [2,7,8,16].

The multiplicative fading process $\tilde{y}(t)$ will be assumed to be zero-mean and have the known covariance function

$$E[\tilde{y}(t)\tilde{y}^*(u)] = \tilde{K}_y(t,u) \qquad (3.3)$$

Then the covariance function for the signal component $\tilde{s}(t)$ is

$$\tilde{K}_s(t,u) = \tilde{f}(t) \tilde{K}_y(t,u)\tilde{f}^*(u) \qquad (3.4)$$

The energy in the transmitted signal $\tilde{f}(t)$ is

$$\int_0^T |\tilde{f}(t)|^2 \, dt \triangleq E_t \qquad (3.5)$$

The expected value of the received energy in s(t) is

$$E[\int_{T_o}^{T_f} |\tilde{s}(t)|^2 \, dt \,] \;=\; E[\int_0^T |f(t)|^2 \tilde{K}_{\tilde{y}}(t,t)dt]$$

$$\stackrel{\Delta}{=} \; E_r \qquad\qquad (3.6)$$

The zero-mean, additive white noise $\tilde{w}(t)$ has the covariance function

$$E[\tilde{w}(t)\tilde{w}^*(u)] \quad = N_o \delta(t-u) \qquad\qquad (3.7)$$

The model above has a convenient state-variable description whenever the fading process $\tilde{y}(t)$ has a state-variable representation. Suppose $\tilde{y}(t)$ is the output of a linear system driven by white noise

$$\dot{\tilde{\underline{x}}}_f(t) \;=\; \tilde{\underline{F}}_f(t) \, \tilde{\underline{x}}_f(t) + \tilde{\underline{G}}_f(t) \, \tilde{\underline{u}}_f(t)$$

$$\tilde{y}(t) \;=\; \quad \tilde{\underline{C}}_f(t) \, \tilde{\underline{x}}_f(t) \qquad\qquad (3.8)$$

$$E[\tilde{\underline{u}}_f(t) \, \tilde{\underline{u}}_f^\dagger(\sigma)] \;=\; \quad \underline{Q}_f \delta(t-\sigma)$$

$$E[\tilde{\underline{x}}_f(T_o) \, \tilde{\underline{x}}_f^\dagger(T_o)] \;=\; \underline{P}_{of} \qquad\qquad (3.9)$$

Then the signal $\tilde{s}(t)$ is described by the model of (2.86 - 2.88) if

$$\tilde{\underline{F}}(t) = \tilde{\underline{F}}_f(t)$$

$$\tilde{\underline{G}}(t) = \tilde{\underline{G}}_f(t)$$

$$\tilde{\underline{C}}(t) = \tilde{\underline{C}}_f(t)\tilde{f}(t) \qquad\qquad (3.10)$$

$$\underline{Q} \;\;=\; \underline{Q}_f$$

$$\underline{P}_o \;=\; \underline{P}_{of}$$

This state-variable model permits a direct application of the results of

Chapter II. A diagram of the model is shown in Figure 3.1.

When $\tilde{y}(t)$ is a stationary random process, the channel model

is a special case of the "wide-sense stationary uncorrelated scatterer"

(WSSUS) channel model [6,8,16] that will be discussed in Chapter V. In

this case the covariance function of $\tilde{y}(t)$ is written $\tilde{K}_y(t-u)$, and the

matrices $\tilde{F}_f(t)$, $\tilde{C}_f(t)$ and $\tilde{C}_f(t)$ in (3.10) are all constant. Also

(3.6) reduces to

$$E_r = \tilde{K}_y(0) \int_0^T |f(t)|^2 dt$$

(3.11)

$$= PE_t$$

where P is the average power in $\tilde{y}(t)$. Although $\tilde{y}(t)$ is stationary, the

process $\tilde{s}(t)$ is still non-stationary, in general.

The examples that follow is this chapter are limited to the

case of stationary fading. First and second order state-variable models

are used for the numerical results. The model of (3.8) for the first

order case is

$$\tilde{F}_f(t) = -k_1, \qquad k_1 > 0$$

$$\tilde{C}_f(t) = \tilde{C}_f(t) = 1$$

$$Q_f = 2Pk_1$$

(3.12)

$$P_{fo} = P$$

The constant k_1 is chosen to be real since any imaginary part would

represent a pure doppler shift [8]. For the second order model

FADING PROCESS GENERATION
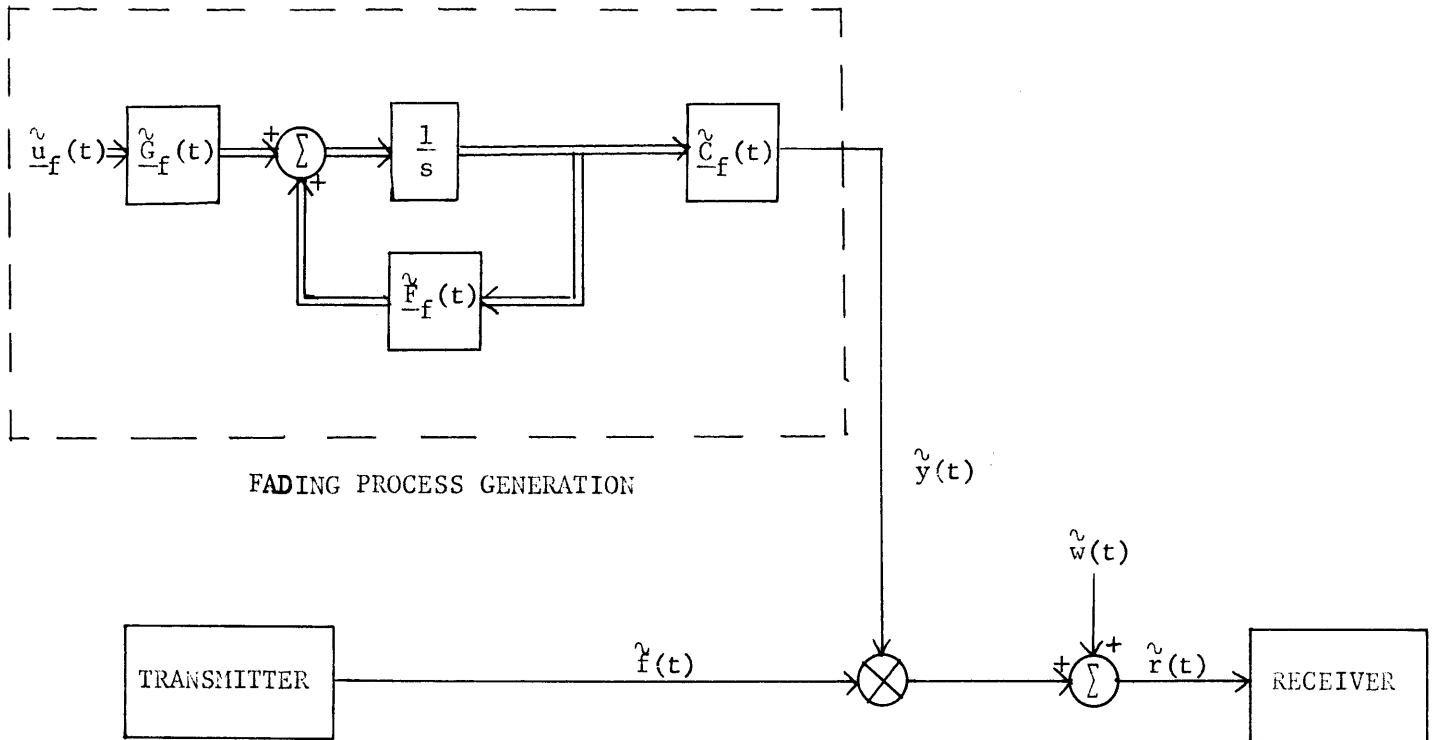
Figure 3.1. A complex state-variable model for the bandpass doppler-spread channel.

$$\tilde{F}_f(t) = \begin{bmatrix} 0 & 1 \\ -\tilde{k}_1 \tilde{k}_2 & -(\tilde{k}_1 + \tilde{k}_2) \end{bmatrix}$$

$$\tilde{G}_f(t) = \begin{bmatrix} 0 \\ 1 \end{bmatrix} \tag{3.13}$$

$$\tilde{C}_f(t) = [1 , 0]$$

and $\tilde{Q}_f$ and $\tilde{P}_{of}$ are functions of P, $\tilde{k}_1$ and $\tilde{k}_2$ given in [8,15,24]. The constants $\tilde{k}_1$ and $\tilde{k}_2$ are complex with positive real parts. This is not the most general second order process possible, but it is a reasonably flexible model. For details about complex state-variable models, see [8,15,24].

B. The Optimum Receiver and its Performance

This section reviews several configurations for the optimum receiver for the doppler-spread model given above. The performance of the optimum receiver for binary symmetric orthogonal communication for various channel parameters is summarized. The contents of this section are not new [8], but they provide a framework for the results of the following sections.

When the doppler-spread channel state-variable model of (3.8 - 3.10) is valid, the realizable branch structure of Figure 1.4 can be used in each branch of the optimum receiver for the binary

detection or the M-ary communication problems of Chapter 1. This state-variable receiver branch is shown in Figure 3.2. This realization of the optimum receiver has the widest applicability of the structures reviewed in Chapter I.

When low-energy-coherence conditions prevail and the fading is stationary, Price [2,7] has shown that the filter-squarer-integrator receiver branch of Figure 3.3 is optimum. Note that the post-detection integration interval here is infinite. The realizable filter $\hat{G}_{opt}(j\omega)$ is specified by

$$\hat{G}_{opt}(j\omega) = [\hat{S}_y(\omega)]^+ \tag{3.14}$$

where

$$\hat{S}_y(\omega) = \int_{-\infty}^{\infty} \hat{K}_y(\tau)\, e^{-j\omega\tau}\, d\tau \tag{3.15}$$

and the superscript $+$ indicates the non-unique factor of the argument which contains poles and zeros in the left-half complex plane. Note that the structure in Figure 3.3 is similar to the filter-squarer-integrator receiver of Figure 1.3.

A second case for which the structure of Figure 3.1 is optimum occurs when the fading is stationary, $\hat{f}(t)$ is a constant, and the observation interval approaches infinity. The optimum filter in Figure 1.3 is [8]

$$\hat{G}_{opt}(j\omega) = \left[\frac{\hat{S}_s(\omega)}{\hat{S}_s(\omega) + N_o} \right]^+ \tag{3.16a}$$
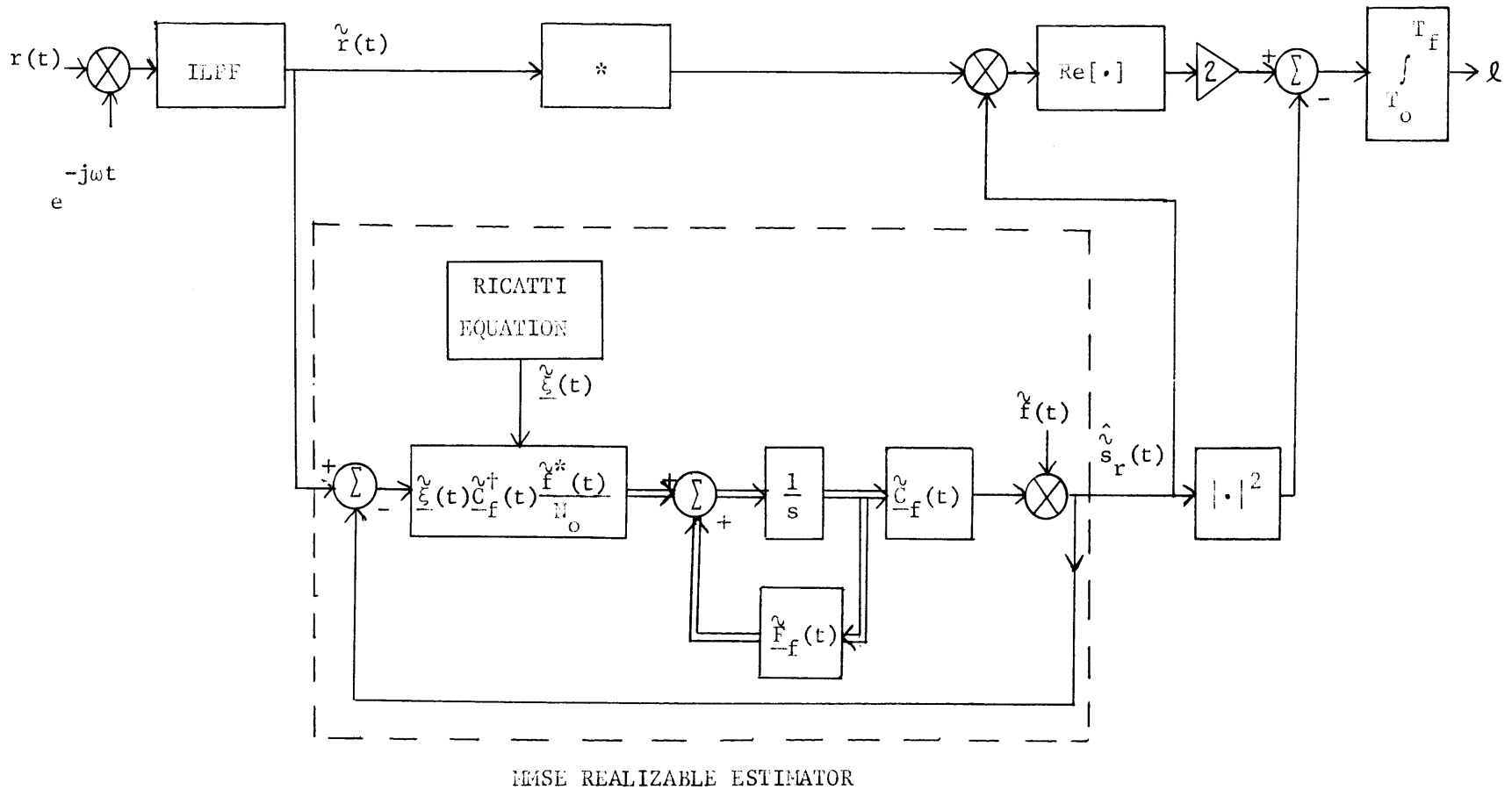
Figure 3.2. Complex state-variable configuration of a realizable optimum receiver branch for the doppler-spread channel.

-67-
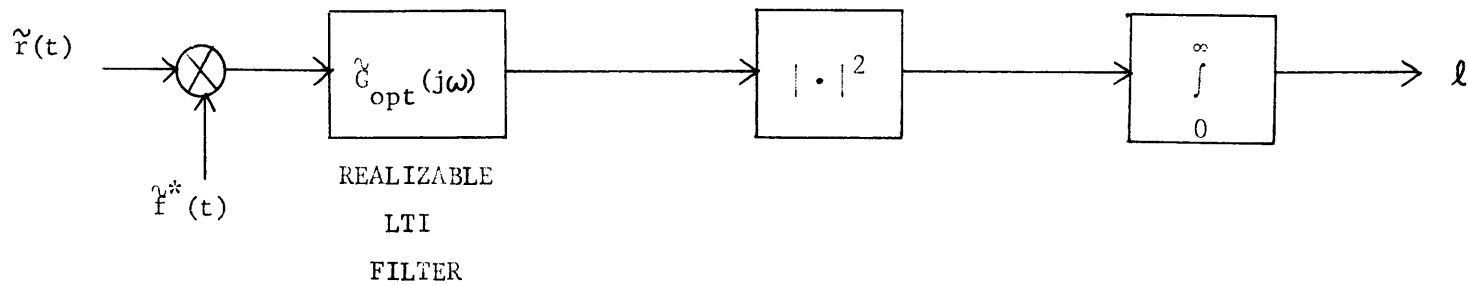
Figure 3.3. A filter-squarer-integrator realization of the optimum receiver for the doppler-spread channel under the stationary low-energy-coherence or the stationary process-long observation assumptions.

where

$$\mathring{S}_{s}(\omega) = \int_{-\infty}^{\infty} \mathring{K}_{s}(\tau) \ e^{-j\omega\tau} d\tau \qquad\qquad (3.16b)$$

Except for these two cases, a filter-squarer-integrator implementation for the optimum receiver is not known for the general doppler-spread channel problem.

The performance of the optimum receiver can be evaluated by the techniques of Collins [13], which are reviewed in Chapter II. In order to compute the error probabilities or evaluate bounds on them, the semi-invariant moment-generating function of the decision statistic is necessary. These are given for the optimum receiver in Chapter II, Section D. When the state-variable model of (3.8 - 3.10) is used, the evaluation of the moment-generating functions is particularly convenient.

The numerical examples which follow involve either the simple binary problem of (1.10) or the binary symmetric orthogonal communication problem of (1.12), with $M = 2$. The latter case is particularly instructive because the tight bounds of (2.77) involve the quantity $\mu_{*bc}(-.5)$, which influences the error probability exponentially. The numerical examples which follow show that the relative performance of a binary symmetric communication system for different signals and fading parameters is closely related to the relative simple binary detection optimum performance for the same sets of parameters. Thus the quantity $\mu_{*bc}(-.5)$ will be used in some cases as a direct measure of relative performance.

Kennedy [6] has shown that the minimum value which $\mu_{*bc}(-.5)$ can assume for any signal $\mathring{f}(t)$ and fading covariance function is

$$\min \mu_{*bc}(-.5) = -.1488 \quad \frac{E_r}{N_o} \tag{3.17}$$

Thus $\mu_{*bc}(-.5)$ normalized by E_r/N_o provides a good measure of the efficiency of a particular binary communication system.

For the doppler-spread channel, the binary symmetric communication performance of the optimum receiver behaves as shown in Figure 3.4. Here $\tilde{f}(t)$ is a constant, as illustrated by Figure 3.5a, and the fading is specified by the first order model of (3.12). Note that there is a value of k_1T which optimizes the normalized $\mu_{*bc}(-.5)$. Figure 3.6 shows this optimum k_1T and the corresponding value of $\mu_{*bc}(-.5)$.

It is evident from Figure 3.6 that in the first order case for some signal-to-noise ratios, a constant $\tilde{f}(t)$ provides nearly the best possible performance, as indicated by (3.17). Note that for such values of E_r/N_o the optimum k_1T is zero. In this case the channel fading is so slow that a Rayleigh fading model s for the channel is appropriate.

Kennedy [6] has provided an approximate description of dispersion channels which is useful for interpreting the results above. He argues that there are roughly

$$N_{dp} = 1 + kT \tag{3.18}$$

degrees of freedom in $\tilde{s}(t)$, where T is the duration of $\tilde{f}(t)$ and k a reasonable measure of the bandwidth of the fading process. N_{dp} may also be thought of as the available number of independent samples of $\tilde{s}(t)$, since such samples are nearly independent if taken 1/k seconds apart. This suggests interpreting the communication system as having an N_{dp}- fold

$$\frac{-\mu_{*bc}(-.5)}{E_r/N_o}$$

1.2

1.0

.8

.6

.4

.2

$$\frac{E_r}{N_o} = 30$$

$$\frac{E_r}{N_o} = 20$$
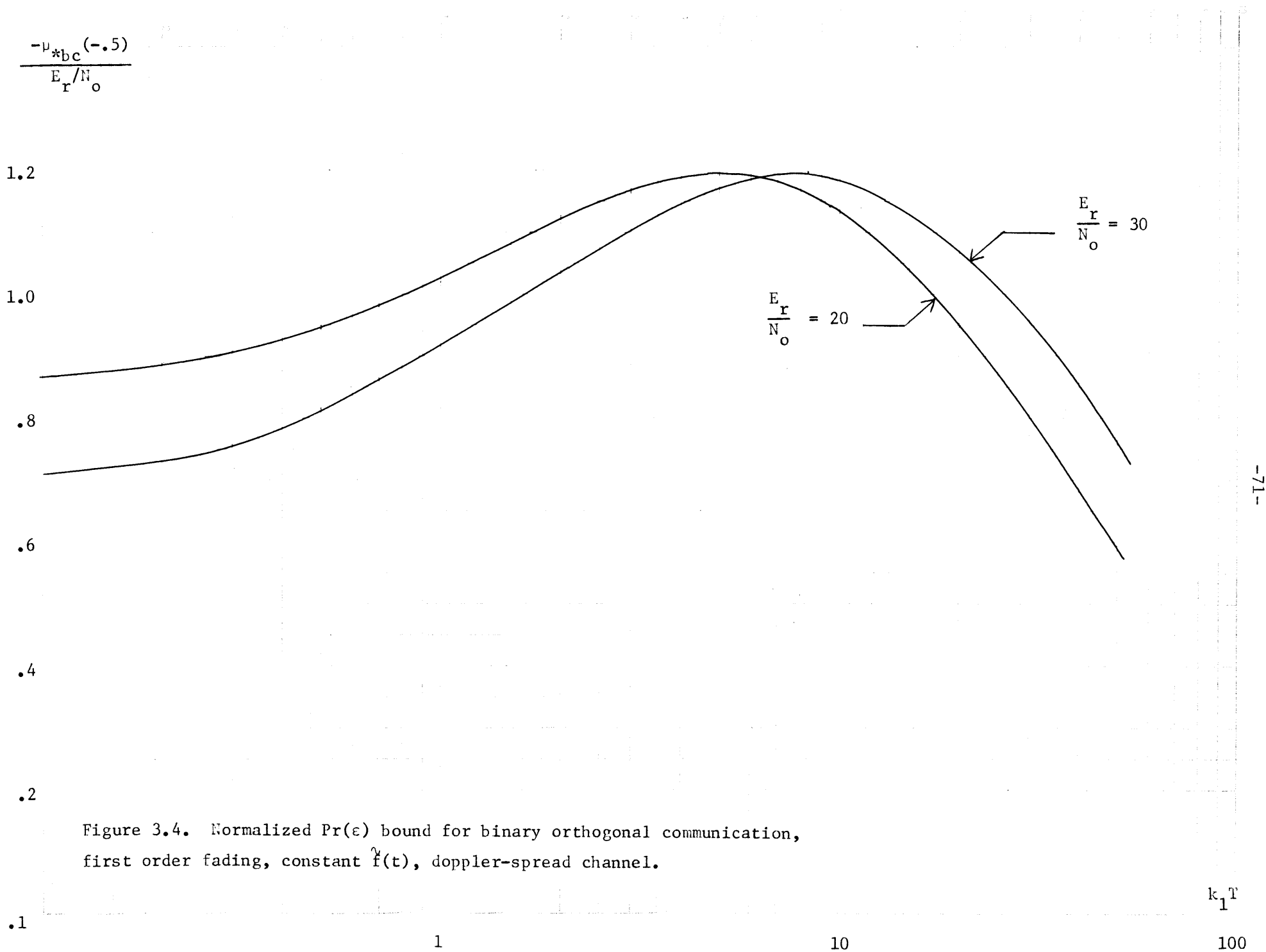
Figure 3.4. Normalized Pr(ε) bound for binary orthogonal communication, first order fading, constant $\hat{f}(t)$, doppler-spread channel.

k_1T

.1

1

10

100

$\hat{f}(t)$

$$\sqrt{\frac{E_t}{T}}$$
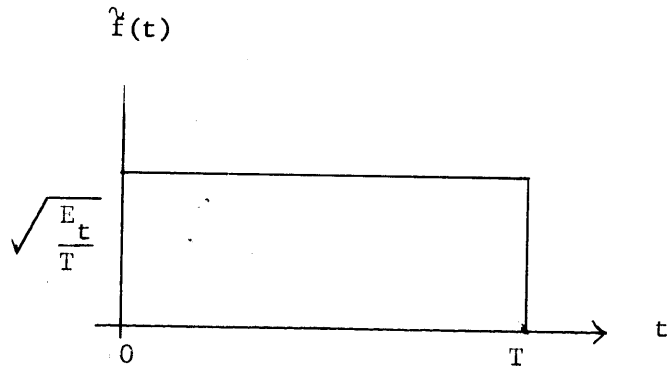
a.) Constant. E_t = signal energy

$\hat{f}(t)$

$$\sqrt{\frac{E_t}{TD}}$$

$$\frac{DT}{N}$$
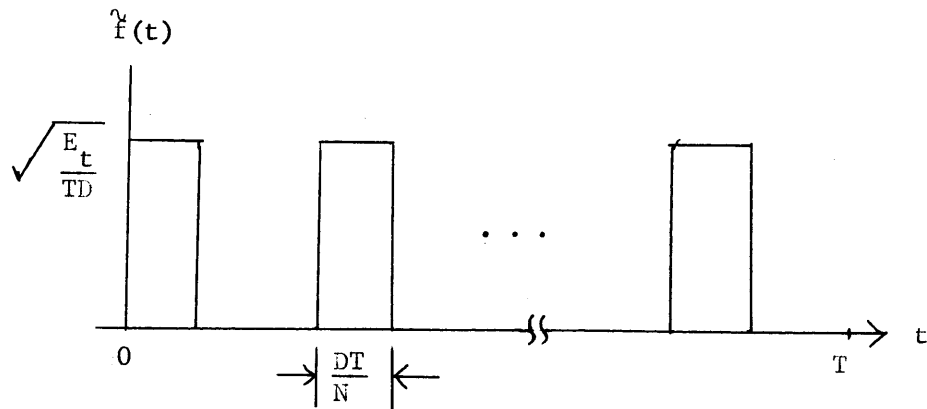
b.) Pulse train. N = number of pulses; D = duty cycle, $0 < D < 1$; E_t = signal energy.

Figure 3.5. Signals for the doppler-spread channel.
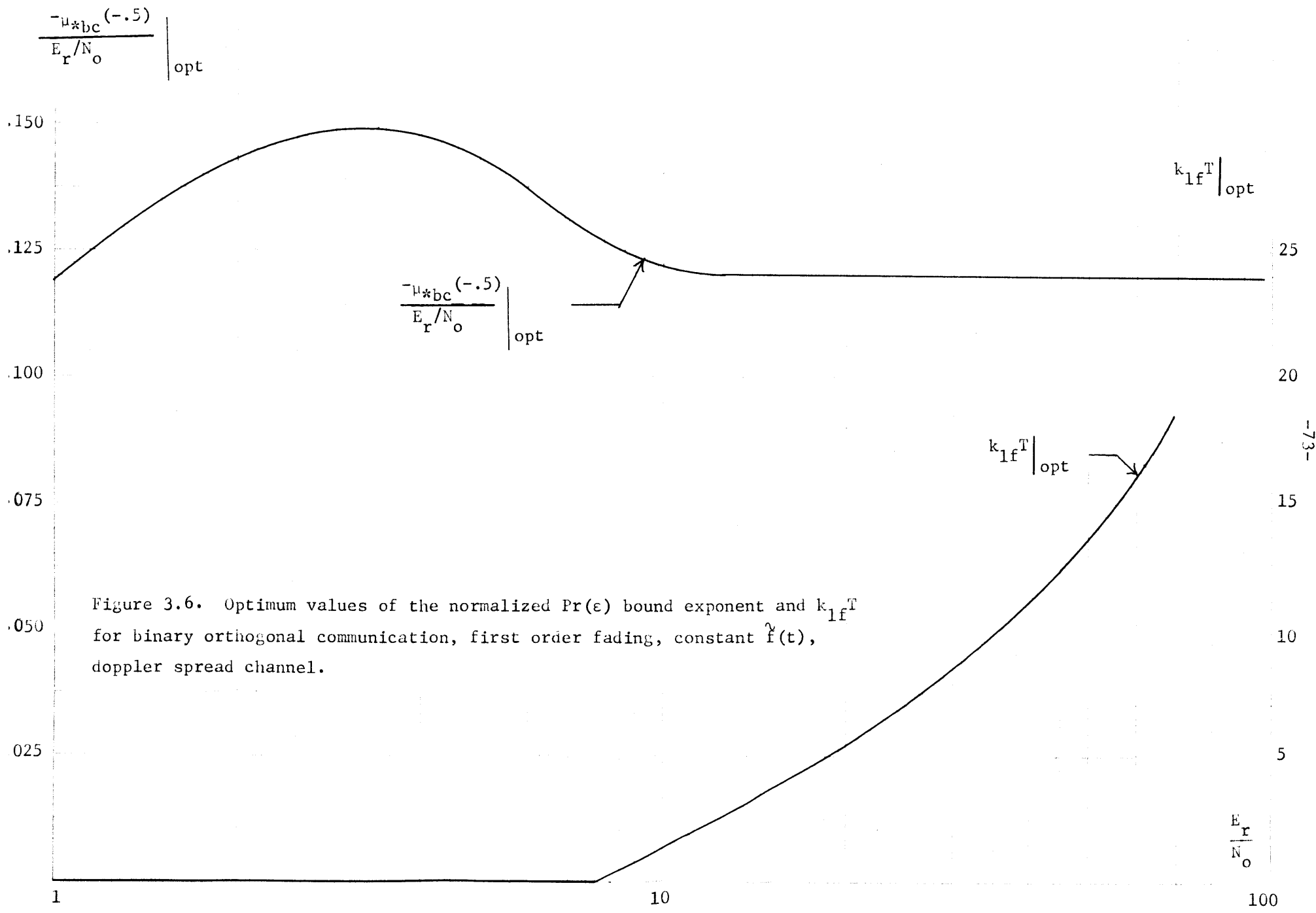
Figure 3.6. Optimum values of the normalized $Pr(\varepsilon)$ bound exponent and $k_{1f}T$ for binary orthogonal communication, first order fading, constant $\hat{f}(t)$, doppler spread channel.

"implicit" diversity.

From the results available on conventional diversity systems [28], it is reasonable to expect that there is an optimum value of N_{dp} which provides the best distribution of signal energy over the implicit diversity elements. For conventional diversity this optimization occurs for N_{dp} such that [6]

$$\left.\frac{E_r/N_o}{N_{dp}}\right|_{opt} = 3.07 \tag{3.19}$$

and provided the diversity paths have equal strength. Of course, for dispersive channels the distribution of energy is determined implicitly by $\hat{\gamma}(t)$.

For the doppler-spread channel and a constant $\hat{\gamma}(t)$, the behavior in Figures 3.4 and 3.6 is consistent with the implicit diversity interpretation, since k_1 is a measure of the fading band-width. Figure 3.4 shows performance maxima at values of $k_1 T$ consistent with (3.18). In Figure 3.6 the best value of $k_1 T$ for low E_r/N_o minimizes the implicit diversity, which agrees with (3.19). Since, in this latter case, the channel is effectively a Rayleigh fading model, the results of Figure 3.6 are in exact agreement with the optimum diversity results of Pierce.

The concept of implicit diversity suggests that when E_r/N_o and $k_1 T$ are such that the optimum number of implicit diversity elements is greater than one, the pulse train $\hat{\gamma}(t)$ of Figure 3.5b may provide a better performance. The reasoning for this expectation is that the

individual pulses divide the signal energy more evenly among the optimum

number of implicit diversity elements. Table 3.1 gives $\mu_{*bc}(-.5)$ for this

$\overset{\gamma}{f}(t)$ with first order fading. Note that the optimum number of pulses in

each example is consistent with the argument above. Also, the better

performance of the lower duty cycle cases can be attributed to a

more even distribution of signal energy over the implicit diversity

elements.

When the second-order fading model (3.13) is used, a similar

behavior is observed. If $\tilde{k}_1 = \tilde{k}_2^*$ in (3.13), the fading process is

called second order Butterworth. Figure 3.7 shows the optimum value

of $Re[\tilde{k}_1 T]$ and the corresponding $\mu_{*bc}(-.5)$ for the case of second

order Butterworth fading and a constant $\overset{\gamma}{f}(t)$. Table 3.2 shows the

values of $\mu_{*bc}(-.5)$ when $\tilde{k}_1$ and $\tilde{k}_2$ are not conjugates. Table 3.3 examines

the performance of the pulse train $\overset{\gamma}{f}(t)$ under second order Butterworth

fading conditions. These results are all consistent with the implicit

diversity ideas discussed above for first-order fading, since the

real parts of $\tilde{k}_1$ and $\tilde{k}_2$ provide a measure of the bandwidth of the

second order fading process.

The notion of implicit diversity is useful in the binary

symmetric orthogonal communication examples above because it permits

an understanding of the important parameters in the optimum reception

problem. As the following examples show, the performance of the

optimum receiver for simple binary detection can be interpreted in

the same manner. In addition, the notion of implicit diversity is

helpful in the choice and design of suboptimum communication systems

k_1T	duty cycle	number of pulses	$\dfrac{-\mu_{*bc}(-.5)}{E_r/N_o}$
5	.5	3	.1235
		4	.1251
		5	.1254
		6	.1252
	.1	3	.1288
		4	.1344
		5	.1359
		6	.1355
1	.5	2	.1036
		3	.1050
		4	.1048
		5	.1045
	.1	2	.1059
		3	.1085
		4	.1080
		5	.1070

Table 3.1. Normalized error probability bound exponent, binary
orthogonal communication, optimum receiver, pulse train
$\hat{f}(t)$, $E_r/N_o = 20$, first order fading, doppler-spread channel.

$$\frac{-\mu_{*bc}(-.5)}{E_r/N_o}\Bigg|_{opt}$$

$Re[\tilde{k}_{1f}T]_{opt}$

.150

.125

$$\frac{-\mu_{*bc}(-.5)}{E_r/N_o}\Bigg|_{opt}$$

25

.100

$Re[\tilde{k}_{1f}T]_{opt}$

20

.075

Figure 3.7. Optimum values of the normalized $Pr(\varepsilon)$ bound exponent and $Re[\tilde{k}_{1f}T]$ for binary orthogonal communication, second order Butterworth fading, constant $\tilde{f}(t)$, doppler spread channel.

.050

15

10

.025

5

1

10

$\dfrac{E_r}{N_o}$

100
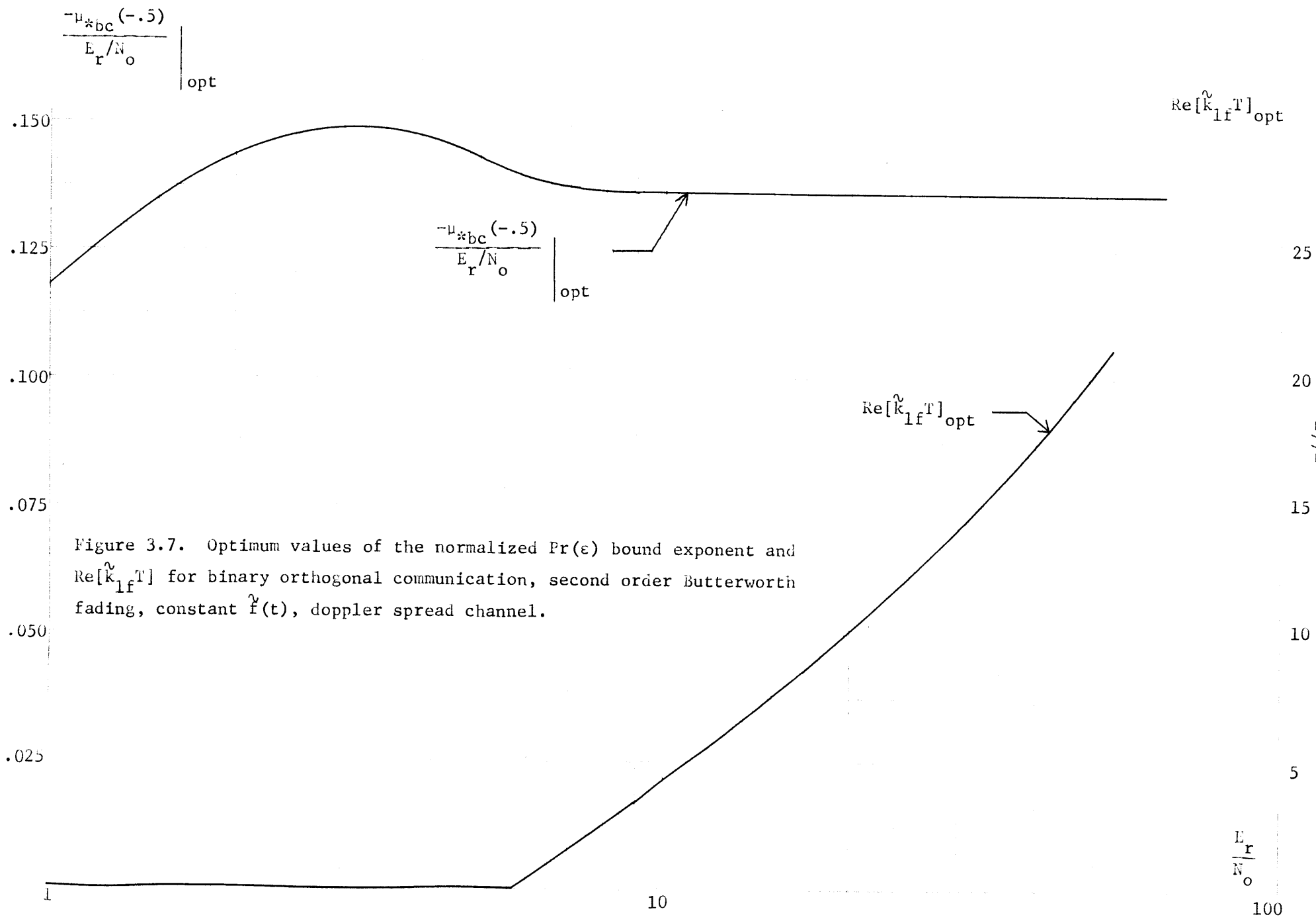
$\hat{k}_1 T$	$\hat{k}_2 T$	$\dfrac{-\mu_{*bc}(-.5)}{E_r/N_o}$
5.9 + 14.7j	3.9 − 14.7j	.1374
7.5 + 13 j	7.5 − 13 j	.1377
10.6 + 10.6j	10.6 − 10.6j	.1358
13 + 7.5j	13 − 7.5j	.1340
14.7 + 3.9j	14.7 − 3.9j	.1329
12.6 + 10.6j	8.6 − 10.6j	.1353
14.6 + 10.6j	6.6 − 10.6j	.1336
16.6 + 10.6j	4.6 − 10.6j	.1294
14.7 + 3.9j	3.9 − 14.7j	.1289

Table 3.2. Normalized error probability bound exponent, binary
orthogonal communication, optimum receiver, constant
$\hat{f}(t)$, $E_r/N_o = 20$, second order fading, doppler-spread
channel.

$\tilde{k}_1 T$	$\tilde{k}_2 T$	duty cycle	number of pulses	$-\mu_{*bc}(-.5)$
4 + 4j	4 - 4j	.5	2	.1374
			3	.1400
			4	.1386
			5	.1375
		.1	2	.1419
			3	.1445
			4	.1410
			5	.1387

Table 3.3. Normalized error probability bound exponent, binary orthogonal communication, optimum receiver, pulse train $\tilde{f}(t)$, $E_r/N_o = 10$, second order Butterworth fading, doppler-spread channel.

and detectors, which is considered in the next two sections.

C. A Filter-Squarer-Integrator Suboptimum Receiver

This section applies the results of Chapter II to the performance

analysis of a suboptimum receiver for the doppler-spread channel: the

filter-squarer-integrator structure of Figure 2.1. The equations of

section C, Chapter II are used to evaluate approximations to the error

probabilities for the simple binary detection problem (1.10) and binary

symmetric communication problem of (1.12) with $M = 2$. The signal $\tilde{s}(t)$

is assumed to have the state-variable representation of (3.9-3.10).

Stationary fading is considered exclusively, although the results of

Chapter II are valid for the non-stationary case also.

To apply the results of Chapter II it is necessary for the

filter in Figure 2.1 to have a finite state-variable representation.

Any such filter fulfills the conditions for convenient evaluation of

the error probability expressions. Of course, it is desirable to have

a FSI suboptimum receiver which performs well.

The structure of Figure 3.3, which the previous section

indicated is optimum for two special cases, provides some insight into

picking a good suboptimum FSI receiver under other conditions. Suppose

the first-order fading model of (3.12) is assumed. Then under low-

energy-coherence conditions $\tilde{G}_{opt}(j\omega)$ in Figure 3.3 is, by (3.14)

$$\tilde{G}_{opt}(j\omega) \;=\; \frac{2k_1 P}{j\omega + k_1} \qquad\qquad (3.20a)$$

This is the same filter which generates the first-order fading process

$\tilde{y}(t)$ from white noise. When $\tilde{f}(t)$ is a constant and $T \to \infty$,

$$\tilde{G}_{opt}(j\omega) = \frac{k_1 \sqrt{\dfrac{2E_r}{N_o k_1 T}}}{j\omega + k_1 \sqrt{\dfrac{2E_r}{N_o k_1 T}} + 1} \qquad (3.20b)$$

by (3.16). This has the same form as the filter of (3.20a) but with a different pole. For these two special cases, then, the filters of (3.20) used in the structure of Figure 3.3 are optimum for first order fading.

The results of the example above suggest that a potentially good suboptimum FSI receiver for the doppler-spread channel is one which multiplies $\tilde{r}(t)$ by $\tilde{f}^*(t)$, passes the result through a filter which has the same order as that which generates the fading process $\tilde{y}(t)$, and squares and integrates the filter output. Figure 3.8 shows this configuration. Equation (3.20b) also indicates that perhaps the bandwidth of the suboptimum receiver filter should be widened for increasing E_r/N_o. This procedure is consistent with (3.20a) since the low-energy-coherence condition for the doppler-spread channel is [8]

$$\frac{E_r}{N_o kT} << 1, \qquad LEC \qquad (3.21)$$

In any case, for a given $\tilde{f}(t)$ and fading model the suboptimum FSI receiver of Figure 3.8 can be optimized numerically over the parameters of the receiver filter. Further design options are replacement of the reference signal $\tilde{f}(t)$ with some other waveform, or use of a different order filter. In the numerical examples that follow, only
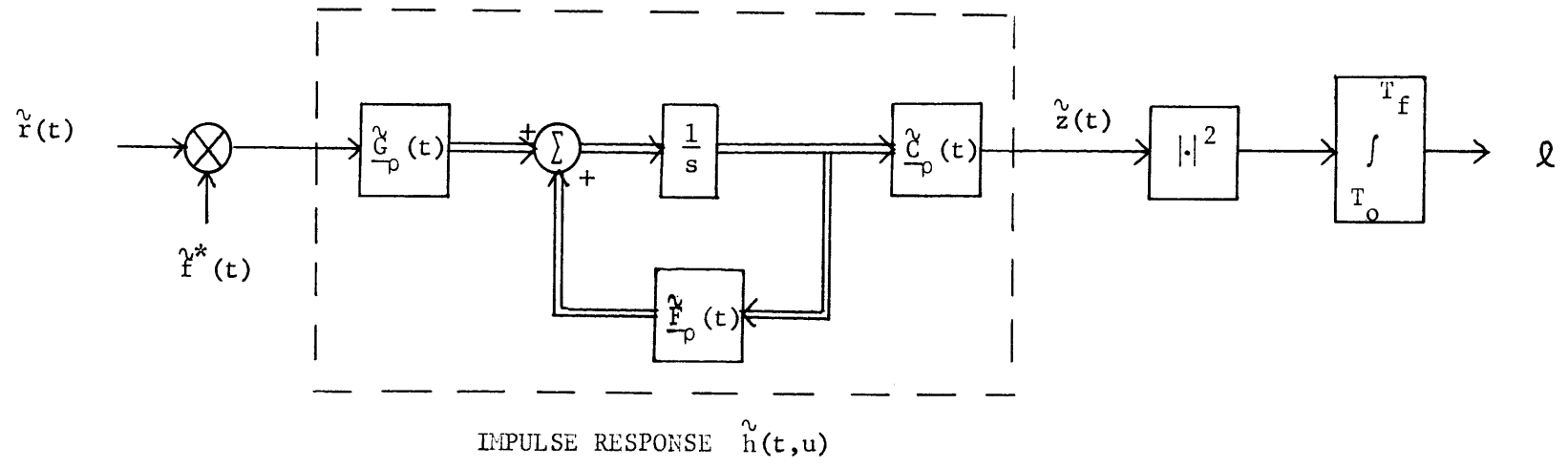
Figure 3.8. A suboptimum filter-squarer-integration receiver branch for the doppler-spread channel.

the structure shown in Figure 3.8 is considered. Note that when the fading is stationary, the filter in the FSI receiver is time-invariant; also, if $\hat{f}(t)$ is a constant, the multiplier may be replaced by a gate.

The performance of the FSI filters follows directly from the results of Chapter II. The composite state-variable model of (2.107 - 2.108) can be used with the following substitutions

$$\underline{\tilde{F}}_r(t) = \underline{\tilde{F}}_\rho(t)$$

$$\underline{\tilde{G}}_r(t) = \hat{f}^*(t) \, \underline{\tilde{G}}_\rho(t)$$

$$\underline{\tilde{C}}_r(t) = \underline{\tilde{C}}_\rho(t)$$

$$\underline{\tilde{F}}_s(t) = \underline{\tilde{F}}_f(t)$$

$$\underline{\tilde{G}}_s(t) = \underline{\tilde{G}}_f(t)$$

$$\underline{\tilde{C}}_s(t) = \hat{f}(t) \, \underline{\tilde{C}}_f(t)$$

(3.22)

where the subscripts f and ρ denote the fading generation filter and the receiver filter, respectively. The moment-generating functions for the simple binary detection problem, (2.98) and (2.99), are calculated by using the composite state variable model on each hypothesis in in (2.89 - 2.91). For binary symmetric orthogonal communication $\mu_{bc}(s)$ follows from (2.102). The probability of error expressions, (2.18), (2.32), and (2.70), and the bounds, (2.37), (2.38) and (2.74), can then be evaluated.

For the simple binary detection problem the following examples compare receiver operating-curves (ROC), which are plots of $Pr(\varepsilon|H_1)$ versus $Pr(\varepsilon|H_0)$, as the decision threshold is varied. It should be

emphasized that the probability of error expressions are approximate, since the series expressions for them have been truncated. Figure 3.9 shows the effect of truncating the series for the suboptimum FSI receiver error probabilities in a particular example. An "Nth order" approximation means that the series of (2.18), (2.32), or (2.70) has been truncated after N terms. As discussed by Collins [13], the first and second order approximations have roughly the same magnitude, as do the third and fourth, and so on; hence Figure 3.9 gives just the second and fourth order approximations. Figure 3.9 also shows the error probability bounds of (2.37) and (2.38). Note that bounds are not tight; this illustrates why it is useful to have the ability to compute the error probabilities.

In the examples which follow, the convergence exhibited by the suboptimum receiver error probabilities in Figure 3.9 was observed for the optimum receiver error probabilities as well. Furthermore, the rates of convergence of the optimum and suboptimum approximations were roughly equal in each case. This provides a justification for using the bounds of (2.37), (2.38), or (2.74) as a measure of the relative performance of several systems, when it is convenient to do so. Unless otherwise indicated, the error probabilities calculated in the following examples will be second-order approximations.

Stationary fading is considered in all of the numerical examples that follow. In each, the filter in the FSI suboptimum receiver also has a zero initial condition; that is, the matrix $\underline{P}_{or}$ in (2.106) is zero. This is convenient but not necessary. Some other value for $\underline{P}_{or}$ may improve the performance of the FSI receiver in a
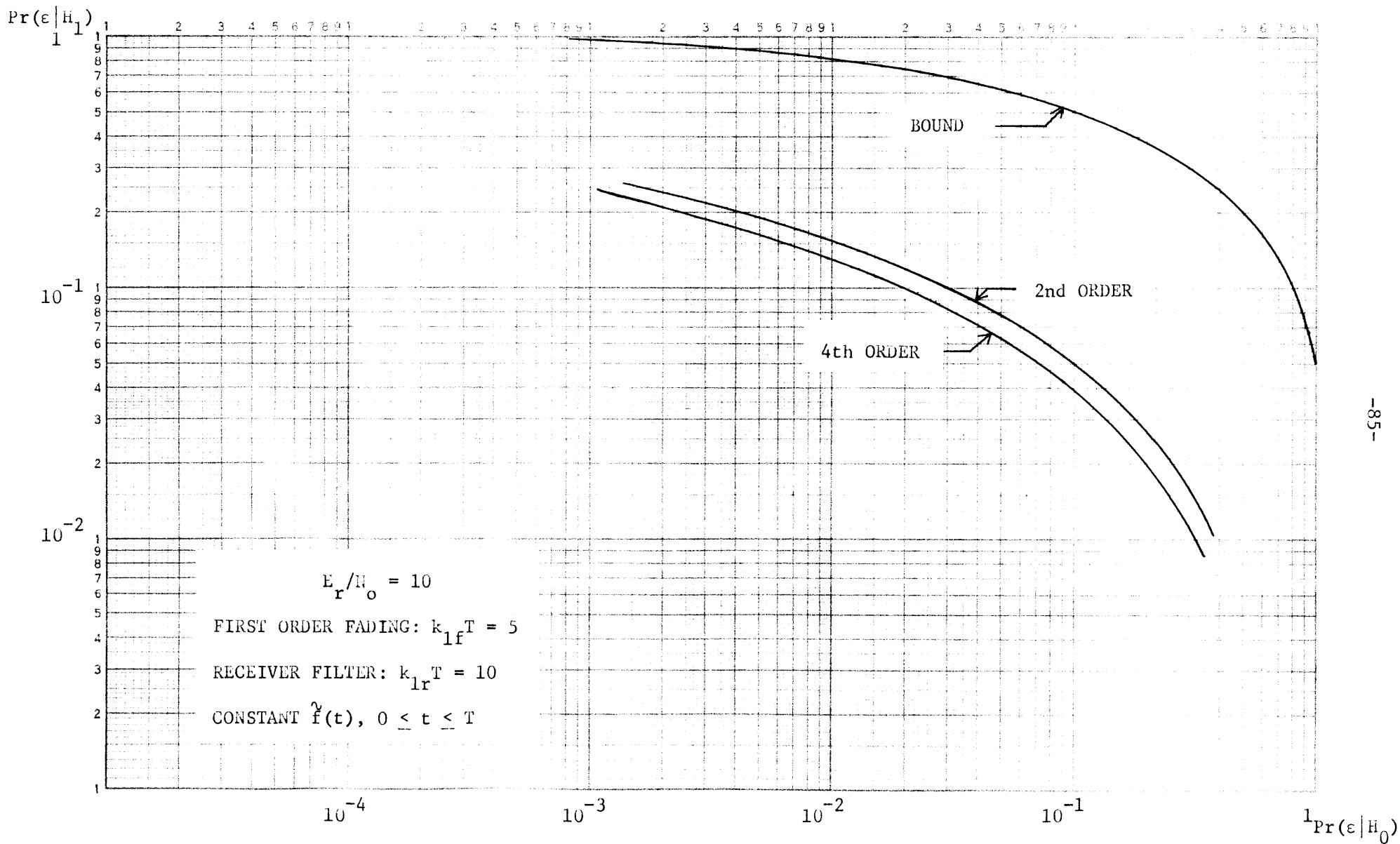
Figure 3.9. Convergence of error probability approximations, FSI suboptimum receiver, doppler-spread channel.

given example.

Figure 3.10 shows the ROC's for the case of first order fading (3.12), a constant $\hat{f}(t)$ (Figure 3.5a), and simple binary detection. The receiver filter is also first order; the poles k_{1f} and k_{1r} refer to the fading process and receiver filter, respectively. The approximate suboptimum error probabilities are shown for several different values of $k_{1r}T$; the optimum value is in approximate agreement with the indications of (3.20b). This example assumes a fading bandwidth, signal duration product, $k_{1f}T$, which is optimum (Figure 3.6).

Figure 3.10 indicates that it is possible to obtain a FSI receiver performance that is quite close to being optimum over a wide range on the ROC's. In order to compare the optimized FSI performance with the optimum receiver performance in terms of the energy difference required to obtain equal performance, it is useful to postulate that the logarithm of the error probabilities is linearly proportional to E_r/N_o. To see that this is approximately so, consider the exponents of the optimum receiver error probability bounds shown in Figure 3.6 and 3.7, which exhibit a roughly linear dependence on E_r/N_o. Under this assumption the FSI receiver performance is within several tenths of a dB of the optimum receiver performance for the example of Figure 3.10. Of course, it is possible to vary E_r/N_o in the probability of error expressions to obtain this comparison directly, but this simple estimate will be sufficient here.

Figure 3.11 compares the FSI and optimum receiver approximate error probabilities for several other first order fading parameter sets. In each case $\hat{f}(t)$ is a constant, and the value of $k_{1r}T$ has been

Figure 3.10. Approximate error probabilities for simple binary detection, first order fading, constant f(t), FSI and optimum receivers, doppler-spread channel.

Pr($\varepsilon|h_1$)

FSI SUBOPTIMUM

RECEIVER B, $k_{1r}T = 10$

OPTIMUM

RECEIVER B

FSI SUBOPTIMUM

RECEIVER A, $k_{1r}T = 10$

OPTIMUM

RECEIVER A

A: $E_r/N_o = 30$

FADING: $k_{1f}T = 1$

B: $E_r/N_o = 10$

FADING: $k_{1f}T = 2$

SECOND ORDER APPROXIMATIONS

10^{-1}

10^{-2}

10^{-4} 10^{-3} 10^{-2} 10^{-1}

Pr($\varepsilon|h_0$)

Figure 3.11. Approximate error probabilities for simple binary detection, first order fading, constant $\overset{\gamma}{f}(t)$, FSI and optimum receivers, doppler-spread channel.

varied to give the best FSI receiver performance. Again the suboptimum

performance is close to that of the optimum receiver.

Figures 3.12 and 3.13 show the optimum and FSI suboptimum

ROC's for first order fading and the pulse train $\hat{f}(t)$ of Figure 3.5b.

Again the suboptimum receiver filter has been roughly optimized. Figures

3.14 and 3.15 give similar plots for the second order fading model of

(3.13). Figure 3.14 assumes Butterworth fading and a constant $\hat{f}(t)$;

Figure 3.15 is an example in which the poles of the fading process are

not conjugates. Figures 3.12-.15 also indicate that it is possible to

obtain good performance with the FSI receiver of 3.8, provided that

the filter in the receiver is properly chosen.

For the binary symmetric communication problem, Table 3.4

compares the performance of the optimum receiver and suboptimum FSI

receiver for a variety of signal and fading parameters. In each case

the receiver parameters are chosen to approximately optimize receiver

performance. Given are the normalized exponents in the $\Pr(\epsilon)$ bounds,

as well as the fourth order approximations to $\Pr(\epsilon)$. Note that the

bound exponents are good indicators of relative performance. Again the

performance of the optimized FSI receiver is close to that of the

optimum receiver.

For orthogonal communication when M is greater than two, the

results above and the bound of (2.59) provide an indication of the

suboptimum FSI receiver performance. The exponent in (2.59) for

rates less than R_{crit} is proportional to R as shown by (2.66). The

zero rate exponent, given by (2.66) with R = 0, is just $\mu_{bc}(s)$ of (2.69)
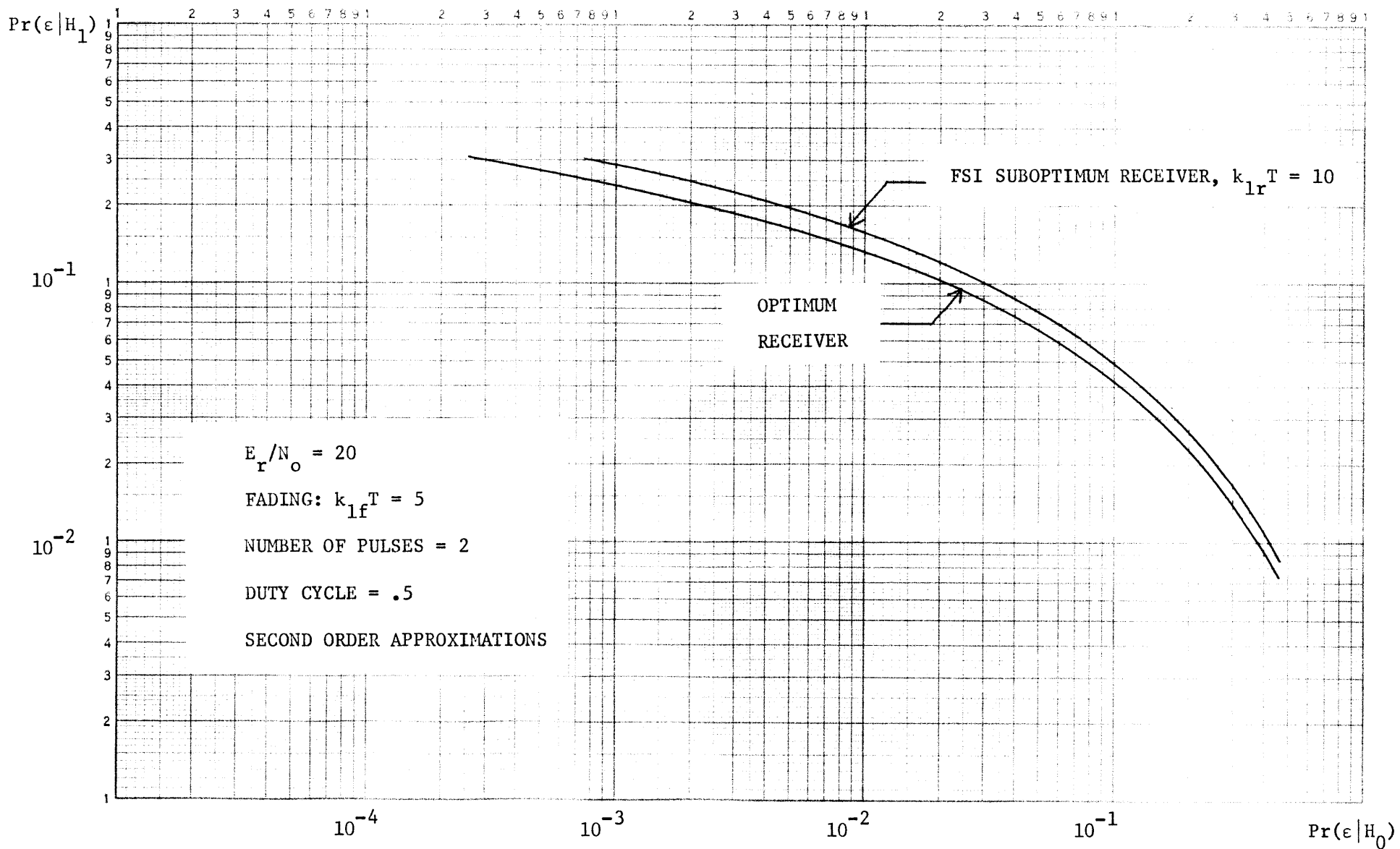
Figure 3.12. Approximate error probabilities for simple binary detection, first order fading, pulse train f(t), FSI and optimum receiver, doppler-spread channel.
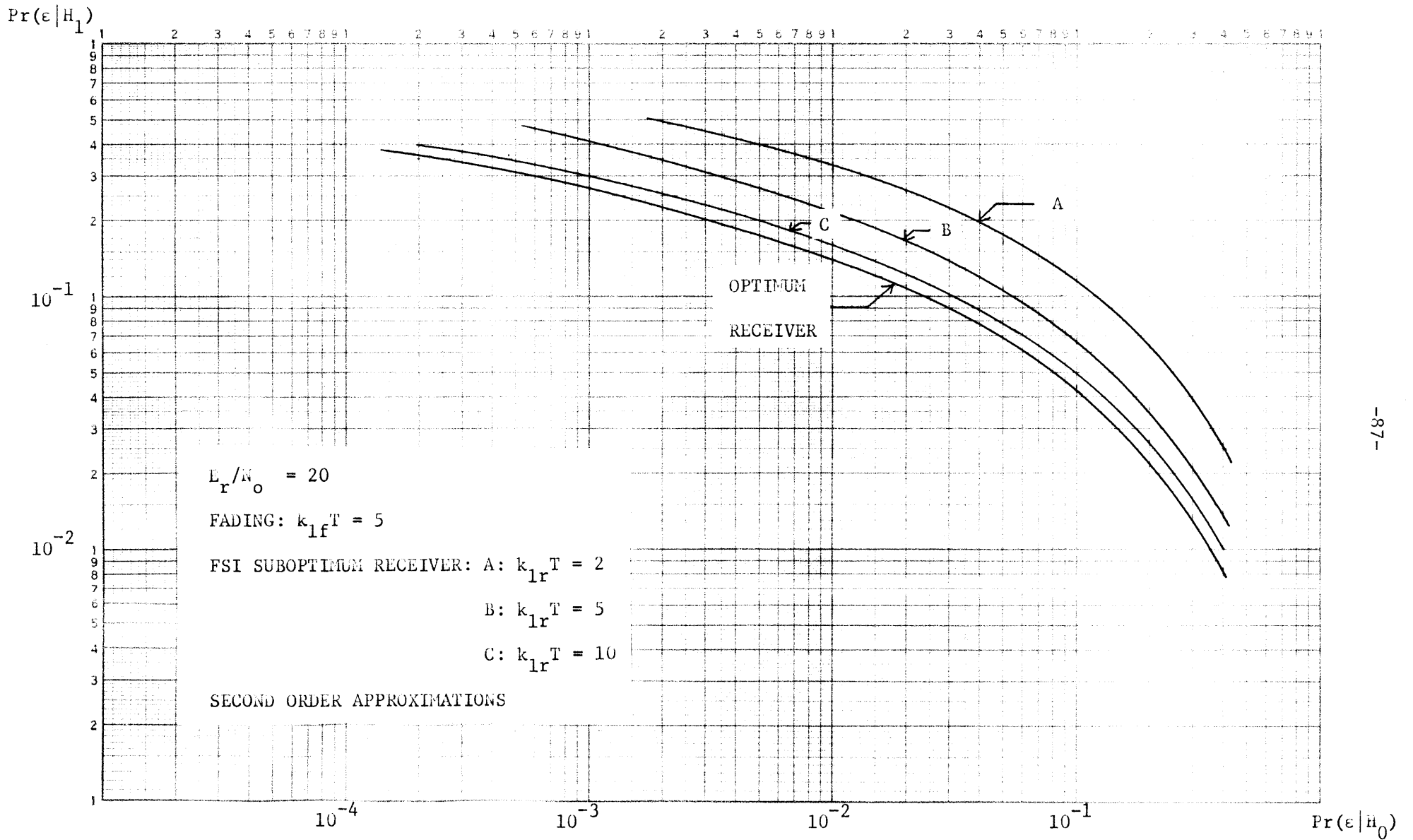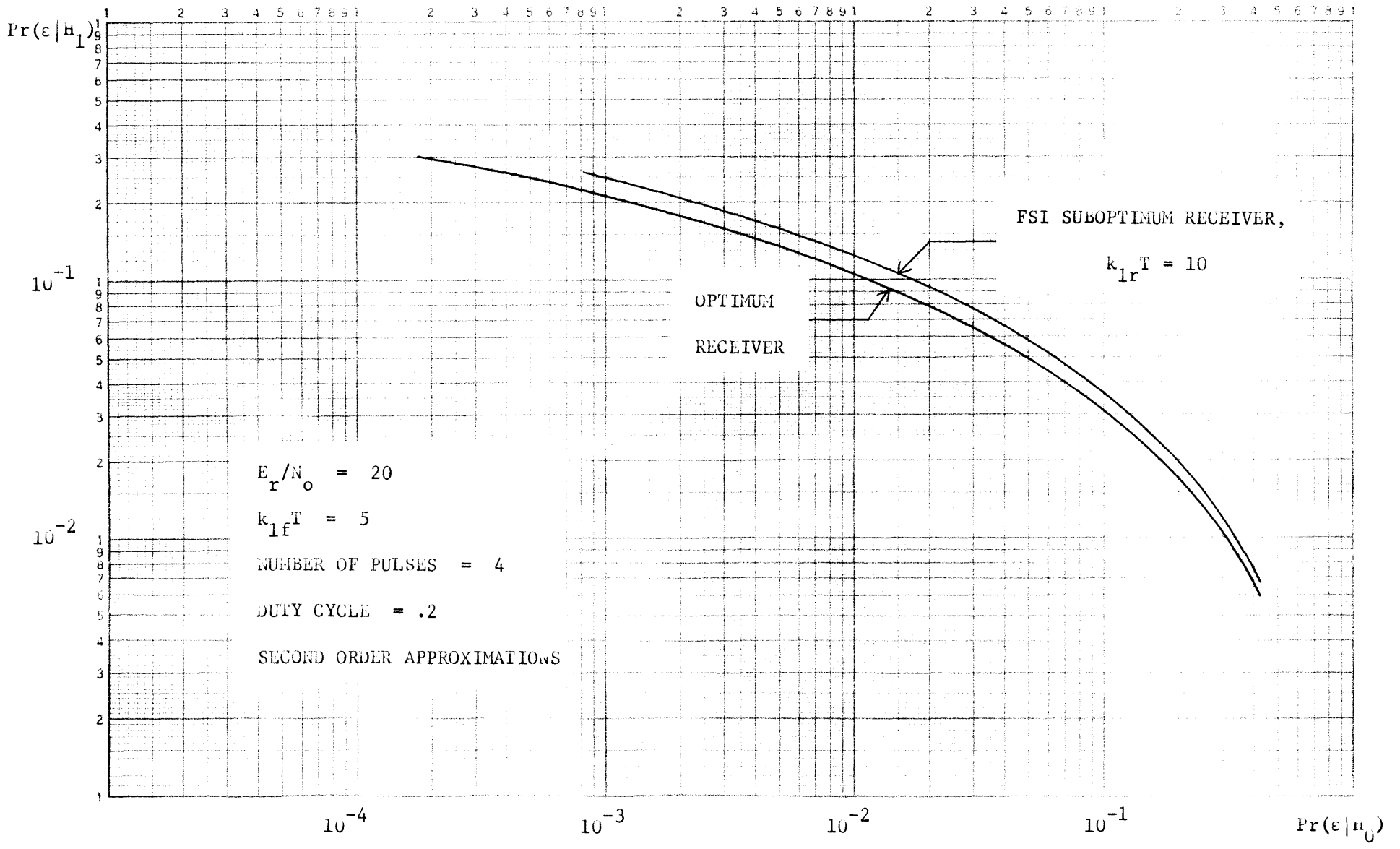
Figure 3.13. Approximate error probabilities for simple binary detection, first order fading, constant $\hat{f}(t)$, FSI and optimum receivers, doppler-spread channel.

FSI SUBOPTIMUM
RECEIVER

OPTIMUM

RECEIVER

$E_r/N_o = 10$

FADING : $k_{1f}T = 4 + 4j$, $k_{2f}T = 4 - 4j$

FSI RECEIVER: $k_{1r}T = 8 + 8j$, $k_{2r}T = 8 - 8j$

SECOND ORDER APPROXIMATIONS

10^{-4} 10^{-3} 10^{-2} 10^{-1} Pr($\epsilon|n_0$)
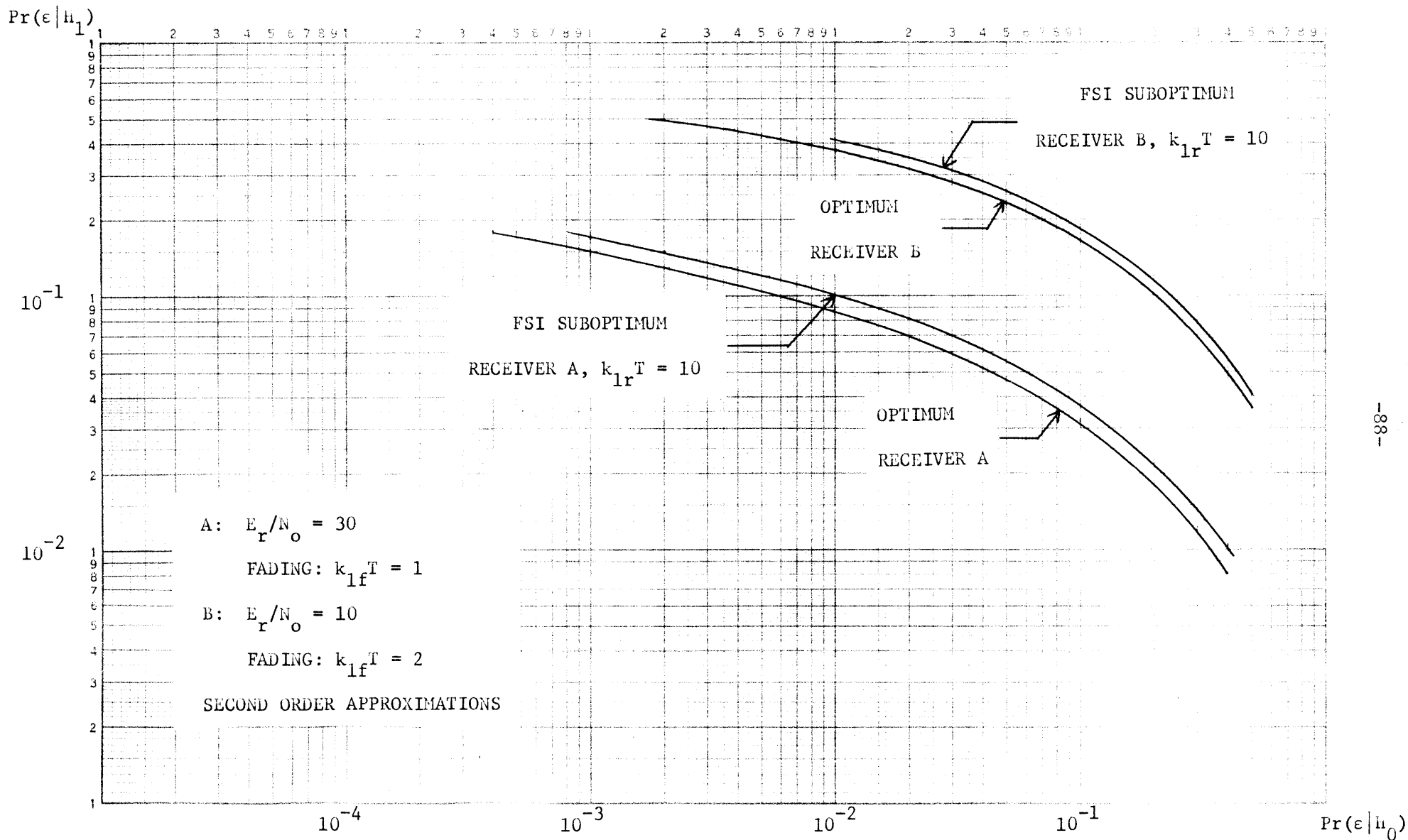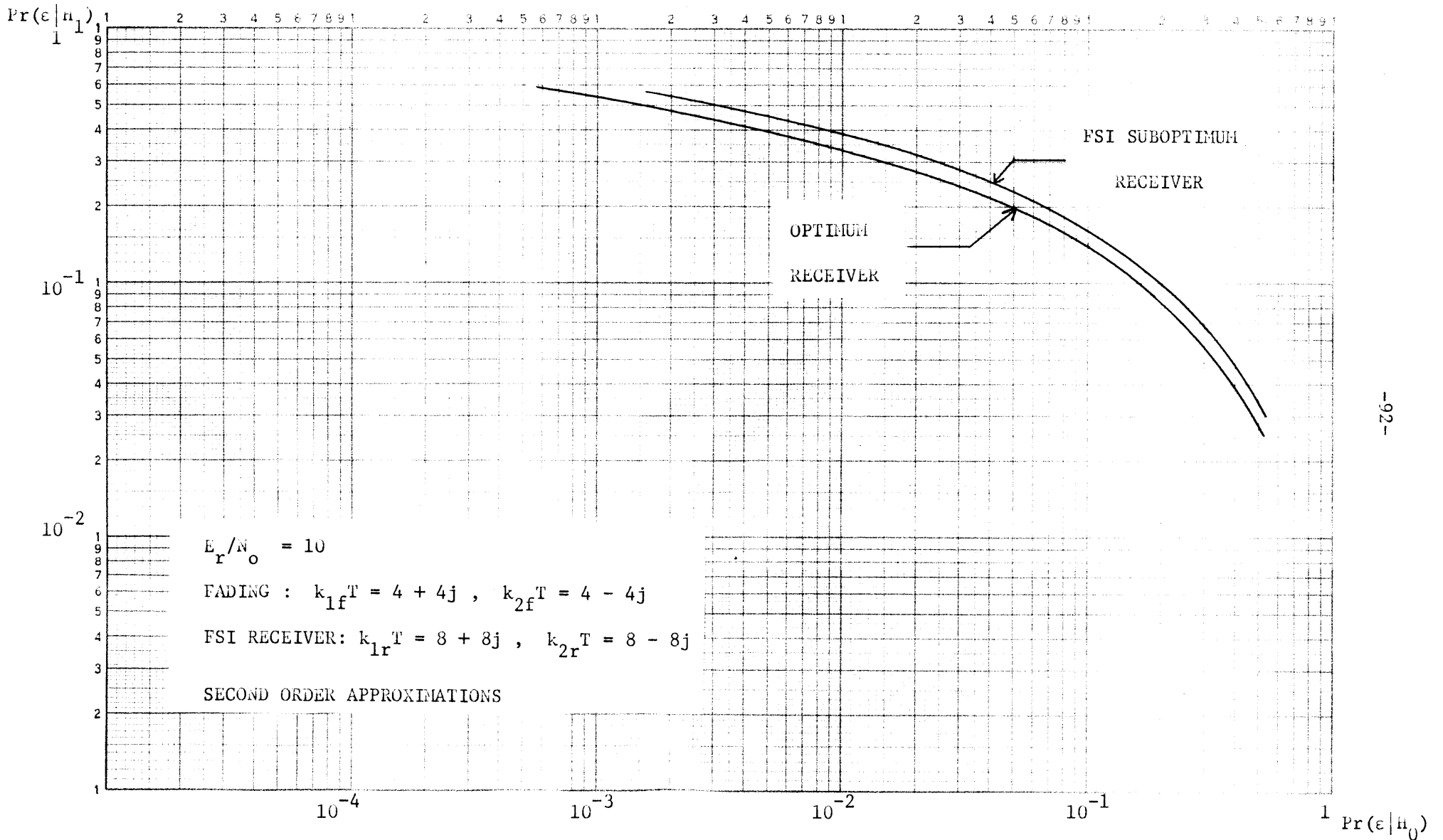
Figure 3.14. Approximate error probabilities for simple binary detection, second order Butterworth fading, constant $\hat{f}(t)$, FSI and optimum receiver, doppler spread channel.
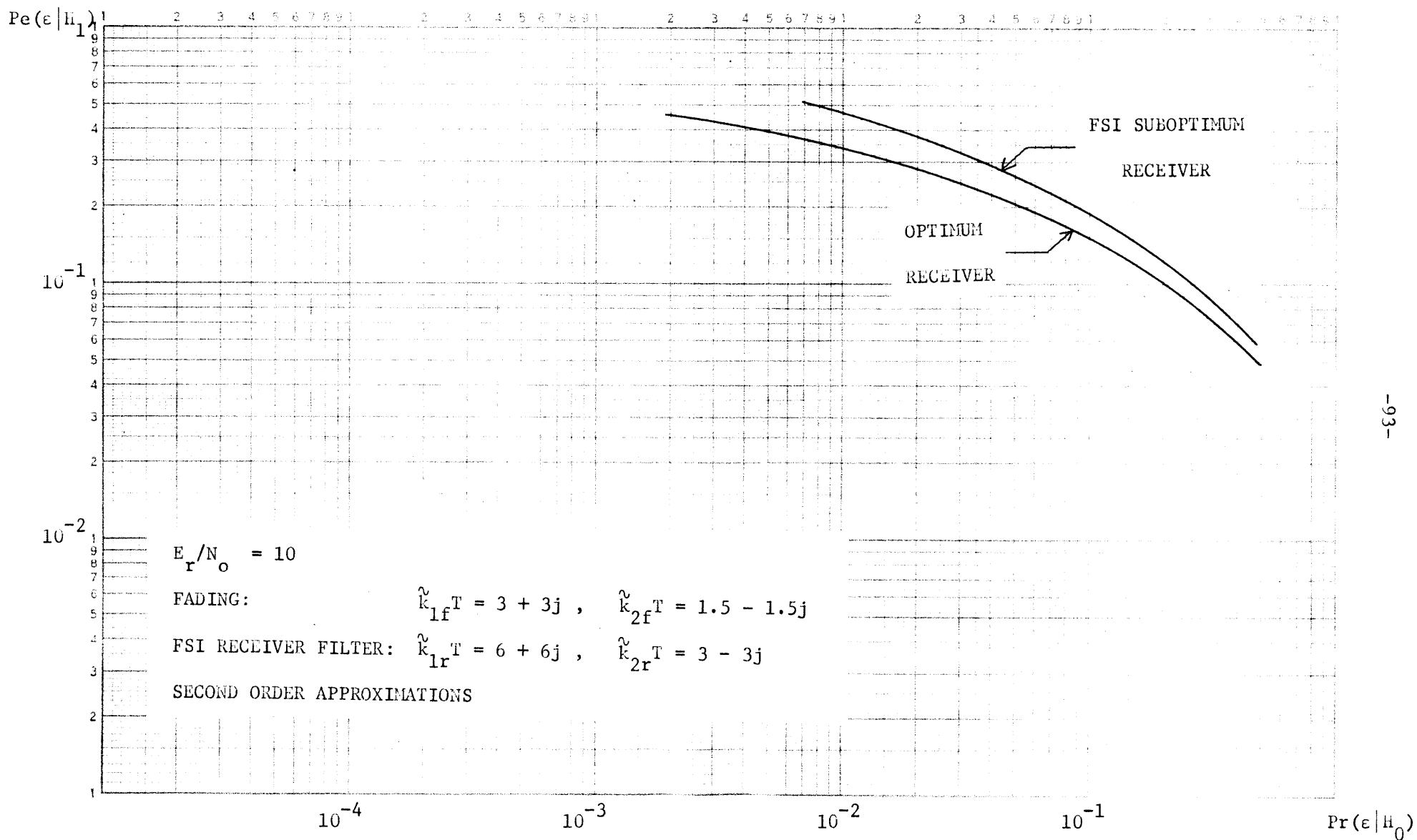
Figure 3.15. Approximate error probabilities for simple binary detection, second order fading, constant $\overset{\gamma}{f}(t)$.

The figure contains the following labels and annotations:

- Vertical axis: $Pe(\epsilon|H_1)$
- Horizontal axis: $Pr(\epsilon|H_0)$
- FSI SUBOPTIMUM RECEIVER
- OPTIMUM RECEIVER
- $E_r/N_o = 10$
- FADING: $\tilde{k}_{1f}T = 3 + 3j$, $\tilde{k}_{2f}T = 1.5 - 1.5j$
- FSI RECEIVER FILTER: $\tilde{k}_{1r}T = 6 + 6j$, $\tilde{k}_{2r}T = 3 - 3j$
- SECOND ORDER APPROXIMATIONS

E_r/N_o	$k_{1f}T$	signal	OPTIMUM		$k_{1r}T$	SUBOPTIMUM FSI	
			$\dfrac{-\mu_{*bc}(-.5)}{E_r/N_o}$	$\dfrac{-\ln Pr(\epsilon)}{E_r/N_o}$ (4th order)		$\dfrac{-\mu_{bc}(s)}{E_r/N_o}$	$\dfrac{-\ln Pr(\epsilon)}{E_r/N_o}$ (4th order)
30	1	constant	.092	.155	10	.087	.148
20	5	constant	.119	.217	10	.113	.209
10	2	constant	.121	.285	10	.116	.277
20	5	2 pulses duty = .5 cycle	.120	.216	10	.115	.201
20	5	4 pulses duty = .1 cycle	.131	.229	10	.130	.219
10	4 + 4j 4 − 4j	constant	.136	.366	8 + 8j 8 − 8j	.123	.288
10	3 + 3j 1.5 − 1.5j	constant	.130	.293	6 + 6j 3 − 3j	.110	.275

Table 3.4. Binary orthogonal communication, optimum and suboptimum receiver fourth order approximations to error probabilities, doppler-spread channel.

normalized by E_r/N_o. For low rates, then, an M-ary communication
system using a suboptimum FSI receiver can be made to perform nearly
as well as the optimum receiver, provided the FSI filter is optimized
as in the binary communication examples above. Comparison of the
optimum and suboptimum M-ary error bounds for higher rates can be
carried out as indicated in Chapter II, but this has not been done here.

For both the **simple** binary detection problem and the binary
symmetric communication problem, the examples above show that a
properly designed suboptimum filter-squarer-integrator receiver will
achieve close to the optimum performance over a doppler-spread channel.
In these cases it is possible to obtain a FSI performance within 1 dB
in E_r/N_o of the optimum, for a wide range of fading parameters and
for several signals. It should be pointed out that the techniques used
can be applied to other signals and higher order fading spectra as
well.

The examples presented in this section provide a rule of
thumb for selecting a good filter in the FSI receiver: choose a filter
bandwidth which is larger than the fading spectrum bandwidth, k, by
a factor of roughly $\sqrt{1 + E_r/N_o kT}$, where T is the signal interval.
Of course, in any particular case the filter optimization can be done
numerically. Figure 3.16 shows the effect of varying the FSI filter
bandwidth in an example. Note that the performance maximum is broad.
Thus the choice of the filter by the criterion above is likely to be a
satisfactory one in most cases.

$-\mu_{bc}(s)$

$\dfrac{}{E_r/N_o}$

.150 $\Big|_{max}$

.100

.050

$\mu_{*bc}(-.5)$, OPTIMUM RECEIVER

$E_r/N_o = 10$

FADING: $k_{1f}T = 2$

RECEIVER FILTER POLE $= k_{1r}$

0   2   4   6   8   10   12   14   16

$k_{1r}T$
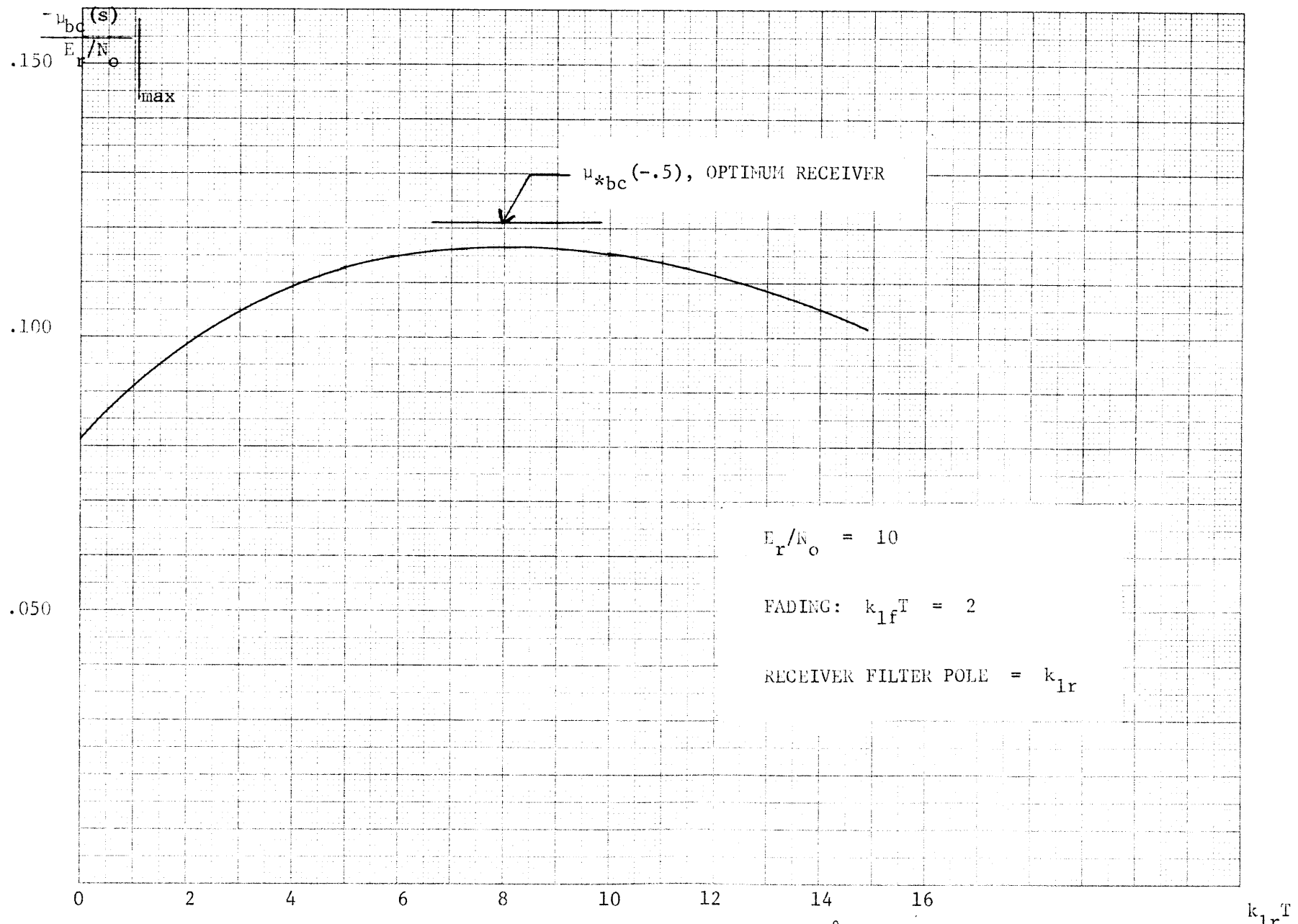
Figure 3.16. Optimization of the FSI suboptimum receiver, constant $\hat{f}(t)$, first order fading, binary orthogonal communication, doppler-spread channel.

D.   A Correlator-Squarer-Sum Suboptimum Receiver

This section considers another class of suboptimum receivers

for the doppler-spread channel detection and communication problems

of Chapter I. The branch structure of the receiver consists of a

bank of correlators followed by square-law devices whose outputs

are weighted and summed to form the decision statistic. This receiver

is called a correlator-squarer-sum (CSS) receiver. Its performance is

analyzed for the doppler-spread channel and compared with that of

the optimum and FSI suboptimum receivers of the previous sections.

There are many ways to choose the reference signals and

correlation intervals for the CSS receiver. The diversity discussion

in Section B of the present chapter suggests one such choice. If

k is the bandwidth of the fading process $\tilde{y}(t)$ in (3.2), then samples

of $\tilde{y}(t)$ taken 1/k seconds apart are approximately uncorrelated. That

is, $\tilde{y}(t)$ is significantly correlated only over time intervals approx-

imately 1/k seconds long. From the model of (3.2) the same statement

can be made about $\tilde{s}(t)$: the correlation between samples of $\tilde{s}(t)$ 1/k

seconds apart is small.

This relation suggests the approximate staircase model for

$\tilde{y}(t)$ shown in Figure 3.17. Here the value of $\tilde{y}_a(t)$ in each segment is

assumed to be a zero-mean complex Gaussian random variable with a

variance equal to $E[\tilde{y}(t_i)\tilde{y}^*(t_i)]$, where t_i is some time between

$(i-1)\tau$ and $i\tau$. The random amplitudes of $\tilde{y}_a(t)$ in different intervals

are assumed to be independent. This staircase approximation to $\tilde{y}(t)$

is, of course, not exact.
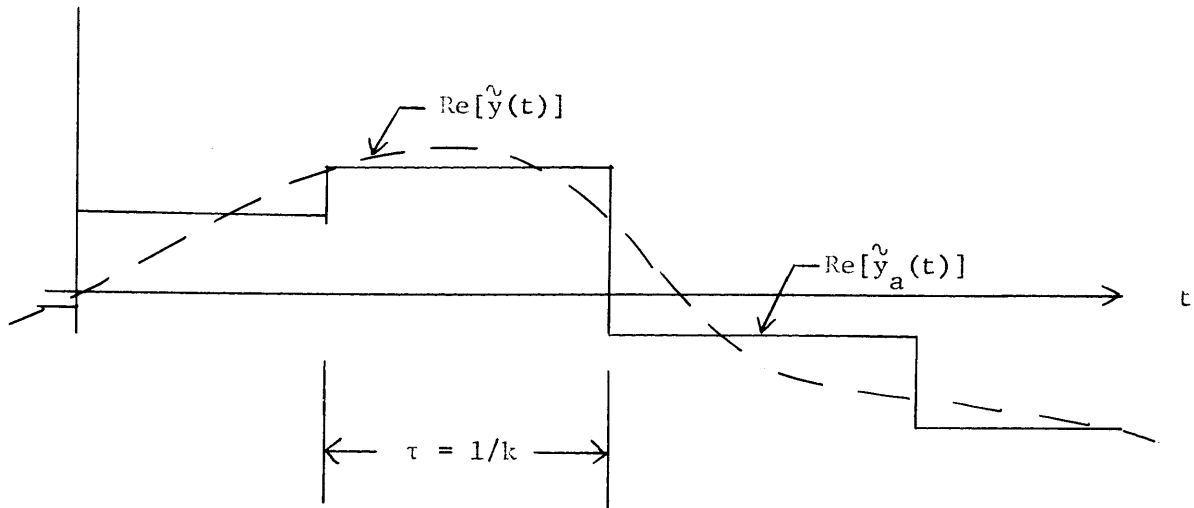
Figure 3.17. A random staircase approximation to the fading process $\tilde{y}(t)$.

The approximation for the fading process $\tilde{y}(t)$ shown in Figure 3.17 suggests the question: if the channel fading were really represented by the model of $\tilde{y}_a(t)$, what would the optimum receiver be for the problem of (3.2)? The answer can be found by realizing that in this hypothetical problem the channel output consists of a signal $\tilde{f}(t)$ multiplied by the staircase $\tilde{y}_a(t)$. This corresponds exactly to a time diversity system in which the segment of $\tilde{f}(t)$ between $(i-1)\tau$ and $i\tau$ is transmitted over a bandpass Rayleigh channel [8,20]. The fading from interval to interval is independent.

The optimum receiver for this diversity model consists of a gate which feeds $\tilde{r}(t)$ to one of N correlators or matched filters [8.20]. Each filter is matched to the appropriate segment of $\tilde{f}(t)$. The filter outputs are sampled, squared, weighted by the expected value of the energy in $\tilde{s}(t)$ during the appropriate interval, and summed. Figure 3.18 gives a block diagram of this receiver; Figure 3.19 shows a simpler realization of the same structure using a τ second correlator.

The correlator-squarer-sum receiver has been derived by assuming the independent, slowly-fading staircase approximation to $\tilde{y}(t)$. It can still be used with the original model for the fading process, in which case it is a suboptimum receiver.

When the transmitted signal $\tilde{f}(t)$ is a constant (Figure 3.5a), the CSS receiver in Figure 3.19 assumes a particularly simple form. The signal $\tilde{r}(t)$ is passed into a τ second integrator. The integrator output is sampled at the times $i\tau$, $i = 1, \ldots, N,$. A weighted sum of the squared samples gives the decision statistic.
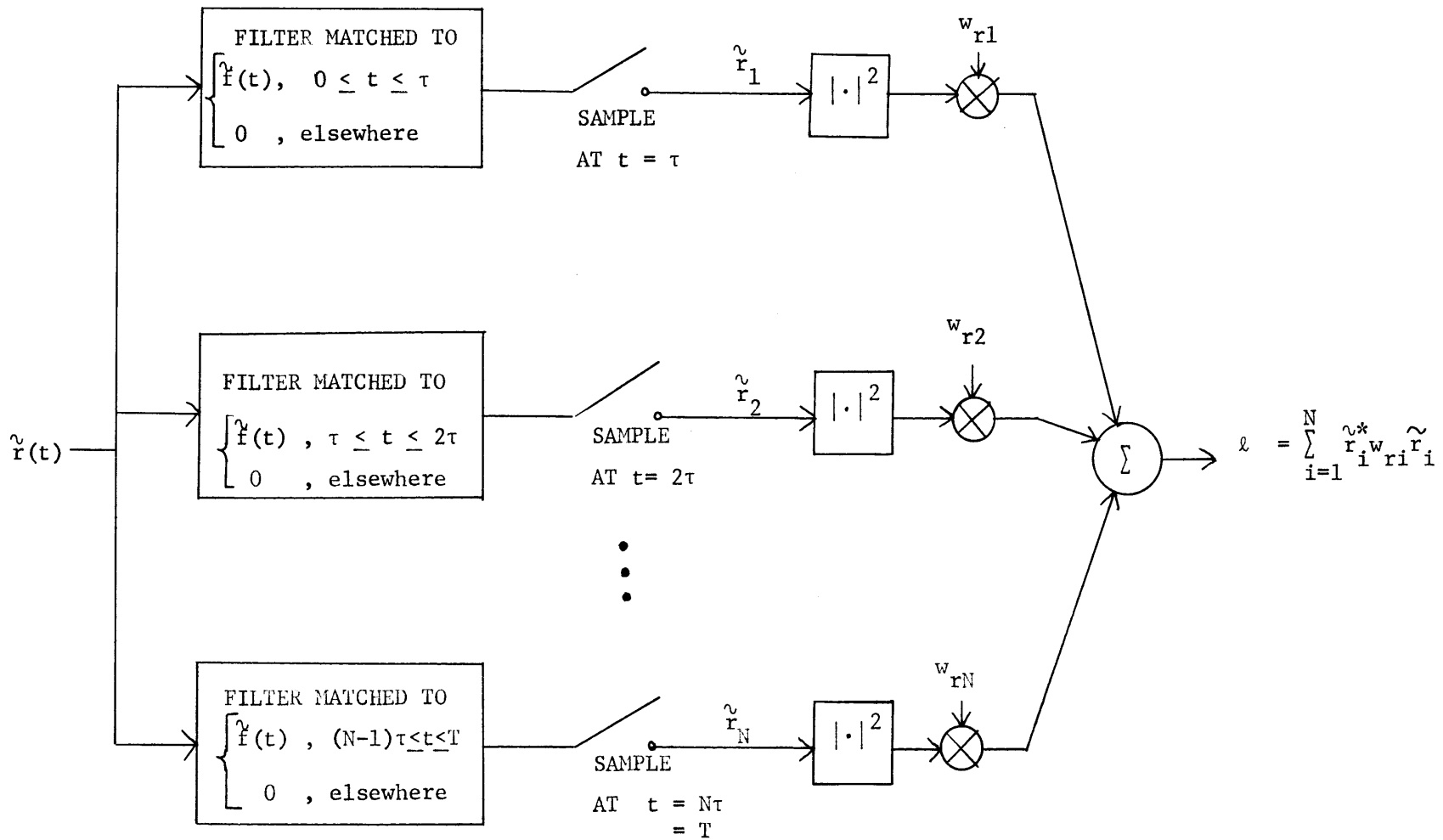
Figure 3.18. Complex version of the conductor-squarer-sum suboptimum receiver, matched filter realization.
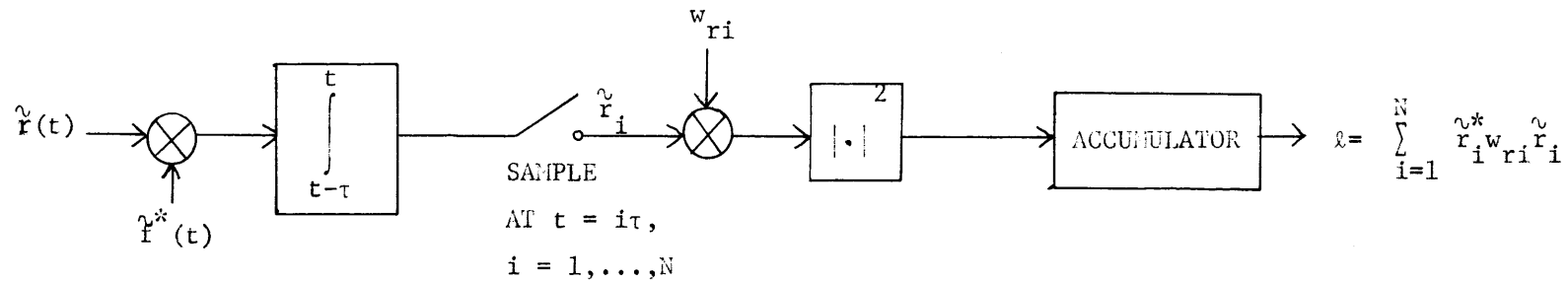
Figure 3.19. Complex version of correlator-squarer-sum suboptimum receiver, gated correlator realization.

Another motivation for using the CSS suboptimum receiver of
Figure 3.18 is provided by considering the case when the correlation
time of the fading, $1/k$, is much larger than the signal duration T.
Then the doppler-spread channel model reduces to that of a known signal
$\overset{\curvearrowright}{f}(t)$ transmitted over a slowly fading Rayleigh channel. By the
argument above the CSS receiver of Figure 3.18 is optimum for this
case, if $N = 1$.

There are several levels of optimization possible for the
CSS receiver of Figures 3.18 and 3.19:

(i). If the weights W_{ri} are chosen in accordance with the
discussion above as

$$W_{ri} = \int_{(i-1)\tau}^{i\tau} \overset{\curvearrowright}{K}_s(t,t)dt$$

$$= \int_{(i-1)\tau}^{i\tau} |\overset{\curvearrowright}{f}(t)|^2 \overset{\curvearrowright}{K}_y(t,t)dt \ , \quad i=1,\ldots N \qquad (3.23)$$

then the number of correlators $N = T/\tau$ is a design
variable. Note that, if $\overset{\curvearrowright}{f}(t)$ is constant and the
fading is stationary, the W_{ri} are equal.

(ii). Both the weights, W_{ri}, and the number of correlations
can be varied. This is a more complicated optimization
problem.

The performance of the CSS receiver for the detection and
communication problems of Chapter I with the doppler-spread channel
model of this chapter can be found by a direct application of the
results of Chapter II. The decision statistic of the CSS receiver in

Figure 3.18 is a finite, weighted sum of squared complex Gaussian random variables. Hence the equations of Chapter II, Section E can be used to find the semi-invariant moment-generating functions required to evaluate error probability expressions and bounds. The following relations enable direct use of the equations of Chapter II, Section E. The vector $\underset{\sim}{\underline{R}}$ in (2.110) has components $\tilde{r}_i$, shown in Figure 3.18. The weighting matrix $\underset{\sim}{W}$ of (2.111) is real and diagonal with elements

$$\tilde{W}_{ij} = W_{ri}\delta_{ij} \tag{3.24}$$

The elements of the N dimensional covariance matrices of (2.113) and (2.114) are

$$\Lambda_{nij} = \int_{(i-1)\tau}^{i\tau} \int_{(j-1)\tau}^{j\tau} \tilde{f}^*(t)\tilde{f}(u) \, E[\tilde{r}(t)\tilde{r}^*(u)| \text{ noise}] \, dtdu$$

$$= N_o \, \delta_{ij} \int_{(i-1)\tau}^{i\tau} |f(t)|^2 dt \tag{3.25}$$

and

$$\Lambda_{sij} = \int_{(i-1)\tau}^{i\tau} \int_{(j-1)\tau}^{j\tau} \tilde{f}^*(t)\tilde{f}^*(u) \, E[\tilde{r}(t)\tilde{r}^*(u)| \text{ signal + noise}] dtdu$$

$$= \int_{(i-1)\tau}^{i\tau} \int_{(j-1)\tau}^{j\tau} |\tilde{f}(t)|^2|\tilde{f}(u)|^2 \, \tilde{K}_y(t,u) dtdu + \Lambda_{nij}$$

$$\tag{3.26}$$

The moment generating functions $\mu_0(s)$ and $\mu_1(s)$ of (2.118) and (2.119) follow directly.

The expressions given above indicate that it is not necessary in this case to have processes which can be represented by state-variable models. Only the integrals in (3.25) and (3.26) need to be evaluated, and they require only knowledge of the covariance function $\overset{\nu}{K}_{y}(t,u)$. Of course, evaluation of the integrals in a given problem may not be easy.

The performance of the CSS receiver can now be compared with that of the optimum and FSI suboptimum receivers. The binary symmetric communication problem is considered here, since computation of the exponents in the error probability bounds, $\mu_{bc}(s)$ and $\mu_{*bc}(-.5)$, provides an accurate comparison of relative performance. The transmitted signal $\overset{\nu}{f}(t)$ is the constant envelope waveform shown in Figure 3.5a. The fading is first order and stationary, as specified by (3.12). The covariance function $\overset{\nu}{K}_{y}(t,u)$ is

$$\overset{\nu}{K}_{y}(t,u) \;=\; P\, e^{-k_1|t-u|} \tag{3.27}$$

The covariance matrices $\underline{\Lambda}_s$ and $\underline{\Lambda}_n$ follow easily from (3.25-.26). The weights W_{ri} in (3.23) are equal for this case. The simplified CSS receiver shown in Figure 3.19 is appropriate in this example. The number of integrator samples N is variable.

Figures 3.20 and 3.21 contrast the performance of the optimum, FSI, and CSS receivers for this example. Plotted in each case are the normalized exponents in the error probability bounds versus $k_1 T$: $\mu_{*bc}(-.5)$ for the optimum receiver, and the minimum value of the appropriate $\mu_{bc}(s)$ for the suboptimum receivers. Figure 3.20 shows the performance comparison for $E_r/N_o = 5$, Figure 3.21 for $E_r/N_o = 20$.
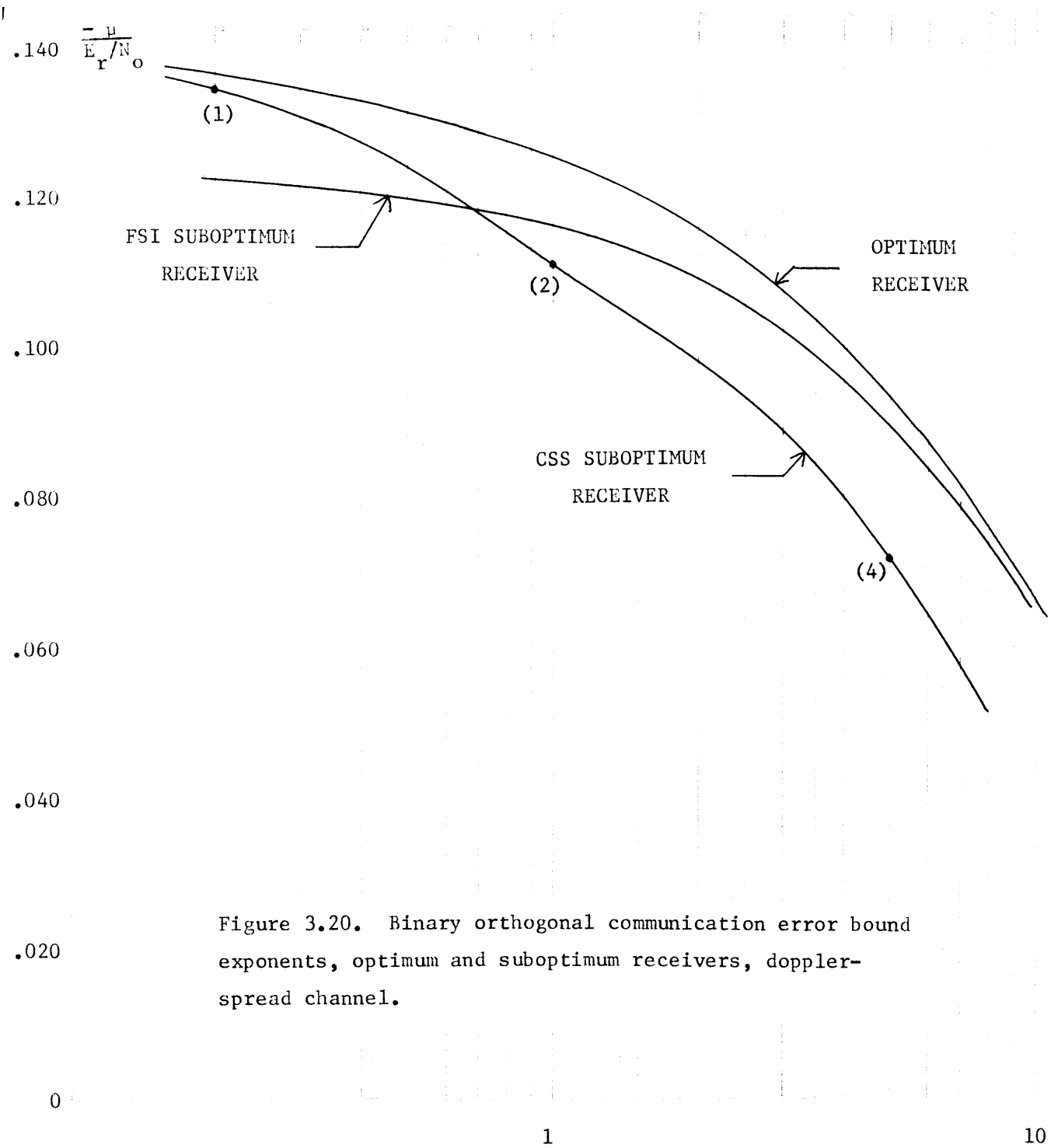
Figure 3.20. Binary orthogonal communication error bound
exponents, optimum and suboptimum receivers, doppler-
spread channel.
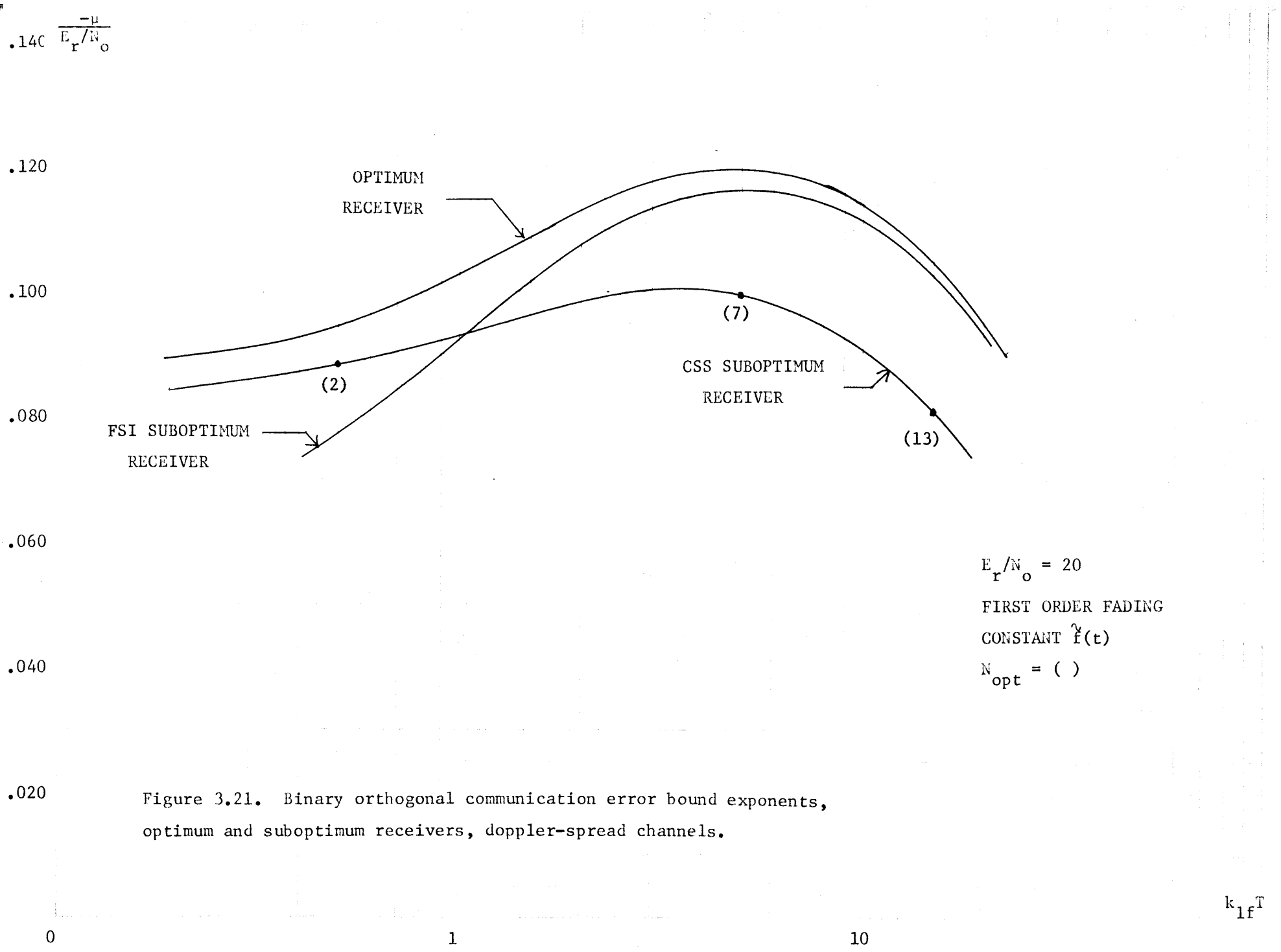
Figure 3.21. Binary orthogonal communication error bound exponents, optimum and suboptimum receivers, doppler-spread channels.

Both suboptimum receivers are optimized: the receiver filter pole is varied in the FSI case, and the number of correlators for the CSS receiver. This resulting value of N_{op} is indicated in parentheses for various points on the CSS curves; the FSI receiver optimum parameters have been indicated previously in this chapter.

The curves of Figures 3.20 and 3.21 show that the optimized FSI and CSS receivers both have a performance that is not far from the optimum. Furthermore, for low k_1T the CSS receiver is the better of the two suboptimum receivers, whereas the FSI gives a better performance for higher values of k_1T. This is not surprising since the CSS receiver becomes optimum in the limit of low k_1T and the FSI receiver becomes optimum in the limit of large k_1T. Note that the optimum number of correlators in the CSS receiver is approximately equal to the implicit diversity of the system, $1 + k_1T$. This provides a rule of thumb of optimizing the CSS receiver without actually calculating the performance.

The results of Figures 3.20 and 3.21 indicate that one of two suboptimum receivers can be used to obtain a performance that is within one dB, in this example, of the optimum receiver performance for binary symmetric communication over a doppler-spread channel. For values of k_1T less than one, the CSS receiver should be used; for other k_1T the FSI receiver is a better choice. This is significant because the CSS and FSI receiver structures are considerably simpler than that of the optimum receiver. It should be pointed out that this performance comparison can be carried out for other signals and higher order fading spectra as well.

E. Summary

This chapter has considered in detail the performance of the optimum receiver and two suboptimum receivers for the doppler-spread channel. A state-variable model for the channel and the performance of the optimum receiver were reviewed. A suboptimum receiver with a filter-squarer-integrator structure was suggested. Its performance was analyzed from the results of Chapter II and compared with the optimum. Proper design of the FSI receiver permitted nearly optimum performance. A second suboptimum receiver was proposed which consists of a bank of correlators followed by square-law detection and a weighted summation. Its performance was compared with the optimum and FSI receivers, again by the techniques of Chapter II.

The numerical examples indicated that either the CSS receiver of the FSI receiver could be used to achieve a performance within one or two dB of the optimum. For low kT the CSS receiver was the better performer; for large kT the FSI receiver was closer to optimum. The parameter k is the fading bandwidth and T is the signalling interval. The significance of this result is that the complicated optimum receiver can be replaced in a given problem by one of two much simpler receivers without much sacrifice in performance.

The numerical examples also provided guidelines for designing the suboptimum receivers. For the FSI receiver, a filter of the same order as the fading provides good performance if its bandwidth is increased by a factor that can be determined from F_r/N_o and kT. The

optimum number of correlations in CSS receiver is roughly the implicit diversity in the system. The performance maxima for either case are broad. Thus these guidelines provide a way to realize good performance without careful numerical optimization in each example.

A final word concerns the applicability of the techniques used to compare the performance of the doppler-spread channel receivers in this chapter. It is not necessary that $\hat{f}(t)$ be a constant or that the fading be first order, a frequent choice in the examples. Other signal and higher order fading, stationary or non-stationary, may be treated.

CHAPTER IV

DETECTION OF KNOWN SIGNALS TRANSMITTED

OVER DELAY-SPREAD CHANNELS

This chapter considers the problem of detecting or communicating

with known signals which are transmitted over delay-spread channels. This

is another special case of the Gaussian signal in Gaussian white noise

model of Chapter I. In contrast to the doppler-spread channel, however,

it is not possible to specify a finite state-variable model for the delay-

spread channel. The ability to do this was essential in much of Chapter

III in order to apply the results of Chapter II.

This chapter considers two approaches to the analysis of the

delay-spread problem. The first is use of time-frequency duality notions

to relate the delay-spread and the doppler-spread models. This was

originally done by Bello [18] and Kennedy [6]. These concepts are

applied to the two suboptimum receiver structures of Chapter III to give

suboptimum receivers for the delay-spread channel. Then an alternate

approach is suggested for the analysis of optimum receiver performance

for the delay-spread channel. It involves reduction of the receiver

decision statistic to an infinite sum of squared Gaussian random vari-

ables. The method is also applied to two suboptimum receiver structures.

The suboptimum and optimum receiver performances are compared in an example.

A. The Delay-Spread Channel Model

The delay-spread channel model used here is similar to the

doppler-spread model of Chapter II. The known narrowband transmitted

signal

$$f(t) = \sqrt{2}\, \text{Re}[\tilde{f}(t)\, e^{j\omega t}] \qquad 0 \le t \le T \qquad (4.1)$$

is reflected by a large collection of small point scatterers. For the delay-spread model it is assumed that the spatial distribution of scatterers has dimensions, in units of signal propagation time, which are significant compared to the transmitted waveform duration, T. Furthermore, it is assumed that the scatterers are moving at a rate which is slow compared to $1/T$. Then the scattered return can be considered as the superposition of returns from slowly fading (Rayleigh) scatterers [8]. The complex amplitude of the total received signal is

$$\tilde{r}(t) = \tilde{s}(t) + \tilde{w}(t)$$

$$= \int_{-\infty}^{\infty} \tilde{f}(t - \lambda)\, \tilde{y}(\lambda)\, d\lambda + \tilde{w}(t), \quad T_o \le t \le T_f \qquad (4.2)$$

where $\tilde{y}(\lambda)$ is a complex Gaussian random process and $\tilde{w}(t)$ is complex white Gaussian noise. The formulation of (4.2) implies that the channel produces no doppler shift. This model is also known as a deep or extended target model and has received considerable attention [2,7,8,16].

The channel process $\tilde{y}(\lambda)$ is zero-mean and has the known covariance function

$$E[\tilde{y}(\lambda)\tilde{y}^*(\sigma)] = \tilde{K}_{\tilde{y}}(\lambda,\sigma) \qquad (4.3)$$

The covariance function for $\tilde{s}(t)$ is

$$\tilde{K}_{\tilde{s}}(t,u) = \int_{-\infty}^{\infty} \int_{-\infty}^{\infty} \tilde{f}(t-\lambda)\tilde{K}_{\tilde{y}}(\lambda,\sigma)\tilde{f}^*(u-\sigma)\, d\lambda\, d\sigma \qquad (4.4)$$

The energy in the transmitted signal is

$$E_t = \int_0^T |\tilde{f}(t)|^2 dt \qquad (4.5)$$

The expected value of the energy in $\tilde{s}(t)$ over the observation interval $[T_o, T_f]$ is

$$E_r = \int_{T_o}^{T_f} \tilde{K}_{\tilde{s}}(t,t) dt$$

$$= \int_{-\infty}^{\infty} \int_{-\infty}^{\infty} \tilde{K}_{\tilde{y}}(\lambda,\sigma) \; [\int_{T_o}^{T_f} \tilde{f}(t-\lambda)\tilde{f}^*(t-\sigma)dt]d\lambda d\sigma \qquad (4.6)$$

Unless $\tilde{K}_{\tilde{y}}(\lambda,\sigma)$ is identically zero outside of some region in the $\lambda-\sigma$ plane, $\tilde{r}(t)$ will contain the scattered return from $f(t)$ over the infinite time interval $[-\infty,\infty]$. Thus the larger the interval $[T_o, T_f]$, the better the optimum receiver will perform. In some cases it is useful to consider scatterers which have a finite spatial distribution. Then $\tilde{K}_{\tilde{y}}(\lambda,\sigma)$ is zero outside a finite region in the $\lambda-\sigma$ plane. For example, suppose $\tilde{K}_{\tilde{y}}(\lambda,\sigma)$ is non-zero only for $0 \leq \lambda,\sigma \leq L$; then the observation interval need not exceed $[0, T + L]$, for $\tilde{r}(t)$ contains only white noise outside this interval.

A special case of the above model arises when the scatterers are assumed to be uncorrelated. That is, the channel process $\tilde{y}(\lambda)$ is assumed to be uncorrelated for different values of λ

$$\tilde{K}_{\tilde{y}}(\lambda,\sigma) = S(\lambda)\delta(\lambda-\sigma) \qquad (4.7)$$

where $S(\lambda)$ is positive and real. $S(\lambda)$ is often called the scattering

function of the channel. The process $\tilde{y}(\lambda)$ is said to be spatially white when (4.7) holds. This model is also a special case of the "wide-sense stationary uncorrelated scatterer" channel described in the next chapter. Introduction of (4.7) into (4.4) and (4.6) gives

$$\tilde{k}_{s}(t,u) = \int_{-\infty}^{\infty} \tilde{f}(t - \lambda)S(\lambda)\tilde{f}^{*}(u - \lambda)d\lambda \qquad (4.8)$$

$$E_{r} = \int_{-\infty}^{\infty} S(\lambda) \ [\int_{T_{o}}^{T_{f}} |f(t - \lambda)|^{2}dt]d\lambda \qquad (4.9)$$

The idea of implicit diversity is also a useful one in the delay-spread channel model. Kennedy [6] has pointed out that samples of the Fourier transform of the complex envelope of the received signal separated in frequency by 1/L are nearly independent. The quantity 1/L is the correlation bandwidth of the channel and is determined by how fast the correlation function $\tilde{k}_{y}(\lambda,\sigma)$ varies in λ and σ. In the case of uncorrelated scattering, 1/L is given by the bandwidth of the Fourier transform of the scattering function $S(\lambda)$. If the transmitted signal bandwidth is W, the bandwidth of $\tilde{s}(t)$ is roughly W + 1/L. Thus it is possible to obtain

$$N_{d\ell} = 1 + LW \qquad (4.10)$$

nearly independent samples of the Fourier transform of $\tilde{s}(t)$. As a result, the delay-spread channel is said to possess $N_{d\ell}$ degrees of freedom, or to have an implicit diversity of $N_{d\ell}$. Such an argument is clearly approximate in nature, but it will be useful both in

interpreting performance results and in providing a guideline for signal design.

B. Duality and Doppler-Spread Channel Receivers

This section discusses the notion of time-frequency duality and its use in the delay-spread channel detection problem. The original application of duality ideas to this channel model was done by Bello [18]. Kennedy [6] considered the performance of the optimum receiver for the delay-spread channel and its relation to a dual doppler-spread channel. These results are briefly reviewed here. Then this section considers the use of several suboptimum receivers for the delay-spread channel. These are related to dual doppler-spread channel suboptimum receivers.

A short description follows of the notion of duality that is used here. For more details see [6,8,18]. A function $\tilde{y}_2(\cdot)$ is said to be the dual of $\tilde{y}_1(\cdot)$ if $\tilde{y}_2(\cdot)$ is related to $\tilde{y}_1(\cdot)$ by the Fourier transform

$$\tilde{y}_2(f) = \int_{-\infty}^{\infty} \tilde{y}_1(t) \, e^{-j2\pi ft} \, dt \triangleq \tilde{Y}_1(f) \tag{4.11a}$$

If $\tilde{y}_1(\cdot)$ is a complex Gaussian random process, then $\tilde{y}_2(\cdot)$ is the statistical dual of $\tilde{y}_1(\cdot)$ if

$$\tilde{K}_{\tilde{y}_2}(f_1, f_2) = E[\tilde{y}_2(f_1)\tilde{y}_2^*(f_2)]$$

$$= \int_{-\infty}^{\infty} \int_{-\infty}^{\infty} \tilde{K}_{\tilde{y}_1}(t_1, t_2) \, e^{-j2\pi(f_1 t_1 - f_2 t_2)} \, dt_1 dt_2 \tag{4.11b}$$

If $\tilde{y}_2(\cdot)$ is the statistical dual of $\tilde{y}_1(\cdot)$, and if both processes are expanded in series with uncorrelated coefficients over the infinite

interval, then both expansions have the same eigenvalues, and the eigenfunctions of $\tilde{y}_2(\cdot)$ are related to those of $\tilde{y}_1(\cdot)$ by (4.11a) [6]. Note that the dual of a stationary white Gaussian process is also a stationary white Gaussian process, by (4.11b).

Consider the deterministic operation $g[\cdot]$. The operator $G[\cdot]$ is defined to be the dual of $g[\cdot]$ if, when

$$\tilde{y}_2 = g[\tilde{y}_1], \tag{4.12a}$$

then

$$\tilde{Y}_2 = G[\tilde{Y}_1] \tag{4.12b}$$

where $\tilde{Y}_2(\cdot)$ and $\tilde{Y}_1(\cdot)$ are the respective Fourier transforms of $\tilde{y}_2(\cdot)$ and $\tilde{y}_1(\cdot)$. The definition of (4.12) is also valid for random operators if $\tilde{Y}_2(\cdot)$ and $\tilde{Y}_1(\cdot)$ are interpreted as statistical duals of $\tilde{y}_2(\cdot)$ and $\tilde{y}_1(\cdot)$, respectively. Some examples are: multiplication by $\exp(-j2\pi fT)$ is the dual of a delay of T; convolution with $\tilde{M}(\cdot)$ is the dual of multiplication by $\tilde{m}(\cdot)$, the inverse Fourier transform of $\tilde{M}(\cdot)$; multiplication by $\tilde{M}(\cdot)$ is the dual of convolution with $\tilde{m}(\cdot)$.

With these definitions it is possible to show that there is a dual relationship between the delay-spread and doppler-spread channel models. [6,8,18]. Let $\tilde{s}_{dp}(t)$ denote the output of the doppler-spread channel in (3.2), and $\tilde{s}_{d\ell}(t)$, the output of the delay-spread channel in the model of (4.2). The process $\tilde{s}_{d\ell}(t)$ is the statistical dual of $\tilde{s}_{dp}(t)$ if the relationship of (4.11b) holds. Introducing (3.4) and (4.4) into (4.11b) it is straightforward to show [8] that this dual relationship exists if

$$\tilde{f}_{d\ell}(t) \leftrightarrow \tilde{F}_{dp}(t) \qquad\qquad (4.13)$$

and

$$\tilde{K}_{y_{dp}}(t,u) \leftrightarrow \int\limits_{-\infty}^{\infty} \int\limits_{-\infty}^{\infty} K_{y_{d\ell}}(\lambda,\sigma)\ e^{j2\pi(\lambda t-\sigma u)}\ d\lambda d\sigma \qquad (4.14)$$

That is, the output of the delay-spread channel is the dual of the doppler-spread channel output if the doppler-spread model transmitted signal $\tilde{f}_{dp}(t)$ is the Fourier transform of the delay-spread channel signal $\tilde{f}_{d\ell}(t)$, and if the corresponding channel covariance functions are related by the double inverse Fourier transform of (4.14).

This dual relationship has important implications for the optimum reception of signals transmitted over the delay-spread channel. If the conditions of (4.13) and (4.14) are satisfied, the received signal in the delay-spread model of (4.2) is the dual of the received signal in the doppler-spread model, since the white noise $\tilde{w}(t)$ is its own dual. Thus the eigenvalues of both processes are the same, which implies that the moment-generating functions of the liklihood ratio and therefore the error probabilities are identical. The delay-spread channel optimum receiver can be specified in terms of the optimum receiver for the dual doppler-spread channel [18,8], as shown in Figure 4.1. The input to the delay-spread channel is $\tilde{f}(t)$ and the received signal $\tilde{r}(t)$ is inverse Fourier transformed. The result, $\tilde{R}(f)$, is operated upon by the optimum receiver for the doppler-spread channel which has a transmitted signal that is the Fourier transform of $\tilde{f}(t)$ and a covariance function related to the delay-spread covariance
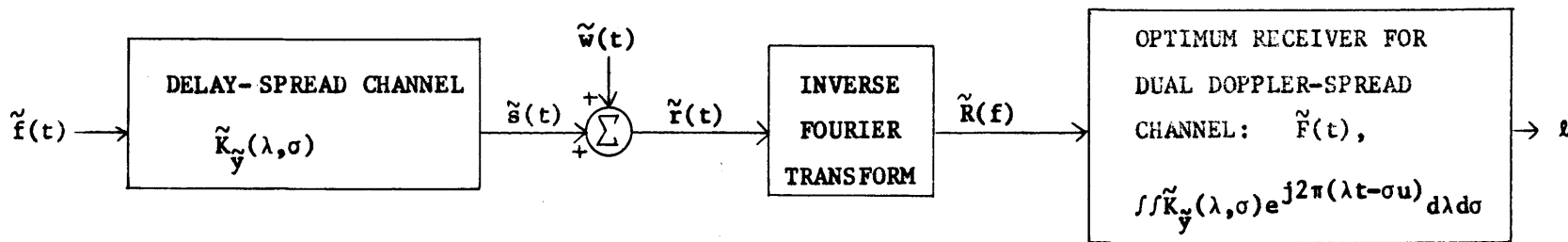
Figure 4.1. Complex version of the optimum receiver for the delay-spread channel, dual realization.

function by (4.14).

The notion of duality thus provides a way of finding the optimum receiver and its performance for the delay-spread channel, provided that the dual doppler-spread receiver and its performance are available. From Chapter III, the most useful class of doppler-spread channels with convenient performance expressions and receiver realizations can be described by state-variable models. This, in turn, has several implications for the delay-spread dual analysis described above. First, the transmitted signals for the doppler-spread state-variable models are strictly time-limited. Thus the duality notion can be conveniently applied without approximations only to delay-spread models with transmitted signals of finite bandwidth and, hence, of infinite duration.

A second limitation of the duality approach becomes apparent after considering the special case of stationary fading in the doppler-spread channel and uncorrelated scattering in the delay-spread channel. Then (4.7) in (4.14) gives the dual relation

$$\tilde{K}_{y_{dp}}(\tau) = \int_{-\infty}^{\infty} S(\lambda) \, e^{j2\pi\lambda\tau} \, d\lambda \qquad (4.15)$$
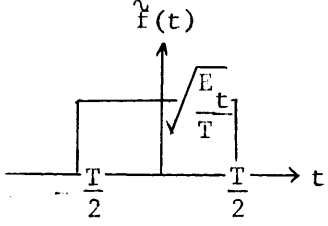
Since (4.15) indicates that $S(\lambda)$ is the Fourier transform of the covariance function of a random process generated by passing white noise through a finite state linear system, $S(\lambda)$ must be a rational function in λ and hence extends over $[-\infty,\infty]$. Without approximations, then, it is not possible to consider performance of a delay-spread model with a finite scatterer distribution, by means of a dual state-variable

doppler-spread channel model.

These limitations are evident in the structure of the optimum receiver of Figure 4.1. It is unrealizable since an infinite segment of $\tilde{r}(t)$ is required in order to take the inverse Fourier transform. Nevertheless, the notion of duality is useful in studying the performance of delay-spread channel models with rational $\tilde{S}(\lambda)$ and bandlimited transmitted signals. For instance, Table 4.1 gives the relationships between a doppler-spread example treated in Chapter III and its dual delay-spread model. Often these constraints can be met by suitable approximations in a particular delay-spread channel problem.

The application of duality above has provided a means to directly apply the results of Chapter III concerning doppler-spread channel optimum receivers for the binary detection or M-ary communication problems. A logical question at this point is: do the duality relationships presented above hold for the two doppler-spread channel suboptimum receiver structures of Chapter III? The answer is yes, which permits application of the remainder of results of Chapter III to the delay-spread channel problem.

From the preceding discussion on duality, a logical approach to finding good suboptimum receivers for the delay spread channel is to inverse Fourier transform the received signal and operate on it with a dual doppler-spread channel suboptimum receiver. The resulting structures are unrealizable, however. A more practical receiver would be obtained if the dual operations could be carried out directly on $\tilde{r}(t)$. This issue will be investigated in the following discussion.

DOPPLER-SPREAD CHANNEL	DELAY-SPREAD CHANNEL
	$\tilde{f}(t) = \sqrt{\dfrac{E_t}{W}} \ \dfrac{\sin \pi Wt}{\pi t}$, $-\infty < t < -\infty$
$\overset{\sim}{K_y}(\tau) = P\,e^{-k_1|\tau|}$ (FIRST ORDER STATIONARY FADING)	$S(\lambda) = \dfrac{2PL}{(2\pi\lambda)^2 + L^2}$ (UNCORRELATED SCATTERING)

Figures 3.5 and 3.6 give the performance in both problems if

$$k_1 T = LW.$$

Table 4.1. A particular delay-spread channel and its dual doppler-model.

Figure 4.2 shows a suboptimum receiver for the delay-spread channel that uses a dual doppler-spread channel FSI receiver. The output of the channel, $\tilde{r}(t)$ is inverse Fourier transformed to give $\tilde{R}(f)$. The sample function $\tilde{R}(f)$ is operated upon by the suboptimum FSI receiver which is designed for the dual doppler-spread channel. That is, if $\hat{f}(t)$ is the transmitted signal and $\tilde{K}_{y}(\lambda,\sigma)$ is the delay-spread channel covariance, then the FSI receiver is designed for a doppler-spread channel with a transmitted signal $\tilde{f}(t)$ and a fading covariance function which is the double Fourier transform of $\tilde{K}_{y}(\lambda,\sigma)$.

The performance of the receiver in Figure 4.2 is identical to the performance of the FSI suboptimum receiver over the dual doppler-spread channel. Thus the techniques of Chapter III for evaluating the FSI receiver error probabilities and designing the FSI receiver can be applied here directly. Note that the receiver in Figure 4.2 requires an inverse Fourier transform, and thus it is unrealizable. Also, since the results of Chapter III for FSI receivers required a state-variable model for the channel, this implies the same restrictions on signals and channel covariance functions as in the optimum receiver case.

The operations indicated in Figure 4.2 can be carried out directly, without the inverse Fourier transform, if the filter $\tilde{h}(t,u)$ is time-invariant. The decision statistic ℓ in Figure 4.2 can be written
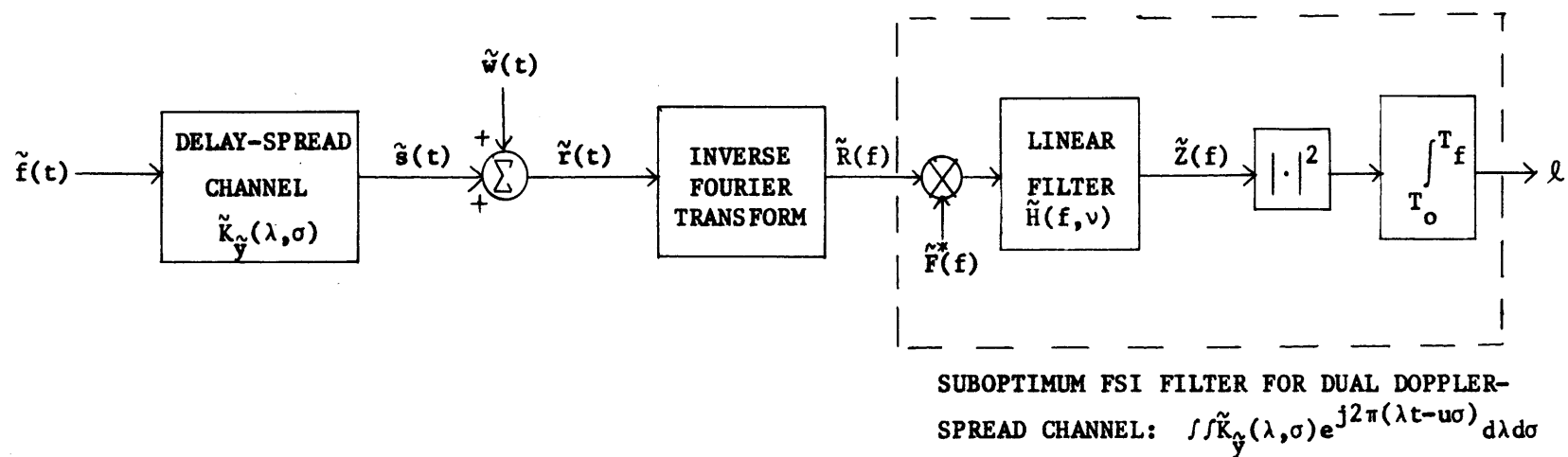
Figure 4.2. Complex version of the suboptimum dual filter-squarer-integrator receiver for the delay-spread channel.

$$\ell = \int_{T_o}^{T_f} |\overset{\vee}{Z}(f)|^2 df$$

$$= \int_{-\infty}^{\infty} |\tilde{z}(\lambda)|^2 d\lambda$$

$$= \int_{-\infty}^{\infty} \left| \int_{-\infty}^{\infty} \tilde{r}(t) \overset{\vee}{f}^*(t-\lambda) dt \right|^2 |\tilde{h}(\lambda)|^2 \, d\lambda \qquad (4.16)$$

where $\tilde{z}(\cdot)$, $\tilde{r}(\cdot)$, $\tilde{f}(\cdot)$, and $\tilde{h}(\cdot)$ are the inverse Fourier transforms

of $\overset{\vee}{Z}(f)$, $\tilde{R}(f)$, $\tilde{F}(f)$, and $\tilde{H}(f)$. Equation (4.16) has been derived by

replacing the operations in Figure 4.2 by their duals, according to

(4.12).

The inner integral in (4.16) can be realized by passing $\tilde{r}(t)$

into a filter matched to $\tilde{f}^*(t)$. The matched filter output is squared,

weighted by $|\tilde{h}(\lambda)|^2$, and integrated. This structure is shown in

Figure 4.3 and is called a two-filter radiometer [2]. It is

interesting to note that if $|\tilde{h}(\lambda)|^2$ is chosen to be $\overset{\vee}{S}(\lambda)$, the

structure of Figure 4.3 is the optimum receiver when a low-energy-

coherence condition exists [2].

The performance of the two-filter radiometer is the same as

that of the receiver in Figure 4.2. Thus the results of Chapter 3

can be applied directly, provided the dual doppler-spread channel with

stationary fading has a state-variable representation. Furthermore,

the dual relationships suggest a design procedure for the TFR receiver.

The gain $\tilde{h}(\lambda)$ in the TFR receiver is the inverse Fourier transform of
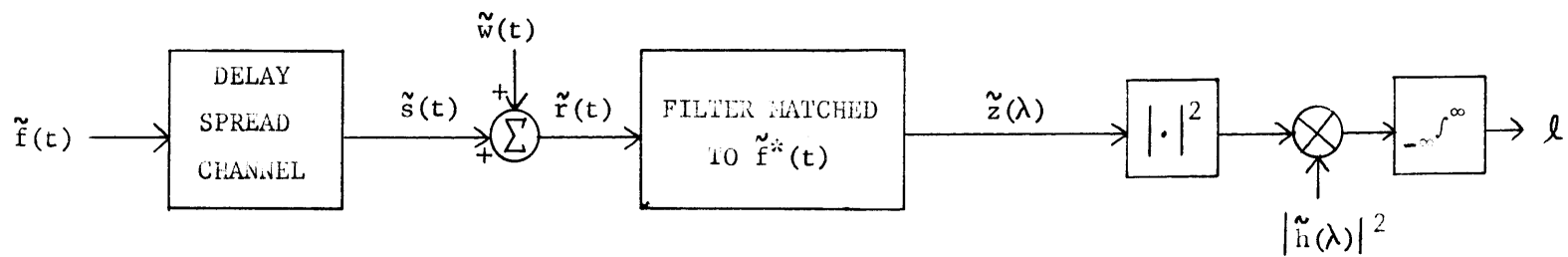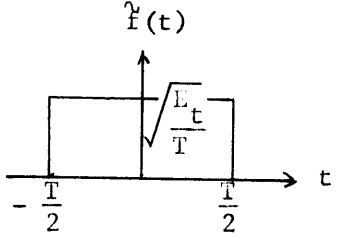
Figure 4.3 Complex version of the two-filter radiometer suboptimum receiver for the delay-spread channel.

$\tilde{H}(f)$, which in the doppler-spread model is the impulse response of a
filter that has the same order as the fading process. Hence the
squared magnitude of the Fourier transform of $\tilde{H}(\cdot)$ has the same form
as the fading spectrum. Since (4.15) indicates that the dual doppler
fading spectrum is just the scattering function $S(\lambda)$, this implies
$|h(\lambda)|^2$ in the TFR of Figure 4.3 should be rational with the same order
as $S(\lambda)$, but with possibly different parameters. Table 4.2 gives this
dual correspondence between the FSI and TFR receiver parameters for the
example considered in Table 4.1. Of course other $|\tilde{h}(\lambda)|^2$ may be used
in the TFR receiver. Convenient performance analysis requires only
that the dual doppler-spread model have a state-variable representation.

The results of Chapter III indicate that the TFR suboptimum
receiver for the binary detection or the M-ary orthogonal communication
problems can be designed to achieve nearly optimum performance. The
general procedure of suboptimum receiver optimization consists of
varying the post-detection weighting, $|\tilde{h}(\lambda)|^2$, depending on the values
of E_r/N_o, the scattering function duration, L, and the signal bandwidth
W. It should be emphasized, however, that the requirements of a rational
scattering function and a band-limited transmitted signal make the TFR
receiver in Figure 4.3 unrealizable. Of course, it may be worthwhile
to satisfy these constraints by approximations, in a given problem.

A second suboptimum receiver for the delay-spread channel is
available by inverse transforming the delay-spread channel output and
applying the result to the correlator-squarer-sum (CSS) receiver for
the dual doppler-spread channel model. Figure 4.4 shows this receiver.
As in the case of the FSI-TFR structures, the performance of the

DOPPLER SPREAD CHANNEL, FSI RECEIVER	DELAY-SPREAD CHANNEL, TFR RECEIVER
	$$\tilde{f}(t) = \sqrt{\frac{E_t}{W}} \ \frac{\sin \pi Wt}{\pi t}$$
RECEIVER FILTER $$\tilde{h}(t) = e^{-k_r t} u_{-1}(t)$$	POST-DETECTION WEIGHTING $$|\tilde{h}(\lambda)|^2 = \frac{2L_r}{(2\pi\lambda)^2 + L_r^2}$$

Figures 3.9 - 3.11 give the performance in both problems if

$$k_r T = L_r W$$

Table 4.2. A particular delay-spread channel TFR receiver and its dual doppler-spread FSI receiver.
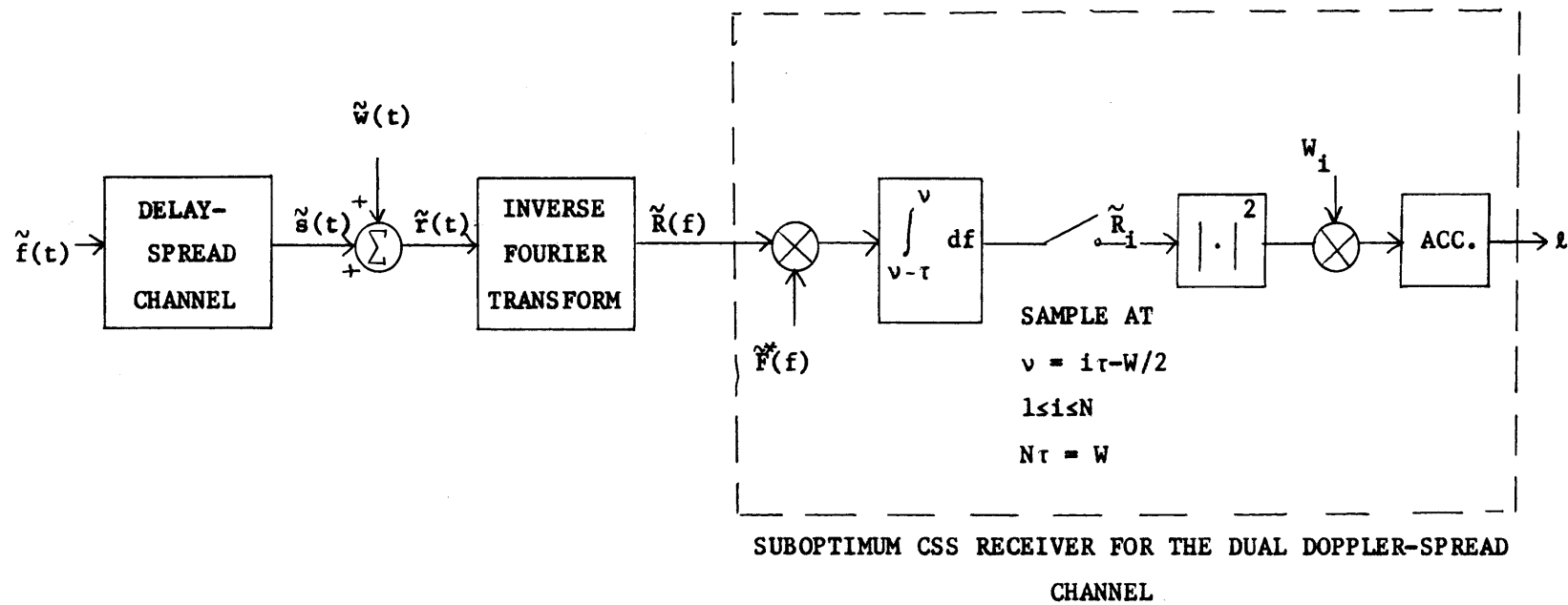
Figure 4.4. Complex version of the suboptimum dual correlator-squarer-sum receiver for the delay-spread channel.

receiver in Figure 4.4 is available from Chapter III when the correct

dual correspondence between the delay-spread and doppler-spread models

is made.

The operations of Figure 4.4 can be implemented without the

use of the inverse Fourier transform. Each $\tilde{R}_i$ in Figure 4.4 is

$$\tilde{R}_i = \int_{(i-1)\tau - \frac{W}{2}}^{i\tau - \frac{W}{2}} \tilde{R}(f)\tilde{F}^*(f)df \qquad (4.17)$$

This can be rewritten by defining

$$F_i(f) = \begin{cases} \tilde{F}(f), & (i-1)\tau - \frac{W}{2} < f < i\tau - \frac{W}{2} \\ \\ 0 & , \quad \text{elsewhere} \end{cases} \qquad (4.18)$$

Then $\tilde{R}_i$ becomes

$$\tilde{R}_i = \int_{-\infty}^{\infty} \tilde{R}(f)\tilde{F}_i^*(f)df$$

$$= \int_{-\infty}^{\infty} \tilde{r}(t)\tilde{f}_i^*(t)dt \qquad (4.19)$$

where $\tilde{f}_i(t)$ is the inverse Fourier transform of $\tilde{F}_i(f)$. The resulting

receiver is shown in Figure 4.5; it produces the same output as the

receiver in Figure 4.4. The reference signals for the correlators in

Figure 4.5 are obtained by passing f(t) through a bank of ideal band-

pass filters. An alternate scheme, derived by writing $\tilde{R}(f)$ in the same

form as (4.18), involves passing r(t) into the same bank of bandpass
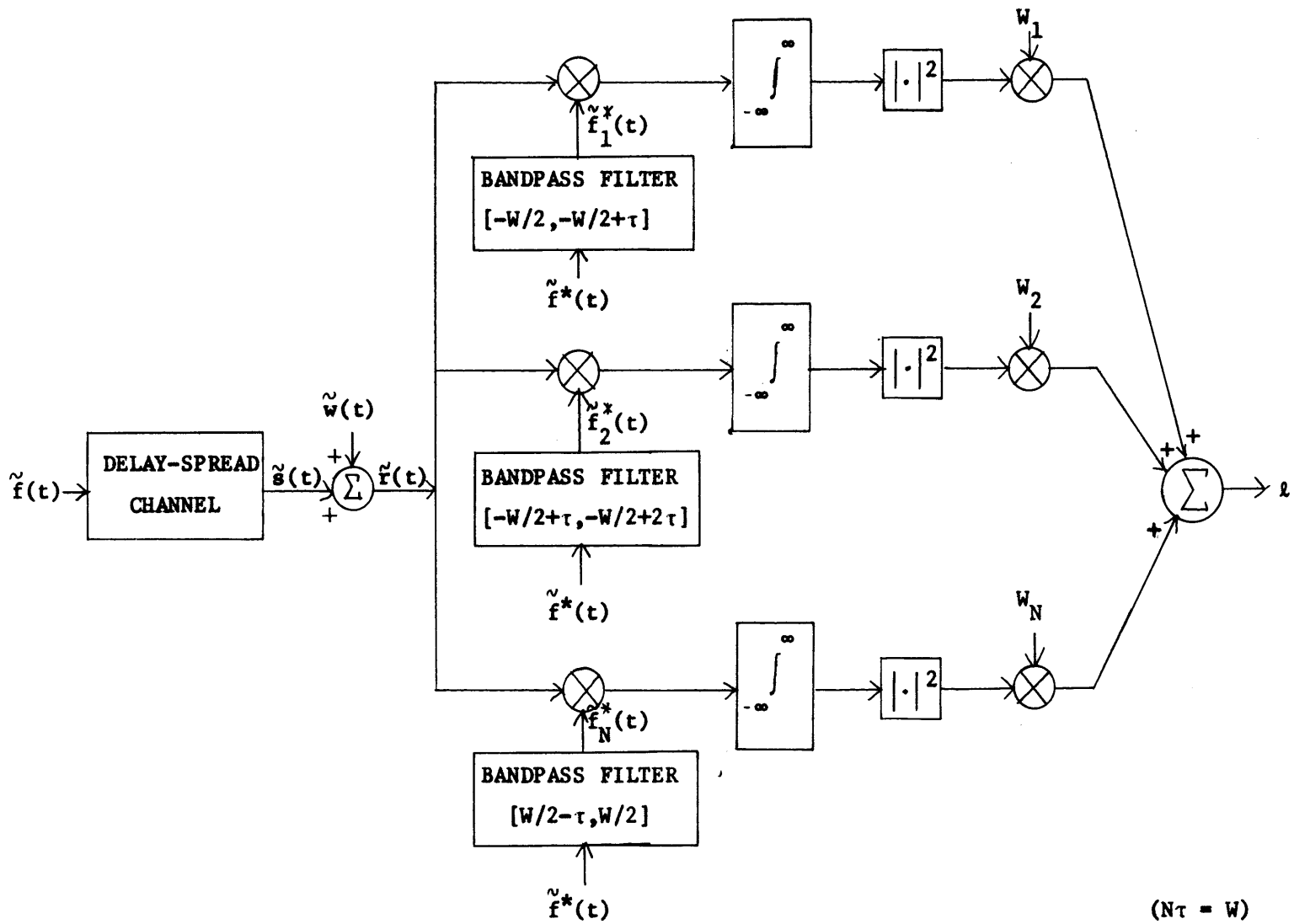
Figure 4.5. Complex version of the suboptimum dual CSS receiver for the delay-spread channel, direct realization.

filters and then correlating each of the outputs with f(t). In either case, the receiver of Figure 4.5 is still unrealizable. However, this model may be practical in some problems if the necessary approximations are made.

This section has discussed a way of applying the results of Chapter III for the doppler-spread channel to the problem of detecting signals transmitted over delay-spread channels. This method provides the performance of the optimum receiver and two suboptimum receivers for a useful class of signals and channels, even though a state-variable model for the delay-spread channel is not available. The drawback of using duality is that it is best suited for band-limited signals and delay-spread channels with scattering distributions of infinite extent. The next sections give an alternate method of finding the performance of the delay-spread channel optimum receiver and several suboptimum receivers. This method is useful for transmitted signals and scattering distributions which have a finite duration.

C. A Series Technique for Obtaining the Optimum Receiver Performance for the Delay-Spread Channel

This section considers an alternate technique for finding the performance of the delay-spread channel optimum receiver for either the binary detection or orthogonal communication problems of Chapter I. The derivation of the method begins by expanding the random process $\tilde{y}(\lambda)$ in (4.2) in the series

$$\tilde{y}(\lambda) = \sum_{i=1}^{\infty} \tilde{y}_i \tilde{\phi}_i(\lambda) \qquad (4.20)$$

where $\{\tilde{\phi}_i(\lambda)\}$ is a complete, orthonormal set of functions over the interval $[L_o, L_f]$,

$$\int_{L_o}^{L_f} \tilde{\phi}_i(\lambda)\tilde{\phi}_j^*(\lambda)d\lambda = \delta_{ij} \qquad (4.21)$$

The $\tilde{y}_i$ in (4.20) are obtained by multiplying (4.20) by $\phi_j^*(\lambda)$ and integrating

$$\tilde{y}_i = \int_{L_o}^{L_f} \tilde{y}(\lambda)\tilde{\phi}_i^*(\lambda)d\lambda \qquad (4.22)$$

Since $\tilde{y}(\lambda)$ is a zero-mean complex Gaussian random process, (4.22) indicates that the $\tilde{y}_i$ are complex Gaussian random variables with covariance

$$E[\tilde{y}_i\tilde{y}_j^*] = \int_{L_o}^{L_f}\int_{L_o}^{L_f} \tilde{K}_y(\lambda,\sigma)\tilde{\phi}_i^*(\lambda)\tilde{\phi}_j(\sigma)d\lambda d\sigma \qquad (4.23)$$

When the scattering is uncorrelated, (4.23) reduces to

$$E[\tilde{y}_i\tilde{y}_j^*] = \int_{L_o}^{L_f} S(\lambda)\tilde{\phi}_i^*(\lambda)\tilde{\phi}_j(\lambda)d\lambda \qquad (4.24)$$

Note that the series of (4.20) has correlated coefficients in general. The set $\{\tilde{\phi}_i(\lambda)\}$ need only be complete and orthonormal; the eigenfunctions of the Karhunen-Loeve expansion, which gives uncorrelated coefficients, comprise just one possible set that may be used in (4.20). The expansion interval $[L_o, L_f]$ is chosen to include the region in σ or λ over which $\tilde{K}_y(\lambda,\sigma)$ is non-zero.

If the series of (4.20) is introduced into (4.2) the complex envelope of the received signal becomes

$$\tilde{r}(t) = \sum_{i=1}^{\infty} \tilde{y}_i \tilde{b}_i(t) + \tilde{w}(t) \qquad T_o \leq t \leq T_f \qquad (4.26)$$

where

$$\tilde{b}_i(t) = \int_{L_o}^{L_f} \tilde{f}(t-\lambda) \tilde{\phi}_i(\lambda) \qquad (4.27)$$

The observation interval is

$$T_o = \min(0, L_o)$$

$$(4.28)$$

$$T_f = \max(T, L_f)$$

since $\tilde{f}(t)$ is non-zero over $[0,T]$.

The form of (4.26) suggests the following approach: truncate the series of (4.26) to N terms, find the optimum receiver for the truncated model, and determine the moment-generating functions of the receiver decision statistic. These, in turn, permit evaluation of the error probabilities for the truncated model optimum receiver. The limiting value of these error probabilities, provided they converge, give the error probabilities of the delay-spread channel optimum receiver.

A secondary issue that will not be treated in detail here is the use of the truncated model's optimum receiver as an approximation to the optimum receiver of the actual delay spread channel. In such

a situation the truncated model receiver is suboptimum for the delay-spread channel. In order to tell how good an approximation to the truly optimum receiver it is, its performance must be found. The techniques of Chapter II can be used to find this suboptimum performance, if such a comparison is desired.

The truncated model is, from (4.26)

$$\tilde{r}(t) = \sum_{i=1}^{N} \tilde{y}_i \tilde{b}_i(t) + \tilde{w}(t) \tag{4.29}$$

Defining the vectors

$$\underline{\tilde{b}}(t) = [\tilde{b}_1(t), \ldots, \tilde{b}_N(t)]$$

$$\underline{\tilde{y}} = \begin{bmatrix} \tilde{y}_1 \\ \cdot \\ \cdot \\ \tilde{y}_N \end{bmatrix} \tag{4.30}$$

permits (4.29) to be written as

$$\tilde{r}(t) = \underline{\tilde{b}}(t)\underline{\tilde{y}} + \tilde{w}(t) \tag{4.31}$$

The model of (4.31) is similar to one which has received considerable attention: the transmission of known signals over a Rayleigh fading channel. The $\tilde{b}_i(t)$ are the known signals, and the covariance of the random gains $\tilde{y}_i$ is given by (4.23) or (4.24).

The optimum receiver for this truncated model can be derived by the procedure given by (4.399 - 4.404) of Van Trees [20], modified to account for the fact that the $\tilde{b}_i(t)$ are not orthogonal and the $\tilde{y}_i$

are correlated. The details of this straightforward derivation are relegated to Appendix II; the result is that the logarithm of the liklihood ratio can be written

$$\ell = \ell n \underline{\Lambda}(\tilde{r}(t))$$

$$= \underline{\tilde{R}}^{\dagger}(\underline{\tilde{K}}^{-1} + \underline{\tilde{B}})^{-1}\underline{\tilde{R}} - \ell n \det (\underline{I} + \underline{\tilde{K}}\,\underline{\tilde{B}}) \qquad (4.32)$$

where

$$\underline{\tilde{R}} = \begin{bmatrix} \tilde{r}_1 \\ \cdot \\ \cdot \\ \cdot \\ \cdot \\ \tilde{r}_N \end{bmatrix} = \frac{1}{N_o} \int_{T_o}^{T_f} \tilde{r}(t)\underline{\tilde{b}}^{\dagger}(t)dt \qquad (4.33)$$

$$\underline{\tilde{B}} = \frac{1}{N_o} \int_{T_o}^{T_f} \underline{\tilde{b}}^{\dagger}(t)\underline{\tilde{b}}(t)dt \qquad (4.34)$$

$$\underline{\tilde{K}} = E[\underline{\tilde{y}}\ \underline{\tilde{y}}^{\dagger}] \qquad (4.35)$$

A branch of the optimum receiver for the truncated model is shown in Figure 4.6. The second term in (4.32), a bias which does not depend on $\tilde{r}(t)$, can be included in the threshold.

The moment generating functions for the statistic ℓ in (4.32) follow directly from Chapter II, Section E, since ℓ is a quadratic form. The details of the derivation are given in Appendix II. For the simple binary problem
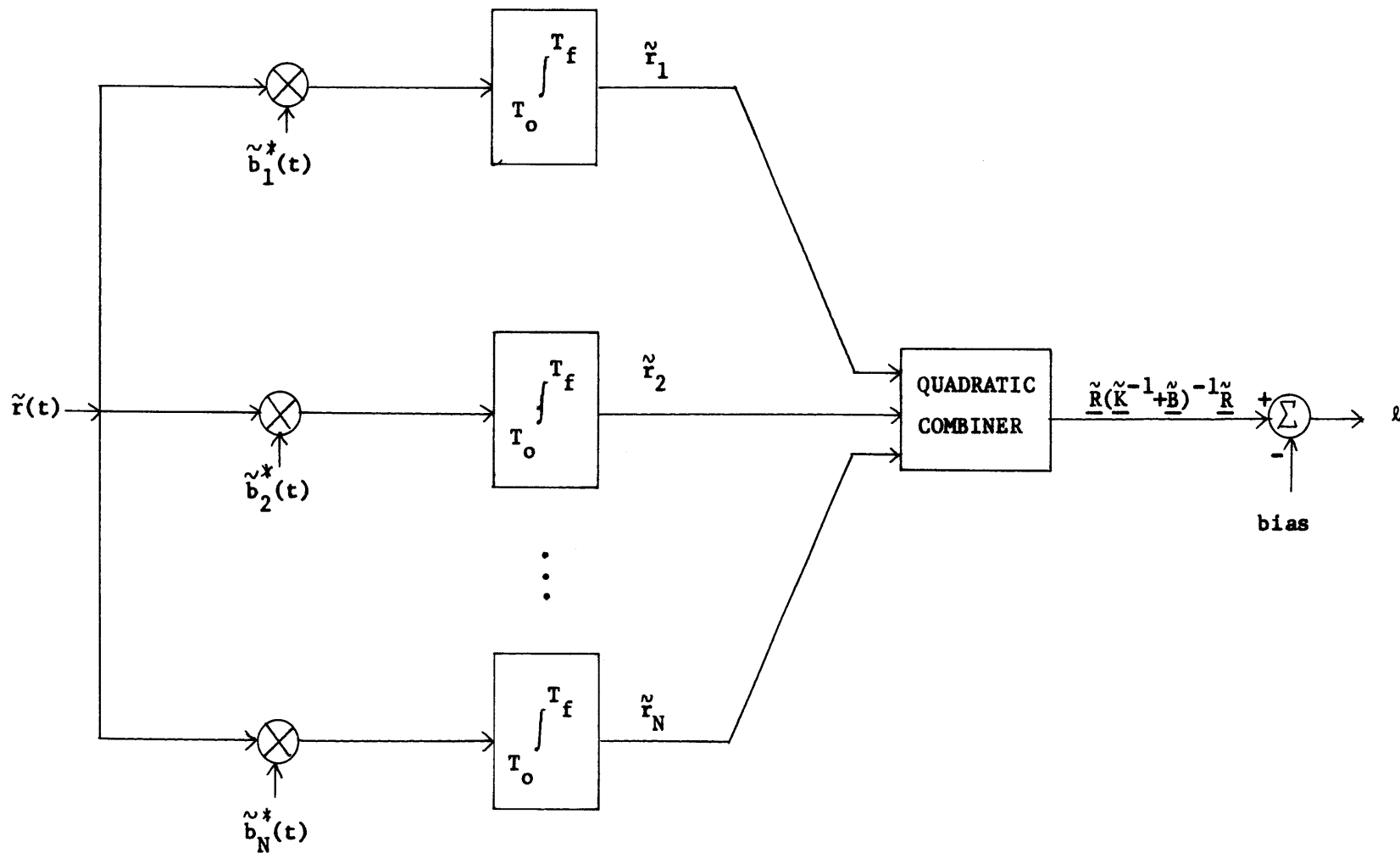
Figure 4.6. Complex version of the optimum receiver branch for the delay-spread channel truncated series model.

$$\mu_{*0}(s) \;\;= -s \ln \det \,(\underline{I} + \underline{\tilde{K}}\, \underline{\tilde{B}})$$

$$- \ln \det \,(\underline{I} - s(\underline{\tilde{K}}^{-1} + \underline{\tilde{B}})^{-1}\underline{\tilde{B}})$$

$$\mu_{*1}(s) \;\;= \;\; \mu_{*0}(s + 1) \tag{4.36}$$

and for the binary orthogonal communication problem

$$\mu_{*bc}(s) \;\;= \;\; \mu_{*0}(s + 1) + \mu_{*0}(-s) \tag{4.37}$$

The error probabilities for the truncated model can be computed from (4.36) and (4.37) as discussed in Chapter II.

Provided that there is convergence, the delay-spread channel optimum receiver error probabilities can be found from the results above, by letting the number of terms in the series, N, go to infinity. In practice, the maximum value of N required to achieve a given accuracy for $\mu_{*0}(s)$, $\mu_{*1}(s)$, or $\mu_{*bc}(s)$ is determined experimentally.

This series expansion approach has several advantages. One is that the method can be applied when the transmitted signal $\tilde{f}(t)$ has a finite duration. Also, there is no constraint on the scattering characteristics. $\tilde{K}_{\tilde{y}}(\lambda,\sigma)$ or $S(\lambda)$ need not be related directly or through duality to a state-variable channel model.

A disadvantage of the series approach is that its usefulness is determined primarily by the amount of work that is required to obtain analytically or numerically the covariance matrix $\underline{\tilde{K}}$, from (4.23) or (4.24), and the matrix $\underline{\tilde{B}}$. It would be convenient to choose

an orthonormal set $\{\overset{\sim}{\phi}_i(x)\}$ that makes these calculations easy. On the other hand, it is desirable that the $\{\overset{\sim}{\phi}_i(x)\}$ provide rapid convergence of the performance expressions. It is not obvious how to make this choice to satisfy either of these wishes.

As an example, consider the case when $\tilde{f}(t)$ has a constant envelope and the scattering is uncorrelated with the scattering function shown in Figure 4.7.

$$\tilde{f}(t) = \begin{cases} \dfrac{E_r}{T} & 0 \le t \le T \\ \\ 0 & \text{elsewhere} \end{cases} \tag{4.38}$$

$$S(\lambda) = \begin{cases} \dfrac{1}{L} \left(1 - \cos \dfrac{2\pi\lambda}{L} \right) & 0 \le \lambda \le L \\ \\ 0 & \text{elsewhere} \end{cases} \tag{4.39}$$

The observation interval is $[0, T + L]$. Let the expansion of (4.20) be a Fourier series over $[0,L]$

$$\overset{\sim}{\phi}_1(\lambda) = \frac{1}{\sqrt{L}} \quad ,$$

$$\overset{\sim}{\phi}_{2k}(\lambda) = \sqrt{\frac{2}{L}} \cos \frac{2\pi k\lambda}{L} \quad ,$$

$$\overset{\sim}{\phi}_{2k+1}(\lambda) = \sqrt{\frac{2}{L}} \sin \frac{2\pi k\lambda}{L} \quad , \quad k \ge 1 \tag{4.40}$$

The elements of the covariance matrix $\overset{\sim}{\underline{K}}$ can be found easily from (4.24). Somewhat more tediously, analytical expressions for the elements of $\overset{\sim}{\underline{B}}$

$$\tilde{f}(t)$$

$$S(\lambda)$$
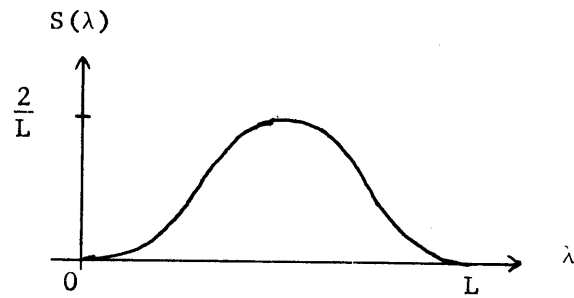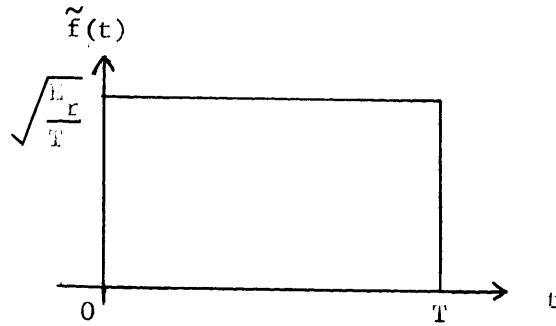
$$S(\lambda) = \begin{cases} \dfrac{1}{L} \left(1 - \cos\dfrac{2\pi}{L}\lambda\right) , & 0 \le \lambda \le L \\ \\ 0 & \text{elsewhere} \end{cases}$$

Figure 4.7. Signal and scattering function for a delay-spread channel example with uncorrelated scattering.

can be obtained from (4.30) and (4.34). The binary detection or orthogonal communication error probabilities may now be computed for this problem.

Figure 4.8 shows the exponent in the binary symmetric error probability bounds of (2.77) for the example presented above. The results of Chapter III indicated $\mu_{*bc}(-.5)$ is a convenient measure of relative performance in the binary symmetric communication case and is useful in assessing relative simple binary detection performance also. The normalized value of $\mu_{*bc}(-.5)$ is plotted; it serves as a measure of efficiency of a system, since .1488 is the maximum attainable value for this quantity. The numbers in parentheses give the number of harmonics, N_h, required to obtain an accuracy of three decimal places in $\mu_{*bc}(-.5)$; the number of terms in the series of (4.20) is $2N_h + 1$.

Note that there is an optimum value of L/T for each E_r/N_o in Figure 4.8. This behavior is similar to that observed in the doppler-spread examples. Figure 4.9 shows the optimum $\mu_{*bc}(-.5)$ and the value of L/T which produces it as a function of E_r/N_o. The concept of implicit diversity is again useful in interpreting these results. As given by (4.10), the signal $\tilde{s}(t)$ has roughly 1 + L/T degrees of freedom (the signal bandwidth is on the order of 1/T). For a given E_r/N_o the optimum L/T should provide a signal-to-noise ratio per degree of freedom of approximately three.

This example illustrates that the truncated series technique is useful for analyzing the delay-spread channel optimum receiver performance. The method may be applied to other signals and scattering functions as well, without constraints such as band-limited signals and
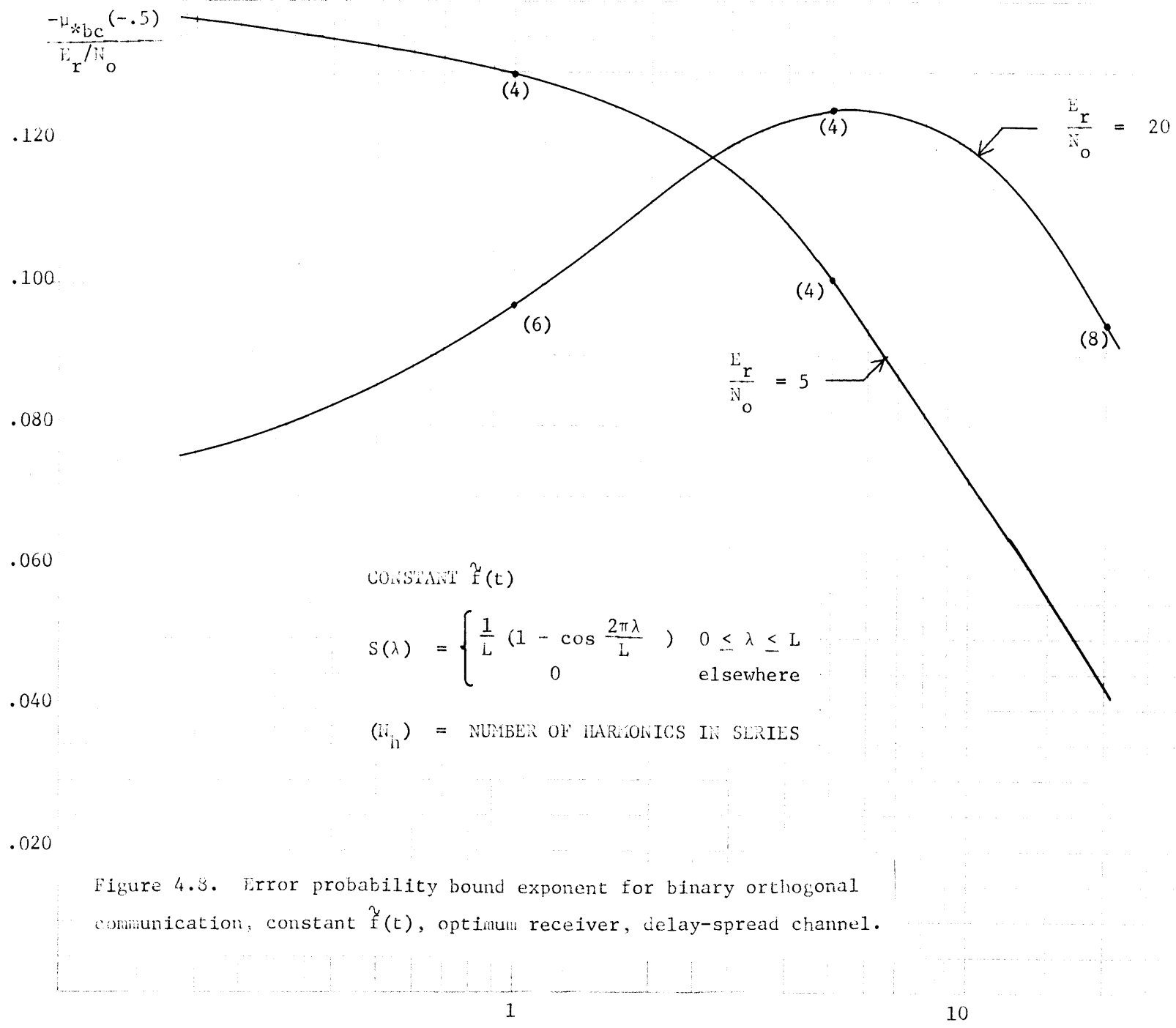
Figure 4.8. Error probability bound exponent for binary orthogonal communication, constant $\overset{\gamma}{f}(t)$, optimum receiver, delay-spread channel.

$$\frac{-\mu_{*bc}(-.5)}{E_r/N_o}\bigg|_{opt}$$

$$\frac{L}{T}\bigg|_{opt}$$

CONSTANT $\overset{\curvearrowright}{f}(t)$

$$S(\lambda) = \begin{cases} \dfrac{1}{L}\left(1 - \cos\dfrac{2\pi\lambda}{L}\right) & 0 \le \lambda \le L \\ 0 & \text{elsewhere} \end{cases}$$

$$\frac{-\mu_{*bc}(-.5)}{E_r/N_o}\bigg|_{opt}$$

$$\frac{L}{T}\bigg|_{opt}$$

$$\frac{E_r}{N_o}$$
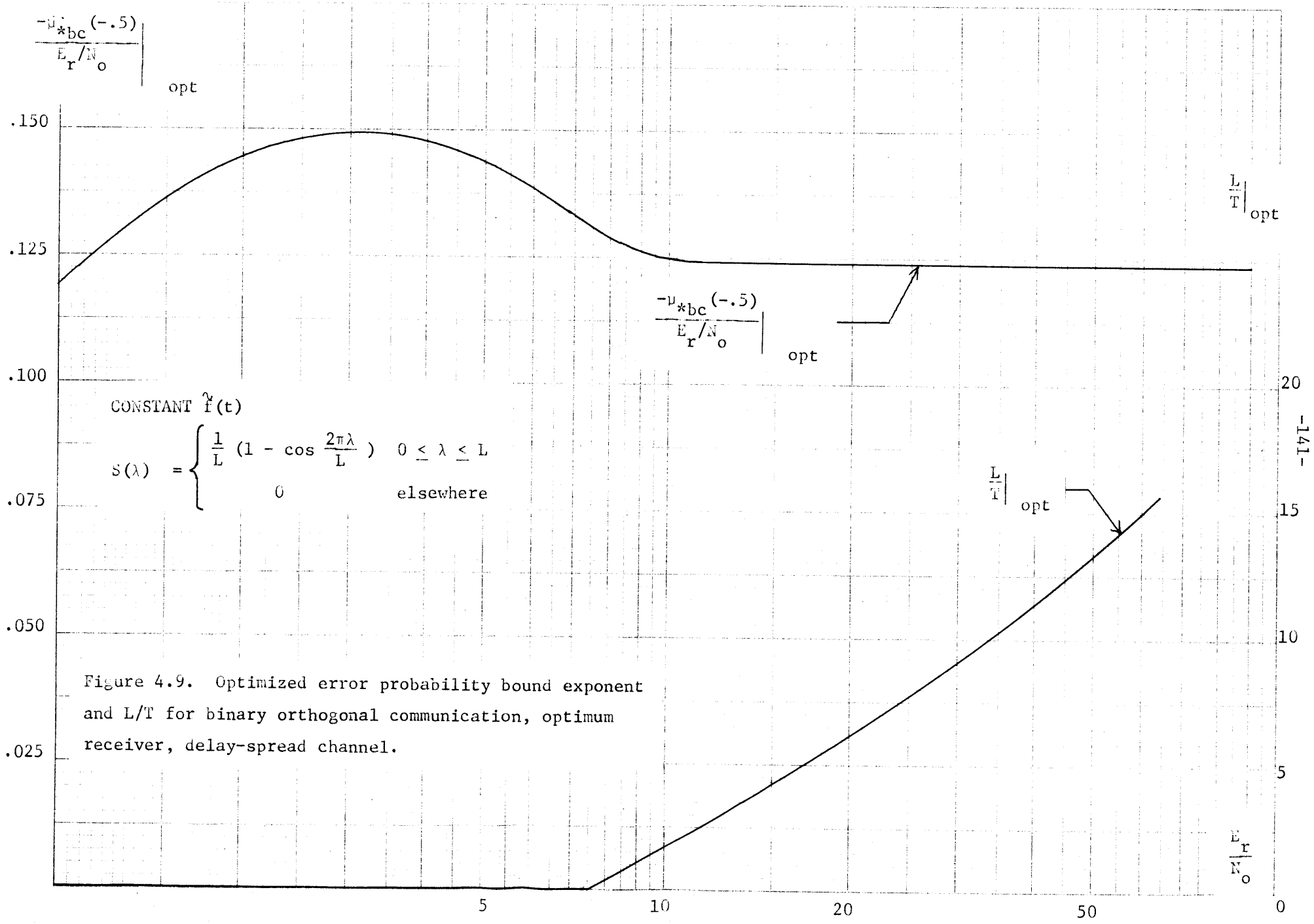
Figure 4.9. Optimized error probability bound exponent and L/T for binary orthogonal communication, optimum receiver, delay-spread channel.

-141-

state-variable representations. The issue of what orthogonal series to use in the expansion is an open one; the Fourier series was chosen in the example above because it permitted easy evaluation of the $\tilde{K}$ and $\tilde{B}$ matrices. The next sections consider application of the truncated series approach to several suboptimum receivers for the delay-spread channel.

D. A Two-Filter Radiometer Suboptimum Receiver for the Delay-Spread Channel

This section applies the series technique, derived above for the optimum receiver performance, to the problem of evaluating the performance of the two-filter radiometer in Figure 4.3. As indicated in Section B, this structure is generally suboptimum. From (4.16) the decision statistic for the TFR receiver is

$$\ell = \int_{L_1}^{L_2} g(\lambda) \int_{T_o}^{T_f} \int_{T_o}^{T_f} \tilde{r}(t)\tilde{f}^*(t-\lambda)\tilde{r}^*(u)\tilde{f}(u-\lambda)\,dt\,du\,d\lambda \qquad (4.41)$$

where

$$g(\lambda) = \left|\tilde{h}(\lambda)\right|^2 \qquad (4.42)$$

The observation interval is $[T_o, T_f]$ and is usually given by (4.28) to obtain the maximum available information about $\tilde{f}(t)$ from $\tilde{r}(t)$. The interval $[L_1, L_2]$ in (4.41) is the extent of $g(\lambda)$. Since the output of the matched filter in Figure 4.3 is significant over the interval $[T_o - T, T_f]$, where the duration of $\tilde{f}(t)$ is $[0,T]$, the interval $[L_1, L_2]$ should not include more than $[T_o - T, T_f]$.

In order to find the performance of the TFR receiver, the signal $\tilde{f}(t-\lambda)$ is written in the complete orthonormal series over $[L_1, L_2]$

$$\tilde{f}(t - \lambda) = \sum_{i=1}^{\infty} \tilde{b}_{is}(t)\tilde{\phi}_i^*(\lambda) \qquad (4.43)$$

$$\tilde{b}_{is}(t) = \int_{L_1}^{L_2} \tilde{f}(t - \lambda)\tilde{\phi}_i(\lambda)d\lambda \qquad (4.44)$$

$$\int_{L_1}^{L_2} \tilde{\phi}_i(\lambda)\tilde{\phi}_j^*(\lambda)d\lambda = \delta_{ij} \qquad (4.45)$$

The subscript s denotes "signal", in order to distinguish $\tilde{b}_{is}(t)$ from $\tilde{b}_i(t)$ of the previous section. Equation (4.43) is substituted in (4.41) to give

$$\ell = \sum_{i=1}^{\infty} \sum_{j=1}^{\infty} \tilde{r}_i^* \tilde{g}_{ij} \tilde{r}_j \qquad (4.46)$$

where

$$\tilde{r}_i = \frac{1}{N_o} \int_{T_o}^{T_f} \tilde{r}(t)\tilde{b}_i^*(t) \qquad (4.47)$$

$$\tilde{g}_{ij} = N_o^2 \int_{L_1}^{L_2} g(\lambda)\tilde{\phi}_i^*(\lambda)\tilde{\phi}_j(\lambda)d\lambda \qquad (4.48)$$

The $\tilde{r}_i$ in (4.47) are complex Gaussian random variables.

The decision statistic ℓ of the TFR receiver has been expressed as an infinite quadratic form. As in the case of the optimum receiver,

the sums in (4.46) will be truncated to N terms each. In this case
the approximate decision statistic can be written

$$\ell = \underset{\sim}{\underline{R}}^{\dagger} \underset{\sim}{\underline{G}} \underset{\sim}{\underline{R}} \tag{4.49}$$

where $\underset{\sim}{\underline{R}}$ is given by (4.33) and the $N \times N$ matrix $\underset{\sim}{\underline{G}}$ has elements $\underset{\sim}{g}_{ij}$
given by (4.48).

The moment generating functions for the finite quadratic form
of (4.49) are available from Chapter II, Section E. This permits
calculation of the suboptimum receiver error probabilities for the
truncated receiver. Then the number of terms in the series is allowed
to increase until acceptable convergence is obtained. This gives the
performance of TFR suboptimum receiver for the delay-spread channel.

In order to calculate the moment-generating functions for (4.49)
it is necessary to have the covariance matrix for $\underset{\sim}{\underline{R}}$ when $\underset{\sim}{r}(t)$ is $\underset{\sim}{w}(t)$
and $\underset{\sim}{s}(t) + \underset{\sim}{w}(t)$, respectively. For noise alone (II-16) in Appendix
II gives

$$\underline{\Lambda}_n = E[\underset{\sim}{\underline{R}} \underset{\sim}{\underline{R}}^{\dagger} | \text{noise}]$$

$$= \frac{1}{N_o} \int_{T_o}^{T_f} \underset{\sim}{\underline{b}}_s^{\dagger}(t) \underset{\sim}{\underline{b}}_s(t) dt$$

$$\overset{\Delta}{=} \underset{\sim}{\underline{B}}_s \tag{4.50}$$

where

$$\underset{\sim}{\underline{b}}_s(t) = [\underset{\sim}{b}_{1s}(t), \ldots, \underset{\sim}{b}_{Ns}(t)] \tag{4.51}$$

When signal plus noise is the input

$$\underline{\Lambda}_s \;=\; E[\underline{\tilde{R}}\,\underline{\tilde{R}}^\dagger|\text{signal + noise}\,]$$

$$=\; \frac{1}{N_o^2}\;\int_{T_o}^{T_f}\int_{T_o}^{T_f}\underline{\tilde{b}}_s^\dagger(t)\tilde{K}_s(t,u)\underline{\tilde{b}}_s(u)dtdu \;+\; \underline{\tilde{B}}_s$$

$$(4.52)$$

If $\tilde{K}_y(\lambda,\sigma)$ is written in the double orthogonal series over $[L_1,L_2]$

$$\tilde{K}_y(\lambda,\sigma) \;=\; \sum_{i=1}^\infty \sum_{j=1}^\infty \tilde{q}_{ij}\tilde{\phi}_i(\lambda)\tilde{\phi}_j^*(\sigma) \qquad (4.53)$$

$$\tilde{q}_{ij} \;=\; \int_{L_1}^{L_2}\int_{L_1}^{L_2}\tilde{K}_y(\lambda,\sigma)\tilde{\phi}_i^*(\lambda)\tilde{\phi}_j(\sigma)d\lambda d\sigma \qquad (4.54)$$

then from (4.4) $\tilde{K}_s(t,u)$ is given by

$$\tilde{K}_s(t,u) \;=\; \sum_{i=1}^\infty \sum_{j=1}^\infty \tilde{b}_{is}(t)\,\tilde{q}_{ij}\tilde{b}_{js}^*(u) \qquad (4.55)$$

If the sums in (4.55) are also truncated at the Nth terms, an approximation for $\tilde{K}_s(t,u)$ is

$$\tilde{K}_s(t,u) \;\cong\; \underline{\tilde{b}}_s(t)\underline{\tilde{Q}}_s\underline{\tilde{b}}_s^\dagger(u) \qquad (4.56)$$

where $\underline{\tilde{Q}}_s$ has elements given by (4.54). Introducing (4.56) into (4.52) and performing the integrations give an approximation for $\underline{\Lambda}_s$

$$\underline{\Lambda}_s \;\cong\; \underline{\tilde{B}}_s\,\underline{\tilde{Q}}_s\,\underline{\tilde{B}}_s \;+\; \underline{\tilde{B}}_s \qquad (4.57)$$

The approximation of (4.57) can be used for $\underline{\Lambda}_s$ since the number of

terms in the series will be increased until the error probability expressions

converge.

The appropriate moment-generating functions are available

from Section E of Chapter II. For simple binary detection

$$\mu_0(s) = -\ell n \det (I - s\underline{\tilde{G}} \underline{\Lambda}_n)$$

$$(4.58)$$

$$\mu_1(s) = -\ell n \det (I - s\underline{\tilde{G}} \underline{\Lambda}_s)$$

and for binary symmetric orthogonal communication

$$\mu_{bc}(s) = \mu_1(s) + \mu_0(-s) \tag{4.59}$$

The calculation of $\underline{\tilde{B}}_s$, $\underline{\tilde{G}}$, and $\underline{\tilde{Q}}_s$ for the N-term truncated series

enables (4.58) and (4.59) to be evaluated. Then N is increased until

the desired error probabilities or their bounds converge. As in the

optimum receiver case, it is not clear how to choose the orthonormal

set $\{\tilde{\phi}_i(\lambda)\}$; rapid convergence and easy calculation of $\underline{\tilde{B}}_s$, $\underline{\tilde{G}}$, and

$\underline{\tilde{Q}}_s$ are desirable.

For the uncorrelated scattering example of the preceding

section it is informative to compare performance of a TFR suboptimum

receiver with the optimum receiver performance. Insight into choosing

a good $g(\lambda)$ in (4.41) can be gained by considering the doppler-spread

channel FSI suboptimum receiver results of Chapter III and applying

duality. The filter in the FSI receiver was of the same order as the

filter which generated the fading process, but with a different bandwidth.

For the TFR receiver this implies choosing a $g(\lambda)$ which is similar in shape to the scattering function $S(\lambda)$ and including a parameter which permits adjustment of the effective width of $g(\lambda)$.

For the delay-spread channel model of Figure 4.9, let the TFR receiver post-detection weighting be

$$g(\lambda) = \begin{cases} \dfrac{1}{L} (A - \cos \dfrac{2\pi\lambda}{L}) & 0 \le \lambda \le L \\ \\ 0 & \text{elsewhere} \end{cases} \tag{4.60}$$

The parameter A is variable; for large A the weighting is uniform over λ. The matrices $\overset{\sim}{\underline{B}}_s$, $\overset{\sim}{\underline{G}}$, and $\overset{\sim}{\underline{Q}}_s$ follow directly. Note that $[L_0, L_f]$ and $[L_1, L_2]$ are identical in this example, and that $\overset{\sim}{\underline{B}}_s$ and $\overset{\sim}{\underline{Q}}_s$ are the same as $\underline{B}$ and $\underline{K}$, respectively, which were calculated for the optimum receiver in the previous section.

The suboptimum TFR receiver performance for binary orthogonal communication can be contrasted to the optimum performance indicated in Figure 4.8 by evaluating $\mu_{bc}(s)$ and finding its minimum. This has been done for the above example. The results will be presented in the next section along with those for a second suboptimum receiver for the delay-spread channel.

E. A Correlator-Squarer-Sum Suboptimum Receiver for the Delay-Spread Channel

A second suboptimum receiver for the delay-spread channel is considered in this section. The structure of this receiver is suggested by the form of the TFR receiver output in (4.16)

$$\ell = \int_{-\infty}^{\infty} \left| \int_{-\infty}^{\infty} \tilde{r}(t) \overset{\sim}{\Upsilon}^*(t - \lambda) dt \right|^2 |\tilde{h}(\lambda)|^2 d\lambda \tag{4.61}$$

Suppose the integral in (4.61) is approximated by the sum

$$\ell \overset{\thicksim}{=} \sum_{i=1}^{N} \left| \int_{-\infty}^{\infty} r(t)f(t - i\Delta\lambda)dt \right|^2 \left| \overset{\thicksim}{h}(i\Delta\lambda) \right|^2 i\Delta\lambda \qquad (4.62)$$

Each term in (4.62) can be considered the squared magnitude of a correlator output. As in the doppler-spread CSS receiver it may be advantageous to break down the correlation integral T into subintervals and add the squared subinterval correlator outputs.

The result is the suboptimum correlator-squarer-sum receiver of Figure 4.10. The reference signals $\overset{\thicksim}{f}{}^{*}(t - i\Delta\lambda)$ for each branch of the receiver can be provided by a tapped-delay-line with an input $\overset{\thicksim}{f}(t)$. The number of branches in the receiver is $M = L/\Delta\lambda - 1$ where $L = L_f - L_o$, the duration of the scattering; the number of correlation subintervals is at least $N = T/\tau$ in each branch, where T is the duration of $\overset{\thicksim}{f}(t)$. The squared outputs of each correlation are weighted by W_{ij}, and the branch sums are weighted by $|h(i\Delta\lambda)|^2$.

Insight gained from the TFR receiver performance analyzed with the technique of the previous section can be used in choosing the weights for the CSS receiver. Note that the CSS receiver of Figure 4.10 does not have the same structure as the dual doppler-spread CSS receiver in Figure 4.5.

When $\overset{\thicksim}{f}(t)$ is a constant and the number of branches and correlation sub-intervals is such that $\Delta\lambda = m\tau$ for some integer m, then the simplified structure of Figure 4.11 is possible. Figure 4.11 is constructed by noting that certain sampled correlator outputs in different branches of Figure 4.10 are identical under the assumed conditions. The structure of Figure 4.11 is particularly simple. The weights
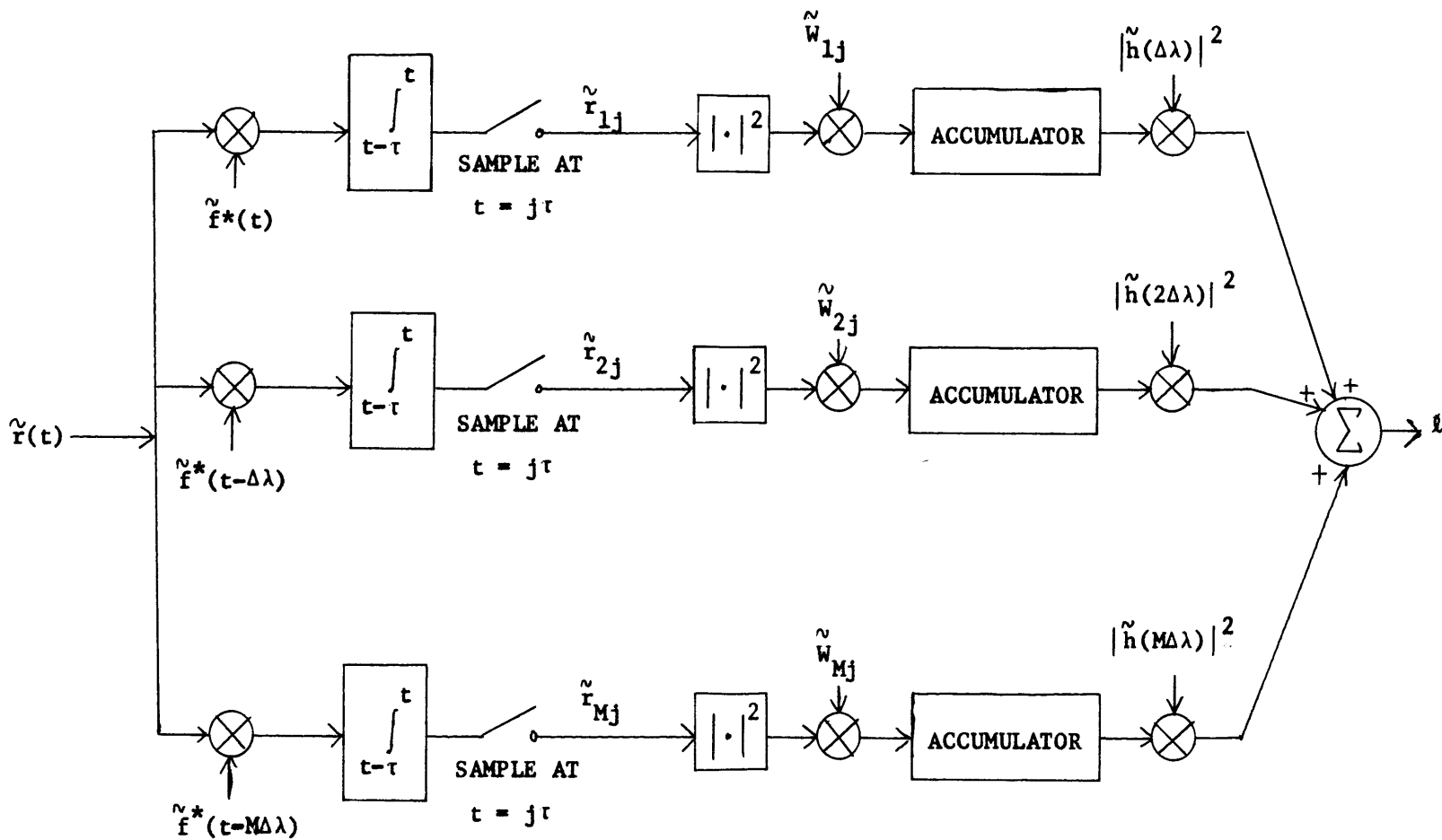
Figure 4.10. Correlator-squarer-sum suboptimum receiver for the delay-spread channel.

$$\tilde{r}(t) \longrightarrow \boxed{\int_{t-\tau}^{t}} \quad \text{SAMPLE AT}$$

$$t = j\tau$$
$$1 \leq i \leq N$$
$$N = \frac{T_f - T_o}{\tau}$$

$$\tilde{r}_i \longrightarrow \boxed{|\cdot|^2} \longrightarrow \bigotimes \xleftarrow{W_i} \longrightarrow \boxed{\text{ACCUMULATOR}} \longrightarrow \ell = \sum_{i=1}^{N} W_i |\tilde{r}_i|^2$$
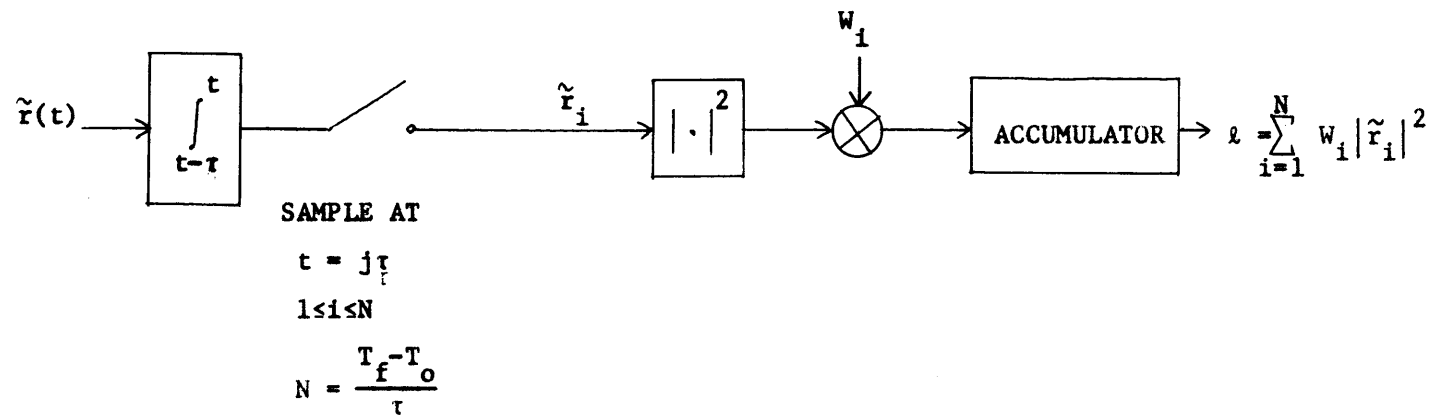
Figure 4.11. Simplified suboptimum CSS receiver for a constant $\tilde{f}(t)$.

W_i can be determined as appropriate combinations of the $\tilde{W}_{ij}$ and $|\tilde{h}(i\Delta\lambda)|^2$ in Figure 4.10.

Since the decision statistic for the delay-spread channel CSS receiver is a finite weighted sum of squared complex Gaussian random variables, the moment-generating functions for computing the error probabilities can be obtained from the equations of Chapter II, Section E. For simple binary detection

$$\mu_0(s) = -\ln \det(\underline{I} - s\underline{W}'\underline{\Lambda}_n)$$

$$\mu_1(s) = -\ln \det(\underline{I} - s\underline{W}'\underline{\Lambda}_s) \tag{4.63}$$

and for binary symmetric communication

$$\mu_{bc}(s) = \mu_1(s) + \mu_0(-s) \tag{4.64}$$

For the CSS receiver of Figure 4.10 the weighting matrix $\underline{W}'$ is diagonal with elements $W_i\delta_{ij}$.

Computation of the covariance functions $\underline{\Lambda}_s$ and $\underline{\Lambda}_n$ is straight-forward but generally tedious. In Figure (4.10)

$$E[\tilde{r}_{ij}\tilde{r}_{k\ell} | noise] = \int_{(\ell-1)\tau}^{\ell\tau} \int_{(j-1)\tau}^{j\tau} \tilde{f}(t-i\Delta\lambda)N_0\delta(t-u)\tilde{f}^*(u-k\Delta\lambda)dtdu \tag{4.65}$$

$$E[\tilde{r}_{ij}\tilde{r}_{k\ell}^* | signal + noise]$$

$$= \int_{(\ell-1)\tau}^{\ell\tau} \int_{(j-1)\tau}^{j\tau} \tilde{f}(t-i\Delta\lambda)[\tilde{K}_s(t,u) + N_0\delta(t-u)] \tilde{f}^*(u-k\Delta\lambda)dtdu \tag{4.66}$$

Evaluation of (4.65) and (4.66) provides the elements of $\underline{\Lambda}_n$ and $\underline{\Lambda}_s$.

For the special case of Figure 4.11, when $\overset{\curvearrowright}{f}(t)$ is a constant,

$$E[\overset{\curvearrowright}{r}_i \overset{\curvearrowright}{r}_j^* \mid \text{noise}] = \int_{(j-1)\tau}^{j\tau} \int_{(i-1)\tau}^{i\tau} N_o \delta(t-u)dtdu$$

$$= N_o \tau \delta_{ij} \tag{4.67}$$

$$E[\overset{\curvearrowright}{r}_i \overset{\curvearrowright}{r}_j^* \mid \text{signal} + \text{noise}] = \int_{(j-1)\tau}^{j\tau} \int_{(i-1)\tau}^{i\tau} \overset{\curvearrowright}{K}_s(t,u)dtdu + N_o \tau \ \delta_{ij}$$

$$\tag{4.68}$$

where $\overset{\curvearrowright}{K}_s(t,u)$ is given by (4.4) or (4.8). Note that no restrictions on

the form of $\overset{\curvearrowright}{K}_s(t,u)$ are required to compute the error probabilities for

this suboptimum receiver.

Figures 4.12 and 4.13 give a performance comparison of the

optimum, the TFR, and the CSS receiver for the binary symmetric

communication problem and the model of Figure 4.7. The TFR suboptimum

weighting of (4.60) is used, and the CSS structure of Figure 4.11 is

assumed with the weighting

$$W_i = 1 + \cos \frac{2\pi}{N} (i-.5), \quad i = 1,\ldots,N \tag{4.69}$$

For each receiver the normalized value of the appropriate error bound

exponent is plotted: $\mu_{*bc}(-.5)$ for the optimum, and the minimized

$\mu_{bc}(s)$ for the suboptimum receiver. In each case the appropriate sub-

optimum receiver parameter is also optimized, A in (4.60) for the TFR
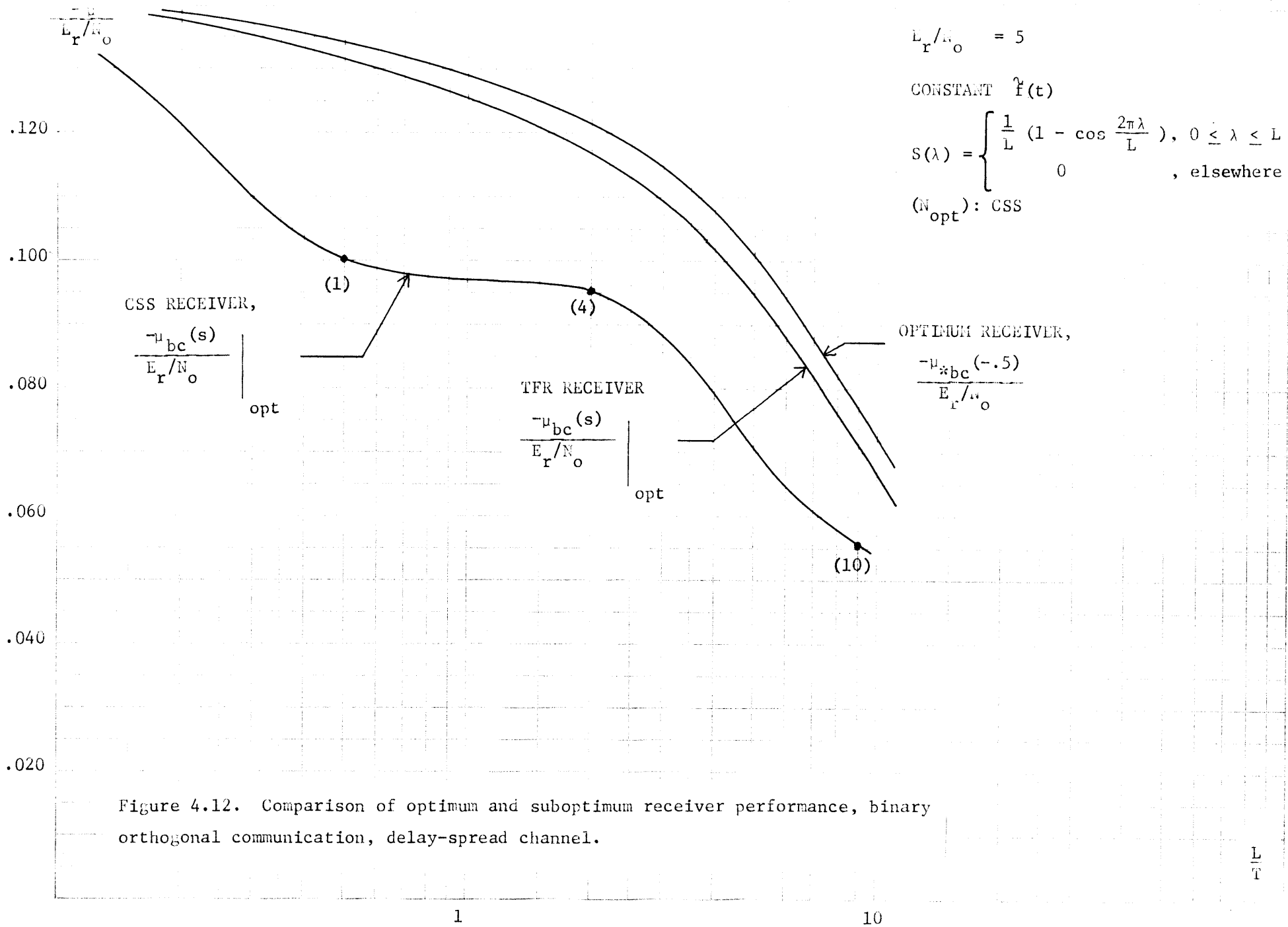
Figure 4.12. Comparison of optimum and suboptimum receiver performance, binary orthogonal communication, delay-spread channel.

E_r / N_o (vertical axis label)

$E_r / N_o = 5$

CONSTANT $\hat{f}(t)$

$$S(\lambda) = \begin{cases} \dfrac{1}{L}\left(1 - \cos\dfrac{2\pi\lambda}{L}\right), & 0 \le \lambda \le L \\ 0, & \text{elsewhere} \end{cases}$$

(N_{opt}): CSS

CSS RECEIVER,

$$\left. \frac{-\mu_{bc}(s)}{E_r/N_o} \right|_{opt}$$

TFR RECEIVER

$$\left. \frac{-\mu_{bc}(s)}{E_r/N_o} \right|_{opt}$$

OPTIMUM RECEIVER,

$$\frac{-\mu_{*bc}(-.5)}{E_r/N_o}$$

(1)   (4)   (10)

Vertical axis values: .120, .100, .080, .060, .040, .020

Horizontal axis label: $\dfrac{L}{T}$ with values 1 and 10

Figure 4.13. Comparison of optimum and suboptimum receiver performance, binary orthogonal communication, delay-spread channel.

receiver, and the number of correlations, N in (4.69) for the CSS

receiver. The TFR performance is quite insensitive to the value of A;

the optimum N for the CSS receiver is shown at various points on the

curves.

Figures 4.12 and 4.13 indicate that the TFR and CSS receivers

can achieve a performance which is no more than a few dB worse than

optimum in this example. Note that the TFR provides consistently good

performance over a wide range of L/T and E_r/N_o. Also the TFR becomes

optimum as L/T gets small, since for L << T there is little post-

detection integration in the TFR; the result is just a matched filter.

The number of correlators which optimize the CSS receiver for a given

L/T and E_r/N_o is consistent with the implicit diversity description of

the channel presented earlier in this chapter. It is possible, of

course, that there exist different choices for the TFR post-detection

weighting, $g(\lambda)$, and the CSS weights, W_i, that yield better performances

for some or all of L/T and E_r/N_o.

F. Summary

This chapter has considered in detail the problem of detecting,

or communicating with, known signals which are transmitted over the

delay-spread channel. The notion of time-frequency duality and the

dual relationships between delay-spread and doppler-spread channel

optimum receivers were reviewed. Their duality was applied to obtain a

correspondence between two delay-spread channel suboptimum receivers

and their doppler-spread counterparts. The fact that the doppler-

spread channel performance and receiver structure results of Chapter III

required state-variable models and time-limited transmitted signals implied that the duality concept is most useful for delay spread channels whose scattering distributions are infinite in extent and which use band-limited signals.

A second method of performance analysis has been proposed in which the channel model is expanded in an infinite series. Truncation of the series provides an approximate optimum receiver whose performance can be readily evaluated with the techniques of Chapter II. As the number of terms in the series becomes large, the performance of the delay-spread channel optimum receiver results. The method of analysis is attractive for problems in which the transmitted signal and the scattering have finite durations. The technique was then applied to evaluating the performance of a suboptimum receiver, the two-filter radiometer. This structure is a promising one because it is the dual of the doppler-spread channel FSI receiver. A second delay-spread sub-optimum receiver, the correlator-squarer-sum receiver, was suggested. Its structure is similar to that of the dopper-spread receiver of the same name, and its performance can be found in a similar manner.

The optimum, TFR, and CSS receivers for binary symmetric communication over a particular delay-spread channel were compared. The scattering was uncorrelated and the transmitted signal had a constant envelope. The results showed that the TFR and CSS receivers can be chosen, in this example, to achieve performance levels close to the optimum.

CHAPTER V

A DISTRIBUTED-PARAMETER STATE-VARIABLE MODEL FOR

KNOWN SIGNALS TRANSMITTED OVER DOUBLY-SPREAD CHANNELS

This chapter considers the problem of detecting known signals transmitted over channels which produce both delay and doopler spreading of the original waveform. Chapter III showed that error probabilities for the optimum receiver and several suboptimum receivers could be computed for the doppler-spread channel provided the problem had a finite state-variable representation. Chapter IV indicated that delay-spread channel receiver performance could be obtained either by relating the delay-spread problem to a dual doppler-spread model which has a state-variable model, or by applying an orthogonal expansion technique directly to the delay-spread channel model. The doubly-spread channel does not have a finite state-variable representation, and it cannot be related by duality to a doppler-spread channel. Hence the techniques discussed up to this point cannot be directly applied to the doubly-spread problem.

This chapter presents a distributed-parameter state-variable model for the doubly-spread channel which permits evaluation of the performance of the optimum receivers for the detection and communication problems of Chapter I. The finite state-variable models of the previous chapters will be called lumped-parameter models to distinguish them from the distributed-parameter case. From the distributed parameter state-variable model for the doubly-spread channel a realizable optimum detector structure is derived. A method of finding the moment-generating function of the decision statistic by means of an orthogonal expansion technique is proposed. This in turn permits calculation of the optimum receiver error probabilities. An example is then examined in detail.

A. The Doubly-Spread Channel: a Scattering Function Model

The doubly-spread channel model considered in this chapter can be derived by assuming that the narrowband transmitted signal

$$\tilde{f}(t) = \sqrt{2}\, \text{Re}[\tilde{f}(t)e^{j\omega t}] \quad 0 \leq t \leq T \tag{5.1}$$

is reflected by a collection of moving point scatterers. As in the delay-spread model the dimensions of the scatterer distribution, in units of propagation time, are significant compared to the transmitted waveform duration, T. And, as in the doppler-spread case, the scatterers are moving at a rate which is comparable to 1/T. Thus it is possible to consider the doubly-spread channel as a continuum of doppler-spread targets. That is, the scattering element at a delay λ effectively multiplies the complex envelope of the transmitted signal by a random process $\tilde{Y}(\lambda,t)d\lambda$. Integrating over all possible delays (scattering elements) yields the complex envelope of the total received signal

$$\tilde{r}(t) = \int_{-\infty}^{\infty} \tilde{f}(t-\lambda)\tilde{Y}(\lambda,t)d\lambda + \tilde{w}(t)$$

$$= \tilde{s}(t) + \tilde{w}(t), \quad T_o \leq t \leq T_f \tag{5.2}$$

where $\tilde{w}(t)$ is complex white Gaussian noise.

The $\tilde{Y}(\lambda,t)$ in (5.2) is a complex, two parameter Gaussian random process. The model of (5.2) indicates that the signal $\tilde{f}(t)$ undergoes both delay and doppler spreading in the doubly-spread channel; that is, both time-selective and frequency-selective fading can be observed in the received signal. For a more thorough discussion of the features of this model, a number of references are available [2,6,7,8,16]. It is also

called a deep fluctuating target model.

The covariance function of the zero-mean Gaussian process is denoted by

$$E[\tilde{Y}(x,t)\tilde{Y}^*(y,u)] = \tilde{K}_Y(x,t;y,u) \tag{5.3}$$

The covariance function for $\tilde{s}(t)$ in (5.2) is

$$\tilde{K}_s(t,u) = \int_{-\infty}^{\infty} \int_{-\infty}^{\infty} \tilde{f}(t-\lambda)\,\tilde{K}_Y(\lambda,t;\sigma,u)\tilde{f}^*(u-\sigma)d\lambda d\sigma \tag{5.4}$$

The energy in $\tilde{f}(t)$ over $[0,T]$ is E_t. The expected value of the received energy in $\tilde{s}(t)$ over the observation interval $[T_o,T_f]$ is

$$E_r = \int_{T_o}^{T_f} \tilde{K}_s(t,t)dt$$

$$= \int_{-\infty}^{\infty} \int_{-\infty}^{\infty} \int_{T_o}^{T_f} \tilde{f}(t-\lambda)\tilde{K}_Y(\lambda,t;\sigma,t)\tilde{f}^*(t-\sigma)d\lambda d\sigma \tag{5.5}$$

The comments of Chapter IV on the choice of the observation interval for the delay spread channel are relevant here also. The non-zero extent of $\tilde{K}_Y(\lambda,t;\sigma,u)$ in the variables λ and σ determines the duration of the scattered signal $\tilde{s}(t)$.

The doppler-spread and delay-spread channels of the previous chapters can be derived from the doubly-spread model above. For the delay-spread model, the fluctuations of $\tilde{Y}(\lambda,t)$ in t are negligible; then $\tilde{K}_Y(\lambda,t;\sigma,u)$ can be replaced by $\tilde{K}_y(\lambda,\sigma)$, given in (4.3), and $\tilde{Y}(\lambda,t)$ by $\tilde{y}(\lambda)$. For the doppler-spread case, the distribution of scatters

behaves as a point target. Then $\tilde{Y}(\lambda,t)$ becomes $\tilde{y}(t)$ and $\tilde{K}_Y(\lambda,t;\sigma,u)$ is replaced by $\tilde{K}_y(t,u)\delta(\lambda)\delta(\sigma)$.

A special case of the doubly-spread channel model arises when the scattering is spatially uncorrelated and temporally stationary. That is, the random process $\tilde{Y}(\lambda,t)$ is uncorrelated for different values of λ and stationary in the variable t. The covariance function for $\tilde{Y}(\lambda,t)$ becomes

$$\tilde{K}_Y(x,t;y,\tau) = \tilde{K}_D(x,t-\tau)\delta(x-y) \tag{5.6}$$

When the condition of (5.6) holds, the model is said to represent a "wide-sense stationary, uncorrelated scatterer" (WSSUS) channel [6,8,16]. From (5.6) the signal covariance function reduces to

$$\tilde{K}_S(t,u) = \int_{-\infty}^{\infty} \tilde{f}(t-\lambda)\tilde{K}_D(\lambda,t-u)\tilde{f}^*(u-\lambda)d\lambda \tag{5.7}$$

and the average received energy is

$$E_r = \int_{-\infty}^{\infty} \tilde{K}_D(\lambda,0) \left[\int_{T_o}^{T_f} |\tilde{f}(t-\lambda)|^2 dt \right] d\lambda \tag{5.8}$$

The Fourier transform of $\tilde{K}_D(\lambda,\tau)$ in the   variable is called the scattering function

$$\tilde{S}(\lambda,f) = \int_{-\infty}^{\infty} \tilde{K}_D(\lambda,\tau) e^{-j2\pi f\tau} d\tau \tag{5.9}$$

The doppler-spread and delay-spread channels which are derived from the WSSUS doubly-spread model have stationary fading and uncorrelated scattering, respectively.

Kennedy [6] has provided several measures of the implicit diversity of a doubly-spread channel which will be useful in interpreting

the results of this chapter. One such approximate measure takes into account the observation that time samples of the process $\tilde{s}(t)$ are approximately uncorrelated if they are taken 1/k seconds apart. The quantity 1/k is called the correlation time of the channel. Its magnitude is the smallest value for which $\tilde{K}_{\tilde{Y}}(\lambda,t;\sigma,t + 1/k)$ is approximately zero for all t,λ, and σ. For the WSSUS channel k corresponds to the bandwidth of the scattering function $\tilde{S}(x,f)$ in the f variable.

As in the doppler-spread channel, samples of the Fourier transform of the complex envelope of the doubly-spread channel output taken at frequency intervals of 1/L are approximately uncorrelated. The quantity 1/L is the correlation bandwidth of the channel and is determined by how fast the correlation function $\tilde{K}_{\tilde{Y}}(\lambda,t;\sigma,\tau)$ varies in λ and σ. For instance, in the WSSUS case, 1/L is given by the bandwidth of the Fourier transform of $\tilde{S}(x,f)$ in the x variable.

If the transmitted signal has a duration T and a bandwidth W, then there are approximately (1 + kT) independent time samples and (1 + LW) independent frequency samples of the channel output. This suggests assigning

$$N_{db} = (1 + kT)(1 + LW) \tag{5.9a}$$

degrees of freedom to the channel. This argument is not precise, of course, and Kennedy [6] indicates that other measures of the implicit diversity may be more accurate. However, (5.10) will be useful in interpreting performance results that are presented later in this chapter. For various definitions for the quantities L, k, T, and W in terms of the transmitted signal and the correlation function $\tilde{K}_{\tilde{Y}}(\lambda,t;\sigma,\tau)$, see Kennedy [6].

B. A Distributed-Parameter State-Variable Channel Model

The doubly-spread channel model of the previous section does
not have a lumped-parameter (finite state) state-variable model. This
prohibits direct application of the results of Chapter II to realizing
optimum receivers and calculating optimum and suboptimum receiver
error probabilities. This section shows that it is possible to represent
the doubly-spread channel by a distributed-parameter state-variable model,
and thereby obtain a realizable optimum receiver and its performance.

The distributed-parameter state-variable model presented here
is an application of the model given by Tzafestas and Nightingale [33].
The complex formulation is added according to Van Trees, Baggeroer, and
Collins [15]. For further discussions of distributed-parameter state-
variables see [8,29,33-35].

For the distributed-parameter state-variable model the complex
Gaussian random process $\overset{\vee}{Y}(x,t)$ is considered to be the output of a
distributed parameter linear system driven by a noise process $\underset{\sim}{\overset{\vee}{U}}(x,t)$.
The system is described by the linear partial differential equation

$$\frac{\partial \underset{\sim}{\overset{\vee}{X}}(x,t)}{\partial t} = \underset{\sim}{\overset{\vee}{F}}(x,t)\underset{\sim}{\overset{\vee}{X}}(x,t) + \underset{\sim}{\overset{\vee}{G}}(x,t)\underset{\sim}{\overset{\vee}{U}}(x,t)$$

(5.10)

$$\overset{\vee}{Y}(x,t) = \underset{\sim}{\overset{\vee}{C}}(x,t)\underset{\sim}{\overset{\vee}{X}}(x,t)$$

The model of (5.10) is a specialization of one given by Tzafestas and
Nightengale [33]; note that partial differential equation can be consid-
ered as an ordinary differential equation with x as a parameter. The

n-dimensional vector process $\underset{\sim}{X}(x,t)$ is the state of the distributed

system at time t. The gain matrices $\underset{\sim}{\underline{F}}(x,t)$, $\underset{\sim}{\underline{G}}(x,t)$, and $\underset{\sim}{\underline{C}}(x,t)$ are

known functions. The p-dimensional input process $\underset{\sim}{\underline{U}}(x,t)$ is temporally

white with a covariance

$$E[\underset{\sim}{\underline{U}}(x,t)\underset{\sim}{\underline{U}}^{\dagger}(y,\tau)] = \underset{\sim}{\underline{Q}}(x,y,t)\delta(t-\tau)$$

$$E[\underset{\sim}{\underline{U}}(x,t)\underset{\sim}{\underline{U}}^{T}(y,\tau)] = \underline{0}$$

$$E[\underset{\sim}{\underline{U}}(x,t)] = \underline{0} \tag{5.11}$$

The state vector at time t can be related to the state of the

system at some earlier time t_o by

$$\underset{\sim}{\underline{X}}(x,t) = \underset{\sim}{\underline{\Psi}}(x,t,t_o)\underset{\sim}{\underline{X}}(x,t_o) + \int_{t_o}^{t} \underset{\sim}{\underline{\Psi}}(x,t,\tau)\underset{\sim}{\underline{G}}(x,\tau)\underset{\sim}{\underline{U}}(x,\tau)d\tau, \quad t > t_o$$

$$\tag{5.12}$$

The distributed-parameter transition matrix $\underset{\sim}{\underline{\Psi}}(x,t,\tau)$ satisfies the partial

differential equation

$$\frac{\partial\underset{\sim}{\underline{\Psi}}(x,t,\tau)}{\partial t} = \underset{\sim}{\underline{F}}(x,t)\underset{\sim}{\underline{\Psi}}(x,t,\tau)$$

$$\underset{\sim}{\underline{\Psi}}(x,t,t) = \underline{I} \tag{5.13}$$

The covariance function of the state vector is

$$E[\underset{\sim}{\underline{X}}(x,t)\underset{\sim}{\underline{X}}^{\dagger}(y,\tau)] = \underset{\sim}{\underline{K}}_{X}(x,t;y,\tau) \tag{5.14}$$

Since

$$E[\underset{\sim}{\underline{X}}(x,t)\underset{\sim}{\underline{U}}^{\dagger}(y,\tau)] = \underline{0} , \quad \tau > t \tag{5.15}$$

$\overset{\sim}{\underline{K}}_X(x,t;y,\tau)$ can be written from (5.12) as

$$\overset{\sim}{\underline{K}}_X(x,t;y,\tau) = \begin{cases} \overset{\sim}{\underline{\Psi}}(x,t,\tau) \ \overset{\sim}{\underline{K}}_X(x,\tau;y,\tau) & t > \tau \\ \\ \\ \overset{\sim}{\underline{K}}_X(x,t;y,t)\overset{\sim}{\underline{\Psi}}^\dagger(y,\tau,t) & t < \tau \end{cases} \qquad (5.16)$$

Note that

$$\overset{\sim}{\underline{K}}_X^\dagger(x,t;y,\tau) = \overset{\sim}{\underline{K}}_X(y,\tau;x,t) \qquad (5.17)$$

The matrix $\overset{\sim}{\underline{K}}_X(x,t;y,t)$ in (5.16) is the solution of a partial differential equation. Differentiating $\overset{\sim}{\underline{K}}_X(x,t;y,t)$ gives

$$\frac{\partial \overset{\sim}{\underline{K}}_X(x,t;y,t)}{\partial t} = E\left[\frac{\partial \overset{\sim}{\underline{X}}(x,t)}{\partial t} \overset{\sim}{\underline{X}}^\dagger(y,t)\right] + E\left[\overset{\sim}{\underline{X}}(x,t) \frac{\partial \overset{\sim}{\underline{X}}^\dagger(y,t)}{\partial t}\right]$$

$$(5.18)$$

The first term on the right hand side of (5.18) is from (5.10)

$$E\left[\frac{\partial \overset{\sim}{\underline{X}}(x,t)}{\partial t} \overset{\sim}{\underline{X}}^\dagger(y,t)\right] = \overset{\sim}{\underline{F}}(x,t)\overset{\sim}{\underline{K}}_X(x,t;y,t) + \overset{\sim}{\underline{G}}(x,t)E[\overset{\sim}{\underline{U}}(x,t)\overset{\sim}{\underline{X}}^\dagger(y,t)]$$

$$(5.19)$$

From (5.11) and (5.12)

$$E[\overset{\sim}{\underline{X}}(x,t) \ \overset{\sim}{\underline{U}}^\dagger(y,t)] = \frac{1}{2} \overset{\sim}{\underline{G}}(x,t)\overset{\sim}{\underline{Q}}(x,y,t) \qquad (5.20)$$

Substitution of (5.20) in (5.19) and a similar procedure applied to the second term of (5.18) gives the desired equation

$$\frac{\partial \tilde{\underline{K}}_X(x,t;y,t)}{\partial t} = \tilde{\underline{F}}(x,t)\tilde{\underline{K}}_X(x,t;y,t) + \tilde{\underline{K}}_X(x,t;y,t)\tilde{\underline{F}}^\dagger(y,t)$$

$$+ \tilde{\underline{G}}(x,t)\tilde{\underline{Q}}(x,y,t)\tilde{\underline{G}}^\dagger(y,t) \qquad (5.21)$$

with an initial condition at t_o of

$$\tilde{\underline{K}}_X(x,t_o;y,t_o) = \tilde{\underline{P}}_o(x,y) \qquad (5.22)$$

From the assumption that

$$E[\tilde{\underline{x}}(x,t_o)\tilde{\underline{X}}^T(y,t_c)] = \underline{0}$$

it follows by an argument similar to Van Trees, Baggeroer, and Collins [15] that

$$E[\tilde{\underline{X}}(x,t)\tilde{\underline{X}}^T(y,\tau)] = \underline{0}$$

for all x,y,t, and τ. From (5.10) the covariance for the output vector is

$$\tilde{\underline{K}}_Y(x,t;y,\tau) = E[\tilde{Y}(x,t)\tilde{Y}^*(y,\tau)]$$

$$= \tilde{\underline{C}}(x,t)\tilde{\underline{K}}_X(x,t;y,\tau)\tilde{\underline{C}}^\dagger(y,\tau)$$

$$E[\tilde{Y}(x,t)\tilde{Y}(y,\tau)] = 0 \qquad (5.23)$$

The distributed-parameter state-variable model for the doubly-spread channel is given by (5.10) and (5.11).. The covariance function for the state vector is specified by (5.16) and the solution to (5.21) with the initial condition (5.22). The output covariance is given in (5.23).

Figure 5.1 shows a block diagram for the distributed-parameter state-variable model.

For the special case of the WSSUS channel the output covariance $\tilde{K}_Y(x,t;y,\tau)$ can be written in the form of (5.6). That is, $\tilde{Y}(x,t)$ is spatially white and temporally stationary. From (5.23) this condition is achieved if $\underline{\tilde{C}}(x,t)$ does not depend on t and if

$$\underline{\tilde{K}}_X(x,t;y,\tau) = \underline{\tilde{K}}(x,t-\tau)\delta(x-y) \tag{5.24}$$

For (5.24) to hold, inspection of (5.16) and (5.21) indicates that $\underline{\tilde{F}}(x,t)$, $\underline{\tilde{G}}(x,t)$ and $\underline{\tilde{Q}}(x,y,t)$ should be constant with respect to t, and furthermore that

$$\underline{\tilde{Q}}(x,y,t) = \underline{\tilde{Q}}(x)\delta(x-y) \tag{5.25}$$

Thus the distributed state-variable model for the WSSUS doubly-spread channel is

$$\frac{\partial \underline{\tilde{X}}(x,t)}{\partial t} = \underline{\tilde{F}}(x)\underline{\tilde{X}}(x,t) + \underline{\tilde{G}}(x)\underline{\tilde{U}}(x,t)$$

$$\underline{\tilde{Y}}(x,t) = \underline{\tilde{C}}(x)\underline{\tilde{X}}(x,t) \tag{5.26}$$

with

$$E[\underline{\tilde{U}}(x,t)\underline{\tilde{U}}^{\dagger}(y,\tau)] = \underline{\tilde{Q}}(x)\delta(x-y)\delta(t-\tau) \tag{5.26}$$

$$E[\underline{\tilde{U}}(x,t)\underline{\tilde{U}}^{T}(y,\tau)] = \underline{0} \tag{5.27}$$

The covariance matrices for the WSSUS model follow directly from the more general expressions above. From (5.6), (5.24) and (5.26)
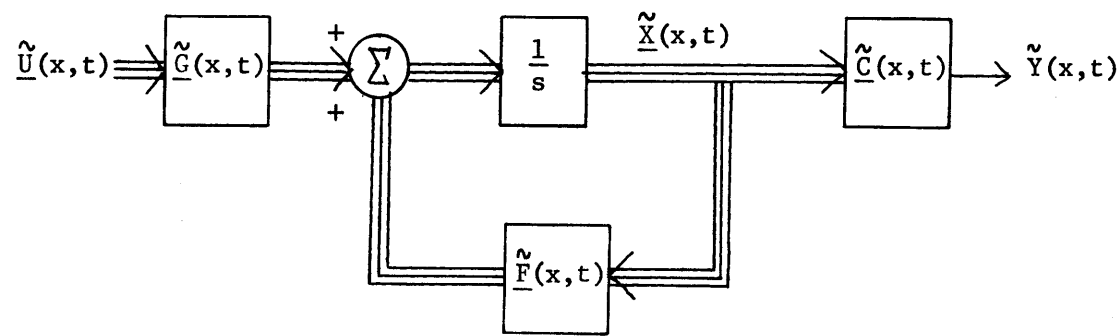
Figure 5.1. Distributed-parameter state-variable model for the doubly-spread channel.

$$\widetilde{\underline{K}}_{D}(x,\tau) = \widetilde{\underline{C}}(x)\widetilde{\underline{K}}(x,\tau)\widetilde{\underline{C}}^{\dagger}(x) \tag{5.28}$$

From (5.13) and (5.16)

$$\widetilde{\underline{K}}(x,\tau) = \begin{cases} \widetilde{\underline{\Theta}}(x,\tau)\widetilde{\underline{K}}_{o}(x), & \tau > 0 \\ \\ \widetilde{\underline{K}}_{o}(x)\widetilde{\underline{\Theta}}^{\dagger}(x,-\tau), & \tau < 0 \end{cases} \tag{5.29}$$

where $\widetilde{\underline{\Theta}}(x,\tau)$ is the solution to

$$\frac{\partial\widetilde{\underline{\Theta}}(x,t)}{\partial t} = \widetilde{\underline{F}}(x)\widetilde{\underline{\Theta}}(x,t)$$

$$\widetilde{\underline{\Theta}}(x,0) = \underline{I} \tag{5.30}$$

The matrix $\widetilde{\underline{K}}_{o}(x)$ is the steady-state solution of (5.21)

$$\underline{0} = \widetilde{\underline{F}}(x)\widetilde{\underline{K}}_{o}(x) + \widetilde{\underline{K}}_{o}(x)\widetilde{\underline{F}}^{\dagger}(x) + \widetilde{\underline{G}}(x)\widetilde{\underline{Q}}(x)\widetilde{\underline{G}}^{\dagger}(x) \tag{5.31}$$

The scattering function for the WSSUS channel is defined by (5.9). $\widetilde{S}(x,f)$ is positive and real for all x and f, since $\widetilde{\underline{Q}}(x)$ is Hermetian with a non-negative definite real part.

For an example of the WSSUS channel model, consider a first order system for (5.26)

$$\widetilde{\underline{F}}(x) = -\widetilde{k}(x) = -k_{r}(x) - jk_{i}(x)$$

$$\widetilde{\underline{G}}(x) = \widetilde{\underline{C}}(x) = 1$$

$$\widetilde{\underline{Q}}(x) = Q(x) \tag{5.32}$$

with

$$Q(x) \geq 0$$

$$k_r(x) > 0 \tag{5.33}$$

From (5.29), (5.30), and (5.31)

$$\underline{\tilde{\theta}}(x,\tau) = \exp[-k_r(x) |\tau| -jk_i(x)\tau]$$

$$\underline{\tilde{K}}_o(x) = \frac{Q(x)}{2k_r(x)} \tag{5.34}$$

Thus

$$\tilde{K}_D(x,\tau) = \frac{Q(x)}{2k_r(x)} \quad \exp[-k_r(x)|\tau| -jk_i(x)\tau] \tag{5.35}$$

and the scattering function is

$$\tilde{S}(x,f) = \frac{Q(x)}{[2\pi f + k_i(x)]^2 + k_r^2(x)} \tag{5.36}$$

The scattering function in (5.36), considered as a function of frequency at any value of x, is a one-pole spectrum centered at $f_o = k_i(x)/2\pi$ and 3 dB points $\pm k_r(x)/2\pi$ about f_o. Except for the constraints of (5.33), $Q(x)$ and $\tilde{k}(x)$ are arbitrary. This permits considerable flexibility in the choice of $\tilde{S}(x,f)$, even for this first order model. For instance if $k_i(x)$ is linearly proportioned to x, then $\tilde{S}(x,f)$ is sheared in the $x - f$ plane. Also, $Q(x)$ can be chosen so that $\tilde{S}(x,f)$ is multimodal in the x direction. Figure 5.2 shows several examples of possible scattering functions for the first order model.
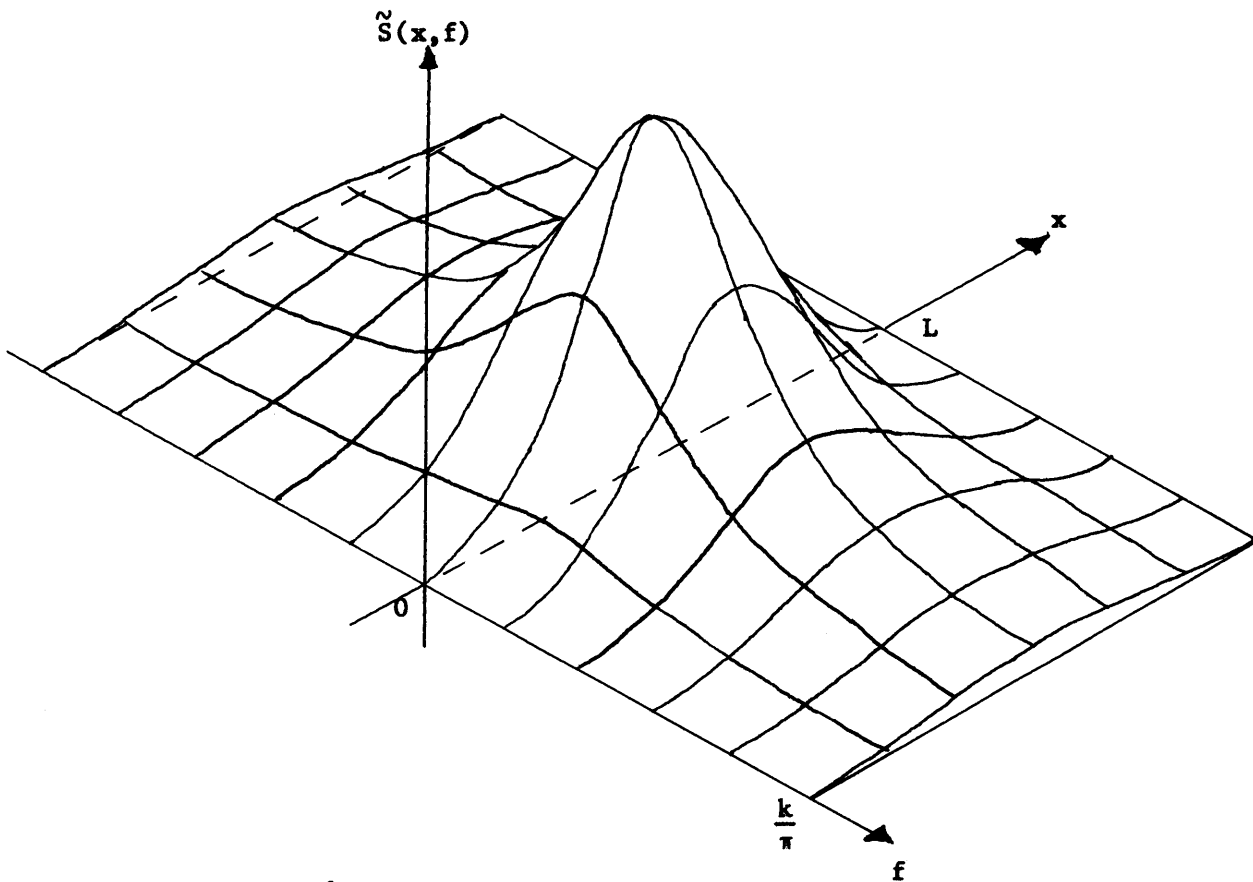
$$\tilde{Q}(x) = \begin{cases} 1 - \cos \dfrac{2\pi x}{L} & , \quad 0 \le x \le L \\[2em] \quad 0 & \quad \text{elsewhere} \end{cases}$$

$$\tilde{k}(x) = k(1 - \frac{1}{2} \sin \frac{\pi x}{L})$$

Figure 5.2a. Example of a scattering function for a first order model.
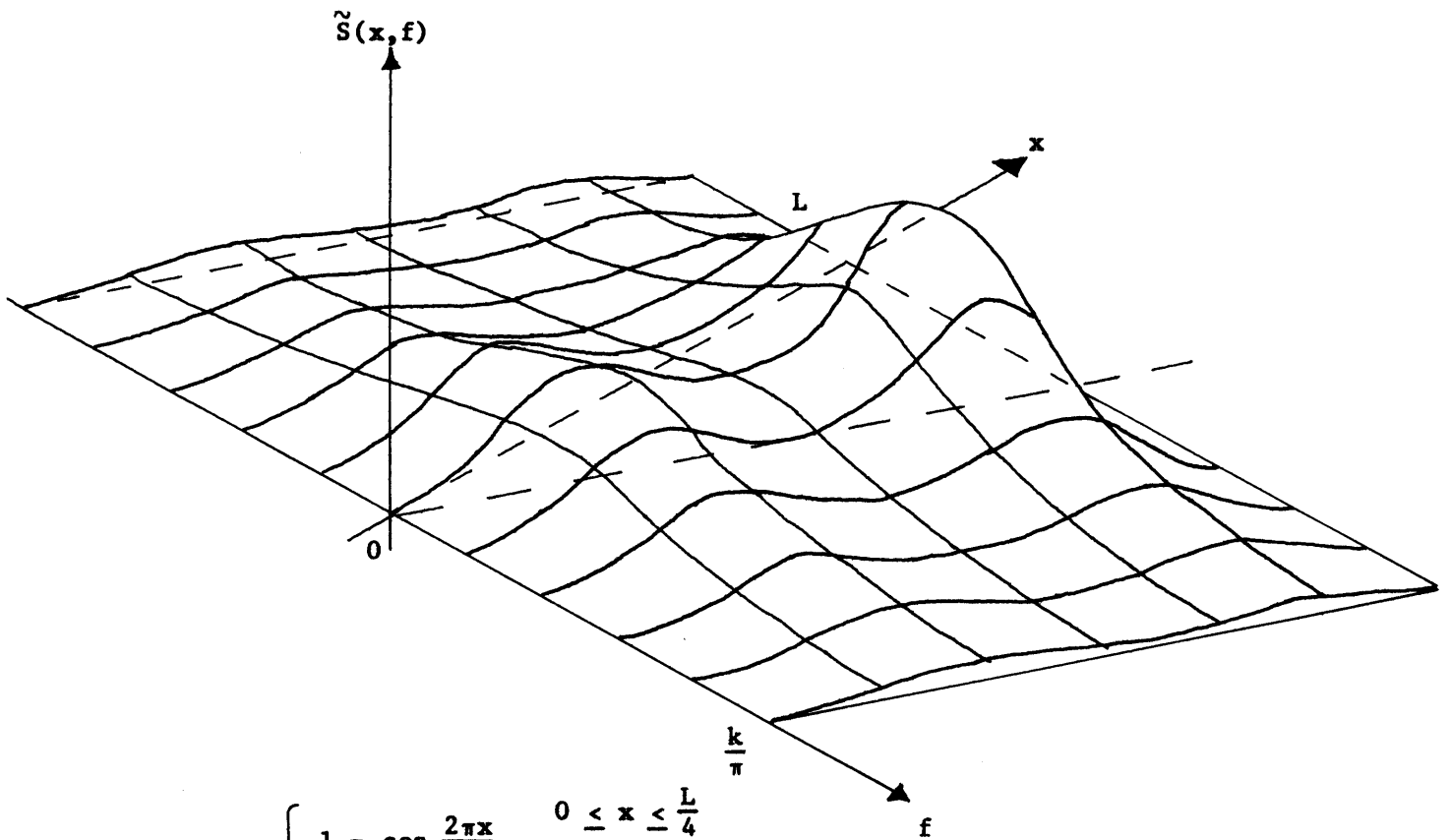
$$\tilde{Q}(x) = \begin{cases} 1 - \cos \dfrac{2\pi x}{L}, & \begin{array}{l} 0 \le x \le \dfrac{L}{4} \\[2mm] \dfrac{3L}{4} \le x \le L \end{array} \\[6mm] 2 + \cos \dfrac{\pi x}{L}, & \dfrac{L}{4} \le x \le \dfrac{3L}{4} \\[4mm] 0 & \text{elsewhere} \end{cases}$$

$$\tilde{k}(x) = k\left(1 - \frac{x}{2L}\right) - j\,\frac{3kx}{5\pi L}$$

Figure 5.2b. Example of a scattering function for a first order model.

The first order case above indicates that the class of scattering functions which can be described by the model of (22) are those for which $\tilde{S}(x,f)$ is a rational function in f. The poles and zeros of this particular function may depend on x in an arbitrary manner, except for conditions such as those of (30). Thus higher order distributed-parameter state-variable models permit more degrees of freedom in the specification of the scattering function. For example, a $\tilde{S}(x,f)$ which exhibits multimodal behavior in f can be obtained from a second or higher order model.

C. A Realizable Detector and its Performance

This section considers the implementation of the optimum receiver for the transmission of known signals over doubly-spread channels which are described by the distributed-parameter state-variable model presented in the previous section. Figure 1.4 shows a realizable version of the optimum receiver branch which can be constructed if the minimum mean-square error (MMSE) realizable estimate of $\tilde{s}(t)$ is available. This section derives the MMSE realizable estimator for the doubly-spread channel output when the distributed-parameter state-variable model of Section B is valid.

The performance of the optimum receiver for the binary detection or orthogonal communication problems can be computed using the techniques of Chapter II. The moment-generating functions necessary for these computations all involved the Fredholm determinant for the random process $\tilde{s}(t)$. The Fredholm determinant can be expressed in terms of the MMS realizable filtering error

$$\tilde{\xi}_P(t) = E[|\tilde{s}(t) - \hat{\tilde{s}}(t)|^2] \tag{5.37}$$

A by-product of the MMSE realizable estimator derivation of this section is an equation for $\tilde{\xi}_P(t)$. Solving this equation permits evaluation of the performance of the doubly-spread channel optimum receiver.

The MMSE realizable estimate of $\tilde{s}(t)$ is related to the MMSE realizable estimate of the channel output $\tilde{Y}(x,t)$ by

$$\hat{\tilde{s}}(t) = \int_{-\infty}^{\infty} \tilde{f}(t-x) \, \hat{\tilde{Y}}(x,t) dt \tag{5.38}$$

The estimate $\hat{\tilde{Y}}(x,t)$ can be obtained from the MMSE realizable estimate of the state vector $\underline{\tilde{X}}(x,t)$ in the distributed-parameter state-variable model of (5.10)

$$\hat{\tilde{Y}}(x,t) = \underline{\tilde{C}}(x,t)\underline{\hat{\tilde{X}}}(x,t) \tag{5.39}$$

Thus

$$\hat{\tilde{s}}(t) = \int_{-\infty}^{\infty} \tilde{f}(t - x) \, \underline{\tilde{C}}(x,t)\underline{\hat{\tilde{X}}}(x,t) dx \tag{5.40}$$

The expected value of the state vector estimation error matrix is denoted by

$$\underline{\tilde{\xi}}(x,y,t) \overset{\Delta}{=} E\left\{ [\underline{\tilde{X}}(x,t) - \underline{\hat{\tilde{X}}}(x,t)][\underline{\tilde{X}}^{\dagger}(x,t) - \underline{\hat{\tilde{X}}}^{\dagger}(x,t)] \right\} \tag{5.41}$$

The error $\tilde{\xi}_P(t)$ in (5.37) is then given by

$$\tilde{\xi}_P(t) = \int_{-\infty}^{\infty} \int_{-\infty}^{\infty} \tilde{f}(t-\sigma)\underline{\tilde{C}}(\sigma,t)\underline{\tilde{\xi}}(\sigma,\alpha,t)\underline{\tilde{C}}^{\dagger}(\alpha,t)\tilde{f}^*(t-\alpha)d\sigma d\alpha \tag{5.42}$$

The MMSE realizable estimate of $\underline{\tilde{X}}(x,t)$ is given by the linear

operation or $\tilde{r}(t)$

$$\overset{\wedge}{\underline{X}}(x,t) - \int\limits_{T_0}^{t} \overset{\sim}{\underline{h}}_0(x,t,\sigma)\ \overset{\sim}{\underline{r}}(\sigma)d\sigma, \qquad t > T_0 \qquad (5.43)$$

where $\overset{\sim}{\underline{h}}_0(x,t,\tau)$ is the n x 1 realizable matrix impulse response which minimizes $\overset{\sim}{\underline{\xi}}(x,y,t)$ in (5.41). The details of the derivation of the estimator structure are given in Appendix III. The steps in the derivation follow those of Van Trees [20] for the lumped-parameter state-variable estimation problem. The result is an estimator structure which is a modification of one given by Tzafestas and Nightingale.[33].

The results of Appendix III are that the MMSE realizable estimate of $\overset{\sim}{\underline{X}}(x,t)$ is the solution of the vector partial differential equation

$$\frac{\partial \overset{\wedge}{\underline{X}}(x,t)}{\partial t} = \overset{\sim}{\underline{F}}(x,t)\overset{\wedge}{\underline{X}}(x,t) + \overset{\sim}{\underline{h}}_0(x,t,t)[\tilde{r}(t) - \hat{s}(t)] \qquad (5.44)$$

where

$$\overset{\sim}{\underline{h}}_0(x,t,t) = \frac{1}{N_0} \int\limits_{-\infty}^{\infty} \overset{\sim}{\underline{\xi}}(x,\sigma,t)\overset{\sim}{\underline{C}}{}^{\dagger}(\sigma,t)\tilde{f}{}^{*}(\sigma-t)d\sigma \qquad (5.45)$$

$$\hat{s}(t) = \int\limits_{-\infty}^{\infty} \tilde{f}(t-\sigma)\overset{\sim}{\underline{C}}(\sigma,t)\overset{\wedge}{\underline{X}}(\sigma,t)d\sigma \qquad (5.46)$$

$$\overset{\wedge}{\underline{X}}(x,T_0) = \underline{0} \qquad (5.47)$$

In addition, the covariance matrix $\overset{\sim}{\underline{\xi}}(x,y,t)$ is the solution of a matrix partial differential equation of the Ricatti type

$$\frac{\partial \overset{\sim}{\underline{\xi}}(x,y,t)}{\partial t} = \overset{\sim}{\underline{F}}(x,t)\overset{\sim}{\underline{\xi}}(x,y,t) + \overset{\sim}{\underline{\xi}}(x,y,t)\overset{\sim}{\underline{F}}{}^{\dagger}(y,t) + \overset{\sim}{\underline{G}}(x,t)\overset{\sim}{\underline{Q}}(x,y,t)\overset{\sim}{\underline{G}}{}^{\dagger}(y,t)$$

$$- \frac{1}{N_0} \left[\int\limits_{-\infty}^{\infty} \overset{\sim}{\underline{\xi}}(x,\sigma,t)\overset{\sim}{\underline{C}}{}^{\dagger}(\sigma,t)\tilde{f}{}^{*}(t-\sigma)d\sigma \right] \left[\int\limits_{-\infty}^{\infty} \tilde{f}(t-\alpha)\overset{\sim}{\underline{C}}(\alpha,t)\overset{\sim}{\underline{\xi}}(\alpha,y,t)d\alpha \right] \quad (5.48)$$

with initial conditions

$$\tilde{\underline{\xi}}(x,y,T_o) = \underline{\tilde{P}}_o(x,y) \tag{5.49}$$

Note that (5.48) may be considered an ordinary differential equation with x and y as parameters. Figure 5.3 shows the estimator structure.

For the special case of the WSSUS channel model, the estimator gain matrix $\underline{\tilde{F}}(x,t)$ is replaced by $\underline{\tilde{F}}(x)$. The equation for $\tilde{\underline{\xi}}(x,y,t)$ becomes

$$\frac{\partial \tilde{\underline{\xi}}(x,y,t)}{\partial t} = \underline{\tilde{F}}(x)\tilde{\underline{\xi}}(x,y,t) + \tilde{\underline{\xi}}(x,y,t)\underline{\tilde{F}}^{\dagger}(y) + \underline{\tilde{G}}(x)\underline{\tilde{Q}}(x)\underline{\tilde{G}}^{\dagger}(y)\delta(x-y)$$

$$- \frac{1}{N_o}\left[\int_{-\infty}^{\infty}\tilde{\underline{\xi}}(x,\sigma,t)\underline{\tilde{C}}^{\dagger}(\sigma)\tilde{\underline{r}}^{*}(t-\sigma)d\sigma\right]\left[\int_{-\infty}^{\infty}\tilde{\underline{r}}(t-\alpha)\underline{\tilde{C}}(\alpha)\tilde{\underline{\xi}}(\alpha,y,t)d\alpha\right] \tag{5.50}$$

with

$$\tilde{\underline{\xi}}(x,y,T_o) = \underline{\tilde{K}}_o(x)\delta(x-y) \tag{5.51}$$

$\underline{\tilde{K}}_o(x)$ is specified by (5.31).

An alternate set of equations for $\tilde{\underline{\xi}}(x,y,t)$ can be derived for the WSSUS case by assuming the solution of (5.50) has the form

$$\tilde{\underline{\xi}}(x,y,t) = \tilde{\underline{\xi}}_o(x,t)\delta(x-y) + \tilde{\underline{p}}(x,y,t) \tag{5.52}$$

Substitution of (5.52) into (5.50) gives

$$\tilde{\underline{\xi}}_o(x,t) = \underline{\tilde{K}}_o(x)$$

$$\underline{\tilde{h}}_o(x,t,t) = \frac{1}{N_o}\underline{\tilde{K}}_o(x)\underline{\tilde{C}}^{\dagger}(x)\tilde{\underline{r}}^{*}(t-x) + \frac{1}{N_o}\int_{-\infty}^{\infty}\tilde{\underline{p}}(x,\sigma,t)\underline{\tilde{C}}^{\dagger}(\sigma)\tilde{\underline{r}}^{*}(t-\sigma)d\sigma \tag{5.53}$$
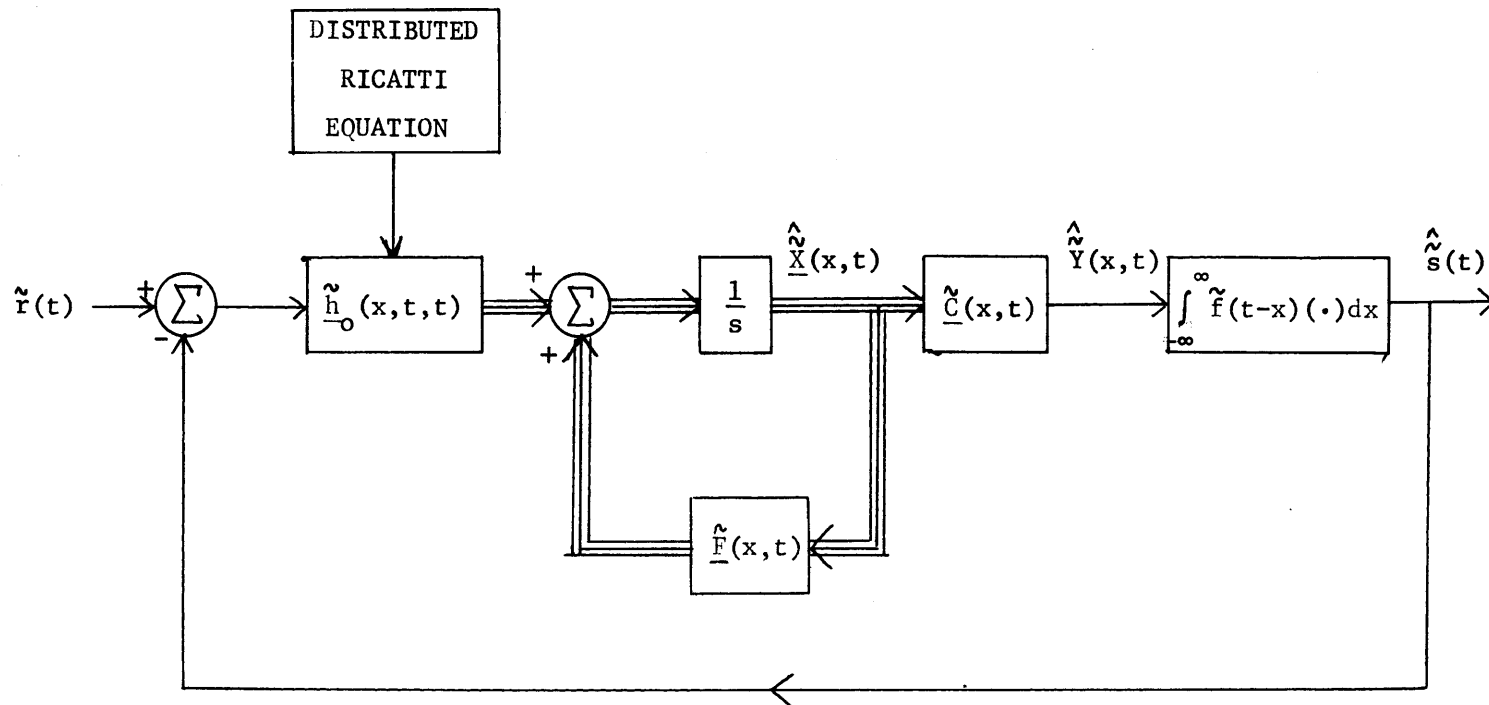
Figure 5.3. Realizable MMSE estimator for the doubly-spread channel distributed-parameter state-variable model.

where $\tilde{\underline{p}}(x,y,t)$ is the solution to

$$\frac{\partial \tilde{\underline{p}}(x,y,t)}{\partial t} = \hat{\underline{F}}(x)\tilde{\underline{p}}(x,y,t) + \tilde{\underline{p}}(x,y,t)\hat{\underline{F}}^{\dagger}(y)$$

$$- \frac{1}{N_o} [\hat{\underline{K}}_o(x)\underline{\hat{C}}^{\dagger}(x)\hat{F}^*(t-x) + \int_{-\infty}^{\infty} \tilde{\underline{p}}(x,\sigma,t)\underline{\hat{C}}^{\dagger}(\sigma)\hat{F}^*(t-\sigma)d\sigma]$$

$$\cdot [\hat{F}(t-y)\underline{\hat{C}}(y)\hat{\underline{K}}_o(y) + \int_{-\infty}^{\infty} \hat{F}(t-\sigma)\underline{\hat{C}}(\sigma)\tilde{\underline{p}}(\sigma,y,t)d\sigma] \qquad (5.54)$$

$$\tilde{\underline{p}}(x,y,T_o) = \underline{0} \qquad (5.55)$$

The formulation of (5.52-.55) is more attractive for numerical solution because the effect of the spatial impulse has been removed from (5.50).

The MMSE realizable estimator for $\tilde{s}(t)$ is given by (5.46). This allows the construction of the optimum receiver configuration in Figure 1.4, which can be used in branches of the doubly-spread channel optimum receivers for the detection or communication problems. The distributed parameter state-variable estimator of Figure 5.3 is realizable in a temporal sense, but it is not clear how to implement physically the distributed-parameter system. The next section considers this problem in more detail.

A by-product of the optimum receiver above is the error covariance matrix $\tilde{\underline{\xi}}(x,y,t)$. By (5.42) the MMS estimation error for $\tilde{s}(t)$ is also available. This implies that the performance of the optimum receivers can be found. Equation (2.85) relates this filtering error to the Fredholm determinant. The various moment-

generating functions which are used for computing the optimum receiver

error probabilities can all be expressed in terms of Fredholm determinants.

In order to find the error probabilities it is necessary to

solve (5.48),(5.50), or (5.52-.54) for $\overset{\sim}{\underline{\xi}}(x,y,t)$. In even the simplest

cases an analytic solution is difficult. Since these equations can be

considered ordinary differential equations with parameters x and y,

they can be numerically integrated, however. Thus one approach is to

obtain $\overset{\sim}{\underline{\xi}}(x,y,t)$ at a set of discrete points, (x_i,y_i,t_i) by numerical

integration of (5.48). Such an approach may become rapidly impractical

as the number of points in the grid grows and the dimension of $\overset{\sim}{\underline{\xi}}(x,y,t)$

increases. The next section discusses this issue in more detail.

It is worthwhile to investigate the form of the estimator in

Figure 5.3 as the model parameters are adjusted towards the limiting

doppler-spread and delay-spread cases. For the doppler-spread channel

it is sufficient to let $\overset{\sim}{\underline{Q}}(x,y,t)$, the covariance of the driving noise in

(5.10), become impulsive in x and y

$$\overset{\sim}{\underline{Q}}(x,y,t) = \underline{Q}\delta(x)\delta(y) \qquad\qquad (5.56)$$

Then the error covariance $\overset{\sim}{\underline{\xi}}(x,y,t)$ is impulsive in x and y, and both

the state variable model of (5.10) and the estimator of Figure 5.3

reduce to lumped-parameter models. The estimator of Figure 3.2 results.

For the delay-spread case it is sufficient to consider the

first order distributed-parameter state-variable model. The gain $\tilde{F}(x,t)$

is allowed to go to zero provided that $\tilde{Q}(x,\mathbf{y},t)$ is chosen such that the

average energy in $\tilde{s}(t)$ over the observation interval remains constant.

The result is the doppler spread model. In the diagram of Figure 5.3,

$\overset{\text{v}}{\underline{F}}(x,t)$ is set to zero.

D. A Modal Technique for Finding the Optimum Receiver Performance

The previous section derived a partial differential equation for the error covariance matrix $\overset{\text{v}}{\underline{\xi}}(x,y,t)$ which is needed for the computation of the doubly-spread channel optimum receiver error probabilities. It was pointed out that one way to solve this equation is to integrate it numerically on a grid in the x-y plane. As the dimension of the state vector increases, this approach rapidly becomes unwieldy. It would be useful to have a more efficient way of computing $\overset{\text{v}}{\underline{\xi}}(x,y,t)$

This section proposes a modal approach to the problem. Such approaches are commom in distributed-parameter systems [29,33,34]. Here the method involves expanding the state vector estimates and the covariance matrix in orthogonal series in their spatial variables.

$$\overset{\wedge}{\underline{X}}(x,t) = \sum_{i=1}^{\infty} \overset{\wedge}{\underline{X}}_i(t)\overset{\text{v}}{\phi}_i(x) \tag{5.57}$$

$$\overset{\text{v}}{\underline{\xi}}(x,y,t) = \sum_{i=1}^{\infty} \sum_{j=1}^{\infty} \overset{\text{v}}{\underline{\xi}}_{ij}(t)\overset{\text{v}}{\phi}_i(x)\phi_j^*(y) \tag{5.58}$$

The set $\{\phi_i(x)\}$ is an arbitrary complete orthonormal set over the interval $[L_o, L_f]$

$$\int_{L_o}^{L_f} \overset{\text{v}}{\phi}_i(x)\overset{\text{v}*}{\phi}_j(x)dx = \delta_{ij} \ . \tag{5.59}$$

How to choose the set $\{\overset{\text{v}}{\phi}_i(x)\}$ will be discussed later. The time-varying

coefficients in (5.57) are

$$\hat{\underline{X}}_i(t) = \int_{L_o}^{L_f} \hat{\underline{X}}(x,t) \overset{\vee}{\phi}{}^*_i(x) dx \qquad (5.60)$$

$$\overset{\vee}{\underline{\xi}}_{ij}(t) = \int_{L_o}^{L_f} \int_{L_o}^{L_f} \overset{\vee}{\underline{\xi}}(x,y,t) \overset{\vee}{\phi}{}^*_i(x) \overset{\vee}{\phi}_j(y) dx dy \qquad (5.61)$$

The series of (5.58) is substituted into the partial differential

equation for the error covariance, (5.48), to give

$$\sum_{i,j} \frac{d\overset{\vee}{\underline{\xi}}_{ij}(t)}{dt} \overset{\vee}{\phi}_i(x) \overset{\vee}{\phi}{}^*_j(y) = \overset{\vee}{\underline{F}}(x,t) \sum_{i,j} \overset{\vee}{\underline{\xi}}_{ij}(t) \overset{\vee}{\phi}_i(x) \overset{\vee}{\phi}{}^*_j(y)$$

$$+ \sum_{i,j} \overset{\vee}{\underline{\xi}}_{ij}(t) \overset{\vee}{\phi}_i(x) \overset{\vee}{\phi}{}^*_j(y) \overset{\vee}{\underline{F}}{}^\dagger(y,t) + \overset{\vee}{\underline{G}}(x,t) \overset{\vee}{\underline{Q}}(x,y,t) \overset{\vee}{\underline{G}}{}^\dagger(y;t)$$

$$- \frac{1}{N_o} \left[\sum_{i,j} \overset{\vee}{\underline{\xi}}_{ij}(t) \overset{\vee}{\phi}_i(x) \int_{-\infty}^{\infty} \overset{\vee}{\phi}{}^*_j(\sigma) \overset{\vee}{\underline{C}}{}^\dagger(\sigma,t) \overset{\vee}{f}{}^*(t-\sigma) d\sigma \right]$$

$$\cdot \left[\sum_{i,j} \int_{-\infty}^{\infty} \overset{\vee}{\phi}_i(\alpha) \overset{\vee}{f}(t-\alpha) \overset{\vee}{\underline{C}}(\alpha,t) d\alpha \; \overset{\vee}{\underline{\xi}}_{ij}(t) \overset{\vee}{\phi}{}^*_j(y) \right] \qquad (5.62)$$

Multiplying both sides of (5.62) by $\overset{\vee}{\phi}{}^*_k(x) \overset{\vee}{\phi}_m(y)$ and integrating over x

and y yields a set of ordinary differential equations for the coefficient

matrices $\overset{\vee}{\underline{\xi}}_{ij}(t)$

$$\frac{d\tilde{\underline{\xi}}_{ij}(t)}{dt} = \sum_k \tilde{\underline{a}}_{ik}(t)\, \tilde{\underline{\xi}}_{kj}(t) + \sum_k \tilde{\underline{\xi}}_{ik}(t)\tilde{\underline{a}}_{kj}^\dagger(t) + \tilde{\underline{q}}_{ij}(t)$$

$$- \frac{1}{N_o}\left[\sum_k \tilde{\underline{\xi}}_{ik}(t)\tilde{\underline{b}}_k^\dagger(t)\right]\left[\sum_k \tilde{\underline{b}}_k(t)\, \tilde{\underline{\xi}}_{kj}(t)\right] \tag{5.63}$$

where

$$\tilde{\underline{a}}_{ij}(t) = \int_{L_o}^{L_f} \tilde{\underline{F}}(x,t)\tilde{\phi}_i^*(x)\tilde{\phi}_j(x)\,dx \tag{5.64}$$

$$\tilde{\underline{q}}_{ij}(t) = \int_{L_o}^{L_f}\int_{L_o}^{L_f} \tilde{\underline{G}}(x,t)\tilde{\underline{Q}}(x,y,t)\tilde{\underline{G}}^\dagger(y,t)\tilde{\phi}_i^*(x)\tilde{\phi}_j(y)\,dx\,dy \tag{5.65}$$

$$\tilde{\underline{b}}_i(t) = \int_{L_o}^{L_f} \tilde{\phi}_i(x)\tilde{F}(t-x)\tilde{\underline{G}}(x,t)\,dx \tag{5.66}$$

The initial conditions for (5.63) are given by

$$\tilde{\underline{\xi}}_{ij}(T_o) = \int_{L_o}^{L_f}\int_{L_o}^{L_f} \tilde{\underline{P}}_o(x,y)\tilde{\phi}_i^*(x)\tilde{\phi}_j(y)\,dx\,dy$$

$$\triangleq \tilde{\underline{P}}_{oij} \tag{5.67}$$

The orthogonal expansion of (5.58) has reduced the partial differential equation for $\underline{\xi}(x,y,t)$ to an infinite set of ordinary differential equations. If the orthonormal set $\{\phi_i(x)\}$ is truncated

at the Nth member, then the system of equations (5.63) is finite. Solution of the finite set of ordinary differential equations provides an approximation for $\overset{\vee}{\xi}(x,y,t)$. The number of terms, N, is increased until $\overset{\vee}{\xi}(x,y,t)$ converges. It is possible, of course, that there may not be convergence in some situations.

The truncated set of differential equations (5.63) can be more compactly described by defining the partitioned matrices

$$\overset{\vee}{\underline{\Sigma}}(t) = \begin{bmatrix} \overset{\vee}{\underline{\xi}}_{11}(t) & \overset{\vee}{\underline{\xi}}_{12}(t) & \cdots & \overset{\vee}{\underline{\xi}}_{1N}(t) \\ & & \vdots & \\ \overset{\vee}{\underline{\xi}}_{N1}(t) & \overset{\vee}{\underline{\xi}}_{N2}(t) & & \overset{\vee}{\underline{\xi}}_{NN}(t) \end{bmatrix} \tag{5.68}$$

$$\overset{\vee}{\underline{A}}(t) = [\overset{\vee}{\underline{a}}_{ij}(t)]$$

$$\overset{\vee}{\underline{Q}}(t) = [\overset{\vee}{\underline{q}}_{ij}(t)]$$

$$\overset{\vee}{\underline{B}}(t) = [\overset{\vee}{\underline{b}}_1(t), \overset{\vee}{\underline{b}}_2(t), \ldots, \overset{\vee}{\underline{b}}_N(t)]$$

$$\overset{\vee}{\underline{P}}_o = [\overset{\vee}{\underline{P}}_{oij}]$$

Then (5.63) and (5.67) are given by

$$\frac{d}{dt}\overset{\vee}{\underline{\Sigma}}(t) = \overset{\vee}{\underline{A}}(t)\overset{\vee}{\underline{\Sigma}}(t) + \overset{\vee}{\underline{\Sigma}}(t)\overset{\vee}{\underline{A}}(t) + \overset{\vee}{\underline{Q}}(t) - \frac{1}{N_o}\overset{\vee}{\underline{\Sigma}}(t)\overset{\vee}{\underline{B}}^\dagger(t)\overset{\vee}{\underline{B}}(t)\overset{\vee}{\underline{\Sigma}}(t)$$

$$\overset{\vee}{\underline{\Sigma}}(T_o) = \overset{\vee}{\underline{P}}_o \tag{5.69}$$

The matrix differential equation (5.69) has the form of the

error covariance differential equation for a finite state, lumped-

parameter state variable estimation problem. The solution of this

equation has received considerable attention [20,24,32]. On the other

hand, the form of (5.48) is unfamiliar. With (5.48) the spatial behavior

of $\underset{\sim}{\xi}(x,y,t)$ must be computed at many more points (x,y) than the number

of terms (submatrices) required in (5.69). This suggests that solving

(5.69) is a considerably more efficient approach than integrating (5.48).

An approximation for the estimator equation can be derived by

applying the expansion of (5.57) to (5.44) and (5.46)

$$\sum_i \frac{d\underset{\sim}{\hat{X}}_i(t)}{dt} \underset{\sim}{\phi}_i(x) = \sum_i \underset{\sim}{F}(x,t)\underset{\sim}{\hat{\underline{X}}}_i(t)\phi_i(x) + \underset{\sim}{\hat{h}}_o(x,t,t)[\underset{\sim}{r}(t)-\hat{\underset{\sim}{s}}(t)] \quad (5.70)$$

$$\hat{\underset{\sim}{s}}(t) = \sum_i (\int_{-\infty}^{\infty} \underset{\sim}{f}(t-\sigma)\underset{\sim}{\underline{C}}(\sigma,t)\underset{\sim}{\phi}_i(\sigma)d\sigma)\underset{\sim}{\hat{\underline{X}}}_i(t)$$

$$= \sum_i \underset{\sim}{b}_i(t)\underset{\sim}{\hat{\underline{X}}}_i(t) \quad (5.70a)$$

Multiplying (5.70) by $\phi_j^*(x)$ and integrating over x gives

$$\frac{d\underset{\sim}{\hat{X}}_i(t)}{dt} = \sum_k \underset{\sim}{a}_{ik}(t)\underset{\sim}{\hat{X}}_k(t) + \int_{L_o}^{L_f} \underset{\sim}{h}_o(x,t,t)\underset{\sim}{\phi_i^*}(x)dx)[\underset{\sim}{r}(t) - \sum_k \underset{\sim}{b}_k(t)\underset{\sim}{\hat{X}}_k(t)]$$

$$(5.71)$$

From (5.74)

$$\int_{L_o}^{L_f} \underset{\sim}{h}_o(x,t,t)\underset{\sim}{\phi_i^*}(x)dx = \sum_k \underset{\sim}{\xi}_{ik}(t) \underset{\sim}{b}_k^\dagger(t) \quad (5.72)$$

The estimator equation of (5.44) has been reduced to an infinite set of ordinary linear differential equations, (5.71). If the series (5.57) is truncated to N terms and the composite vector $\underline{\tilde{X}}(t)$ is defined

$$\underline{\overset{\wedge}{\tilde{X}}}(t) \;=\; \begin{bmatrix} \underline{\overset{\wedge}{\tilde{X}}}_1(t) \\ \cdot \\ \cdot \\ \cdot \\ \underline{\overset{\wedge}{\tilde{X}}}_N(t) \end{bmatrix} \tag{5.73}$$

then the approximate set of equations can be written as

$$\frac{d}{dt}\,\underline{\overset{\wedge}{\tilde{X}}}(t) \;=\; \underline{\tilde{A}}(t)\underline{\overset{\wedge}{\tilde{X}}}(t) \;+\; \frac{1}{N_o}\,\underline{\overset{\sim}{\Sigma}}(t)\underline{\tilde{B}}^{\dagger}(t)[\tilde{r}(t) - \overset{\wedge}{\tilde{s}}(t)] \tag{5.74}$$

$$\overset{\wedge}{\tilde{s}}(t) \;\overset{\sim}{=}\; \underline{\tilde{B}}(t)\underline{\overset{\wedge}{\tilde{X}}}(t) \tag{5.75}$$

The approximate estimate of $\tilde{X}(x,t)$ is

$$\underline{\overset{\wedge}{\tilde{X}}}(x,t) \;\overset{\sim}{=}\; \underline{\overset{\sim}{\Phi}}(x)\underline{\overset{\wedge}{\tilde{X}}}(t) \tag{5.76}$$

$$\underline{\overset{\sim}{\Phi}}(x) \;=\; [\overset{\sim}{\phi}_1(x),\; \ldots,\; \overset{\sim}{\phi}_N(x)] \tag{5.77}$$

The covariance matrix $\underline{\overset{\sim}{\xi}}(x,y,t)$ is approximately

$$\underline{\overset{\sim}{\xi}}(x,y,t) \;\overset{\sim}{=}\; \underline{\overset{\sim}{\Phi}}(x)\underline{\overset{\sim}{\Sigma}}(t)\underline{\overset{\sim}{\Phi}}^{\dagger}(y) \tag{5.78}$$

and the estimation error $\overset{\sim}{\xi}_p(t)$ is, from (5.42)

$$\overset{\sim}{\xi}_p(t) \;\overset{\sim}{=}\; \underline{\tilde{B}}(t)\underline{\overset{\sim}{\Sigma}}(t)\underline{\tilde{B}}^{\dagger}(t) \tag{5.79}$$

The expansions of (5.57) and (5.58) have led to ordinary dif-
ferential equation approximations for the partial differential equations
which specify the optimum state vector estimator and the error covariance
matrix. The form of the resulting equations, (5.69), (5.74) and (5.75)
is exactly that assumed by the appropriate equations in a lumped-parameter
state-variable. This suggests that the truncated orthogonal expansions
of (5.57) and (5.58) effectively reduce the doubly-spread channel model
to a finite state system. To see this, it is instructive to expand the
state vector $\underline{\tilde{X}}(x,t)$ in (5.10) in a similar series over $[L_o, L_f]$

$$\underline{\tilde{X}}(x,t) = \sum_{i=1}^{\infty} \underline{\tilde{X}}_i(t) \tilde{\phi}_i(x) \tag{5.80}$$

$$\underline{\tilde{X}}_i(t) = \int_{L_o}^{L_f} \underline{\tilde{X}}(x,t) \phi_i^*(x) dx \tag{5.81}$$

If this series is truncated to M terms and substituted in (5.10) and
(5.2) the resulting approximation for $\tilde{r}(t)$ is

$$\tilde{r}(t) \cong \underline{\tilde{B}}(t) \underline{\tilde{X}}(t) + \tilde{w}(t) \tag{5.82}$$

where $\underline{\tilde{x}}(t)$ is defined by adjoining the vectors $\underline{\tilde{x}}_i(t)$, $i=1,\ldots,N$. If
one starts with the finite-state model of (5.82) and finds the MMSE
estimator for $\underline{\tilde{X}}(t)$, the result is just the set of equations derived
above.

Note that if the performance of the optimum delay-spread channel
receivers is desired, $\tilde{\xi}_p(t)$ in (5.79) is all that is necessary for the
computations. The matrix $\underline{\tilde{\Sigma}}(t)$ is available from (5.69). The number

of terms in the approximation may be increased until $\overset{\vee}{\xi}_p(t)$ converges

to a desired accuracy.

Another important observation is that (5.75) provides a way of

approximately implementing the distributed-parameter receiver of Figure

5.3. The finite state equations of (5.74) can be integrated in real

time, since $\overset{\vee}{\underline{\Sigma}}(t)$ can be precomputed. An indication of the dimensions

of the system (5.74) required to approximate the optimum receiver per-

formance to a desired degree can be obtained from the number of terms

required for accurate performance evaluation.

For the WSSUS case, the equations above are modified by

replacing $\overset{\vee}{\underline{F}}(x,t)$, $\overset{\vee}{\underline{C}}(x,t)$, $\overset{\vee}{\underline{G}}(x,t)$, $\overset{\vee}{\underline{P}}_o(x,y)$, $\overset{\vee}{\underline{Q}}(x,y,t)$ with $\overset{\vee}{\underline{F}}(x)$, $\overset{\vee}{\underline{C}}(x)$, $\overset{\vee}{\underline{G}}(x)$,

$\overset{\vee}{\underline{K}}_o(x)\delta(x-y)$, and $\overset{\vee}{Q}(x)\delta(x-y)$, respectively, in (5.64-.67). It is possible

to obtain a modal expansion for the alternate covariance matrix equations

of (5.52-.55). The result is that $\overset{\vee}{\underline{\Sigma}}(t)$ in the equations above is

replaced by the partioned matrices

$$\overset{\vee}{\underline{\Sigma}}(t) = \overset{\vee}{\underline{\Sigma}}_o + \overset{\vee}{\underline{P}}(t) \tag{5.83}$$

where

$$\overset{\vee}{\underline{\Sigma}}_{oij} = \int_{L_o}^{L_f} \overset{\vee}{\underline{K}}_o(x)\overset{\vee}{\phi}_i^*(x)\overset{\vee}{\phi}_j(x)dx$$

$$\overset{\vee}{\underline{P}}_{ij}(t) = \int_{L_o}^{L_f}\int_{L_o}^{L_f} \overset{\vee}{\underline{P}}(x,y,t)\overset{\vee}{\phi}_i^*(x)\overset{\vee}{\phi}_j(y)dxdy \tag{5.84}$$

and $\underline{P}(t)$ satisfies the matrix differential equation

$$\frac{d\overset{\vee}{\underline{P}}(t)}{dt} = \overset{\vee}{\underline{A}}(t)\overset{\vee}{\underline{P}}(t) + \overset{\vee}{\underline{P}}(t)\overset{\vee}{\underline{A}}^\dagger(t) - \frac{1}{N_o}(\overset{\vee}{\underline{\Sigma}}_o + \overset{\vee}{\underline{P}}(t))\overset{\vee}{\underline{B}}^\dagger(t)\overset{\vee}{\underline{B}}(t)(\overset{\vee}{\underline{P}}(t)+\overset{\vee}{\underline{\Sigma}}_o)$$

$$\overset{\vee}{\underline{P}}(T_o) = \underline{0} \tag{5.85}$$

This alternate formulation may provide better convergence because it separates that part of $\tilde{\underline{\Sigma}}(t)$ which comes from the impulsive behavior of $\tilde{\underline{\xi}}(x,y,t)$.

There are several computational issues that must be considered for the technique described in this section. First, the dimension of the approximate lumped-parameter system is nN, where n is the order of the distributed-parameter model and N is the number of terms in the truncated series. Thus the computation required increases rapidly with N. Also the higher order expansion functions $\tilde{\phi}_i(x)$ are likely to vary more rapidly. This implies that the sampling intervals for integration of $\tilde{\underline{\Sigma}}(t)$ must be shortened as N gets larger. This implies an even more rapid rate of increase in the computation time as N increases.

Another issue that affects the desirability of using the modal method is the effort that must be expended to calculate the matrices $\tilde{\underline{A}}(t)$, $\tilde{\underline{B}}(t)$, and $\tilde{\underline{Q}}(t)$, either analytically or numerically. It is not clear how to pick the orthonormal set $\{\phi_i(x)\}$ for the expansion. Certainly a desirable choice is one which permits easy calculation of the system matrices, while still providing rapid convergence. No procedure for making such a choice is obvious, however.

It is interesting to compare the delay-spread channel finite-state approximation of this section with one which has been suggested for the WSSUS model [16,19]. If the transmitted signal complex envelope $\tilde{f}(t)$ is strictly bandlimited to $[-W/2,W/2]$, the sampling theorem gives the representation

$$\overset{\gamma}{f}(t-x) = \sum_{i=-\infty}^{\infty} \overset{\gamma}{f}(t- \frac{i}{W_s})\frac{1}{W_s} \frac{\sin\pi W_s (x- \frac{i}{W_s})}{\pi(x- \frac{i}{W_s})} \tag{5.86}$$

where $W_s > W$. The channel output in (5.2) can be written

$$\tilde{s}(t) = \sum_{i=-\infty}^{\infty} \overset{\gamma}{f}(t- \frac{i}{W_s})\tilde{y}(\frac{i}{W_s},t)\frac{1}{W_s} \tag{5.87}$$

where the random processes $\tilde{Y}(\frac{i}{W_s}, t)$ are defined by

$$\tilde{y}(\frac{i}{W_s},t) = \int_{-\infty}^{\infty} \tilde{Y}(x,t) \frac{\sin \pi W_s (x- \frac{i}{W_s})}{\pi(x - \frac{i}{W_s})} dx \tag{5.88}$$

and have covariances

$$E[\tilde{y}(\frac{i}{W_s},t)\tilde{y}^*(\frac{j}{W_s},\tau)] = \int_{-\infty}^{\infty} \overset{\gamma}{K}_D(x,t-\tau)\frac{\sin \pi W_s (x- \frac{i}{W_s}) \sin\pi W_s (x- \frac{j}{W_s})}{\pi(x - \frac{i}{W_s})\pi(x- \frac{j}{W_s})}$$

$$\tag{5.89}$$

This model is called a tapped delay line model for the doubly-spread channel. If the sum in (5.87) is truncated to a finite number of terms, $\tilde{s}(t)$ is the output of a tapped delay line which has $\overset{\gamma}{f}(t)$ as an input and the $\tilde{Y}(i/W_s,t)$ as tap gains.

In order to obtain a lumped-parameter state-variable model from (5.87-.89) it is necessary to truncate the sum in (5.87) to N terms and to assume that the $\tilde{Y}(i/W_s,t)$ are uncorrelated. This assumption is not strictly valid, as (5.89) indicates. But a justification for it is provided by noting that, as W_s increases, $E[\tilde{Y}(i/W_s,t)\tilde{Y}^*(j/W_s,t)]$

grows roughly linearly with W_s for $i = j$, and remains approximately constant when $i \neq j$. Under this condition, a state-variable model results by specifying a state-variable representation for each tap gain $\tilde{Y}(i/W_s, t)$. It is not really necessary to have uncorrelated tap gains, but if this assumption is not made, then it is not clear how to specify the tap gain state-variable model.

The tapped delay line state-variable model derived in this fashion is not the same as the approximate model obtained by the modal analysis of the distributed-paramter model. However, the tapped-delay line model converges to the distributed-parameter state-variable model for the WSSUS doubly-spread channel as $W_s \rightarrow \infty$, provided that the length of the tapped delay line is held constant and the tap spacing goes to zero. In this case, the sum in (5.87) is replaced by the integral in (5.2). The densely tapped delay line tap gains become the distributed process $\tilde{Y}(x, t)$, with the covariance determined by holding i/W_s and j/W_s constant in (5.89) as W_s goes to ∞.

The disadvantage of the tapped delay line approach is that it assumes strictly bandlimited signals and uncorrelated tap gains. This modal technique presented in this section can be applied under much more general circumstances, in particular to signals and scattering distributions of finite duration. The set of expansion functions need only be complete and orthonormal. When the transmitted signal is band-limited and when the WSSUS channel scattering function $\tilde{S}(x, f)$ has a Fourier transform in the variable x which is also bandlimited, an appropriate set of expansion functions in the modal approach is the sin x/x set used in the tapped delay line model. However, the

approximate system which results from the modal approach is different than the tapped delay line model above, since the state variables in the former are correlated.

This section has derived an approximate method for finding the distributed-parameter state estimate and covariance matrix for the doubly-spread channel model in Section B. This modal analysis replaces the partial differential equations of Section C with a set of ordinary differential equations. To determine whether this approach is useful for analyzing the doubly-spread channel problem, it is necessary to perform the computations in a practical example.

E. Optimum Receiver Performance: An Example

This section uses the model method of the previous section to evaluate the doubly-spread channel optimum receiver performance for a particular example. Some details of the computational techniques that are used are discussed. The performance curves which are obtained also provide some insight into the problems of signalling over doubly-spread channels.

The example which is considered here involves the transmission of a waveform with a constant envelope

$$
\tilde{f}(t) = \begin{cases} \sqrt{\dfrac{E_r}{T}} & 0 \le t \le T \\ \\ 0 & \text{elsewhere} \end{cases}
\tag{5.90}
$$

A first order, WSSUS distributed-parameter state-variable model is assumed for the channel. The parameters of the model of (5.26-.27) are

$$\overset{\curlyvee}{\underline{F}}(x) = -k$$

$$\overset{\curlyvee}{\underline{G}}(x) = \underline{C}(x) = 1$$

$$\overset{\curlyvee}{\underline{Q}}(x) = \begin{cases} \dfrac{2k}{L} (1 - \cos \dfrac{2\pi x}{L}) & 0 \le x \le L \\ \\ 0 & \text{elsewhere} \end{cases}$$

(5.91)

The scattering function for this channel is

$$\overset{\curlyvee}{S}(x,f) = \begin{cases} \dfrac{\dfrac{2k}{L} (1 - \cos \dfrac{2\pi x}{L})}{(2\pi f)^2 + k^2} & \begin{array}{l} 0 \le x \le L \\ \\ -\infty \le f < \infty \end{array} \\ \\ 0 & \text{elsewhere} \end{cases}$$

(5.92)

and is similar to the one shown in Figure 5.2a. The observation interval is $[0, T + L]$, the maximum that is useful. From (5.8), the average received energy in $\overset{\curlyvee}{s}(t)$ over this interval is E_r.

The binary symmetric orthogonal communication problem of Chapter I is treated, since the bounds on the optimum receiver error probability in (2.77) are strongly influenced by the quantity $\mu_{*bc}(-.5)$. This function is given by (2.83), whose terms can be related to the Fredholm determinant, (2.84). The Fredholm determinant is computed for the example of this section by integrating the MMSE estimation error $\overset{\curlyvee}{\xi}_p(t)$, as indicated by (2.85). Relative performance of the optimum receiver for

different L,T, k, and E_r/N_o will be indicated by comparing the values of $\mu_{*bc}(-.5)$.

For the modal technique of the previous section the orthonormal set used in this example is

$$\overset{\sim}{\phi}_1(x) = \sqrt{\frac{1}{L}}$$

$$\overset{\sim}{\phi}_{2k}(x) = \sqrt{\frac{2}{L}} \cos \frac{2\pi k}{L} x$$

$$\overset{\sim}{\phi}_{2k+1}(x) = \sqrt{\frac{2}{L}} \sin \frac{2\pi k}{L} x, \ k \geq 1 \qquad (5.93)$$

over the interval [0,L]. The matrices $\overset{\sim}{\underline{A}}(t)$, $\overset{\sim}{\underline{B}}(t)$, and $\overset{\sim}{\underline{Q}}(t)$ follow directly from (5.64)-.66). The matrices $\overset{\sim}{\underline{P}}_{oij}$ follow from (5.67) by noting that $\overset{\sim}{\underline{K}}_o(x) = \frac{1}{L} (1-\cos \frac{2\pi x}{L})$ in this example. The alternate covariance matrix computation of (5.83-.85) is used. $\overset{\sim}{\underline{P}}(t)$ is obtained from (5.85) by fourth order Runga-Kutta numerical integration. The filtering error $\overset{\sim}{\xi}_p(t)$ is evaluated from (5.79). The number of terms in the truncated series is increased in each case until the value of $\mu_{*bc}(-.5)$ stabilizes, that is, remains constant to three decimal places.

Figure 5.4 shows $\mu_{*bc}(-.5)$, normalized by E_r/N_o, versus T, with k and L each equal to .5. For E_r/N_o less than 5 there is an optimum value of T, near 1. For higher E_r/N_o there are two relative maxima in the curves as T is varied. Note that for all values of E_r/N_o it is possible to find a value of T such that efficient performance is obtained; that is, the normalized value of $\mu_{*bc}(-.5)$ is above .120

$$\frac{-\mu_{*bc}(-.5)}{E_r/N_o}$$

.120

.100

.080

.060

$E_r/N_o = 20$

$E_r/N_o = 10$

$E_r/N_o = 5$

$E_r/N_o = 2.5$

$\left.\begin{array}{l} k = .5 \\ L = .5 \end{array}\right\}$ $kL = .25$

CONSTANT $\tilde{f}(t)$

.040

.020
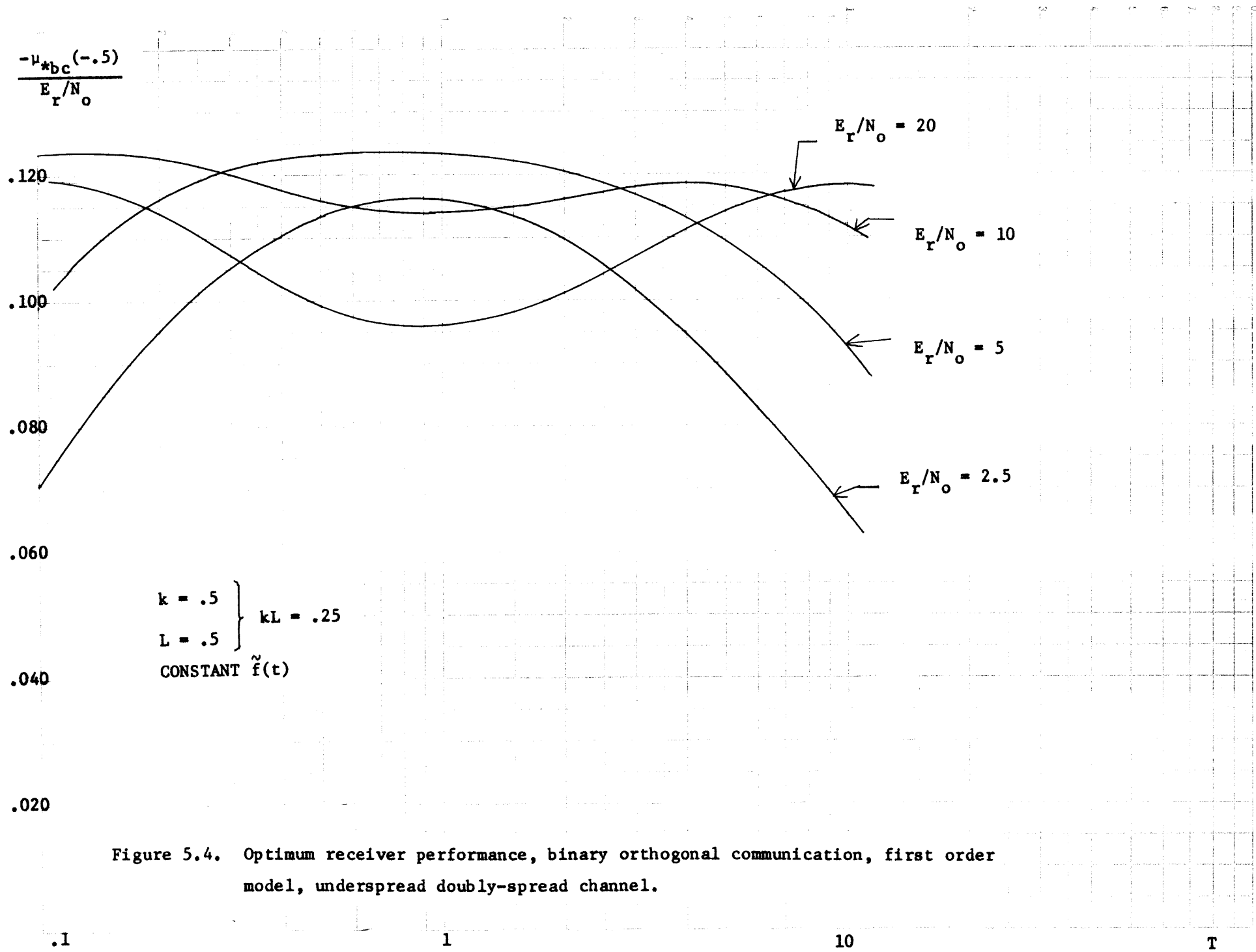
Figure 5.4.   Optimum receiver performance, binary orthogonal communication, first order
model, underspread doubly-spread channel.

.1   1   10   T

(recall that .1488 is an upper bound for this quantity). Since the product kL is .25 in this example, the channel is said to be "under spread" (kL << 1). The significance of this property will be discussed shortly.

Figure 5.5 shows curves of the normalized value of $\mu_{*bc}(-.5)$ when the channel has unity spread. That is, kL is one, since both k and L are one. A behavior similar to that in Figure 5.4 is evident here. However, in Figure 5.5 efficient performance is possible only for E_r/N_o greater than 5. Also the signal-to-noise ratio at which the double maxima with respect to T begins to appear is higher in Figure 5.5.

Figure 5.6 shows another set of curves for k and L each equal to 2.5. The kL product is thus 6.25, which permits the channel to be classified as somewhat overspread. The differences which were observed between Figures 5.4 and 5.5 are more pronounced in Figure 5.6. For low E_r/N_o no value of T provides efficient performance. And the value of E_r/N_o at which the double maximum begins to occur is greater than that in Figure 5.5.

Figures 5.4 - .6 provide some insight into the role of the product kL in this example. It appears that as kL increases, the value of E_r/N_o required to obtain efficient performance increases. Or from a different point of view, if E_r/N_o and T are held fixed and kL is increased, the absolute performance first increases and then decreases.

A useful interpretation of the behavior that is exhibited by the curves of Figures 5.4 - .6 is available from the idea of implicit diversity discussed in the first section of this chapter. For the low time-bandwidth product signal in this example, (5.9a) gives an estimate

$$\frac{-\mu_{*bc}(-.5)}{E_r/N_o}$$

.120

.100

.080

.060

.040

.020

$E_r/N_o = 20$

$E_r/N_o = 10$

$E_r/N_o = 5$

$E_r/N_o = 2.5$

$k = 1$
$L = 1$ } $kL = 1$
CONSTANT $\tilde{f}(t)$

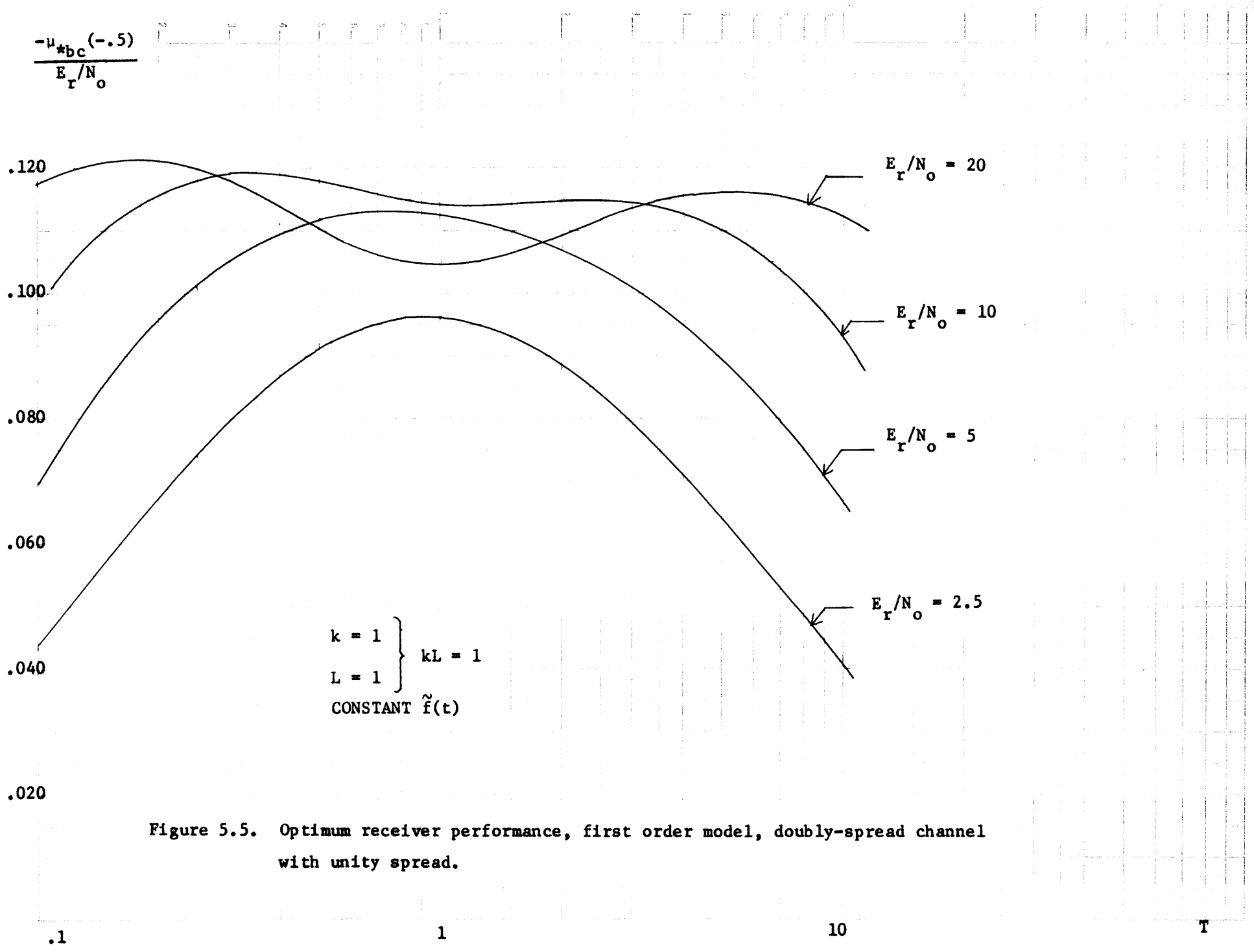Figure 5.5. Optimum receiver performance, first order model, doubly-spread channel
with unity spread.

.1   1   10   T
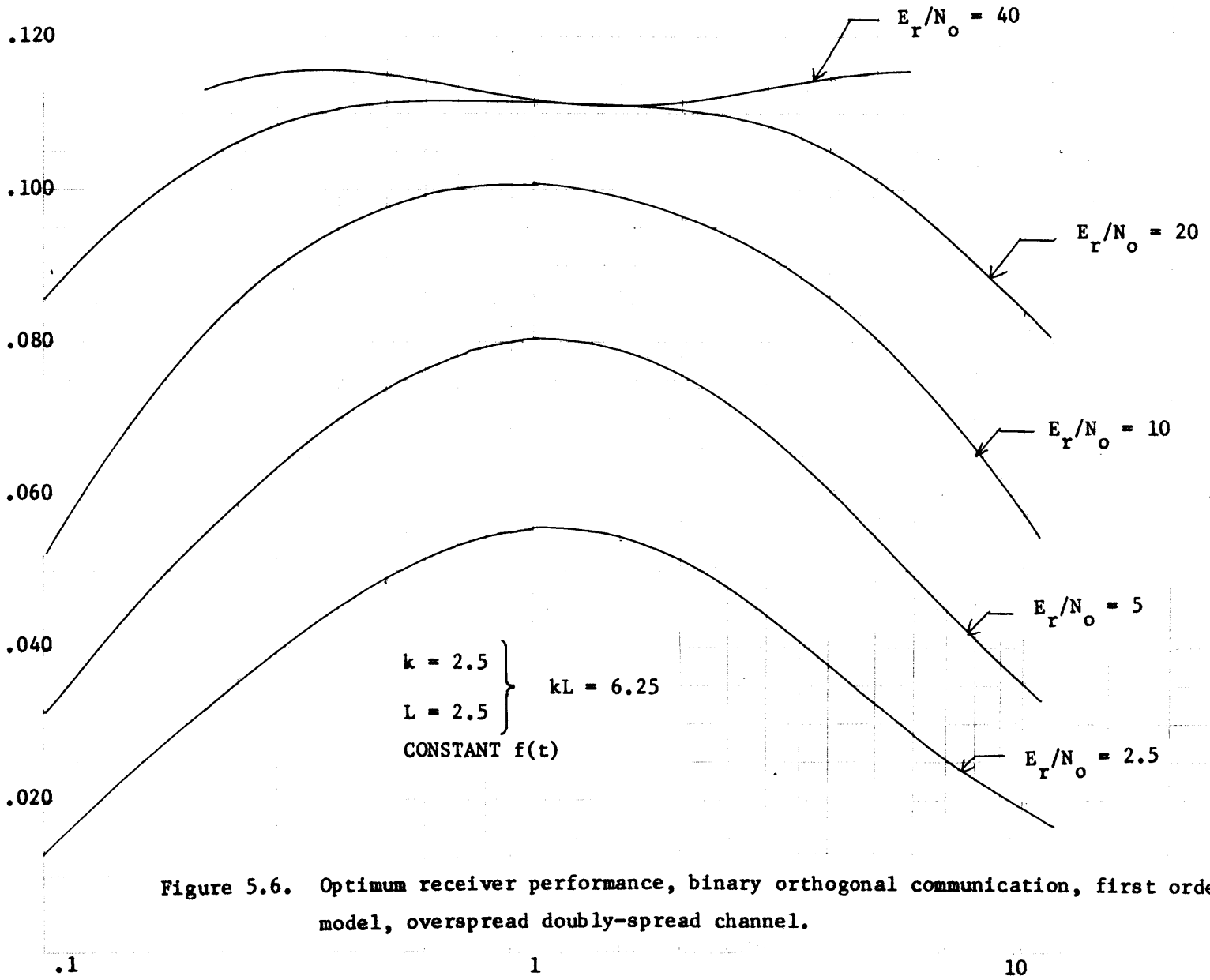
Figure 5.6. Optimum receiver performance, binary orthogonal communication, first order model, overspread doubly-spread channel.

of the approximate number of implicit diversity elements in the system

$$N_{db} = (1 + \frac{L}{T})(1 + kT) \qquad (5.94)$$

The quantities L and k in (5.94) refer to measures of the spread of the scattering function $\tilde{S}(x,f)$ in x and f, respectively; in this example a one-to-one correspondence may be made with these parameters. N_{db} in (5.94) is plotted versus T in Figure 5.7. Note the minimum at L/k.

Figure 5.7 is informative when it is kept in mind that, from an optimum diversity viewpoint, the most efficient choice of L, T, and k will provide a signal-to-noise ratio per diversity element of about 3. The fact that there is a minimum value of N_{db} which may be a good deal greater than 1 for large kL indicates that for low E_r/N_o, even the minimum N_{db} may spread the energy too thinly among the diversity elements. Increasing or decreasing T increases the diversity in this situation, and the performance worsens.

At some higher E_r/N_o, the minimum possible value of N_{db} may not spread the available energy enough. This increasing or decreasing T improves the performance, unless, of course, N_{db} is made too large. Note that the transition E_r/N_o, for which the minimum N_{db} is just optimum, increases with E_r/N_o.

The behavior shown by the performance curves of Figures 5.4-.6 agrees closely with the observations made from the implicit diversity description of the channel. Although this idea is only an approximate one, it gives quite accurately the location of the single and double minima in Figure 5.4 and 5.6. In addition the differences arising from different kL products are easily interpreted with the implicit diversity
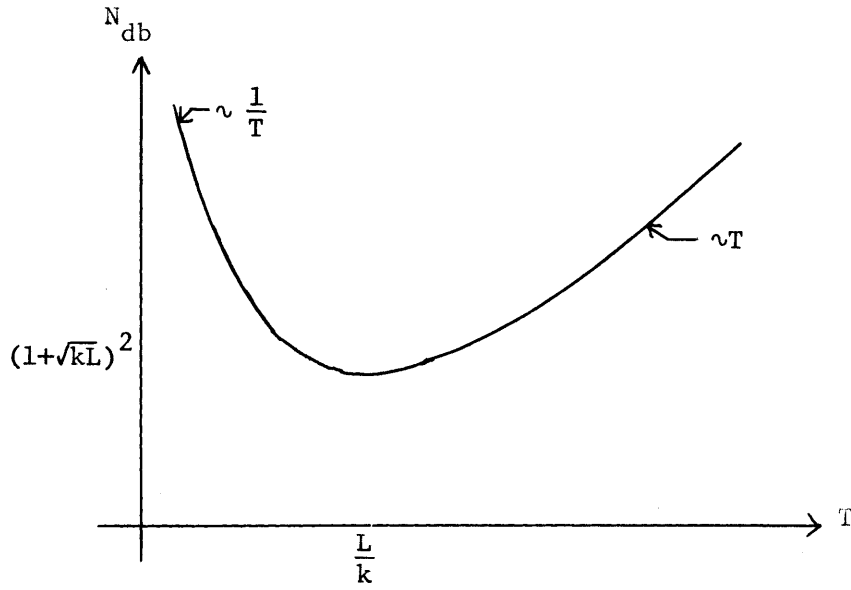
Figure 5.7. Doubly-spread channel implicit diversity; small TW signals.

argument.

The behavior of the optimum receiver performance versus kL is more clearly shown in Figures 5.8 and 5.9. Here $\mu_{*bc}(-.5)$ is plotted without normalization, to show relative level of performance rather than efficiency. The dotted line shows the ultimate bound on $\mu_{*bc}(-.5)$. Figure 5.8 shows that for T = 1 and large signal-to-noise ratios, an overspread channel provides better performance than an underspread channel. In this case large implicit diversity is required to adequately spread out the available E_r/N_o. Figure 5.9 shows the receiver performance for T = 10. Here the implicit diversity is already too large for the underspread channel; hence the overspread channel performance is even worse. Figures 5.8 and 5.9 indicate the importance of properly choosing the signal parameters.

Figure 5.10 shows $\mu_{*bc}(-.5)$ versus E_r/N_o for several values of kL, with T being chosen in each case to optimize the performance. It is evident that if there are no constraints on T it is possible, at least in this example, to achieve efficient performance over doubly-spread channels with a simple signal, even if the channel is overspread (kL >> 1). There is some decrease in performance in Figure 5.10 as kL increases, but it is moderate. For E_r/N_o greater than 20, the kL = 25 case is only about 1.5 dB worse than when kL = 1, provided T can be chosen optimumly. However, for overspread channels it is necessary to have a high enough E_r/N_o to overcome the large implicit diversity that is built into the channel, in order to obtain efficient performance.

Table 5.1 gives the number of harmonics, N_h, in the truncated Fourier series required to compute some of the points in Figures 5.4-.6

$-\mu_{*_{bc}}(-.5)$

BOUND $(.1488\ E_r/N_o)$

1.0

kL = .25

T = 1
k = L

kL = 6.25

kL = 1

.1
1

10

E_r/N_o
100

Figure 5.8. Optimum receiver performance for T = 1, constant f(t), binary orthogonal
communication over a doubly-spread channel.

$-\mu_{*bc}(-.5)$

BOUND $(.1488\ E_r/N_o)$ —→

1.0

T = 10

k = L

kL = 6.25

kL = .25 —→

kL = 1

.1

1

10

E_r/N_o

100
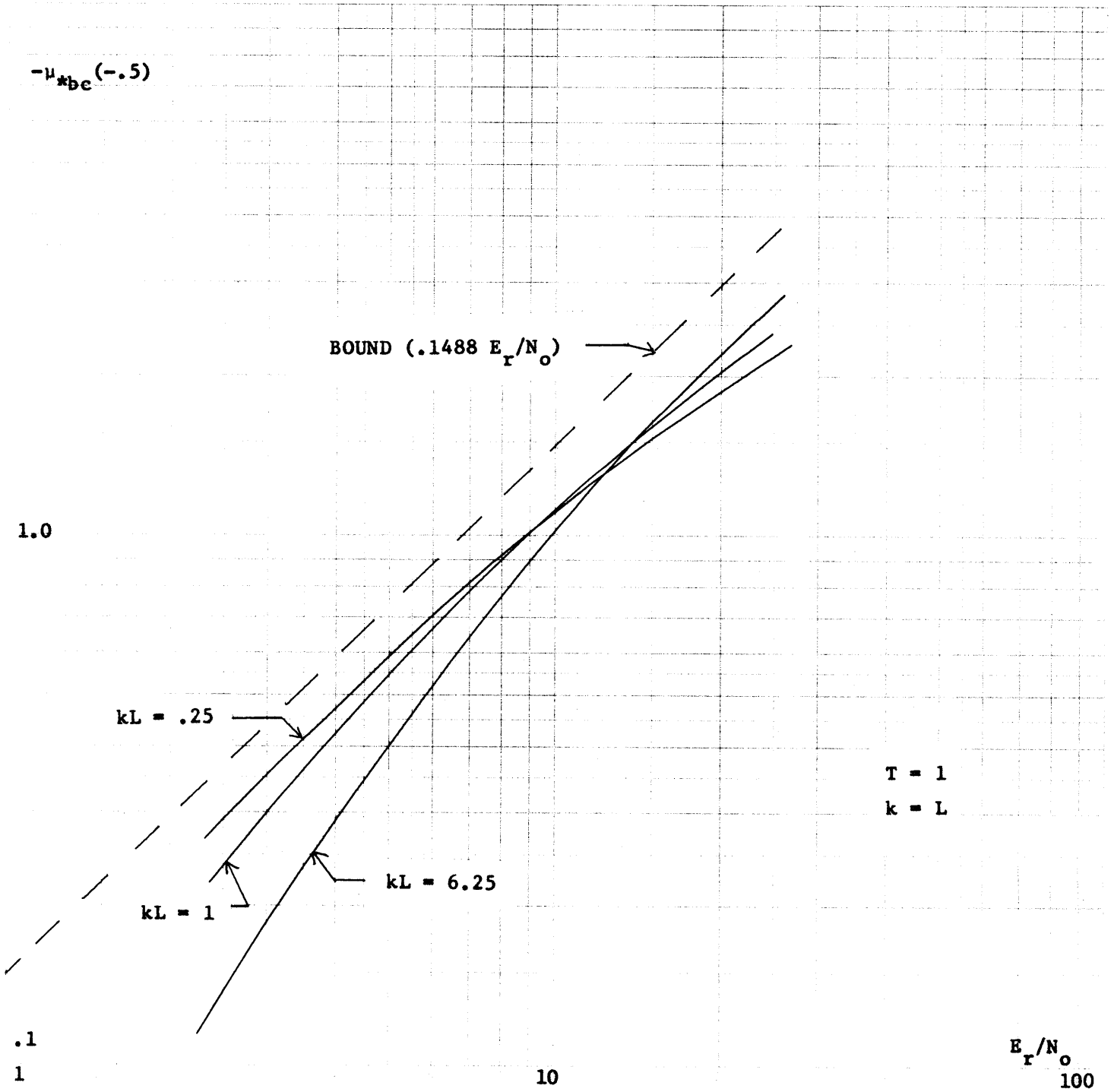
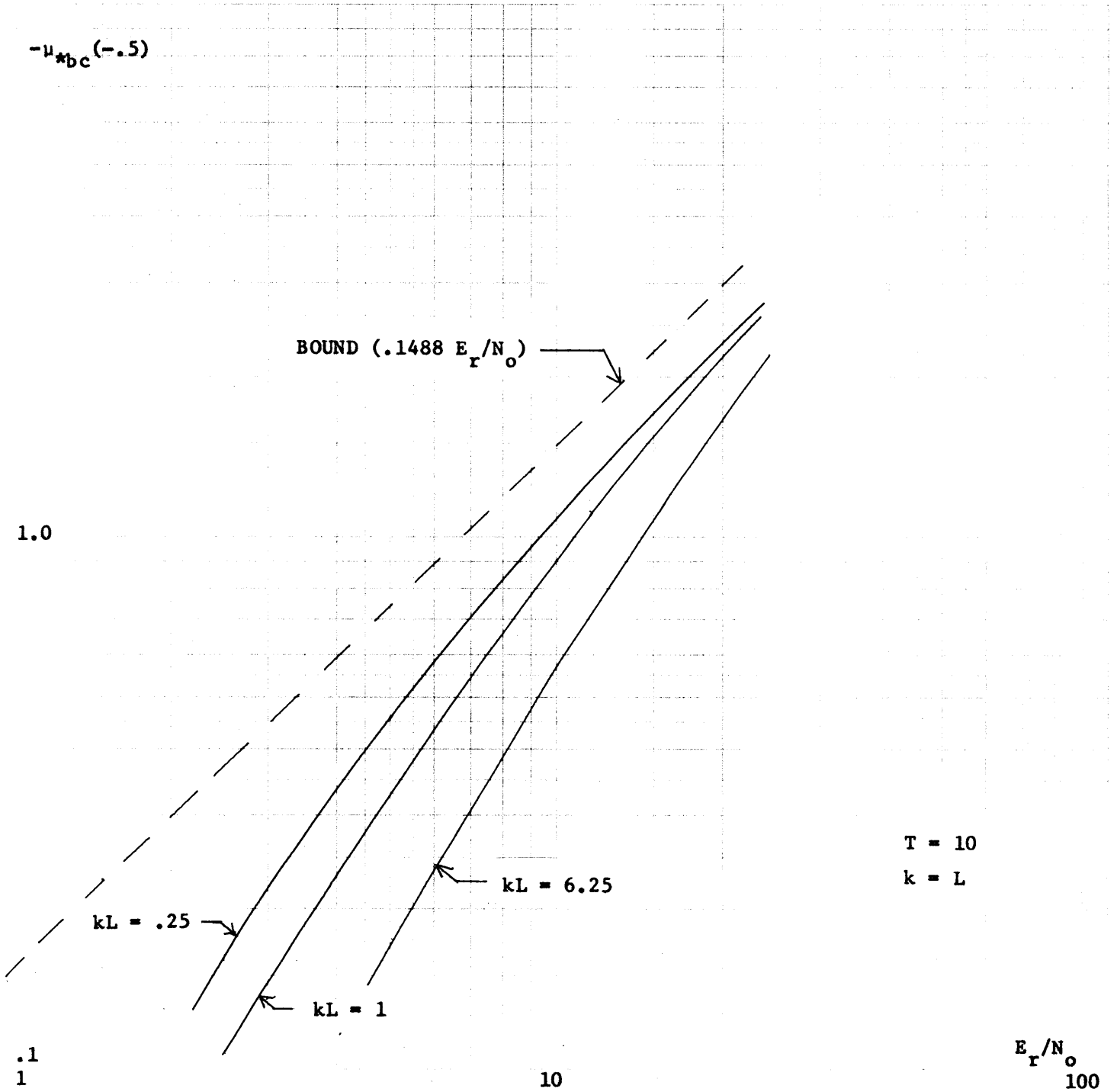Figure 5.9. Optimum receiver performance for T = 10, constant f(t), binary orthogonal communication over a doubly-spread channel.

$-\mu_{*bc}(-.5)$

BOUND $(.1488\ E_r/N_o)$ ⟶

1.0

kL = .25

OPTIMUM T

k = L

kL = 25

kL = 1

kL = 6.25

.1

1

10

E_r/N_o

100
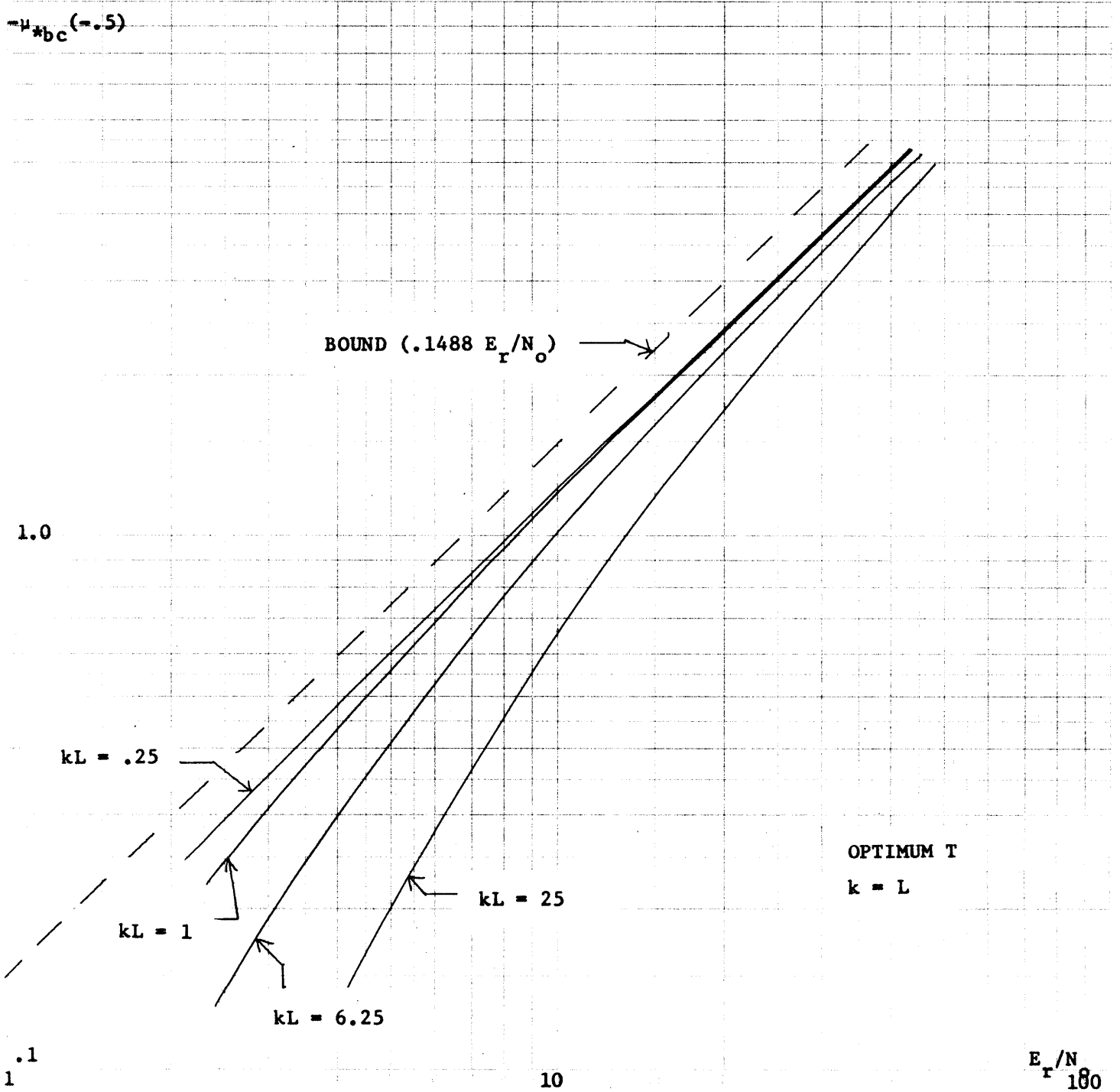
Figure 5.10.   Optimum receiver performance for optimum T, constant f(t), binary
orthogonal communication over a doubly-spread channel

E_r/N_o	k	L	T	N_h
5	.5	.5	.1	8
5	.5	.5	1	6
5	.5	.5	10	10
20	.5	.5	1	6
5	1	1	1	6
5	1	1	10	10
20	1	1	1	8
5	2.5	2.5	.1	12
5	2.5	2.5	1	8
20	2.5	2.5	1	8
20	2.5	2.5	10	12

Table 5.1. Number of harmonics required for at least three place accuracy in $\mu_{*bc}(-.5)$, doubly-spread channel example.

to three place accuracy. Note that the number of terms in the series is actually $2N_h + 1$. For $L << T$ or $T << 1/k$, and the higher values of E_r/N_o, more harmonics are required. It should be pointed out that for these extremes, the doubly-spread channel model is nearly doppler-spread or delay-spread, respectively, and then the approximate optimum receiver performance can be found from Chapters III or IV. The computer time required to evaluate $\mu_{*bc}(.5)$ ranged from a few seconds for low N_h to about 20 seconds for the highest N_h, on the IBM 360/65.

Direct integration of the partial differential equation for the error covariance, (5.48), was carried out for comparison with the modal approach. For the first order model $\tilde{\xi}(x,y,t)$ was computed at a grid of points in the x-y plane; integration was performed by the fourth order Runga-Kutta method. The computer time required to compute $\mu_{*bc}(.5)$ in this manner was higher by a factor of 10 over that required by the modal approach, and often it was impossible to obtain the equivalent accuracy. At least in this example, the modal approach is significantly better, and in fact, the only practical way of finding the optimum receiver performance.

This section has considered an example of the transmission of a known signal over a doubly-spread channel. The optimum receiver performance has been investigated for the binary symmetric communication problem by using the modal technique of Section D to find $\mu_{*bc}(-.5)$, the exponent in the error probability bounds. The results for the underspread, unity spread, and overspread cases were interpreted by considering the concept of implicit diversity. Although only one signal and scattering

205-

function was investigated, the modal approach to the evaluation of the optimum receiver performance can be applied to other signals and scattering functions with an equal effort.

F. Summary

This chapter has considered the problem of finding the optimum receiver for the detection of known signals transmitted over doubly-spread channels, and evaluating its performance. A distributed-parameter state-variable model for the doubly-spread channel has been proposed in which the random processes are generated by passing a temporally white, distributed Gaussian noise through a linear system described by partial differential equations. The model is also valid for a particular case of the doubly-spread channel, the WSSUS channel. For the WSSUS condition, the scattering functions $\tilde{S}(x,f)$ which can be represented by the distributed-parameter state-variable need only be rational function if f. This permits a wide variety of doubly-spread channel models.

A realizable optimum receiver structure was derived by finding the MMSE realizable estimate of the channel output, $\tilde{s}(t)$. This estimate can be obtained directly from the MMSE realizable estimate of the distributed-parameter state-vector in the doubly-spread channel model. The structure of this estimator was derived; it is a linear distributed-parameter state-variable system. A by-product of the derivation is a partial integro-differential equation for the estimation error covariance matrix. Solution of this equation permits the calculation of the moment-generating functions of the optimum receiver decision statistic and therefore the error probabilities.

A modal approach for the solution of the estimator and covariance matrix equations was proposed. The method involves orthogonal expansions of the estimate and the covariance matrix in their spatial variables. The distributed-parameter system is effectively reduced to a lumped-parameter model with finite states. The moment-generating functions are calculated directly using the techniques of Chapter II. The number of states in the truncated model is increased until the performance measure converges.

An example was considered in which a known signal with a constant envelope is transmitted over WSSUS channel with a first order scattering function. The modal technique provided the binary symmetric communication error probability bounds with a modest expenditure of computer time. The notion of implicit diversity was useful in interpreting the results. In this example, proper selection of the signal duration T permitted efficient performance of the communication system over a wide range of channel parameters, including the overspread condition.

The example presented illustrated the feasibility of using the modal approximation for finding the delay-spread channel optimum receiver and its performance. It should be emphasized that other signals and any channel which fits the distributed-parameter state-variable model can be analyzed with this technique. The amount of computer time required for such an analysis apprears to be quite reasonable.

CHAPTER VI

SUBOPTIMUM RECEIVERS FOR THE DOUBLY-SPREAD CHANNEL

The previous chapter presented a distributed-parameter state-variable model for the doubly-spread channel and derived a realizable structure for the optimum receiver when a known signal is transmitted over the doubly-spread channel. The configuration for the resulting optimum receiver included a distributed-parameter system, that is, a linear system whose dynamics are described by a vector partial differential equation. This structure, although temporally realizable, is difficult to implement directly. This suggests using a suboptimum receiver.

Several suboptimum receivers for the doubly-spread channel are suggested by the results of the previous chapters. In Chapter V a modal technique for finding the optimum receiver performance was given. Included in the formulation was a finite state approximation, (5.74-.76), to the distributed parameter state vector estimator which is an essential part of the realizable optimum receiver. One possibility is to use this approximate estimator in place of the distributed-parameter system in the optimum receiver. This may well provide a good suboptimum receiver, but it will not be discussed further in this chapter.

Several other suboptimum receiver structures are suggested by the results for the doppler-spread and delay-spread channels. In the doppler-spread case a filter-squarer-integrator structure provided good performance if properly designed, as did its dual, the two-filter

radiometer, for the delay-spread channel. This chapter considers a receiver for the doubly-spread channel which is closely related to both the FSI and TFR receivers. It consists of a distributed-parameter linear filter whose output is squared and integrated over its space and time variables. This doubly-spread suboptimum receiver will be called a distributed filter-squarer-integrator (DFSI) receiver. The following section discusses the DFSI suboptimum receiver in detail and presents a method for evaluating its performance.

Another suboptimum receiver for the doubly-spread channel which is considered in this chapter is called a correlator-squarer-sum (CSS) receiver. It is essentially a combination of the suboptimum receivers of the same name that were specified for the doppler-spread and delay-spread channels. The performance of the doubly-spread channel CSS receiver is analyzed so that it may be compared with the optimum receiver.

A. A Distributed Filter-Squarer-Integrator Suboptimum Receiver

This section considers a distributed filter-squarer integrator suboptimum receiver for the doubly-spread channel. It is related to both the FSI and TFR receivers for the doppler-spread and delay-spread channels, respectively. The design of the DFSI receiver is investigated and a method for evaluating its performance is presented.

The first section of Chapter V gave the doubly-spread channel model as a superposition of doppler-spread channels. Since the FSI structure proved to be a good suboptimum receiver for the doppler-spread channel, this suggests that a "superposition" of FSI receivers would be a reasonable choice for a doubly-spread channel suboptimum receiver.

This superposition can be accomplished by distributing the doppler-spread FSI filter over a continuum of delays and integrating the output over the spatial variable. That is, the received signal is passed through a time-varying realizable, distributed linear filter with impulse response $\tilde{g}(\lambda,t,u)$. The output is squared and integrated temporally over the observation interval. The result is then integrated over the spatial variable . Thus the decision statistic can be written

$$= \int_{L_o}^{L_f} \int_{T_o}^{T_f} \left| \int_{T_o}^{T_f} \tilde{g}(\lambda,t,u)\tilde{r}(u)du \right|^2 dt \, d\lambda \qquad (6.1)$$

The observation interval is $[T_o,T_f]$. Figure 6.1 shows this receiver structure. Note that the order of the integrations over λ and t may be reversed.

The choice of the distributed filter can be made in many ways. In light of the results for the FSI and TFR suboptimum receivers in the doppler-spread and delay-spread cases, respectively, it is reasonable to look for a $\tilde{g}(\lambda,t,u)$ such that the structure of (6.1) reduces to the FSI or TFR receivers when the doubly-spread channel becomes singly-spread. In the limit of the doppler-spread channel, then, the extent of $\tilde{g}(\lambda,t,u)$ in λ should become negligible and the time behavior should be a multiplication by $\tilde{f}^*(t)$ followed by a filter which has the same order as the fading spectrum. For the delay-spread case, the $\tilde{g}(\lambda,t,u)$ should reduce to a filter matched to $\tilde{f}(t)$ with a post-detection weighting over λ.

A choice for $\tilde{g}(\lambda,t,u)$ which satisfies these conditions is

$\tilde{r}(t) \longrightarrow$ | $\tilde{g}(\lambda,t,u)$ | $\xrightarrow{\tilde{Z}(\lambda,t)}$ | $|\cdot|^2$ | $\longrightarrow$ | $\int_{L_o}^{L_f} \cdot \, d\lambda$ | $\longrightarrow$ | $\int_{T_o}^{T_f} \cdot \, dt$ | $\longrightarrow \quad \ell$
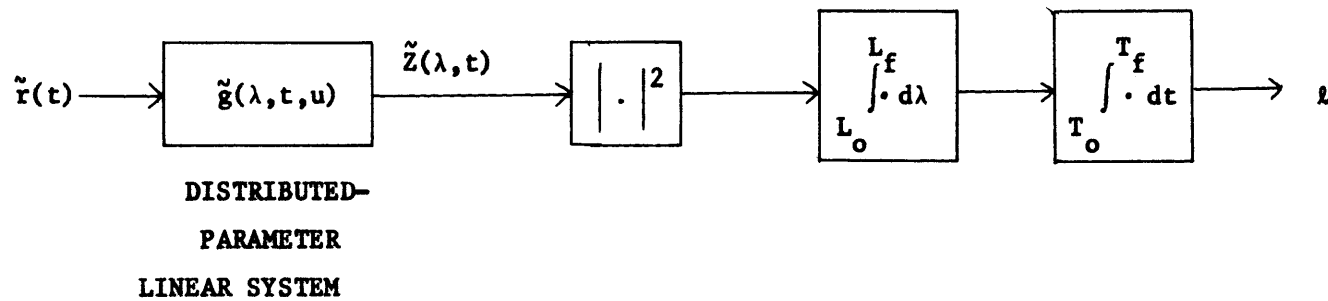
DISTRIBUTED-
PARAMETER
LINEAR SYSTEM

Figure 6.1. Distributed filter-squarer-integrator suboptimum receiver for the delay-spread
channel.

shown in Figure 6.2. The distributed parameter filter consists of multiplication of $\tilde{r}(t)$ by $\tilde{f}^*(t-\lambda)$ followed by a distributed-parameter system which has the same order as the channel model filter in (5.10). As the doubly-spread channel model reduces to the doppler-spread or delay-spread cases, so does the distributed filter in Figure 6.2. The result is a FSI or TFR receiver structure. Another motivation for using the particular structure of Figure 6.2 is that the optimum receiver for the doubly-spread channel under low-energy-coherence conditions is similar in form to the receiver of Figure 6.2 [2]. In this case the filter in Figure 6.2 should be identical to that in the channel model, and the post-detection temporal integration should be infinite in extent.

The receiver structure in Figure 6.2 is simpler than the optimum receiver given in Chapter V. It does involve a distributed-parameter system, which presents some problems in physically implementing the DFSI receiver. However, it is still informative to compare the performance of the DFSI receiver with the optimum receiver performance. And in the process an approximation to the structure of Figure 6.2 will be obtained which can be realized physically.

The evaluation of the suboptimum DFSI receiver error probabilities is carried out by application of the modal technique which was used in Chapter V to evaluate the optimum receiver performance. As in Chapter V, a series expansion is applied to the receiver filter state vector. Truncation of the series effectively reduces the DFSI receiver to a finite state FSI receiver. If the modal technique is applied to the doubly-spread channel model as well, and the appropriate series
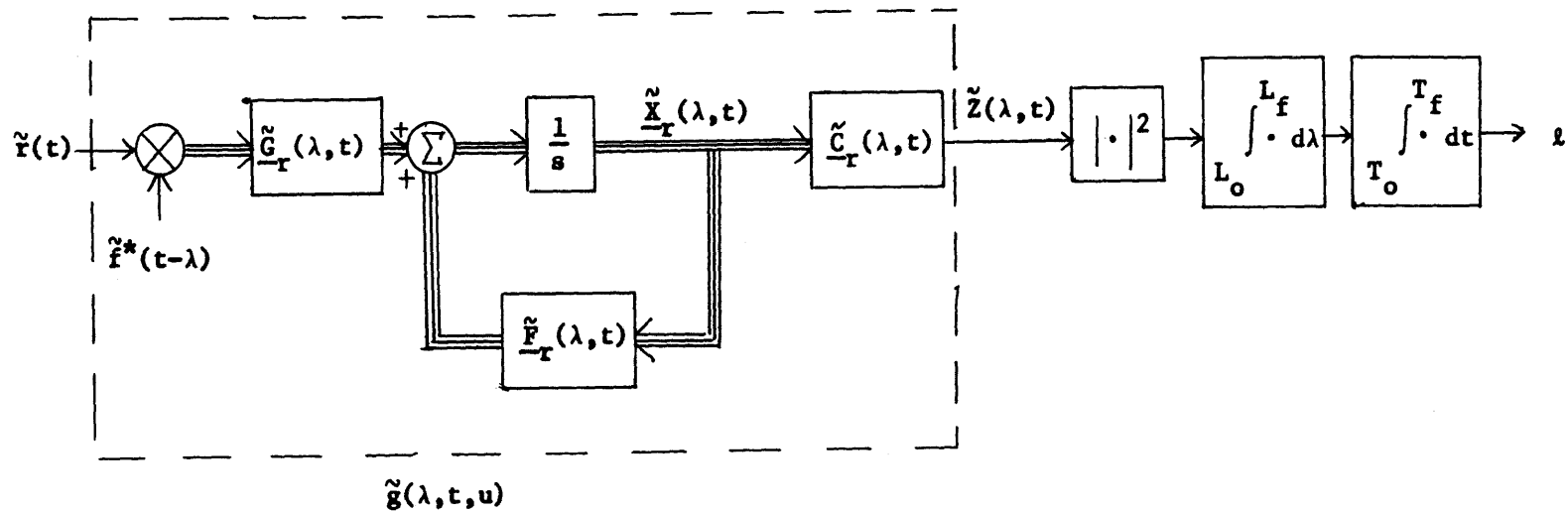
Figure 6.2. A particular choice for the distributed filter-squarer-integrator suboptimum receiver.

expansion is truncated, then the suboptimum receiver performance follows from the state-variable FSI receiver. The number of terms in the truncated series is increased until the performance converges.

The analysis begins by expanding the filter output, $\tilde{Z}(x,t)$ in Figure 6.2, in an orthogonal series

$$\tilde{Z}(x,t) = \sum_{i=1}^{\infty} \tilde{z}_i(t)\tilde{\phi}_i(x) \tag{6.2}$$

$$\int_{L_o}^{L_f} \tilde{\phi}_i(x)\tilde{\phi}_j^*(x)dx = \delta_{ij} \tag{6.3}$$

Then

$$\ell = \int_{T_o}^{T_f} \int_{L_o}^{L_f} |\tilde{Z}(x,t)|^2 dx \, dt$$

$$= \int_{T_o}^{T_f} \sum_{i=1}^{\infty} |\tilde{z}_i(t)|^2 dt \tag{6.4}$$

Suppose the series in (6.4) is truncated to N terms. Defining the vector $\underline{\tilde{Z}}(t)$ as

$$\underline{\tilde{Z}}(t) = \begin{bmatrix} \tilde{z}_1(t) \\ \tilde{z}_2(t) \\ \cdot \\ \cdot \\ \cdot \\ \tilde{z}_N(t) \end{bmatrix} \tag{6.5}$$

permits (6.4) to be approximated by

$$\ell = \int_{T_o}^{T_f} \underline{\tilde{Z}}^*(t)\underline{\tilde{Z}}(t)dt \tag{6.6}$$

The vector process $\tilde{\underline{Z}}(t)$ can be written in a Karhunen-Loeve expansion

$$\tilde{\underline{Z}}(t) = \sum_{i=1}^{\infty} \tilde{z}_i \, \tilde{\underline{\phi}}_i(t), \quad T_o \le t \le T_f \tag{6.7}$$

$$\int_{T_o}^{T_f} \tilde{\underline{\phi}}_i^{\dagger}(t) \tilde{\underline{\phi}}_j(t) dt = \delta_{ij} \tag{6.8}$$

$$E[\tilde{z}_i \tilde{z}_j^*] = \delta_{ij} \lambda_i \tag{6.9}$$

where the $\{\lambda_i\}$ are eigenvalues of the vector process $\tilde{\underline{Z}}(t)$. Note that the $\{\tilde{\underline{\phi}}_i(\cdot)\}$ are different from the $\{\tilde{\phi}_i(\cdot)\}$. If (6.7) is introduced into (6.6), the relationship of (6.9) gives

$$\ell \; \tilde{=} \; \sum_{i=1}^{\infty} \; |\tilde{z}_i|^2 \tag{6.10}$$

The moment-generating function for the right hand side of (6.10) is given by (2.96)

$$E[e^{s \Sigma |\tilde{z}_i|^2}] = - \sum_{i=1}^{\infty} \ell n (1 - s\lambda_i) \tag{6.11}$$

where the $\{\lambda_i\}$ are the eigenvalues of $\tilde{\underline{Z}}(t)$ given H_1 or H_0. Equation (6.11) can be evaluated by the techniques of Chapter II provided that $\tilde{\underline{Z}}(t)$ has a finite (lumped-parameter) state-variable representation.

Such a model can be obtained by treating the receiver filter and the doubly-spread channel model with the modal technique of the previous chapter. The receiver filter in Figure 6.2 is described by

the equations

$$\frac{\partial \underline{\tilde{X}}_r(x,t)}{\partial t} = \underline{\tilde{F}}_r(x,t)\underline{\tilde{X}}_r(x,t) + \underline{\tilde{G}}_r(x,t)\tilde{f}^*(t-x)\tilde{r}(t)$$

$$\underline{\tilde{Z}}(x,t) = \underline{\tilde{C}}_r(x,t)\underline{\tilde{X}}_r(x,t) \tag{6.12}$$

The state vector $\underline{\tilde{X}}_r(x,t)$ is expanded in the series

$$\underline{\tilde{X}}_r(x,t) = \sum_{i=1}^{\infty} \underline{\tilde{X}}_{ir}(t)\tilde{\phi}_i^*(x) \tag{6.13}$$

$$\underline{\tilde{X}}_{ir}(t) = \int_{L_o}^{L_f} \underline{\tilde{X}}_r(x,t)\tilde{\phi}_i^*(x)dx \tag{6.14}$$

Substitution of (6.13) in (6.12), multiplication of both sides of the equation by $\tilde{\phi}_i^*(x)$, and integration over x gives

$$\frac{d}{dt} \underline{\tilde{X}}_{ir}(t) = \sum_{k=1}^{\infty} \underline{\tilde{a}}_{ikr}(t)\underline{\tilde{X}}_{kr}(t) + \underline{\tilde{g}}_{ir}(t)\tilde{r}(t)$$

$$\tilde{z}_i(t) = \sum_{k=1}^{\infty} \underline{\tilde{b}}_{ikr}(t)\underline{\tilde{X}}_{kr}(t) \tag{6.15}$$

where

$$\underline{\tilde{a}}_{ikr}(t) = \int_{L_o}^{L_f} \underline{\tilde{F}}_r(x,t)\tilde{\phi}_i^*(x)\tilde{\phi}_k(x)dx \tag{6.16}$$

$$\underline{\tilde{g}}_{ir}(t) = \int_{L_o}^{L_f} \underline{\tilde{G}}_r(x,t)\tilde{f}^*(t-x)\tilde{\phi}_i^*(x)dx \tag{6.17}$$

$$\tilde{\underline{b}}_{ikr}(t) \quad \int_{L_o}^{L_f} \tilde{\underline{C}}_r(x,t)\tilde{\phi}_i^*(x)\tilde{\phi}_k(x)dx \qquad (6.18)$$

If the series in (6.13) and truncated to N terms, a finite state receiver filter results. Let

$$\tilde{\underline{X}}_r(t) \quad = \begin{bmatrix} \tilde{\underline{X}}_{1r}(t) \\ \cdot \\ \cdot \\ \cdot \\ \tilde{\underline{X}}_{Nr}(t) \end{bmatrix}$$

$$\tilde{\underline{A}}_r(t) \quad = [\tilde{\underline{a}}_{ij}(t)]$$

$$\tilde{\underline{G}}_r(t) \quad = \begin{bmatrix} \tilde{\underline{g}}_{1r}(t) \\ \cdot \\ \cdot \\ \cdot \\ \cdot \\ \tilde{\underline{g}}_{Nr}(t) \end{bmatrix}$$

$$\tilde{\underline{B}}_r(t) = [\tilde{\underline{b}}_{ijr}(t)] \qquad (6.19)$$

Then (6.15) becomes

$$\frac{d}{dt} \tilde{\underline{X}}_r(t) = \tilde{\underline{A}}_r(t)\tilde{\underline{X}}_r(t) + \tilde{\underline{G}}_r(t)\tilde{r}(t)$$

$$\underline{\tilde{Z}}(t) = \tilde{\underline{B}}_r(t)\tilde{\underline{X}}_r(t) \qquad (6.20)$$

The modal approach applied to the doubly-spread channel provides a similar finite state approximation. From (5.10) the distributed-parameter model is

$$\frac{\partial}{\partial t} \; \underline{\tilde{X}}_f(x,t) \;=\; \underline{\tilde{F}}_f(x,t)\underline{\tilde{X}}_f(x,t) \;+\; \underline{\tilde{G}}_f(x,t)\underline{\tilde{U}}(x,t)$$

$$\tilde{Y}(x,t) \;=\; \underline{\tilde{C}}_f(x,t)\underline{\tilde{X}}_f(x,t)$$

$$\tilde{s}(t) \;=\; \int_{-\infty}^{\infty} \tilde{f}(t-x)\tilde{Y}(x,t)dx \qquad\qquad (6.21)$$

The subscript f has been added to distinguish the channel model from the receiver filter. The state vector $\underline{\tilde{X}}_f(x,t)$ is expanded

$$\underline{\tilde{X}}_f(x,t) \;=\; \sum_{i=1}^{\infty} \underline{\tilde{X}}_{if}(t)\tilde{\psi}_i(x)$$

$$\underline{\tilde{X}}_{if}(t) \;=\; \int_{L_o}^{L_f} \underline{\tilde{X}}_f(x,t)\tilde{\psi}_i^*(x) \qquad\qquad (6.22)$$

Note that the orthogonal set here is not necessarily the same as that which is used in the receiver expansion. The driving noise is expanded in the same manner

$$\underline{\tilde{U}}(x,t) \;=\; \sum_{i=1}^{\infty} \underline{\tilde{u}}_i(t)\tilde{\psi}_i(x) \qquad\qquad (6.23)$$

$$\underline{\tilde{u}}_i(t) \;=\; \int_{L_o}^{L_f} \underline{\tilde{U}}(x,t)\tilde{\psi}_i^*(x)dx$$

$$E[\underset{\sim}{u}_i(t)\underset{\sim}{u}_j^\dagger(\tau)] = \delta(t-\tau) \int_{L_o}^{L_f} \int_{L_o}^{L_f} \underline{Q}(x,y,t)\psi^*(x)\psi_j(y)dxdy$$

$$\triangleq \underset{\sim}{q}_{ij}(t)\delta(t-\tau) \tag{6.24}$$

Substituting (6.22) and (6.23), multiplying the result by $\psi_i^*(x)$, and integrating over x gives

$$\frac{d}{dt}\underset{\sim}{\underline{X}}_{if}(t) = \sum_{k=1}^{\infty} \underset{\sim}{\underline{a}}_{ikf}(t)\underset{\sim}{\underline{X}}_{kf}(t) + \sum_{k=1}^{\infty} \underset{\sim}{q}_{ikf}(t)\underset{\sim}{u}_k(t)$$

$$\underset{\sim}{s}(t) = \sum_{k=1}^{\infty} \underset{\sim}{\underline{b}}_{kf}(t)\underset{\sim}{\underline{X}}_{kf}(t) \tag{6.25}$$

The series in (6.22) and (6.23) are truncated at their Nth terms. With the definitions

$$\underset{\sim}{\underline{X}}_f(t) = \begin{bmatrix} \underset{\sim}{\underline{X}}_{1f}(t) \\ \cdot \\ \cdot \\ \cdot \\ \underset{\sim}{\underline{X}}_{Nf}(t) \end{bmatrix}$$

$$\underset{\sim}{\underline{A}}_f(t) = [\underset{\sim}{\underline{a}}_{ij}(t)]$$

$$\underset{\sim}{\underline{G}}_f(t) = [\underset{\sim}{\underline{g}}_{ij}(t)]$$

$$\underset{\sim}{\underline{B}}_f(t) = [\underset{\sim}{\underline{b}}_{1f}(t), \ldots, \underset{\sim}{\underline{b}}_{Nf}(t)]$$

$$\underline{\underset{\sim}{v}}(t) = \begin{bmatrix} \underset{\sim}{u}_1(t) \\ \cdot \\ \cdot \\ \cdot \\ \underset{\sim}{u}_N(t) \end{bmatrix}$$

$$\underset{\sim}{\underline{Q}}_f(t) = [\underset{\sim}{q}_{ij}(t)] \tag{6.26}$$

the finite state approximation to the distributed parameter system of (6.21) is written

$$\frac{d}{dt} \, \tilde{\underline{X}}_f(t) = \tilde{\underline{A}}_f(t)\tilde{\underline{X}}_f(t) + \tilde{\underline{G}}_f(t)\tilde{\underline{U}}(t)$$

$$\tilde{\underline{s}}(t) = \tilde{\underline{B}}_f(t)\tilde{\underline{X}}_f(t) \tag{6.27}$$

$$E[\tilde{\underline{U}}(t)\tilde{\underline{U}}^\dagger(\tau)] = \tilde{\underline{Q}}_f(t)\delta(t-\tau) \tag{6.28}$$

Figure 6.3 shows the composite approximate lumped-parameter state-variable model when signal plus noise is the input to the distributed FSI receiver. As was the case with the doppler-spread channel FSI receiver, the technique given by (2.86-.90) can be used to find the moment-generating functions of (6.11). When signal plus noise is the receiver input, the matrices of (2.86) are

$$\tilde{\underline{x}}(t) = \begin{bmatrix} \tilde{\underline{X}}_f(t) \\ \tilde{\underline{X}}_r(t) \end{bmatrix}$$

$$\tilde{\underline{F}}(t) = \begin{bmatrix} \tilde{\underline{A}}_f(t) & \underline{0} \\ \tilde{\underline{G}}_r(t)\tilde{\underline{B}}_f(t) & \tilde{\underline{A}}_r(t) \end{bmatrix}$$

$$\tilde{\underline{G}}(t) = \begin{bmatrix} \tilde{\underline{G}}_f(t) & \underline{0} \\ 0 & \tilde{\underline{G}}_r(t) \end{bmatrix}$$
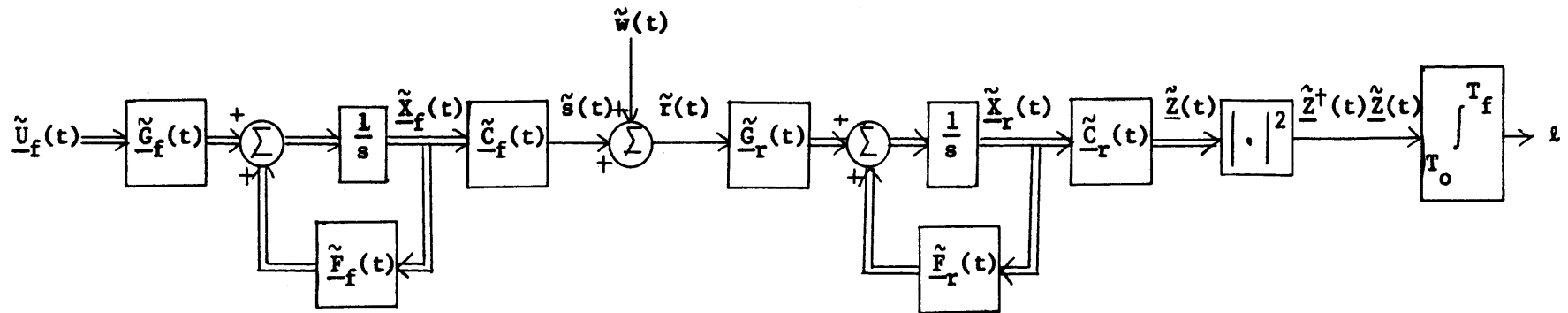
Figure 6.3. Finite state approximation to the DFSI receiver for the doubly-spread channel, signal plus noise input.

$$\underline{Q}(t) \;=\; \begin{bmatrix} \overset{\thicksim}{\underline{Q}}_f(t) & 0 \\[2em] 0 & N_0 \end{bmatrix}$$

$$\overset{\thicksim}{\underline{C}}(t) \;=\; [0,\; \overset{\thicksim}{\underline{B}}_r(t)]$$

$$\overset{\thicksim}{\underline{u}}(t) \;=\; \begin{bmatrix} \overset{\thicksim}{\underline{U}}_f(t) \\[2em] \overset{\thicksim}{\underline{w}}(t) \end{bmatrix}$$

$$\underline{P}_o(t) \;=\; \begin{bmatrix} \overset{\thicksim}{\underline{P}}_{of} & \underline{0} \\[2em] \underline{0} & \overset{\thicksim}{\underline{P}}_{or} \end{bmatrix} \tag{6.29}$$

The matrix $\overset{\thicksim}{\underline{P}}_{of}$ is partitioned into submatrices

$$\overset{\thicksim}{\underline{P}}_{ijf} \;=\; \int\limits_{L_o}^{L_f} \int\limits_{L_o}^{L_f} \overset{\thicksim}{\underline{P}}_o(x,y)\; \overset{\thicksim}{\psi}{}_i^*(x)\overset{\thicksim}{\psi}_j(y)\,dxdy \tag{6.30}$$

and $\overset{\thicksim}{\underline{P}}_{or}$ is any Hermetian matrix with a non-negative definite real part.

When noise alone is the input to the receiver, the model is

$$\overset{\thicksim}{\underline{x}}(t) \;=\; \overset{\thicksim}{\underline{X}}_r(t)$$

$$\overset{\thicksim}{\underline{F}}(t) \;=\; \overset{\thicksim}{\underline{A}}_r(t)$$

$$\overset{\thicksim}{\underline{G}}(t) \;=\; \overset{\thicksim}{\underline{G}}_r(t)$$

$$\overset{\thicksim}{\underline{C}}(t) \;=\; \overset{\thicksim}{\underline{C}}_r(t)$$

$$\tilde{\underline{Q}} = N_0$$

$$\tilde{\underline{u}}(t) = \tilde{\underline{w}}(t)$$

$$\underline{P}_o = \tilde{\underline{P}}_{or} \tag{6.31}$$

Thus the semi-invariant moment-generating functions for the finite state approximation to the DFSI suboptimum receiver can be evaluated. These lead to the error probabilities as discussed in Chapter II. The number of terms in each of the expansions of (6.13), (6.22) and (6.23) is increased in some uniform fashion until the performance converges.

The computer time required to compute the error probabilities for the DFSI receiver in the manner described above is considerably greater than that needed for the evaluation of the optimum error probabilities. The composite state variable model in Figure 6.3 has twice the dimensions of the corresponding approximation used for the optimum receiver calculations. Furthermore, to find the suboptimum receiver error probability bounds, it is necessary to compute the appropriate moment-generating function for a number of different values of s. This implies a computation time that is greater than that used in the optimum receiver case by a factor of 50 or 100.

For this reason no numerical results will be presented here. More efficient programming could significantly reduce the computation required in this problem, so that the method presented above could be

applied. It is likely that the doppler-spread FSI receiver results in Chapter III would provide a useful guide to the DFSI receiver optimization in this case.

B. A Correlator-Squarer-Sum Suboptimum Receiver

This section considers a second suboptimum receiver structure for the doubly-spread channel. It is similar to the correlator-squarer-sum (CSS) receivers used for doppler-spread and delay-spread signals in Chapter III and IV, respectively. Its performance is found by specifying the moment-generating functions of the receiver decision statistic. The performance of the doubly-spread CSS receiver is compared with the optimum receiver in some numerical examples.

The CSS structure used for the doubly-spread channel is just a combination of those of the doppler-spread and delay-spread CSS receivers presented earlier. A motivation for this receiver choice is provided by writing the decision statistic of the DFSI receiver of the previous section as

$$\ell = \int_{L_o}^{L_f} \int_{T_o}^{T_f} \left| \int_{T_o}^{T_f} \tilde{h}(\lambda,t,\tau) \tilde{f}^*(\tau-\lambda) \tilde{r}(\tau) \right|^2 dt \, d\lambda$$

$$= \sum_{i=1}^{M} \int_{T_o}^{T_f} \left| \int_{T_o}^{T_f} \tilde{h}(i\Delta\lambda,t,\tau) \tilde{f}^*(\tau-i\Delta\lambda) \tilde{r}(\tau) \right|^2 dt \; i\Delta\lambda \qquad (6.32)$$

where $\tilde{h}(x,t,\tau)$ is the impulse response of distributed filter following the multiplier in Figure 6.2. Now each term in (6.23) is the output of a FSI receiver. It seems reasonable to replace these FSI receivers with the doppler-spread CSS receiver structure: a subinterval correlator

followed by a sampler, squarer, and weighted summation.

The doubly-spread CSS structure which results is shown in Figure 6.4. The number branches, M, is $(L_f - L_o)/\Delta\lambda - 1$; the number of correlations in each branch, N, is $(T_f - T_o)/\tau$. Note that some of the correlator output samples, r_{ij}, will be zero because $\overset{\gamma}{f}(t - i\Delta\lambda)$ is non-zero only over $[i\Delta\lambda, T + i\Delta\lambda]$. The delayed replicas of $\overset{\gamma}{f}(t)$ used for the correlations can be obtained by passing $\overset{\gamma}{f}(t)$ into a tapped delay line. The variables in the receiver structure of Figure 6.4 are N, M, and the weights, W_{ij}.

The structure of the CSS receiver can be simplified considerably when the envelope $\overset{\gamma}{f}(t)$ is constant and when $\Delta\lambda = m\tau$ for some integer m. In this case many of the sampled correlator outputs in different branches are the same. The simple structure of Figure 6.5 results. The number of correlators, N, and weights W_i are variable in this receiver.

The performance of the CSS receiver for the doubly-spread channel can be obtained since the decision statistic is a finite weighted sum of squared Gaussian random variables, the $\tilde{r}_{ij}$ in Figure 6.4. If a vector $\overset{\sim}{\underline{R}}$ is defined by

$$\overset{\sim}{\underline{R}}^\dagger = [\tilde{r}_{11}, \tilde{r}_{12}, \ldots, \tilde{r}_{1N}, \tilde{r}_{21}, \ldots, \tilde{r}_{MN}]^* \qquad (6.33)$$

then from (2.118) and (2.119)

$$\mu_0(s) = \ln \det (I - s\underline{W}\,\underline{\Lambda}_n)$$

$$\mu_1(s) = \ln \det(I - s\underline{W}\,\underline{\Lambda}_s) \qquad (6.34)$$
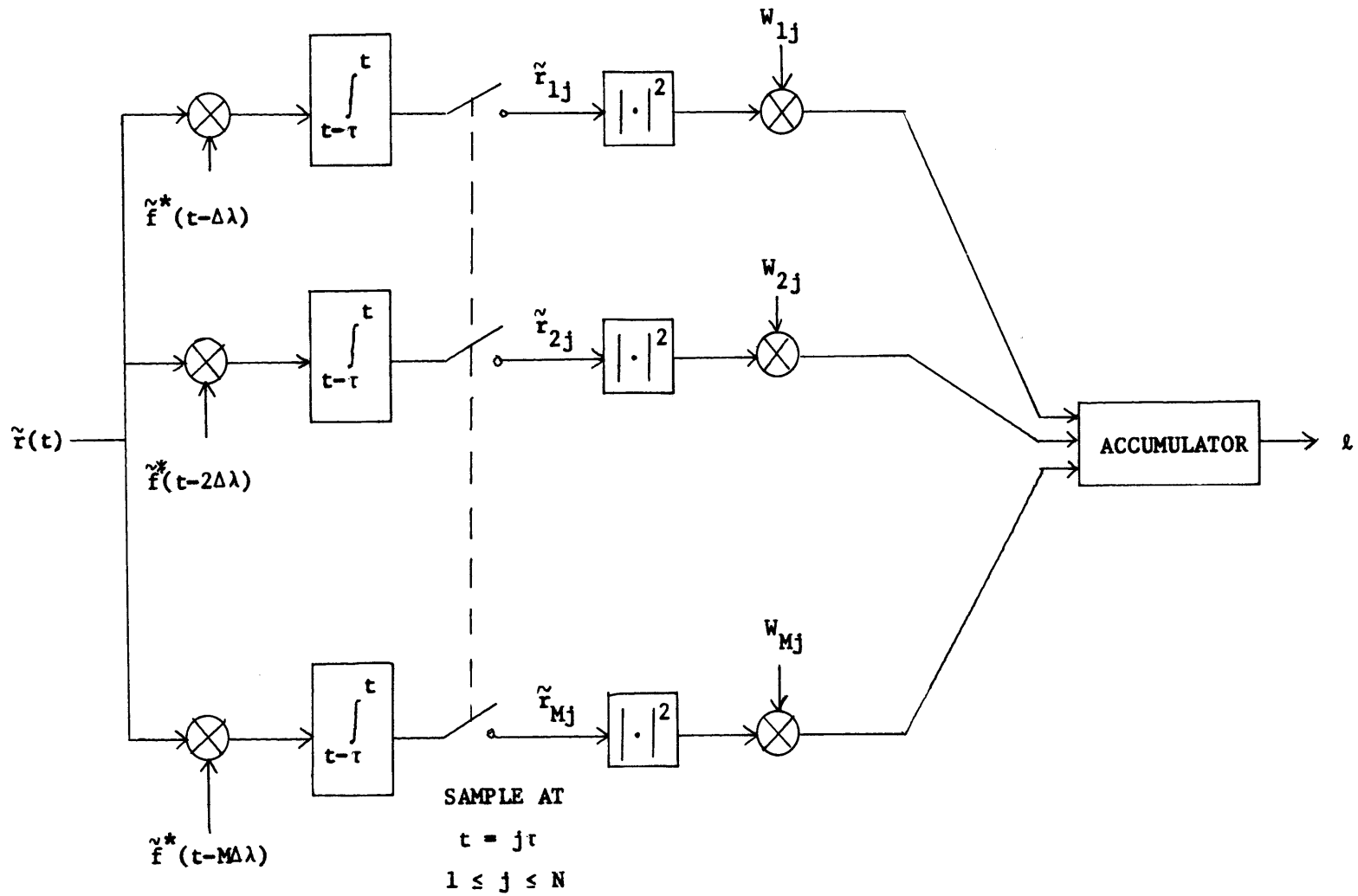
Figure 6.4. Complex version of the doubly-spread channel CSS suboptimum receiver.

$$\tilde{r}(t) \rightarrow \boxed{\int_{t-\tau}^{t}} \quad \text{SAMPLE AT} \quad \tilde{r}_i \rightarrow \boxed{|\cdot|^2} \xrightarrow{W_i} \otimes \rightarrow \boxed{\text{ACCUMULATOR}} \rightarrow \quad \ell = \sum_{i=1}^{N} W_i |\tilde{r}_i|^2$$

SAMPLE AT

$t = j\tau$

$1 \le j \le N$
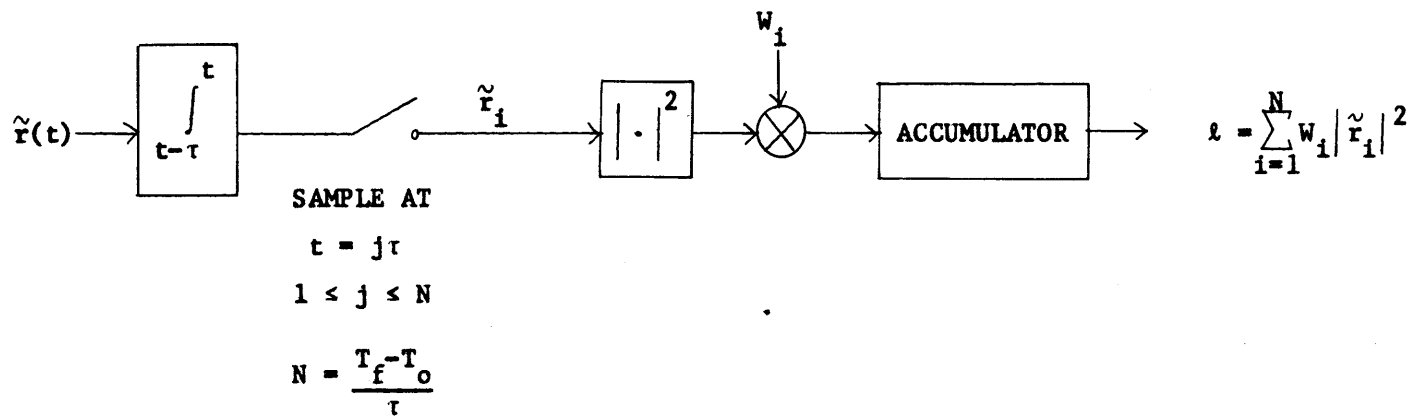
$N = \dfrac{T_f - T_o}{\tau}$

Figure 6.5. Simplified version of the doubly-spread channel CSS receiver for constant $\tilde{f}(t)$ and $m\Delta\lambda = \tau$.

The weighting matrix $\underline{W}$ is diagonal with the weights W_{ij} in Figure 6.4 arranged in the same manner as the $\tilde{r}_{ij}$ in (6.33). The covariance matrices are

$$\underline{\Lambda}_n = E[\overset{\sim}{\underline{R}}^\dagger \overset{\sim}{\underline{R}} \,|\,\text{noise }]$$

$$\underline{\Lambda}_s = E[\overset{\sim}{\underline{R}}^\dagger \overset{\sim}{\underline{R}} \,|\,\text{signal + noise }] \qquad (6.35)$$

The elements of $\underline{\Lambda}_n$ can be found from

$$E[\tilde{r}_{ij} \tilde{r}_{k\ell}^* \,|\,\text{noise}] = \int_{(j-1)\tau}^{j\tau} \int_{(\ell-1)\tau}^{\ell\tau} \tilde{f}^*(t-i\Delta\lambda)\tilde{f}(u-k\Delta\lambda)\tilde{K}_r(t,u)dtdu$$

$$= N_o \int_{(j-1)\tau}^{j\tau} \int_{(\ell-1)\tau}^{\ell\tau} \tilde{f}^*(t-i\Delta\lambda)\tilde{f}(u-k\Delta\lambda)\delta(t-u)dtdu$$

$$\cdot$$

$$(6.36)$$

and those of $\underline{\Lambda}_s$ from

$$E[\tilde{r}_{ij} \tilde{r}_{k\ell} \,|\,\text{signal + noise }] = \int_{(j-1)\tau}^{j\tau} \int_{(\ell-1)\tau}^{\ell\tau} \tilde{f}^*(t-i\Delta\lambda)\tilde{f}(t-k\Delta\lambda)$$

$$[\tilde{K}_s(t,u) + N_o\delta(t-u)]dtdu \qquad (6.37)$$

$\tilde{K}_s(t,u)$ is given by (5.4).

For the simplified structure of Figure 6.5, let the vector $\overset{\sim}{\underline{R}}$ be defined by

$$\overset{\sim}{\underline{R}} = \begin{bmatrix} r_1 \\ \cdot \\ \cdot \\ \cdot \\ \overset{\cdot}{r}_N \end{bmatrix} \qquad (6.38)$$

and $\underline{W}$ be **diagonal** with elements W_i. Then the elements of $\underline{\Lambda}_n$ and $\underline{\Lambda}_s$

can be found by

$$E[\tilde{r}_i \tilde{r}_j^* \,|\text{noise}\,] = \int_{(i-1)\tau}^{i\tau} \int_{(j-1)\tau}^{j\tau} N_o \delta(t-u)dtdu = N_o \tau \delta_{ij} \qquad (6.39)$$

$$E[\tilde{r}_i \tilde{r}_j^* \,|\text{signal + noise}\,] = \int_{(i-1)\tau}^{i\tau} \int_{(j-1)\tau}^{j\tau} \tilde{K}_s(t,u)dtdu + N_o \tau \delta_{ij}$$

$$(6.40)$$

Note that the calculation of the error probabilities for the

CSS receiver does not require the distributed-parameter state-variable model

for the doubly-spread channel. The most difficult feature of the performance

calculation is finding the covariance matrix $\underline{\Lambda}_s$. The integrations

are tedious, if not impossible, so that numerical methods are required

in most cases.

For an example of the relative performances of the CSS receiver

and the optimum receiver, consider the particular doubly-spread

channel of Chapter V, Section E. The channel model is first order

$$\tilde{S}(x,f) = \frac{\dfrac{2k}{L}\left(1-\cos\dfrac{2\pi x}{L}\right)}{(2\pi f)^2 + k^2} \,, \quad \begin{array}{l} 0 \le x \le L \\ -\infty < f < \infty \end{array}$$

$$\qquad\qquad 0 \qquad\qquad \text{elsewhere} \qquad (6.41)$$

and the transmitted signal envelope $\tilde{f}(t)$ is constant over the interval

$[0,T]$. The error probability bound exponent, $\mu_{bc}(s)$, for binary ortho-

gonal communication is computed for the simplified CSS receiver of Figure
6.5. The $\underline{\Lambda}_s$ and $\underline{\Lambda}_n$ matrices are given above; the integration required to
obtain $\underline{\Lambda}_s$ is quite tedious.

The weights W_i in Figure 6.5 are chosen according to the formula

$$W_i = \int_{\min[i\tau-.5,L]}^{\max[0,i\tau-.5-T]} \sqrt{\frac{1}{L}(1-\cos\frac{2\pi x}{L})}\,dx \qquad \begin{array}{l} 1 \leq i \leq N \\ \\ N\tau = T + L \end{array}$$

$$(6.42)$$

This choice is motivated by the weights used in the doppler-spread and
delay-spread CSS receivers. In Figure 6.4, this suggests that within
a branch, each sample be weighed equally, but that from branch to
branch the weightings should be proportional to the scattering function
profile, $\tilde{S}(x,0)$. The choice of (6.42) approximates this weighting,
since the structure of Figure 6.5 is a collapsed version of the CSS
receiver in Figure 6.4.

Figure 6.6 gives a plot of the error probability bound exponents
of the optimum and CSS receivers for this example when the kL product
is less than one (kL = .25). For the optimum receiver $\mu_{*bc}(-.5)$ is
plotted, and for the CSS receiver the minimized value of $\mu_{bc}(s)$ is
shown. The optimum receiver curves come from Figure 5.4. The number of
correlations in the CSS receiver is optimized for each point on the
curves; this value is given in parentheses in Figure 6.6. Note that
the optimized CSS receiver performance is from one to two dB less than
optimum in this example.

Figure 6.6. Relative performance of the CSS and optimum receivers, binary orthogonal communication, underspread delay-spread channel.

Figures 6.7 and 6.8 present similar curves for the cases of
unity spread and overspread (kL = 6.25) channels. In both figures
the optimized CSS receiver performance is again from one to two dB
less than optimum. The optimum receiver curves are taken directly
from Figures 5.5 and 5.6.

In this example the CSS suboptimum receiver performed adequately,
relative to the optimum receiver. The structure of the CSS receiver
is much simpler than that of the optimum receiver, and thus the perfor-
mance degradation may be acceptable from this point of view. It is
likely also that there exists a different choice of weights, W_i, which
would improve the CSS receiver performance in this example. Choosing
both the weights and the number of correlators is a more complicated
optimization problem, however.

The results of the CSS receiver and optimum receiver comparison
in this example suggest that it would be worthwhile to consider the
CSS structure as a suboptimum receiver for other signals and scattering
functions. Of course, there is no guarantee that the CSS receiver
performance will always be within one or two dB of the optimum in all
cases.

C. Summary

This chapter has considered several suboptimum receiver structures
for the doubly-spread channel. The first is a distributed version of
the FSI receiver for the doppler-spread channel. The received signal
$\tilde{r}(t)$ is multiplied by $\tilde{f}^*(t-\lambda)$ and passed through a distributed linear
filter of the same order as that which is used for the channel model.
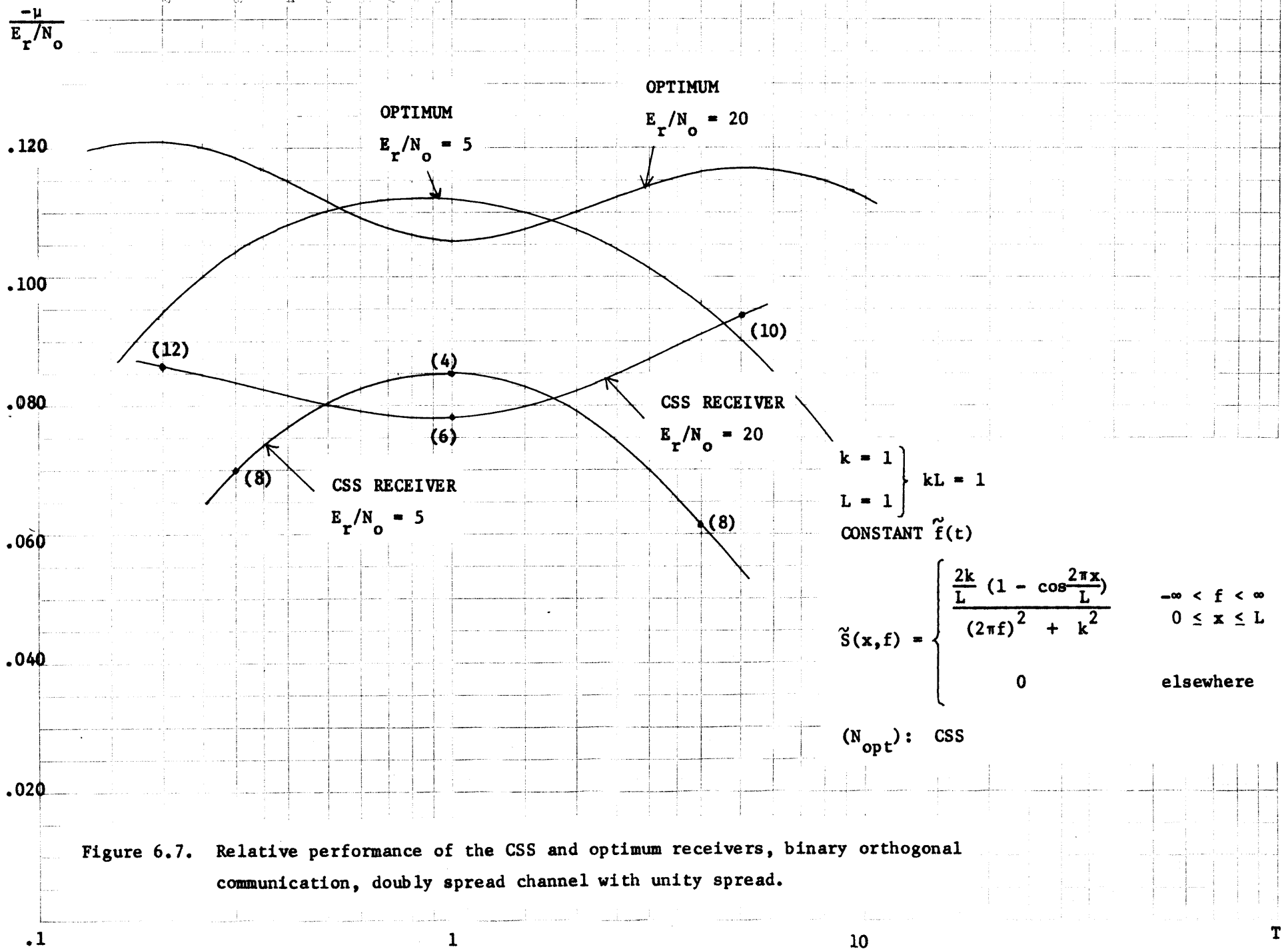The output is squared and integrated over both its time and space

Figure 6.7. Relative performance of the CSS and optimum receivers, binary orthogonal communication, doubly spread channel with unity spread.
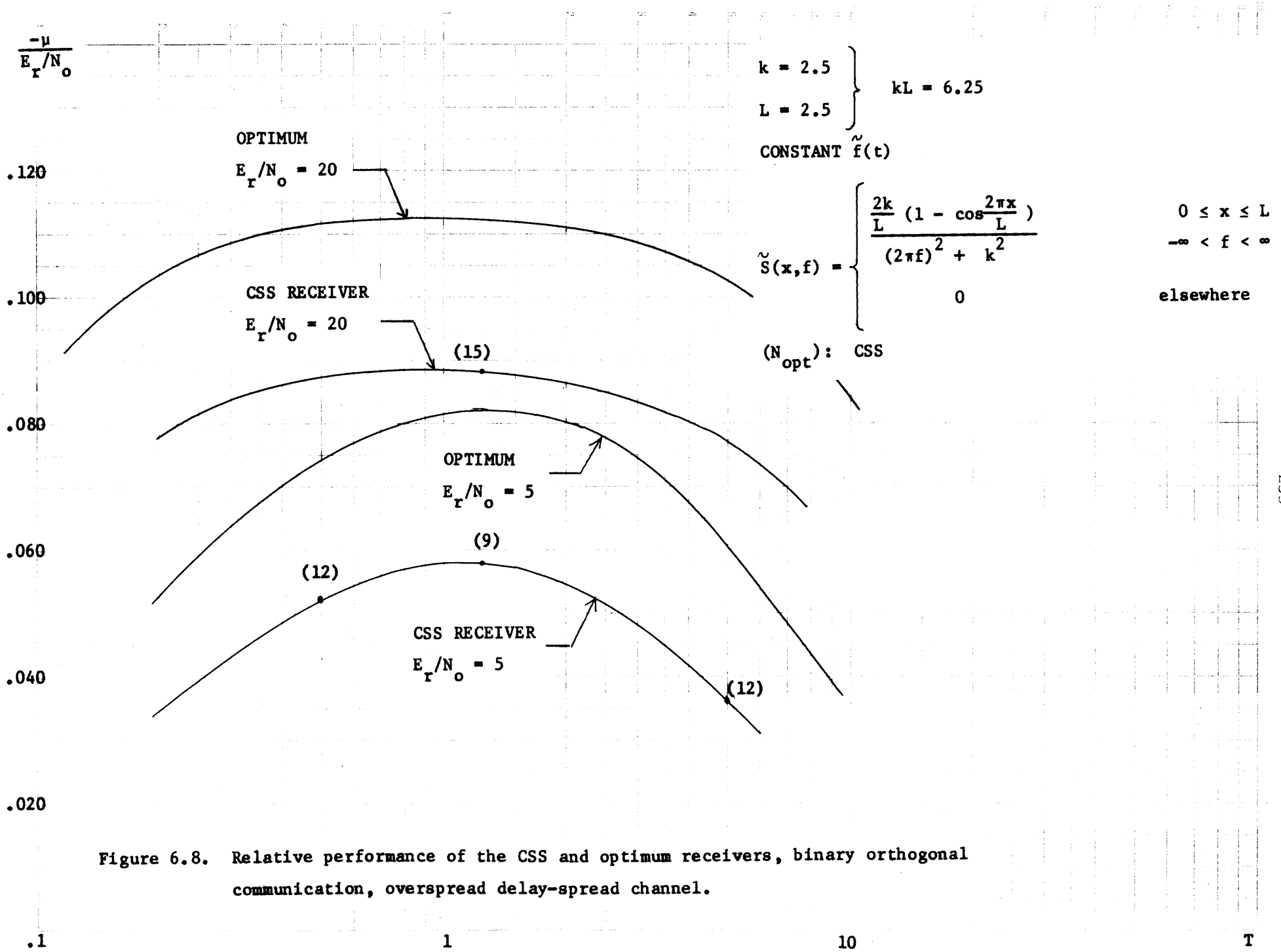
$$\frac{-\mu}{E_r/N_o}$$

OPTIMUM
$$E_r/N_o = 20$$

$$k = 2.5$$
$$L = 2.5$$
$$kL = 6.25$$

CONSTANT $\tilde{f}(t)$

.120

.100

CSS RECEIVER
$$E_r/N_o = 20$$

(15)

$$\tilde{S}(x,f) = \begin{cases} \dfrac{\dfrac{2k}{L}(1 - \cos\dfrac{2\pi x}{L})}{(2\pi f)^2 + k^2} & \begin{array}{l} 0 \le x \le L \\ -\infty < f < \infty \end{array} \\ \\ 0 & \text{elsewhere} \end{cases}$$

(N_{opt}): CSS

.080

OPTIMUM
$$E_r/N_o = 5$$

.060

(9)

(12)

CSS RECEIVER
$$E_r/N_o = 5$$

.040

(12)

.020

Figure 6.8. Relative performance of the CSS and optimum receivers, binary orthogonal
communication, overspread delay-spread channel.

.1   1   10   T

variables.

A method of finding the performance of the FSI receiver was presented. It involved reduction of the receiver distributed filter and the channel model to finite state systems by the modal approach given in Chapter V. The moment-generating functions of the receiver decision statistic were found by the method used for the doppler-spread FSI receiver in Chapter III. No numerical results were presented because the computer time required to evaluate the performance was prohibitive without more efficient programming.

A second suboptimum structure was considered for the doubly-spread channel. It is a combination of the CSS receivers for the doppler-spread and delay-spread channels. The signal $\tilde{r}(t)$ is correlated with a set of delayed replicas of $\tilde{f}(t)$. Each correlator is a gated correlator of the type used in the doppler-spread channel CSS receiver. The correlator samples are squared, weighted, and summed to form the decision statistic.

The performance of the CSS receiver was compared to the optimum receiver performance for the example treated in Chapter V. The optimized CSS receiver performance was within two dB of the optimum over a wide range of parameters.

The treatment of suboptimum receivers for the doubly-spread channel in this chapter is by no means complete. Only two structures were considered here. A number of other possibilities are attractive [6], such as a filter-squarer-filter receiver. The techniques demonstrated in this chapter should be useful in the analysis of these suboptimum receivers.

CHAPTER VII

CONCLUSION

The preceding chapters have considered the problem of detecting known signals transmitted over dispersive channels. This is a special case of the Gaussian signal in white Gaussian noise detection problem. Optimum and suboptimum receiver performance has been investigated for the cases of doppler-spread, delay-spread, and doubly-spread channels. A summary of the results of each chapter is presented below. Topics for further research are then discussed.

Chapter II considered the problem of evaluating the error probabilities for binary detection with a suboptimum receiver. Series expressions for these error probabilities were developed by using tilted probability densities and Edgeworth expansions. Bounds on the suboptimum receiver error probability for M-ary communication with orthogonal Gaussian signals were also found in a similar manner. In order to evaluate these expressions, it was necessary to have the semi-invariant moment-generating function of the receiver decision statistic under both hypotheses. The moment-generating functions for the optimum receiver were reviewed; it was pointed out that efficient computation of the moment-generating functions was possible when the random processes in the problem had state-variable representations. Moment-generating functions for two types of suboptimum receivers were found: filter-squarer-integrator receivers and those with a decision statistic which is a finite, weighted sum of squared complex Gaussian random variables.

Chapter III concerned the reception of known signals transmitted over the doppler-spread channel. The performance of the optimum receiver was reviewed in the case when the channel fading process has a lumped-parameter state-variable representation. Two suboptimum receivers were suggested for the doppler-spread channel. One structure (FSI) consisted of a filter followed by a square-law envelope detector and an integrator. The other (CSS) was a correlator whose output was sampled several times during the observation interval: the samples were squared, weighted, and summed.

The performance of each of these suboptimum receivers was evaluated by the techniques of Chapter II and compared with the optimum receiver performance. By properly designing the suboptimum receivers, it was possible to come within one dB of the optimum receiver performance in a number of examples. The CSS receiver performed better for low values of kT, and the FSI receiver was closer to the optimum for large kT, where k was the fading bandwidth and T the transmitted signal duration. The numerical examples also provided guidelines for optimally choosing the FSI and CSS receiver parameters. Of course, for arbitrary signals and channel fading, it may not be possible to do this well with the FSI and CSS receivers.

Chapter VI investigated the delay-spread channel detection problem. The concept of time-frequency duality was reviewed and the relationship between a delay-spread channel and its dual doppler-spread channel was discussed. It was pointed out that the FSI and CSS suboptimum receivers for the doppler-spread channel have dual structures which are suboptimum for the delay-spread channel. In the case of the

FSI receiver the dual structure was called a two-filter radiometer (TFR).
It consisted of a filter matched to the transmitted signal, followed by
a square law device and weighted integration. The performance of the sub-
optimum receivers was exactly that presented in Chapter III for their
duals. The use of duality is particularly suited to delay-spread
channels with scattering distributions that are infinite in duration
and transmitted signals which are strictly bandlimited.

A more direct approach was given for finding the performance of
the optimum receiver for a delay-spread channel. It involves a series
expansion of the channel model. Truncation of the series yields an
approximation for the delay-spread channel. The optimum receiver and
its performance was found for the truncated model. The number of terms
in the series was allowed to increase until the approximate performance
converged to the optimum receiver performance for the actual delay-spread
channel. A similar technique was applied to the TFR suboptimum receiver.
Also suggested was a second suboptimum receiver which correlated the
received signal with a number of delayed replicas of the transmitted
signal. The correlator outputs were sampled, squared, weighted, and
summed. The two suboptimum receivers were compared with the optimum
receiver in several examples; their performance was within one or two
dB of the optimum. The advantage of this direct approach to the per-
formance analysis is that it is suitable for transmitted signals and
scattering distributions of finite duration. It is not clear, however,
how to obtain the orthogonal expansion to ensure rapid convergence or
easy computation of the semi-invariant moment-generating functions.

Chapter V presented a distributed-parameter state-variable model for the doubly-spread channel. The scattering process was modeled as the output of a distributed linear system whose dynamics are described by a partial differential equation driven by a temporally white, complex, distributed random process. The model was shown to be valid for correlated and non-stationary scattering. The special case of a WSSUS channel model was investigated, and the class of scattering functions which can be described by the distributed-parameter state-variable model was given.

A realizable (causal) structure for the doubly-spread channel optimum receiver was specified. It made use of the MMSE realizable estimate of the distributed state vector in the channel model. The estimation equations were partial differential equations. A by-product of the estimator derivation was an equation which specified the MMSE filtering error for the doubly-spread channel output. This was used to calculate the moment-generating functions for the optimum receiver, from which the error probabilities can be obtained.

In order to find the optimum receiver performance in this manner, it was necessary to solve for the error covariance matrix of the distributed parameter state-vector estimate. This matrix was the solution of a partial integro-differential equation, with partial derivatives in the time variable and integration over the spatial variables. A modal approach to the solution of this equation was given. It involved a double orthogonal expansion of the covariance matrix in its spatial variables. The spatial dependence was integrated out of the equations to give a finite state approximation for the distributed

channel model. The resulting matrix Ricatti equation was solved by conventional techniques. The number of terms in the truncated series was increased until the performance expression converged.

An example using this modal approach was presented. The performance was calculated for a number of cases; the calculations consumed a reasonable amount of computer time. An implicit diversity description of the channel provided an interpretation of the results. The performance of a simple signal over the doubly-spread channel of this example was good, even when the channel was overspread.

Chapter VI investigated the performance of several suboptimum receivers for the doubly-spread channel. One structure was a distributed filter-squarer-integrator (DFSI), an extension of the FSI receiver for the doppler-spread channel. The modal technique of Chapter 5 was applied to the DFSI receiver to reduce it to a finite state model. The techniques used in Chapter III for the FSI receiver were used to find the DFSI moment generating functions. No numerical examples were presented, however, because excessive computer time was required. A second suboptimum receiver was suggested which combined the structures of the CSS receivers for the doppler-spread and delay-spread channels. Its performance was evaluated and compared to the optimum receiver performance in an example. It was suggested that there are other attractive candidates for doubly-spread channel suboptimum receivers that could be analyzed.

One topic for possible further research is the signal design problem. This involves choosing $\tilde{f}(t)$ for transmission over a spread channel and minimizing the error probability or some other measure of

performance, under some set of constraints. Whether or not such study of this problem is of real importance is likely to depend on the set of constraints chosen. The numerical examples presented in the previous chapters showed that it was possible to obtain a performance with simple signals within one DB of the best possible performance. This was observed for a wide variety of channel parameters, but it was necessary that the signal duration or bandwidth assumed the optimum value in each case. With only one dB in performance to be gained, the effort spent in studying the signal design problem might be better spent elsewhere. However, if the constraints on signal parameters, such as peak power, duration, or bandwidth, are such that the simple signals no longer provide efficient performance, then the signal design problem becomes more interesting.

A problem in designing signals for spread channels is finding an approach which actually provides solutions. A signal design method that has been successful in several detection problems [30,31] seeks to formulate the problem so that it fits the results of optimal control theory [32]. This approach has been attempted by Collins [13] for the doppler-spread channel signal design problem. In this case, the binary orthogonal communication error probability bound exponent, $\mu_{*bc}(-.5)$, for the optimum receiver can be expressed as several integrals of MMS realizable filtering errors, as given in Chapter II. When the fading has a state-variable representation, these filtering errors are solutions of differential equations which involve the transmitted signal $\tilde{f}(t)$. This fits the optimal control theory formulation, so that the minimum principle can be applied to find a set of neccessary conditions

for the minimization of $\mu_{*hc}(-.5)$. Collins [13] did this with an

energy constraint on the signal $\tilde{f}(t)$, but he could not obtain realistic

solutions. It appears that one should also impose an amplitude constraint

on $\tilde{f}(t)$ or its derivative in order to make the optimal control problem

meaningful.

In the course of the research for this thesis, the signal optimi-

zation problem for the doppler-spread channel was considered also, this

time with a peak power constraint in addition to the energy constraint.

A set of necessary conditions on the signal waveform was derived in the

form of non-linear differential equations with mixed initial and final

conditions. Since analytic solution of this boundary value problem

appeared impossible, numerical techniques were considered [36,37]. The

necessary conditions indicated that the optimal signal either assumed

its maximum amplitude, or was off, or satisfied a "singular" condition

during the transmission interval. A numerical gradient technique [36,37]

was applied to the problem after assuming an on-off $\tilde{f}(t)$. The signals

which resulted had a performance of the same order as the pulse train

signal considered in Chapter III.

In the doppler-spread case the effort required to apply these

numerical techniques did not seem worth the performance improvement

that resulted. Of course, with different constraints on the signal

there may be a greater performance gain to be realized. Unfortunately,

this approach appears to be less attractive for the delay-spread and

doubly-spread channels. Here the approximate state-variable models of

Chapters IV and V for these channels have large dimensions; the numerical

techniques for finding the optimum signals in the control theory model

are not well suited to this case. For suboptimum receivers the signal

design problem is more complicated, since $\mu_{bc}(s)$ must be minimized over

s as well as the signal shape.

There are several other topics directly related to the thesis in

which further research may be fruitful. One is the modal approach to the

calculation of the doubly-spread channel optimum receiver error probabilities.

It was pointed out in Chapter V that how to choose the orthonormal series

for fast convergence or easy computation was not clear. It would be

helpful to have an organized method for making this choice. More

experience in working examples should provide guidelines in this matter.

Another topic of interest is the performance of various signals

over doubly-spread channels with different scattering functions. Chapter

V discussed only one example in detail. The techniques of Chapter V

can be applied to other signals and scattering functions, however. This

would provide a better understanding of the properties and limitations

of the doubly-spread channel.

The issue of suboptimum receivers for the doubly-spread channel

is one which deserves further attention. Several structures were

considered in Chapter VI, but there are others which are attractive

candidates in the doubly-spread case [6]. The techniques of Chapters V

and VI provide an approach to the analysis of the performance of these

suboptimum receivers which may be useful.

There are other problems which lie outside the context of this

thesis but which may well permit application of the techniques developed

here. For example, the problem of communicating with sequences of

signals is an extension of the single transmission problem considered

here. Another is the detection of signals transmitted over spread

channels and received in non-white Gaussian noise. The application of the

results of this thesis to this problem should be straightforward. Also,

the doubly-spread channel model presented in Chapter V provides a useful

characterization for clutter in some problems. The modal technique

for analyzing the doubly-spread channel optimum receiver performance

can be used in the detection in clutter problem, as discussed by

Van Trees [8].

APPENDIX I

A SYSTEM RELIABILITY FUNCTION FOR FILTER-SQUARER-

INTEGRATOR RECEIVERS, M-ARY ORTHOGONAL COMMUNICATION

This Appendix derives the suboptimum receiver system reliability function, $E^o(\frac{R}{C})$, used in the M-ary orthogonal communication error probability bounds of (2.58) and (2.59). The filter-squarer-integrator receiver has all branches identical except for carrier frequency, and all branch outputs are assumed to be statistically independent and identically distributed when noise alone is the input. The derivation that follows is similar in outline to Kennedy's [6] for the optimum receiver. For suboptimum receivers the derivation is complicated by the fact that the moment-generating functions, $\mu_{1c}(s)$ and $\mu_{0c}(s)$, of the receiver branch outputs are not simply related, as is the case for the optimum receiver.

To begin it is convenient to overbound (2.43) and (2.44) using the results given by (2.14) and (2.31). Equation (2.46) is bounded by

$$Pr(\ell_s \leq h) < e^{\mu_{1c}(s) - s\dot{\mu}_{1c}(s)}$$

(I-1)

$$s \leq 0 , \qquad h = \dot{\mu}_{1c}(s)$$

Similarly, for (2.57)

$$Pr(h < \ell_s \leq \ell_n) \leq e^{\mu_{0c}(t) + \mu_{1c}(r-t) - r\dot{\mu}_{1c}(r-t)}$$

(I-2)

$$r \geq 0 , \qquad t \geq 0 , \qquad h = \dot{\mu}_{1c}(r-t)$$

Since $\mu_{1c}(s)$ is monotonic the conditions of (I-1) and (I-2) imply that $s = r - t$. Then (2.43) is bounded by

$$Pr(\epsilon) \leq e^{\mu_{1c}(s)-s\dot{\mu}_{1c}(s)}\left[1 + Me^{\mu_{0c}(t)-t\dot{\mu}_{1c}(s)}\right]$$

$$\text{(I-3)}$$

$$s \leq 0, \quad t \geq 0, \quad s + t \geq 0$$

The lower bound of (2.44) can be written from (I-1) and (2.14) as

$$Pr(\epsilon) \geq \frac{M}{4} B e^{\mu_{1c}(s)-s\dot{\mu}_{1c}(s)+\mu_{0c}(t)-t\dot{\mu}_{0c}(t)}$$

$$\text{(I-4a)}$$

where B is the product of the bracketed terms in (2.14) and (2.31). Also let s and t be determined by

$$\dot{\mu}_{1c}(s) = \dot{\mu}_{0c}(t) \qquad t \geq 0, \quad s \leq 0$$

$$\text{(I-4b)}$$

and the further condition

$$M e^{\mu_{0c}(t)-t\dot{\mu}_{0c}(t)} \leq 1$$

$$\text{(I-4c)}$$

If (I-4c) holds, then so does (2.45), by virtue of (2.37). For upper bounds on the value of B, see Kennedy [6].

The values of s and t will be chosen to optimize these bounds. The results will be expressed in terms of

$$\tau = T_f - T_o$$

$$\text{(I.5a)}$$

$$R = \frac{\log_2 M}{\tau}$$

$$\text{(I.5b)}$$

$$C = \frac{\alpha}{\tau \, \ln 2} \qquad \text{(I.5c)}$$

$$\alpha = \frac{E_r}{N_o} \qquad \text{(I.5d)}$$

C is the infinite bandwidth, additive white Gaussian noise channel capacity in bits/second, and E_r is the expected value of the received energy in $s_k(t)$ during the observation interval.

A. Properties of $\mu_{1c}(s)$ and $\mu_{0c}(s)$

The semi-invariant moment-generating function of a branch output, ℓ, with signal plus noise as the input to the branch is, from (2.99),

$$\mu_{1c}(s) = E[e^{s\ell} \mid \text{signal + noise}]$$

$$= - \sum_{n=1}^{\infty} \ln(1 - s\lambda_{1n}) \qquad \text{(I.6a)}$$

$$s < \left[\max_n \left\{ \lambda_{1n} \right\} \right]^{-1} \qquad \text{(1.6b)}$$

where the $\{\lambda_{1n}\}$ are the eigenvalues of $\tilde{z}(t)$ in Figure 2.1 given signal plus noise as the input. With noise alone as the branch input

$$\mu_{0c}(s) = E[e^{s\ell} \mid \text{noise}]$$

$$= - \sum_{n=1}^{\infty} \ln(1 - s\lambda_{0n}) \qquad \text{(1.7a)}$$

$$s < \left[\max_n \left\{ \lambda_{0n} \right\} \right]^{-1} \qquad \text{(1.7b)}$$

The $\{\lambda_{0n}\}$ are the eigenvalues of $\tilde{z}(t)$ given that white Gaussian noise is the input to the branch.

Several properites of $\mu_{1c}(s)$ and $\mu_{0c}(s)$ will be useful in the sequel. First,

$$\frac{d^k}{ds^k}\left[\mu_{ic}(s)\right] = \sum_{n=1}^{\infty} (k-1)! \left[\frac{\lambda_{in}}{1 - s\lambda_{in}}\right]^k , \quad k \geq 1, \quad i = 0,1$$

(I.8)

Thus all the derivatives of the $\mu_{ic}(s)$ are positive over values of s given by (I.6b) and (I.7b), and each $d^k/ds^k [\mu_{ic}(s)]$ is a monotonically increasing function of s.

Another property concerns the first derivatives at the origin

$$\dot{\mu}_{ic}(0) = \sum_{n=1}^{\infty} \lambda_{in} \qquad i = 0,1$$

(I.9)

The sum on the right-hand side of (I.9) is just the average energy in $\tilde{z}(t)$ over the observation interval. It is larger when signal plus noise is the input than when r(t) consists of noise alone. Hence

$$\dot{\mu}_{1c}(0) > \dot{\mu}_{0c}(0)$$

(1.10)

Figure I.1 summarizes the two properties.

B. The Upper Bound

If

$$M \, e^{\mu_{0c}(t)-t\dot{\mu}_{1c}(s)} \leq 1$$

(1.11a)
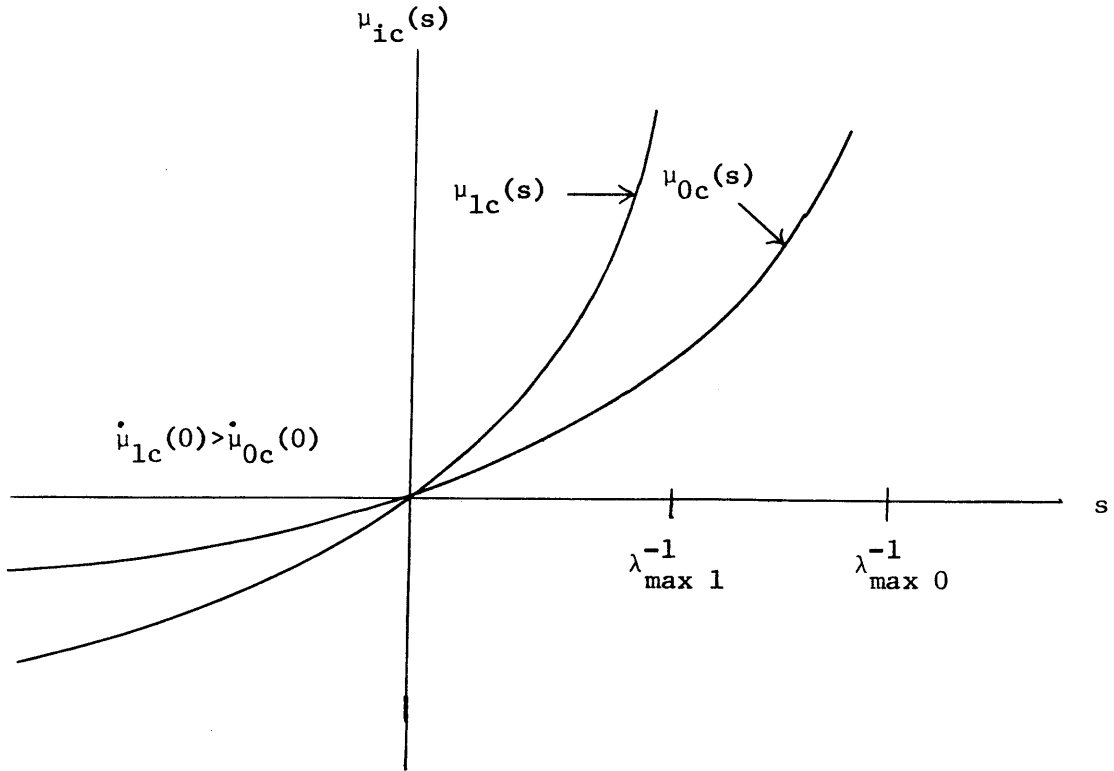
then the upper bound of (1.3) can be further bounded by

Figure I-1. Properties of $\mu_{ic}(s)$.

$$Pr(\epsilon) \leq 2\, e^{\mu_{1c}(s) - s\dot{\mu}_{1c}(s)} \tag{I.11b}$$

Equation (I.11a) can be rewritten using (I.5) as

$$\frac{R}{C} < \frac{1}{\alpha}\left[t\dot{\mu}_{1c}(s) - \mu_{0c}(t) \right] \tag{I.12a}$$

$$s + t \geq 0, \quad t \leq 0, \quad s \leq 0 \tag{1.12b}$$

and (I.11b) similarly as

$$Pr(\epsilon) \leq 2 \cdot 2^{-\tau C E_h\left(\frac{R}{C}\right)} \tag{I.13}$$

where

$$E_h\left(\frac{R}{C}\right) = \frac{1}{\alpha}\left[s\dot{\mu}_{1c}(s) - \mu_{1c}(s) \right], \quad s \leq 0 \tag{I.14}$$

To tighten the bound of (I.13) the function $E_h\left(\frac{R}{C}\right)$ will be maximized over s subject to the constraints of (I.12).

From (I.14), for $s \leq 0$,

$$\frac{d}{ds}\left[E_h\left(\frac{R}{C}\right) \right] = \frac{1}{\alpha}\, s\ddot{\mu}(s) \leq 0$$

and since $E_h\left(\frac{R}{C}\right)$ is zero for $s = 0$, $E_h\left(\frac{R}{C}\right)$ will be maximized by choosing the most negative value of s consistent with (I.12). This constraint may conveniently be rewritten in terms of the function

$$f(s,t) = t\dot{\mu}_{1c}(s) - \mu_{0c}(t) \tag{I.15a}$$

as

$$\frac{R\alpha}{C} < f(s,t), \qquad t \geq 0, \qquad s \leq 0, \qquad s + t \geq 0 \qquad \text{(I.15b)}$$

The nature of the function $f(s,t)$ can be inferred from the derivatives

$$\frac{\partial f}{\partial t} = \dot{\mu}_{1c}(s) - \dot{\mu}_{0c}(t) \qquad \text{(I.16a)}$$

$$\frac{\partial^2 f}{\partial t^2} = -\ddot{\mu}_{0c}(t) \qquad \text{(I.16b)}$$

$$f(s,0) = 0 \qquad \text{(I.16c)}$$

for $t \geq 0$ and $0 \geq s \geq s_0$, where s_0 is determined by

$$\dot{\mu}_{1c}(s_0) = \dot{\mu}_{0c}(0) \qquad \text{(I.16d)}$$

Equation (I.16) and Figure I.1 imply that sections of $f(s,t)$ have the behavior shown in Figure I.2. For the range of s given, $f(s,t)$ has only one inflection point, a maximum at t_a.

Figure 1.2 leads to the sketch of the contours of constant amplitude of $f(s,t)$ in the s-t plane, shown in Figure I.3. The curve A is the locus of the point t_a in Figure I.2. The fact that t decreases along A as s decreases is evident from the definition of A
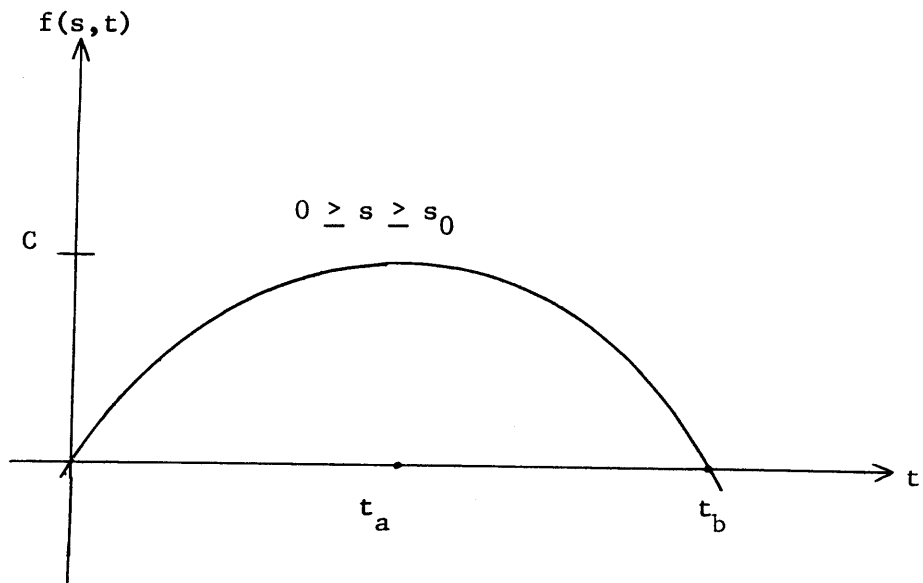
$$t_a: \qquad \dot{\mu}_{1c}(s) = \dot{\mu}_{0c}(t_a)$$

$$t_b: \qquad t_b \dot{\mu}_{1c}(s) = \dot{\mu}_{0c}(t_b)$$

$$s_0: \qquad \dot{\mu}_{1c}(s_0) = \dot{\mu}_{0c}(0)$$

$$C = t_a \dot{\mu}_{0c}(t_a) - \mu_{0c}(t_a)$$

Figure I-2. A section of f(s,t)

locus of A: (s,t) such that $\dot{\mu}_{1c}(s) = \dot{\mu}_{0c}(t)$ $\qquad$ (I.17)

and the properties of the $\mu_{ic}(s)$ illustrated by Figure I.1. The locus
B is that given by $f(s,t) = 0$. Its curvature behaves similar to that
of A. Along A $f(s,t)$ has the value

$$f(s,t)\Big|_A = t\dot{\mu}_{0c}(t) - \mu_{0c}(t) \qquad (I.18)$$

By differentiating (I.18) it can be seen that $f(s,t)\Big|_A$ increases with
increasing t. Hence the maximum of $f(s,t)$ in the region of interest
occurs on A at $s = 0$, as shown in Figure I.3.

$\qquad$ The constraints of (I.11) imply that $f(s,t)$ should exceed $\dfrac{R\alpha}{C}$.
Thus the permissable values of s and t lie within the intersection of
the shaded area and an area like the cross-hatched area, in Figure I.3.
Since $E_h\left(\dfrac{R}{C}\right)$ is maximized by the smallest s, Figure I.3 indicates that
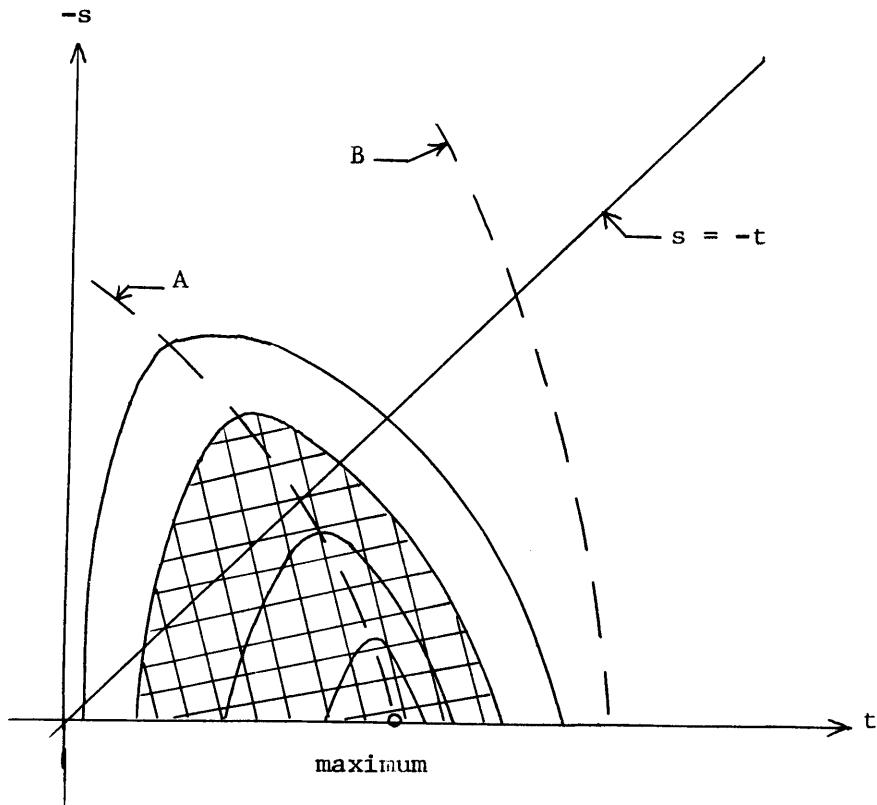there are two types of solutions. If

$$R \geq R_{crit} \qquad (I.19)$$

where

$$\frac{R_{crit}\alpha}{C} = -s'\dot{\mu}_{1c}(s') - \mu_{0c}(-s') \qquad (I.20a)$$

$$\dot{\mu}_{1c}(s') = \dot{\mu}_{0c}(-s'), \qquad s' \leq 0 \qquad (I.20b)$$

then the contour will lie entirely within the allowable region of
the s,t plane. Then the minimum value of s lies on the intersection
of A and the contour

A: locus of $\dot{\mu}_{1c}(s) = \dot{\mu}_{0c}(t)$

B: locus of $t\dot{\mu}_{1c}(s) = \dot{\mu}_{0c}(t)$

Figure I-3.   Contours of constant amplitude of $f(s,t)$.

$$\frac{R}{C} \alpha = t\dot{\mu}_{0c}(t) - \mu_{0c}(t), \qquad t \geq 0 \tag{I.21a}$$

$$\dot{\mu}_{1c}(s_{min}) = \dot{\mu}_{0c}(t), \qquad s_{min} \leq 0 \tag{I.21b}$$

Note that the definition of R_{crit} is the rate for which the contour and the line $s = -t$ just touch.

When $R < R_{crit}$, it is evident from Figure I.3 that the minimum value of s is the lesser of the two solutions determined by the intersection of the line $s = -t$ and the contour; i.e., the minimum of the two values of s that satisfy

$$\frac{R}{C} \alpha = -s\dot{\mu}_{1c}(s) - \mu_{0c}(-s) \qquad s \leq 0 \tag{I.22}$$

To summarize the preceding results, the maximized reliability function for $R \geq R_{crit}$ is given by (I.14) and I.21)

$$E_h^o \left(\frac{R}{C}\right) = \frac{1}{\alpha} \left[s_0 \dot{\mu}_{1c}(s_0) - \mu_{1c}(s_0) \right] \tag{I.23a}$$

$$\dot{\mu}_{1c}(s_0) = \dot{\mu}_{0c}(t_0) \tag{I.23b}$$

$$\frac{R\alpha}{C} = t_0 \dot{\mu}_{0c}(t_0) - \mu_{0c}(t_0) \tag{I.23c}$$

$$t_0 \geq 0, \qquad s_0 \leq 0, \qquad R \geq R_{crit} \tag{I.23d}$$

For $R < R_{crit}$, (I.23a) still holds if s_0 is the minimum of the two solutions to

$$\frac{R\alpha}{C} = -s_0 \dot{\mu}_{1c}(s_0) - \mu_{0c}(-s_0) \qquad R < R_{crit}, \quad s_0 \leq 0 \qquad (I.24)$$

The value of R_{crit} is given by (I.20).

For some values of the rate R a better $E(\frac{R}{C})$ is obtainable. From Eq. (2.70) with h = 0, the $Pr(\epsilon)$ is bounded by

$$Pr(\epsilon) \leq 2 M e^{\mu(s)-s\dot{\mu}(s)}, \qquad s \leq 0 \qquad (I.25)$$

where

$$\mu(s) = \ln E \left[e^{s(\ell_s - \ell_n)} \right]$$

$$= \mu_{1c}(s) + \mu_{0c}(-s) \qquad (I.26)$$

The bound of (I.25) is optimized for $\mu(s) = 0$; then (I.25) may be written

$$Pr(\epsilon) \leq 2 M e^{\mu_{1c}(s) + \mu_{0c}(-s)}$$

$$= 2\, 2^{-\tau C E_\ell^o \left(\frac{R}{C} \right)} \qquad (I.27)$$

by Eq. (I.5), where

$$E_\ell^o \left(\frac{R}{C} \right) = -\frac{R}{C} - \frac{1}{\alpha} \left[\mu_{1c}(s) + \mu_{0c}(-s) \right] \qquad (I.28)$$

$$\dot{\mu}_{1c}(s) = \dot{\mu}_{0c}(-s), \qquad s \leq 0$$

To complete the upper bounding all that remains is to determine which of $E_\ell^o\left(\frac{R}{C}\right)$ and $E_h^o\left(\frac{R}{C}\right)$ is larger, as a function of R. Substitution of R_{crit} into (I.23a) and (I.28) gives

$$E_{\ell}^{o}\left(\frac{R_{crit}}{C}\right) = E_{h}^{o}\left(\frac{R_{crit}}{C}\right) \tag{I.29}$$

For $R \leq R_{crit}$, $E_{h}^{o}\left(\frac{R}{C}\right)$ can be rewritten from (I.23a) and (I.24) as

$$E_{h}^{o}\left(\frac{R}{C}\right) = -\frac{R}{C} - \frac{1}{\alpha}\left[\mu_{1c}(s_0) + \mu_{0c}(-s_0)\right] \tag{I.30}$$

This is just $E_{\ell}^{o}\left(\frac{R}{C}\right)$ evaluated at the s_0 of (I.24). But the value of s which maximizes $E_{\ell}^{o}\left(\frac{R}{C}\right)$ is given by (I.28) and is different; hence

$$E_{\ell}^{o}\left(\frac{R}{C}\right) > E_{h}^{o}\left(\frac{R}{C}\right), \qquad R < R_{crit} \tag{I.31}$$

For $R > R_{crit}$, note that

$$\frac{dE_{\ell}^{o}}{d\left(\frac{R}{C}\right)} = -1, \qquad \text{all } \frac{R}{C} \tag{I.32}$$

From (I.23)

$$\frac{dE_{h}^{o}}{d\left(\frac{R}{C}\right)} = \frac{1}{\alpha} \, s_0 \ddot{\mu}_{1c}(s_0) \, \frac{\partial s_0}{\partial\left(\frac{R}{C}\right)}$$

$$= \frac{1}{\alpha} \, s_0 \ddot{\mu}_{0c}(t_0) \, \frac{\partial t_0}{\partial\left(\frac{R}{C}\right)}$$

$$= \frac{s_0}{t_0} \tag{I.33}$$

by implicit differentiation of (I.23b) and (I.23c). Then by (I.23d)

$$-1 < \frac{dE_h^o}{d\left(\frac{R}{C}\right)} \leq 0 , \qquad R > R_{crit} \tag{I.34a}$$

since $t > -s$ for $R > R_{crit}$. Thus

$$E_h^o\left(\frac{R}{C}\right) > E_\ell^o\left(\frac{R}{C}\right) , \qquad R > R_{crit} \tag{I.34b}$$

The final upper bound is then

$$Pr(\varepsilon) < 2 \cdot 2^{-\tau C E^o\left(\frac{R}{C}\right)} \tag{I.35}$$

where

$$E^o\left(\frac{R}{C}\right) = \begin{cases} E_h^o\left(\frac{R}{C}\right) & R \geq R_{crit} \\ \\ E_\ell^o\left(\frac{R}{C}\right) & R < R_{crit} \end{cases} \tag{I.36}$$

The reliability function $E^o\left(\frac{R}{C}\right)$ is sketched in Figure I.4. Its slope for $R > R_{crit}$ is monotonically decreasing in $\frac{R}{C}$. $E^o\left(\frac{R}{C}\right)$ reaches zero at R_{max} given by

$$\frac{R_{max}}{C} = t\dot{\mu}_{1c}(0) - \mu_{0c}(t) \tag{I.37}$$
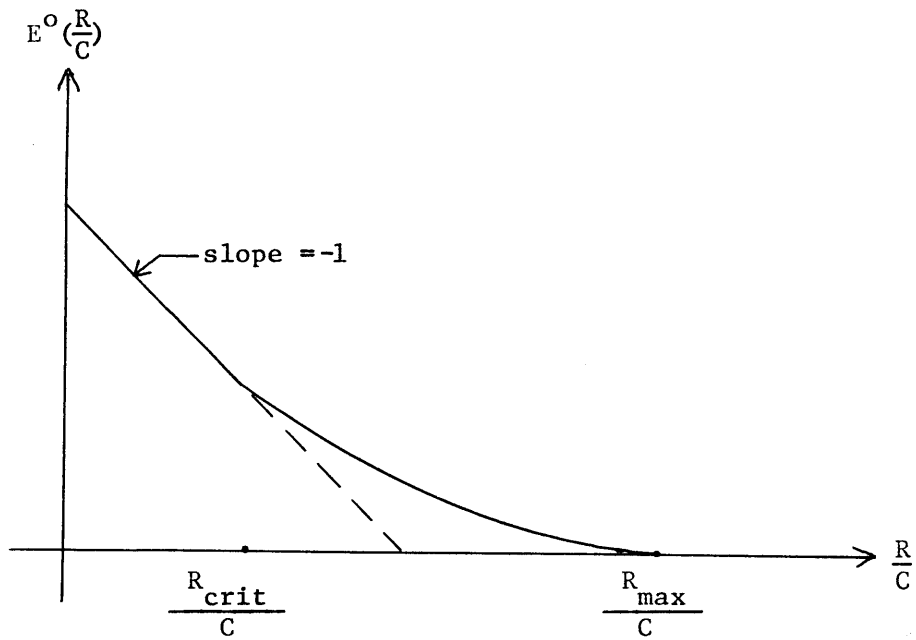
$$\dot{\mu}_{1c}(0) = \dot{\mu}_{0c}(t)$$

Figure I-4. Reliability function for the suboptimum
            filter-squarer-integrator receiver.

At zero rate

$$E^o(0) = \frac{1}{\alpha}\left[\mu_{1c}(s) + \mu_{0c}(-s)\right]$$

(I.38)

$$\dot{\mu}_{1c}(s) = \dot{\mu}_{0c}(-s), \qquad s \leq 0$$

C. The Lower Bound

To optimize the lower bound of (I.4a) subject to the constraints (I.4b,c) it is convenient to recognize that (I.4c) combined with (I.4b) is just

$$\frac{R\alpha}{C} \leq f(s,t)$$

(I.39)

where $f(s,t)$ is given by (I.15a). Thus optimization results from maximizing

$$h(s,t) = \mu_{1c}(s) - s\dot{\mu}_{1c}(s) + \mu_{0c}(t) - t\dot{\mu}_{0c}(t)$$

(I.40)

along the curve A in Figure I.3 for $s \leq 0$ and $t \geq 0$ such that s and t lie inside the contour determined from (I.39).

The derivative of $h(s,t)$ along the curve A is

$$\left.\frac{dh(s,t)}{dt}\right|_A = -s\ddot{\mu}_{1c}(s)\,\frac{ds}{dt} - t\ddot{\mu}_{0c}(t)$$

$$= -(s+t)\ddot{\mu}_{0c}(t)$$

(I.41)

by implicitely differentiating (I.4b). Thus $h(s,t)$ has a maximum at $s = -t$. If $R < R_{crit}$, the contour of (I.39) encloses the point $s = -t$ on A. Then (I.4a) becomes

$$Pr(\varepsilon) \geq \frac{B}{4} \; 2^{-\tau C E_\ell^o\left(\frac{R}{C}\right)}, \qquad R < R_{crit} \qquad (I.42)$$

with

$$E_\ell^o\left(\frac{R}{C}\right) = -\frac{R}{C} - \frac{1}{\alpha} \; h(s_0, -s_0)$$

$$= -\frac{R}{C} - \frac{1}{\alpha} \left[\mu_{1c}(s_0) - \mu_{0c}(-s_0)\right] \qquad (I.43a)$$

$$\dot{\mu}_{1c}(s_0) = \dot{\mu}_{0c}(-s_0), \qquad s_0 \leq 0 \qquad (I.43b)$$

This is the same function derived for the upper bound.

For $R > R_{crit}$, the contour of (I.39) does not enclose $s = -t$ on A, and thus to maximize $h(s,t)$, (s,t) is chosen as the point on A that intersects the given contour. But this is just the point chosen in the upper bound case when $R > R_{crit}$. Thus

$$Pr(\varepsilon) > \frac{B}{4} \; 2^{-\tau C E_h^o\left(\frac{R}{C}\right)}, \qquad R > R_{crit} \qquad (I.44)$$

where $E_h^o\left(\frac{R}{C}\right)$ is given by (I.23). The combination of (I.42) and (I.44) gives a lower bound on the $Pr(\varepsilon)$ that has exactly the same exponential behavior as the upper bound.

In summary, the following bounds have been derived

$$Pr(\varepsilon) < k_u 2^{-\tau C E^o\left(\frac{R}{C}\right)} \qquad (I.45a)$$

$$Pr(\varepsilon) > k_\ell 2^{-\tau C E^o\left(\frac{R}{C}\right)} \qquad (I.45b)$$

where the reliability function $E^o\left(\frac{R}{C}\right)$ is given by (I.36). The results

are expressed in terms of the moment-generating functions of the branch

outputs of the filter-squarer-integrator receiver. In the case of

the optimum receiver, the bounds reduce to those derived by Kennedy [6],

if the proper $\mu_{ic}(s)$ are used. A thorough discussion of this case and

the system reliability function is contained in Kennedy [6]. Although

the derivation above was done for the filter-squarer-integrator suboptimum

receiver, the several necessary properties of the $\mu_{ic}(s)$ should hold for

any suboptimum receiver whose moment generating functions μ_{ic} satisfy the

assumptions given at the beginning of this appendix.

APPENDIX II

THE OPTIMUM RECEIVER FOR A DELAY-

SPREAD CHANNEL TRUNCATED SERIES MODEL

This appendix derives the optimum receiver for the delay-
spread channel truncated series model of (4.29). The derivation is
similar to that for the problem of the transmission of known signals
over a Rayleigh fading channel. In this case the known signals are
not orthogonal and the fading is correlated.

The complex envelope of the received signal in the truncated
model is from (4.29)

$$\tilde{r}(t) = \sum_{i=1}^{N} \tilde{b}_i(t)\tilde{y}_i + \tilde{w}(t) \tag{II-1}$$

The $\tilde{b}_i(t)$ are known signals, $\tilde{w}(t)$ is complex white Gaussian noise, and
the $\tilde{y}_i$ are complex Gaussian random variables. It is convenient to
define the vectors

$$\underline{\tilde{b}}(t) = [\tilde{b}_1(t), \tilde{b}_2(t), \ldots, \tilde{b}_N(t)]$$

$$\underline{\tilde{y}} = \begin{bmatrix} \tilde{y}_1 \\ \cdot \\ \cdot \\ \cdot \\ \tilde{y}_N \end{bmatrix} \tag{II-2}$$

and write $\tilde{r}(t)$ as

$$\tilde{r}(t) = \underline{\tilde{b}}(t)\underline{\tilde{y}} + \tilde{w}(t) \tag{II-3}$$

The covariance matrix for $\underline{\tilde{y}}$ is known and is denoted by

$$E[\underline{\tilde{y}}\,\underline{\tilde{y}}^\dagger] = \underline{\tilde{K}} \tag{II-4}$$

The derivation of the optimum receiver for (II-3) follows the method given by (4.399-4.404) of Van Trees [20]. Given that $\tilde{y}$ in (II-3) has the value $\tilde{Y}$, the likelihood ratio is available from the known signal in white noise problem

$$\Lambda(\tilde{r}(t)|\tilde{Y}) = \exp\left[\frac{1}{N_o} \int_{T_o}^{T_f} \tilde{r}(t)\, \tilde{Y}^\dagger\tilde{b}^\dagger(t)dt \right.$$

$$\left. + \frac{1}{N_o} \int_{T_o}^{T_f} \tilde{r}^*(t)\, \tilde{b}(t)\, \tilde{Y}\, dt - \frac{1}{N_o} \int_{T_o}^{T_f} \tilde{Y}^\dagger\tilde{b}^\dagger(t)\tilde{b}(t)\tilde{Y}dt \right]$$

$$= \exp\left[\tilde{Y}^\dagger\tilde{R} + \tilde{R}^\dagger\tilde{Y} - \tilde{Y}^\dagger\tilde{B}\,\tilde{Y} \right] \tag{II-5}$$

where

$$\tilde{R} = \frac{1}{N_o} \int_{T_o}^{T_f} \tilde{r}(t)\, \tilde{b}^\dagger(t)dt \tag{II-6}$$

$$\tilde{B} = \frac{1}{N_o} \int_{T_o}^{T_f} \tilde{b}^\dagger(t)\, \tilde{b}(t)dt \tag{II-7}$$

The probability density function for the Gaussian random vector $\tilde{y}$ is [8]

$$p_{\tilde{y}}(\tilde{Y}) = \frac{1}{\pi^N \det \tilde{K}}\ \exp\left[-\tilde{Y}^\dagger\tilde{K}^{-1}\tilde{Y} \right] \tag{II-8}$$

Integrating (II-5) over the density (II-8) removes the unwanted variables $\tilde{y}$ to give the likelihood ratio for the problem of (II-3):

$$\Lambda[\tilde{r}(t)] = \int_{-\infty}^{\infty} p\, \underline{\tilde{y}}(\underline{\tilde{Y}})\, \exp\left[\underline{\tilde{Y}}^{\dagger}\underline{\tilde{R}} + \underline{\tilde{R}}^{\dagger}\underline{\tilde{Y}} - \underline{\tilde{Y}}^{\dagger}\underline{B}\,\underline{\tilde{Y}}\right]\, d\underline{\tilde{Y}}$$

$$= \frac{1}{\det(\underline{\tilde{K}}\,\underline{\tilde{\Sigma}}^{-1})}\, \exp\{\underline{\tilde{R}}^{\dagger}\,\underline{\tilde{\Sigma}}\,\underline{\tilde{R}}\}$$

$$\cdot \int_{-\infty}^{\infty} \frac{1}{\pi^N \det \underline{\tilde{\Sigma}}}\, \exp\left[-(\underline{\tilde{Y}}^{\dagger} - \underline{\tilde{R}}^{\dagger}\underline{\tilde{\Sigma}})\underline{\tilde{\Sigma}}^{-1}(\underline{\tilde{Y}} - \underline{\tilde{\Sigma}}\,\underline{\tilde{R}})\right]\, d\underline{\tilde{Y}}$$

$$= \frac{1}{\det(\underline{\tilde{K}}\,\underline{\tilde{\Sigma}}^{-1})}\, \exp\{\underline{\tilde{R}}^{\dagger}\underline{\tilde{\Sigma}}\,\underline{\tilde{R}}\} \qquad (\text{II-9})$$

where

$$\underline{\tilde{\Sigma}}^{-1} = \underline{\tilde{K}}^{-1} + \underline{\tilde{B}} \qquad (\text{II-10})$$

Thus the logarithm of the likelihood ratio is

$$\ell = \underline{\Lambda}(\underline{\tilde{r}}(t))$$

$$= \underline{\tilde{R}}^{\dagger}(\underline{\tilde{K}}^{-1} + \underline{\tilde{B}})^{-1}\underline{\tilde{R}} - \ell n\, \det(\underline{I} + \underline{\tilde{K}}\,\underline{\tilde{B}}) \qquad (\text{II-11})$$

The receiver of (II-11) can also be obtained by writing the ratio of the probability densities of $\underline{R}$ under the signal plus noise and noise alone hypotheses. The branch structure of the optimum receiver of (I-11) is shown in Figure II-1. The signal $\tilde{r}(t)$ is passed into a bank of correlators, or matched filters. The outputs $\tilde{r}_i$, which are the elements of the vector $\underline{\tilde{R}}$, are combined quadratically according to (II-11). The second term in (II-11) is a bias which does not depend on $\tilde{r}(t)$.
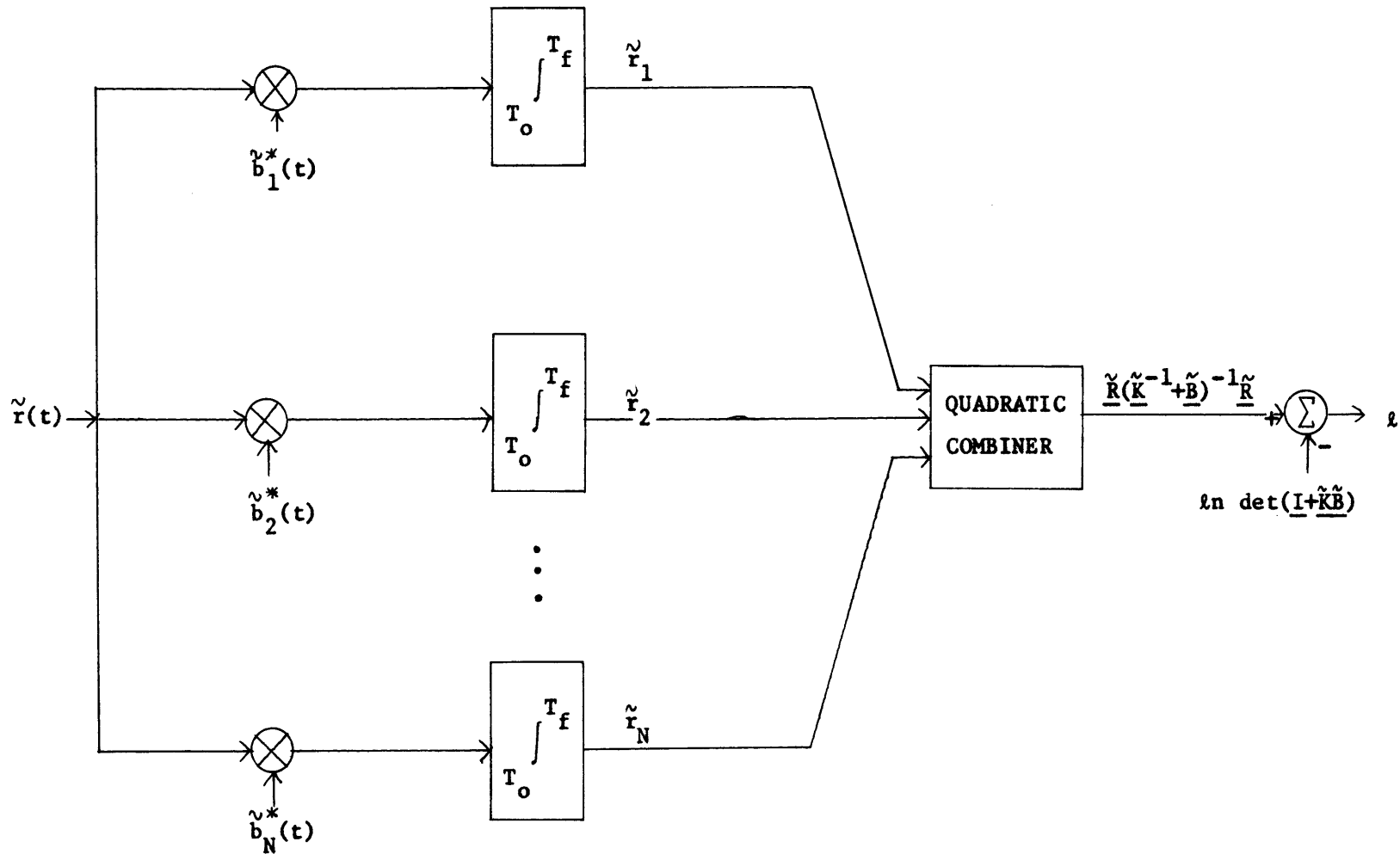
Figure II-1. Complex version of the optimum receiver branch for the delay-spread channel truncated series model.

In order to compute the error probabilities for this receiver with the techniques of Chapter II, it is necessary to find the semi-invariant moment-generating function for ℓ. For either the binary detection or the orthogonal communication problems it is sufficient to find $E[\ e^{s\ell}]$ given that $\tilde{r}(t)$ is just $\tilde{w}(t)$. Then (2.41) and (2.76) give the other moment-generating functions.

Since the decision statistic of II-11 is a finite quadratic form, the expressions of Chapter II, Section E can be used directly to give $\mu_{*0}(s)$. From (2.118)

$$\mu_{*0}(s) = \ln E[\ e^{s\ell}|\ \text{noise}\ ]$$

$$= \ln e^{-s\ \det(\underline{I} + \underline{\tilde{K}}\ \underline{\tilde{B}})}E[\exp(s\ \underline{\tilde{R}}^{\dagger}(\underline{\tilde{K}}^{-1}+\underline{\tilde{B}})^{-1}\underline{\tilde{R}})\ |\ \text{noise}\ ]$$

$$= -s\ \ln\ \det(\underline{I} + \underline{\tilde{K}}\ \underline{\tilde{B}}) - \ln\ \det(\underline{I} - s(\underline{\tilde{K}}^{-1}+ \underline{\tilde{B}})^{-1}\underline{\Lambda}_{n})$$

$$\text{(II-12)}$$

where

$$\underline{\Lambda}_{n} = E[\underline{\tilde{R}}\ \underline{\tilde{R}}^{\dagger}|\ \text{noise}\ ] \tag{II-13}$$

For simple binary detection (2.41) gives

$$\mu_{*1}(s) = \mu_{*0}(s + 1) \tag{II-14}$$

and for the binary symmetric communication, (2.76) gives

$$\mu_{*bc}(s) = \mu_{*0c}(s + 1) + \mu_{*0c}(-s)$$

$$= \mu_{*0c}(s + 1) + \mu_{*0}(-s)$$

$$= -\ell n \ \det \ [\underline{I} + \underline{\tilde{K}} \ \underline{\tilde{B}}] \ [\underline{I} - (s + 1)(\underline{\tilde{K}}^{-1} + \underline{\tilde{B}})^{-1}\underline{\Lambda}_n]$$

$$[\underline{I} + s \ (\underline{\tilde{K}}^{-1} + \underline{\tilde{B}})^{-1}\underline{\Lambda}_n]$$

$$(II-15)$$

The covariance matrix $\underline{\Lambda}_n$ is found from (II-6)

$$\underline{\Lambda}_n = E[\underline{\tilde{R}} \ \underline{\tilde{R}}^\dagger | noise]$$

$$= \frac{1}{N_o^2} \int_{T_o}^{T_f} \int_{T_o}^{T_f} N_o \delta(t-u)\underline{\tilde{b}}^\dagger(t)\underline{\tilde{b}}(u)dtdt$$

$$= \underline{\tilde{B}} \qquad\qquad (II-16)$$

Introduction of (II-16) into (II-12), (II-13) and (II-15) completes the derivation of the moment-generating functions that are used to compute the error probabilities for the truncated optimum receiver.

APPENDIX III

MINIMUM MEAN-SQUARE ERROR ESTIMATION OF

DISTRIBUTED-PARAMETER STATE-VECTORS

This appendix derives the realizable MMSE estimator for the state vector $\underline{\tilde{X}}(x,t)$ in the system of (5.10) and (5.11). The complex envelope of the doubly-spread channel received signal is, from (5.2)

$$\tilde{r}(t) = \int_{-\infty}^{\infty} \tilde{f}(t-x)\tilde{Y}(x,t)dx + \tilde{w}(t)$$

$$= \tilde{s}(t) + \tilde{w}(t), \quad T_o \leq t \leq T_f \tag{III.1}$$

where $\tilde{w}(t)$ is white noise. The MMSE realizable estimate of $\underline{\tilde{X}}(x,t)$ is obtained from $\tilde{r}(t)$ by the linear operation

$$\underline{\hat{X}}(x,t) = \int_{T_o}^{t} \underline{\tilde{h}}_o(x,t,\sigma) \; \tilde{r}(\sigma)d\sigma, \qquad t > T_o \tag{III.2}$$

$$\underline{\tilde{h}}_o(x,t,\tau) = 0, \quad t < \tau \tag{III.3}$$

The $m \times 1$ matrix distributed impulse response $\underline{\tilde{h}}_o(x,t,\tau)$ is chosen to minimize the state estimation error

$$\underline{\tilde{\xi}}(x,y,t) = E\left\{[\underline{\tilde{X}}(x,t) - \underline{\hat{X}}(x,t)][\underline{\tilde{X}}(y,t) - \underline{\hat{X}}(y,t)]^{\dagger}\right\} \tag{III.4}$$

The MMSE realizable estimate of $\tilde{s}(t)$ is then

$$\underline{\hat{\tilde{s}}}(t) = \int_{-\alpha}^{\infty} \tilde{f}(t-\sigma)\underline{\tilde{C}}(\sigma,t)\underline{\hat{\tilde{X}}}(\sigma,t)d\sigma \tag{III.5}$$

with the error

$$\tilde{\xi}_p(t) = E[|\tilde{s}(t) - \hat{\tilde{s}}(t)|^2]$$

$$= \int_{-\infty}^{\alpha} \int_{-\infty}^{\infty} \tilde{f}(t-\sigma)\underline{\tilde{C}}(\sigma,t)\underline{\tilde{\xi}}(\sigma,\alpha,t)\underline{\tilde{C}}^{\dagger}(\alpha,t)\tilde{f}^*(t-\alpha)d\sigma d\alpha \tag{III.6}$$

The derivation of the realizable MMSE estimator for the distributed-parameter state vector $\underset{\sim}{\underline{X}}(x,t)$ parallels that presented by Van Trees [20] for the lumped-parameter state-variable estimation problem. The derivation is extended here to the distributed-parameter case, and the complex notation is added. The result is an estimator structure which is a specialization of one obtained by Tzafestas and Nightingale [33] by a different procedure.

The starting point of the derivation is the generalized Wiener-Hopf equation [20] for $\tilde{h}_o(x,t,\tau)$

$$E[\underset{\sim}{\underline{X}}(x,t)\tilde{r}^*(\tau)] = \int_{T_o}^{t} \overset{\sim}{\underline{h}}_o(x,t,\sigma)\, \tilde{K}_r(\sigma,\tau)d\sigma, \quad T_o < \tau < t \qquad (III.7)$$

$\tilde{K}_r(\sigma,\tau)$ is the covariance function of $\tilde{r}(t)$. The left hand side of (III.7) is, from (III.1)

$$E[\overset{\sim}{\underline{X}}(x,t)\tilde{r}^*(\tau)] = \int_{-\infty}^{\infty} \overset{\sim}{\underline{K}}_X(x,t;\sigma,\tau)\underline{\tilde{C}}^\dagger(\tau,\sigma)\tilde{f}^*(\tau-\sigma)d\sigma \qquad (III.8)$$

since $\tilde{w}(t)$ and $\tilde{r}(\tau)$ are uncorrelated for $\tau < t$. $\underset{\sim}{\underline{K}}_X(x,t;y,\tau)$ is given by (5.14). Substitution of (III.8) into (III.7) and differentiation of the result gives

$$\int_{-\infty}^{\infty} \frac{\partial \underline{K}_X(x,t,\sigma,\tau)}{\partial t} \underline{\tilde{C}}^\dagger(\sigma,\tau)\tilde{f}^*(\tau-\sigma)d\sigma = \underline{\tilde{h}}_o(x,t,t)\tilde{K}_r(t,\tau) + \int_{T_o}^{t} \frac{\partial \overset{\sim}{\underline{h}}_o(x,t,\sigma)}{\partial t} \tilde{K}_r(\sigma,\tau)d\sigma$$

$$T_o < \tau < t \qquad (III.9)$$

To eliminate $\underset{\sim}{\underline{K}}_X(x,t;y,\tau)$ from (III.9), consider (5.18)

$$\frac{\partial \underset{\sim}{\underline{K}}_X(x,t;\sigma,\tau)}{\partial t} = E\left[\frac{\partial \underset{\sim}{\underline{X}}(x,t)}{\partial t} \underset{\sim}{\underline{X}}^{\dagger}(\sigma,\tau)\right]$$

$$= \underset{\sim}{\underline{F}}(x,t)\underset{\sim}{\underline{K}}_X(x,t;\sigma,\tau) \quad , \quad \tau < t \quad (III.10)$$

from (5.19), since $\underset{\sim}{\underline{U}}(x,t)$ and $\underset{\sim}{\underline{X}}(y,\tau)$ are uncorrelated for $\tau < t$. Then the left hand side of (III.9) becomes

$$\int_{-\infty}^{\infty} \frac{\partial \underset{\sim}{\underline{K}}_X(x,t;\sigma,\tau)}{\partial t} \underset{\sim}{\underline{C}}^{\dagger}(\sigma,\tau)\underset{\sim}{\underline{f}}^*(\tau-\sigma)d\sigma = \int_{-\infty}^{\infty} \underset{\sim}{\underline{F}}(x,t)\underset{\sim}{\underline{K}}_X(x,t;\sigma,\tau)\underset{\sim}{\underline{C}}^{\dagger}(\sigma,\tau)\underset{\sim}{\underline{f}}^*(\tau-\sigma)d\sigma$$

$$= \int_{T_o}^{t} \underset{\sim}{\underline{F}}(x,t)\underset{\sim}{\underline{h}}_o(x,t,\sigma)\underset{\sim}{\underline{K}}_r(\sigma,\tau)d\sigma \quad , \quad T_o < \tau < t \quad (III.11)$$

where the latter expression is derived from (III.7) and (III.8). From (III.1), (III.7), and (III.8), the first term on the right hand side of (III.9) becomes

$$\underset{\sim}{\underline{h}}_o(x,t,t)\underset{\sim}{\underline{K}}_r(t,\tau)$$

$$= \underset{\sim}{\underline{h}}_o(x,t,t) \int_{-\infty}^{\infty}\int_{-\infty}^{\infty} \underset{\sim}{\underline{f}}(t-\alpha)\underset{\sim}{\underline{C}}(\alpha,t)\underset{\sim}{\underline{K}}_X(\alpha,t;\sigma,\tau)\underset{\sim}{\underline{C}}^{\dagger}(\sigma,\tau)\underset{\sim}{\underline{f}}^*(\tau-\alpha)d\sigma d\alpha$$

$$= \int_{T_i}^{t}\int_{-\infty}^{\infty} \underset{\sim}{\underline{h}}_o(x,t,t)\underset{\sim}{\underline{f}}(t-\alpha)\underset{\sim}{\underline{C}}(\alpha,t)\underset{\sim}{\underline{h}}_o(\alpha,t,\sigma)\underset{\sim}{\underline{K}}_r(\sigma,\tau)d\alpha d\sigma, \quad T_o < \tau < t$$

$$(III.12)$$

since $E[\underset{\sim}{\underline{r}}(t)\underset{\sim}{\underline{w}}^*(\tau)]$ is zero for $\tau < t$. Substitution of (III.11) and (III.12) into (III.9) yields a partial differential equation for $\underset{\sim}{\underline{h}}_o(x,t,\sigma)$

$$\frac{\partial \underset{\sim}{\underline{h}}_o(x,t,\sigma)}{\partial t} = \underset{\sim}{\underline{F}}(x,t)\underset{\sim}{\underline{h}}_o(x,t,\sigma) + \int_{-\infty}^{\infty} \underset{\sim}{\underline{h}}_o(x,t,t)\underset{\sim}{\underline{f}}(t-\alpha)\underset{\sim}{\underline{C}}(\alpha,t)\underset{\sim}{\underline{h}}_o(\alpha,t,\sigma)d\alpha \quad (III.13)$$

Partial differentiation of (III.2) with respect to t gives an equation which $\underset{\sim}{\underline{X}}(x,t)$ must satisfy

$$\frac{\partial \underset{\sim}{\underline{X}}(x,t)}{\partial t} = \underline{\underset{\sim}{F}}(x,t)\underset{\sim}{\underline{X}}(x,t) + \underset{\sim}{\underline{h}}_o(x,t,t)[\underset{\sim}{r}(t) - \underset{\sim}{s}(t)] \qquad (III.14)$$

where MMSE realizable estimate of $\underset{\sim}{s}(t)$ is

$$\underset{\sim}{s}(t) = \int_{-\infty}^{\infty} \underset{\sim}{f}(t-\sigma)\underset{\sim}{\underline{C}}(\sigma,t)\underset{\sim}{\underline{X}}(\sigma,t)d\sigma \qquad (III.15)$$

The initial condition for (III.14) is

$$\underset{\sim}{\underline{X}}(x,T_o) = E[\underset{\sim}{\underline{X}}(x,T_o) = \underline{0} \qquad (III.16)$$

The MMSE estimate of $\underset{\sim}{\underline{X}}(x,t)$ is the solution to the linear partial differential equation (III.14). The homogeneous system that is associated with this equation is identical to that for the equations which generate $\underset{\sim}{\underline{X}}(x,t)$, (5.10). The estimate of $\underset{\sim}{s}(t)$ is fed back and subtracted from $\underset{\sim}{r}(t)$ to drive the estimator. The matrix gain $\underset{\sim}{\underline{h}}_o(x,t,t)$ is not a function of $\underset{\sim}{r}(t)$.

The nest step is to obtain an equation for $\underset{\sim}{\underline{h}}_o(x,t,t)$. The Wiener-Hopf equation given by (III.7) and (III.8),with $t = \tau$ is

$$\int_{-\infty}^{\infty} \underset{\sim}{\underline{K}}_X(x,t;\sigma,t)\underset{\sim}{\underline{C}}^\dagger(\sigma,t)\underset{\sim}{f}^*(t-\sigma)d\sigma = N_o \underset{\sim}{\underline{h}}_o(x,t,t)$$

$$+ \int_{T_o}^{t} \int_{-\infty}^{\infty} \int_{-\infty}^{\infty} \underset{\sim}{\underline{h}}_o(x,t,\sigma)\underset{\sim}{f}(\sigma-\alpha)\underset{\sim}{\underline{C}}(\alpha)\underset{\sim}{\underline{K}}_X(\alpha,\sigma;\beta,t)\underset{\sim}{\underline{C}}^\dagger(\beta)\underset{\sim}{f}^*(t-\beta) \, d\alpha d\beta d\sigma$$

$$(III.17)$$

From (III.4), (III.7), and (III.8)

$$\underset{\sim}{\underline{\xi}}(x,\beta,t) = E\left\{ [\underset{\sim}{\underline{X}}(x,t) - \int_{T_o}^{t} \underset{\sim}{\underline{h}}_o(x,t,\tau)\underset{\sim}{\underline{r}}(\tau)d\tau][\underset{\sim}{\underline{X}}(\beta,t) - \int_{T_o}^{t} \underset{\sim}{\underline{h}}_o(\beta,t,\tau)\underset{\sim}{\underline{r}}(\tau)d\tau]^{\dagger} \right\}$$

$$= \underset{\sim}{\underline{K}}_X(x,t;\beta,t) - \int_{T_o}^{t} \int_{-\infty}^{\infty} \underset{\sim}{\underline{h}}_o(x,t,\sigma)\underset{\sim}{\underline{f}}(\sigma-\alpha)\underset{\sim}{\underline{C}}(\alpha)\underset{\sim}{\underline{K}}_X(\alpha,\sigma;\beta,t)d\alpha d\sigma \quad (III.18)$$

Post-multiplying (III.18) by $\underset{\sim}{\underline{C}}^{\dagger}(\beta)\underset{\sim}{f}^{*}(t-\beta)$, integrating over β, and combining the result with (II.17) gives

$$\underset{\sim}{\underline{h}}_o(x,t,t) = \frac{1}{N_o} \int_{-\infty}^{\infty} \underset{\sim}{\underline{\xi}}(x,\sigma,t)\underset{\sim}{\underline{C}}^{\dagger}(\sigma,t)\underset{\sim}{f}^{*}(t-\sigma)d\sigma \quad (III.19)$$

This specifies the gain $\underset{\sim}{\underline{h}}_o(x,t,t)$ in terms of the error covariance matrix.

The error covariance matrix $\underset{\sim}{\underline{\xi}}(x,y,t)$ satisfies a partial differential equation which can be derived by recognizing from (5.10) and (III.14) that the error

$$\underset{\sim}{\underline{X}}_{\varepsilon}(x,t) = \underset{\sim}{\underline{X}}(x,t) - \overset{\wedge}{\underset{\sim}{\underline{X}}}(x,t) \quad (III.20)$$

satisfies the partial differential equation

$$\frac{\partial\underset{\sim}{\underline{X}}_{\varepsilon}(x,t)}{\partial t} = \underset{\sim}{\underline{F}}(x,t)\underset{\sim}{\underline{X}}_{\varepsilon}(x,t) - \underset{\sim}{\underline{h}}_o(x,t,t) \int_{-\infty}^{\infty} \underset{\sim}{f}(t-\sigma)\underset{\sim}{\underline{C}}(\sigma,t)\underset{\sim}{\underline{X}}_{\varepsilon}(\tau,t)d\tau$$

$$+ \underset{\sim}{\underline{G}}(x,t)\underset{\sim}{\underline{U}}(x,t) - \underset{\sim}{\underline{h}}_o(x,t,t)\underset{\sim}{w}(t) \quad (III.21)$$

Now

$$\frac{\partial \tilde{\xi}(x,y,t)}{\partial t} = E[\frac{\partial \tilde{X}_\epsilon(x,t)}{\partial t} \tilde{X}_\epsilon^\dagger(y,t)] + E[\tilde{X}_\epsilon(x,t)\frac{\partial \tilde{X}_\epsilon^\dagger(y,t)}{\partial t}]$$

(III.22)

From (III.21) and (5.18), the first term in (III.22) is

$$E[\frac{\partial \tilde{X}_\epsilon(x,t)}{\partial t} \tilde{X}_\epsilon^\dagger(y,t)] = \tilde{F}(x,t)\tilde{\xi}(x,y,t)$$

$$- \tilde{h}_o(x,t,t) \int_{-\infty}^{\infty} \tilde{F}(t-\sigma)\tilde{C}(\sigma,t)\tilde{\xi}(\sigma,y,t)d\sigma$$

$$+ \frac{1}{2} \tilde{G}(x,t)\tilde{Q}(x,y,t)\tilde{G}^\dagger(y,t) + \tilde{h}_o(x,t,t) \frac{N_o}{2} \tilde{h}_o^\dagger(y,t,t)$$

(III.23)

Evaluating the other term in (III.22) in a like manner gives the matrix partial differential equation for the error covariance

$$\frac{\partial \tilde{\xi}(x,y,t)}{\partial t} = \tilde{F}(x,t)\tilde{\xi}(x,y,t) + \tilde{\xi}(x,y,t)\tilde{F}^\dagger(y,t) + \tilde{G}(x,t)\tilde{Q}(x,y,t)\tilde{G}^\dagger(y,t)$$

$$- \frac{1}{N_o}\left[\int_{-\infty}^{\infty} \tilde{\xi}(x,\sigma,t)\tilde{C}^\dagger(\sigma,t)\tilde{F}^*(t-\sigma)d\sigma\right]\left[\int_{-\infty}^{\infty} \tilde{F}(t-\alpha)\tilde{C}(\alpha,t)\tilde{\xi}(\alpha,y,t)d\alpha\right]$$

(III.24)

The initial condition for (III.24) is

$$\underline{\xi}(x,y,T_o) = \underset{-X}{\tilde{K}}(x,T_o;y,T_o)$$

$$= \underset{-o}{\tilde{P}}(x,y) \qquad\qquad\qquad (III.25)$$

from (5.22).

The derivation of the MMSE realizable estimator for $\overset{\sim}{\underline{X}}(x,t)$
is complete. The gain $\underset{-o}{\tilde{h}}(x,t,t)$ in the estimator (III.14) is related
to $\overset{\sim}{\underline{\xi}}(x,y,t)$ by (III.19). The error covariance matrix is the solution
of (III.24) with the initial conditions (III.25). Thus $\underset{-o}{\tilde{h}}(x,t,t)$
does not depend on $\tilde{r}(t)$ and can therefore be precomputed. Note that
partial differential equation (III.25) can be integrated directly,
since its right had side is only a function of $\overset{\sim}{\underline{\xi}}(x,y,t)$ and integrals
of $\overset{\sim}{\underline{\xi}}(x,y,t)$ over x and y.

REFERENCES

1. R. Price, "Optimum Detection for Random Signals in Noise, With
    Application to Scatter-Multipath Communication,I" IRE Transactions
    on Information Theory, PGIT, pp.125-135, December, 1965.

2. R. Price and P. E. Green, "Signal Processing in Radar Astronomy-
    Communication via Fluctuating Multipath Media", M.I.T.,
    Lincoln Laboratory, Technical Report No.234, October, 1960.

3. G. L. Turin, "Communication Through Noisy, Random-Multipath
    Channels", M.I.T., Lincoln Laboratory, Technical Report 116,
    May, 1956.

4. D. Middleton, "On the Detection of Stochastic Signals in Additive
    Normal Noise", IRE Transaction on Information Theory, PGIT-3,
    pp. 86-121, June, 1957.

5. A. J. Viterbi, "Performance of an M-ary Orthogonal Communication
    System Using Stationary Stochastic Signals", IEEE Transactions
    on Information Theory, Vol. IT-13, No.3, pp. 414-422, July, 1967.

6. R. S. Kennedy, Coding and Modulation Theory for Dispersive Fading
    Channels, (unpublished monograph).

7. R. Price, "Detectors for Radar Astronomy", Radar Astronomy,
    T. Hagfors and J. V. Evans, Eds., Wiley, 1968.

8. H. L. Van Trees, Detection, Estimation, and Modulation Theory,
    Part II, John Wiley, New York, (to appear).

9. F. Schweppe, "Evaluation of Likelihood Functions for Gaussian
    Signals", IEEE Transactions on Information Theory, Vol. IT-11,
    No.1, pp. 61-70, January, 1965.

10. A. B. Baggeroer, "A State-Variable Approach to the Solution of
    Fredholm Integral Equations", M.I.T., Research Laboratory of
    Electronics, Technical Report 459, November, 1967.

11. R. Price, "Output Signal to Noise Ratio as a Criterion in Spread-
    Channel Signaling", M.I.T., Lincoln Laboratory, Technical Report
    338, May, 1965.

12. T. Kailath, "The Divergence and Bhattacharyya Distance Measures
    in Signal Selection", IEEE Transactions on Communication
    Technology, Vol. COM-15, No.1, pp. 52-60, February, 1967.

13. L. D. Collins, "Asymptotic Approximations to the Error Probability
    for Detecting Gaussian Signals", Sc.D. Thesis, Department
    of Electrical Engineering, M.I.T., June, 1968.

14. L. D. Collins. "Asymptotic Approximations to the Error Probability for Detecting Gaussian Signals", Technical Paper 6-1, WESCON, Los Angeles, Calif., August, 1968.

15. H. L. Van Trees, A. B. Baggeroer and L. D. Collins, "Complex State Variables: Theory and Applications", Technical Paper 6-3, WESCON, Los Angeles, Calif., August, 1968.

16. P. A. Bello, "Characterization of Randomly Time-Variant Linear Channels", IEEE Transactions on Communications Systems, Vol. CS-11, No.4, pp. 360-393, December, 1963.

17. E. J. Kelly, "Random Scatter Channels", M.I.T., Lincoln Laboratory, Group Report 1964-61, November, 1964.

18. P. A. Bello, "Time-Frequency Duality", IEEE Transactions on Information Theory, Vol. IT-10, No.1, pp.18-33, January, 1964.

19. T. Kailath, "Sampling Models for Linear Time-Invariant Filters", M.I.T., Research Laboratory of Electronics, Technical Report 352, May, 1959.

20. H. L. Van Trees, Detection, Estimation, and Modulation Theory Part I, John Wiley, New York, 1968.

21. H. Cramer, Mathematical Methods of Statistics, Princeton University Press, New Jersey, 1965, pp. 222-231.

22. W. Davenport and W. Root, An Introduction to the Theory of Random Signals and Noise, McGraw-Hill, New York, 1958.

23. D. Slepian, "Fluctuations of Random Noise Power", Bell System Technical Journal, Vol. 37, No.1, pp. 163-184, January, 1958.

24. A. B. Baggeroer, "State Variables, the Fredholm Theory, and Optimal Communications", Sc.D. Thesis, Department of Electrical Engineering, Massachusetts Institute of Technology, January, 1968.

25. C. W. Helstrom, Statistical Theory of Signal Detection, MacMillan, New York, 1960.

26. L. D. Collins, "Closed Form Expressions for the Fredholm Determinant for State-Variable Covariance Functions", Proceedings of the IEEE, Vol. 56, No.4, April, 1968.

27. J. N. Pierce, "Approximate Error Probabilities for Optimal Diversity Combining", IEEE Transactions on Communications Systems, Vol. CS-11, No.3, pp.352-354, September, 1963.

28. J. N. Pierce, "Theoretical Limitations on Frequency and Time Diversity for Fading Binary Transmissions", IRE Transactions on Communications Systems, Vol. CS-9, No.2, pp. 186-187, June, 1961.

29. M. Murray-Lasso, "The Modal Analysis and Synthesis of Linear Distributed Control Systems", Sc.D. Thesis, Department of Electrical Engineering, Massachusetts Institute of Technology, June, 1965.

30. M. Athans and F. Schweppe, "Optimal Waveform Design via Control Theoretic Concepts", Information and Control, Vol. 10, No.4, pp. 335-377, April, 1967.

31. A. B. Baggeroer, "Optimal Signal Design for Additive Colored Noise Channels Via State Variables", Technical Paper 6.1, WESCON, Los Angeles, Calif., August, 1968.

32. M. Athans and P. Falb, Optimal Control, McGraw-Hill Co., New York, 1966.

33. S. G. Tzafestas and J. M. Nightingale, "Optimal Filtering, Smoothing and Prediction in Linear Distributed-Parameter Systems", Proceedings of the IEE, Vol. 115, No.8, August, 1968.

34. S. G. Tzafestas and J. M. Nightingale, "Concerning the Optimal Filtering Theory of Linear Distributed-Parameter Systems", Proceedings of the IEE, Vol. 115, No.11, November, 1968.

35. D. Snyder and E. Hoversten, "An Application of State-Variable Estimation Techniques to the Detection of a Spatially Distributed Signal". Quarterly Progress Report, Research Laboratory of Electronics, Massachusetts Institute of Technology, No. 93, April, 1969.

36. A. E. Bryson and W. F. Denham, "A Steepest-Ascent Method for Solving Optimum Programming Problems", Transactions of the ASME, Journal of Applied Mathematics, pp. 247-257, June, 1962.

37. W. F. Denham and A. E. Bryson, "Optimal Programming Problems with Inequality Constraints II: Solution by Steepest Ascent", AIAA Journal, Vol. 2, No.1, pp. 25-34, January, 1964.

BIOGRAPHY

Richard R. Kurth was born on May 27, 1942, in Asbury Park, New Jersey. He graduated in 1960 from the Norwich Free Academy, Norwich, Connecticut. He received the B. S. and M. S. degrees in Electrical Engineering from the Massachusetts Institute of Technology in August, 1965, and the E. E. degree from M. I. T. in June, 1968.

He has held summer positions with the U. S. Navy Underwater Sound Laboratory, the Institute for Defense Analyses, the RAND Corporation, and the Sperry Rand Research Center. He has done extensive teaching while completing his graduate work and is currently an Instructor in the Department of Electrical Engineering at M. I. T.

He is a member of Eta Kappa Nu, Tau Beta Pi, Sigma Xi, and the Institute of Electrical and Electronics Engineers.